Effect of hydrostatic pressure on the resistance and critical temperature of $YBa_2Cu_3O_{7-\delta}$ single crystals

D. D. Balla, A. V. Bondarenko, R. V. Vovk, M. A. Obolenskii, and A. A. Prodan

Kharkov State University, 310077 Kharkov, Ukraine[*]

(Submitted March 11, 1997)
Fiz. Nizk. Temp. **23**, 1035–1040 (October 1997)

The effect of hydrostatic pressure on the resistance and resistive transition to the superconducting state in $YBa_2Cu_3O_{7-\delta}$ single crystals with different oxygen contents is studied experimentally. It is found that, following the application (or removal) of pressure, the resistance relaxes to an equilibrium value that depends on pressure, the relaxation time at room temperature being about two days. It is shown that the value of the superconducting transition temperature depends on the pressure, but the width and shape of the transition depend mainly on the degree of resistance relaxation to the equilibrium value. It is concluded that the decrease in resistance under hydrostatic pressure is associated with the ordering of labile oxygen in the Cu–O plane. The possible mechanisms of variation of the superconducting transition temperature are discussed. [S1063-777X(97)00110-2]

As hydrostatic pressure is applied to the high-T_c superconductor $YBa_2Cu_3O_{7-\delta}$, its transition temperature T_c increases but its resistance R decreases.[1–5] The magnitude of variation $|dT_c/dP|$ of transition temperature and $|dR/dP|$ of resistance under a pressure P depends significantly on the oxygen index and increases with δ. A characteristic feature of samples with a reduced oxygen concentration is a broadening of their resistive transitions under hydrostatic pressure.[2,3] The reason behind such a behavior has not been established so far.

In all the works mentioned above, investigations were carried out on monocrystalline samples having an oxygen deficiency $\delta \leqslant 0.1$.[4,5] For a significant oxygen deficit $\delta \sim 0.5$, measurements were made on ceramic samples.[1–3] The aim of the present work is to study experimentally the effect of hydrostatic pressure on resistance in the ab-plane and on the superconducting transition temperature of $YBa_2Cu_3O_{7-\delta}$ single crystals with an oxygen index $\delta \sim 0.4$–0.6.

The $YBa_2Cu_3O_{7-\delta}$ single crystals were grown by the solution–melt technique in a gold crucible.[6] The crystals were subjected to thermal treatment in oxygen flow at temperatures 420–650 °C for two–three days. Measurements were made on three crystals. The resistivity of the crystal $K1$ at room temperature was $\rho_k \sim 200\ \mu\Omega\cdot$cm, the transition temperature $T_c = 92$ K and $\Delta T_c = 0.3$ K. The corresponding characteristics for crystals $K2$ and $K3$ are $\rho_r = 750\ \mu\Omega\cdot$cm, $T_c = 50$ K, $\Delta T_c = 2.4$ K and $\rho_r = 7\ \mu\Omega\cdot$cm, $T_c = 46$ K, $\Delta T_c = 4$ K, respectively. A comparison with the data available in the literature on the dependence of the transition temperature and resistivity on the oxygen index leads to the estimates $\delta \leqslant 0.1, \delta \leqslant 0.5$, and $\delta \leqslant 0.6$ for the value of δ in the crystals $K1$, $K2$ and $K3$, respectively.

The hydrostatic pressure was created with the help of a multiplicator by using the technique described in Ref. 7. The pressure in the multiplicator was measured by a manganine probe placed in the vicinity of the sample. The resistance was measured in a constant current by the standard four-probe technique. A transport current $I = 0.1$–$10\ \mu$A was passed through the ab-plane. The value of T_c was determined at the middle of the resistive transition to the superconducting state, i.e., at the level $R = R_N/2$, where R_N is the electrical resistance in the normal state. The width ΔT_c of the superconducting transition was determined as the difference in temperatures corresponding to the values $0.95\,R_N$ and $0.05\,R_N$ of the resistance.

Isothermal measurements of resistance at room temperature in $YBa_2Cu_3O_{7-\delta}$ crystals with oxygen deficiency $\delta \sim 0.5$ showed that after cooling of the samples from 620–650 °C, the resistance relaxes to the equilibrium value over a few days.[8] Hence all measurements were made after holding the samples at room temperature for four days. Test measurements show that the sample resistance did not change with time after such a holding.

Temperature dependences of the resistance R were measured during heating of the multiplicator (at first, under the atmospheric pressure). The pressure was then raised slowly at room temperature, the multiplicator was cooled to a temperature below the superconducting transition temperature, and measurements of $R(T)$ were started. The pressure was decreased to the atmospheric level after the attainment of maximum pressure, and $R(T)$ dependences were measured again.

In some cases, isothermal measurements of resistance as a function of time were made. The following procedure was adopted: after the application (removal) of pressure, the multiplicator was placed in a thermostat and resistance was measured after the attainment of a particular temperature. The time interval between measurements was 100 h.

Curves *1, 2, 3* in Fig. 1 show the temperature dependence of the reduced resistance of the samples $K1$, $K2$ and $K3$, respectively. The upper and lower insets to Fig. 1 show the transition to the superconducting state for the crystals $K1$

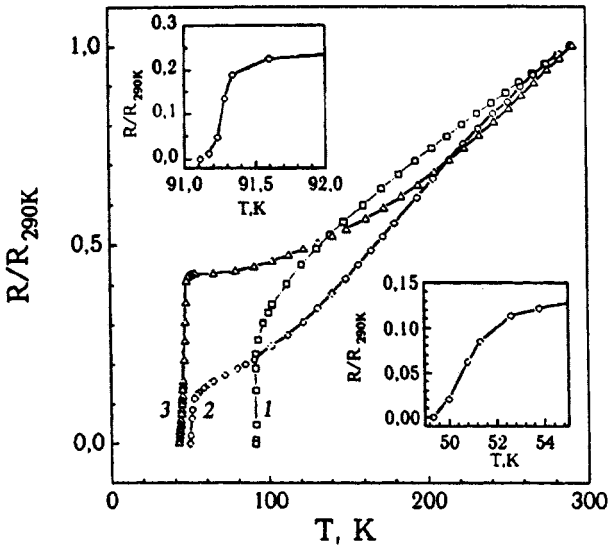

FIG. 1. Temperature dependence of the reduced resistance of single crystals $K1$ (curve *1*), $K2$ (curve *2*), and $K3$ (curve *3*). The upper inset shows the resistive transition to the superconducting state for the crystal $K1$, while the lower inset shows the corresponding transition for the crystal $K2$.

and $K2$, while Fig. 2 shows the corresponding transition for the sample $K3$. It can be seen that the width of the resistive transition increases with decreasing concentration of oxygen. This is in accord with the results available in the literature.[2]

Figure 2 shows the evolution of the superconducting transition for the crystal $K3$ under hydrostatic pressure. The results of measurements made under the application of pressure are shown by light circles on curve *1*. Curve *2* shows the $R(T)$ dependence measured directly after the application of a pressure of 4.2 kbar. Measurements were repeated after holding the sample under pressure at room temperature for three days. The results of these measurements are shown by curve *3*. The pressure was then removed, and the measurements at atmospheric pressure were made immediately after this (curve *4*). After this, the sample was held at room temperature for three days, and the resistance was measured repeatedly. The dark circles on curve *1* correspond to the results of measurements made three days after the removal of pressure.

It can be seen from Fig. 2a that the results of measurement of $R(T)$ depend not only on pressure, but also on the time of holding of the sample at room temperature under a constant pressure. A comparison of curves *1* and *2* shows that the shape and width of the resistive transition does not change upon the application of pressure, and only the magnitude of resistance and transition temperature changes. However, a comparison of curves *2* and *3* shows that holding of a sample under pressure at room temperature changes not only the resistance of the sample, but also the width and shape of the superconducting transition, while the transition temperature T_c remains unchanged (see Fig. 2b). Such a regularity was also observed as the pressure was reduced to the atmospheric level, at which the resistance and transition temperature change, but the width and shape of the superconducting transition remain unchanged. The resistance as well as the width and shape of the superconducting transition change as the sample is held for another three days at room

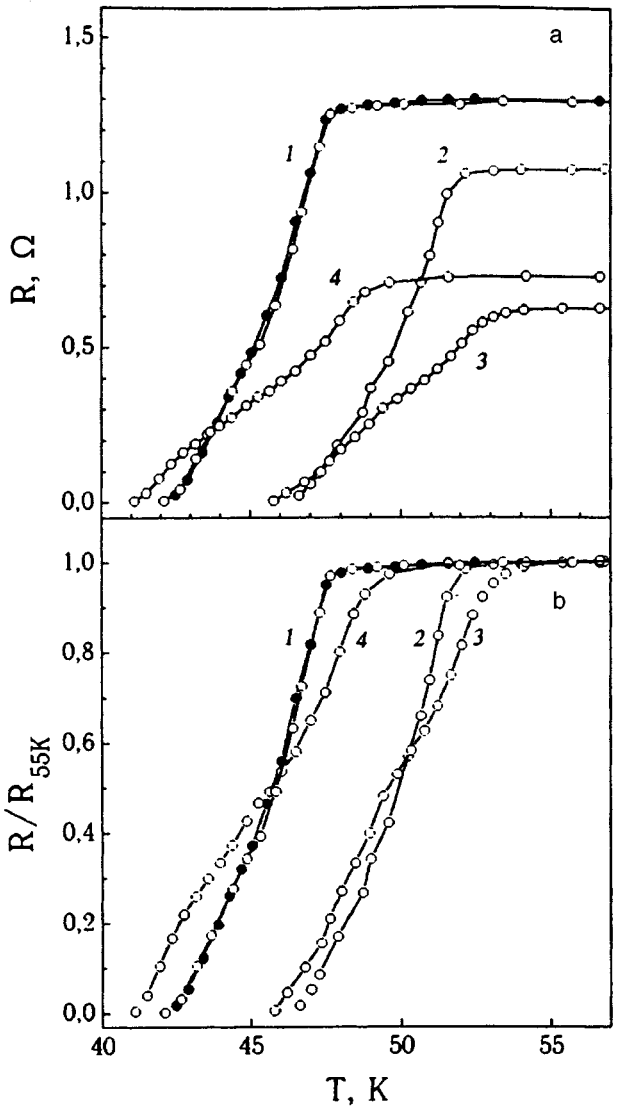

FIG. 2. Evolution of superconducting transitions in the crystal $K3$ in the process of application and removal of pressure (see text).

temperature. However, the additional holding of the sample at room temperature does not change the value of T_c. It is interesting to note that as the pressure is lowered to the atmospheric level and the sample is held at room temperature for three days, the $R(T)$ dependence coincides with the dependence obtained before the application of pressure. Thus, the observed variation of $R(T)$ is reversible during the application–removal of pressure. This is also confirmed by the results of measurements of resistance relaxation to the equilibrium value corresponding to the room temperature measurement.

The dependence of the resistance of the sample $K3$ on time, measured after the application and removal of pressure, is shown in Fig. 3.Before the application of the pressure, the sample resistance was $3.22\,\Omega$. The following sequence of measurements was adopted. After mounting the sample, a pressure $P=4.2$ kbar was produced in the high-pressure chamber. Curve *1* shows the results of measurements of the $R(T)$ dependence made at 293 K about one hour after the application of pressure. The pressure was then increased to

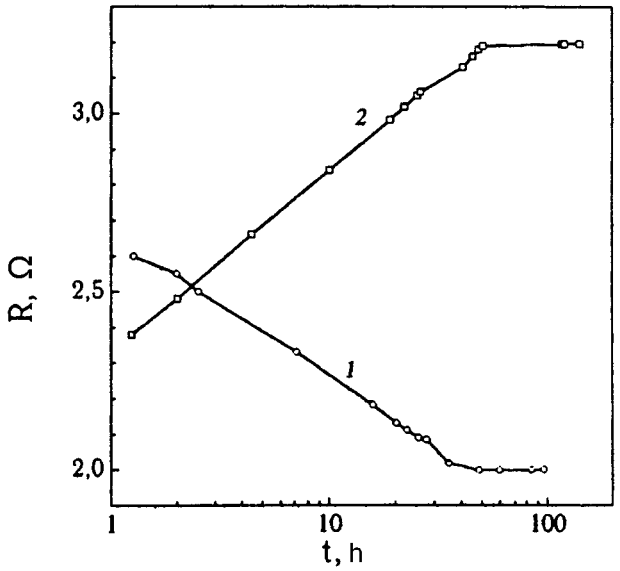

FIG. 3. Isothermal relaxation of resistance of the crystal $K3$ during application of pressure $P=4.2$ kbar (curve *1*) and removal of pressure $P=6.3$ kbar (curve *2*).

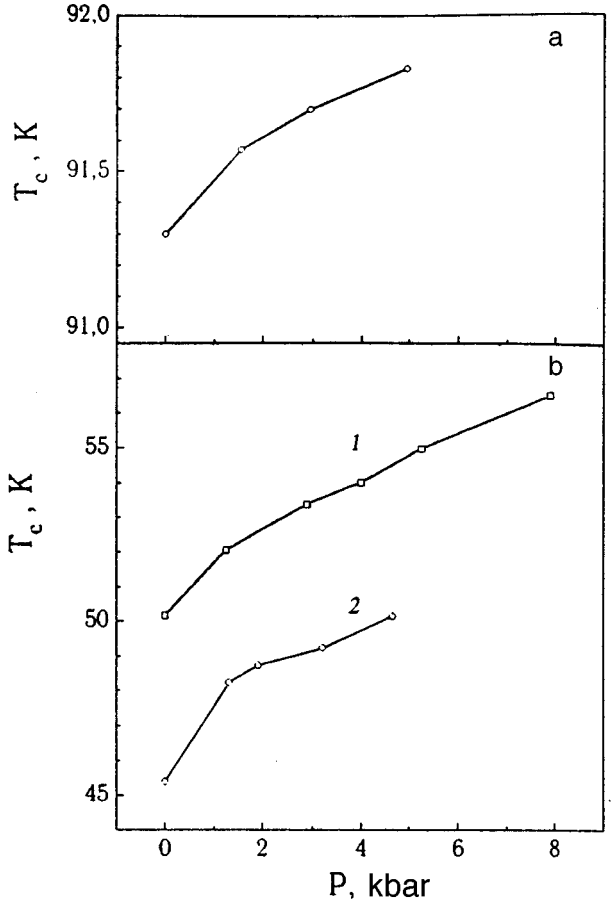

FIG. 4. Pressure dependence of the superconducting transition temperature of crystals $K1$ (a) , $K2$ (curve *1*) and $K3$ (curve *2*) (b).

6.3 kbar and the sample was held at room temperature for three days under this pressure. Test measurements show that the sample resistance after such a holding was 2 Ω, and did not change subsequently with time. The pressure was then reduced to the atmospheric value, and the time dependence of the resistance was measured at $T=293$ K. Curve *2* shows the results of these measurements. It can be seen that after the passage of 50 hours, the resistance attains its equilibrium value equal to the resistance value before the application of the pressure.

It can be seen from Fig. 3 that the time of relaxation of the resistance to the equilibrium value is about 50 hours at a temperature 293 K. It must be remarked that the relaxation of the resistance after the application (removal) of pressure was also observed at low temperatures. However, the relaxation rate decreases rapidly with temperature, and no variations in the resistance were observed at liquid nitrogen temperature for a period of seven days, which points towards the thermal activation mechanism of resistance relaxation.

The above peculiarities in the temperature and time dependences of resistance under hydrostatic pressure were also observed during investigations of crystals $K1$ and $K2$. The relative variations of the critical temperature and resistance for $K2$ and $K3$ crystals were nearly identical, while the variation for the crystal $K1$ was considerably smaller. By way of an example, Fig. 4 shows the dependence of the critical temperature on pressure.

The ordering of oxygen in Cu–O planes may be the most plausible reason behind the decrease in resistance with time under hydrostatic pressure. Such an assumption is supported by the thermal activation nature of the process of resistance relaxation. Moreover, the time of resistance relaxation to the equilibrium value at room temperature is approximately equal to the time of oxygen ordering in single crystals with oxygen deficiency $\delta\sim 0.5$.[8] Finally, neutron diffraction studies carried out during room-temperature annealing of samples quenched from high temperatures show that the ordering of oxygen in the Cu–O plane is accompanied by a decrease in the lattice parameters.[9] Thus, a higher degree of oxygen ordering corresponds to lower values of the lattice parameters. The reverse relation also seems to be logical, i.e., smaller values of the lattice parameters must correspond to a higher ordering in the oxygen–vacancy system. The modulus of hydrostatic compression of $YBa_2Cu_3O_{7-\delta}$ single crystals is estimated at 230 GPa.[10] Hence the application of a pressure of 2 kbar must lead to a decrease in the unit cell volume by 0.09 %. The application of a pressure of 2 kbar followed by the relaxation of resistance to its equilibrium value reduced the resistance of the samples $K2$ and $K3$ by about 15 %. Hence a decrease in the volume of a unit cell by 0.09% under a hydrostatic pressure of 2 kbar corresponds to a decrease in resistance by 15%. In the course of oxygen ordering in samples with an oxygen deficit $\delta\sim 0.6$, the lattice parameters c and a decrease by 0.04 % while the parameter b decrease by 0.004 %.[9] In other words, the decrease in the unit cell volume amounts to about 0.09 %. The decrease in the sample resistance in the course of oxygen ordering is about 20 %.[8] Thus, there is a satisfactory agreement between the decrease in the unit cell volume and the decrease in the sample resistance, which are associated with the oxygen ordering and the application of hydrostatic pressure. In the light of the above arguments, it can be stated that the de-

crease in resistance upon the application of hydrostatic pressure is associated with oxygen ordering in the Cu–O plane.

Magnetic,[11,12] resistive,[8] optical,[13,14] and structural[9] studies of monocrystalline and ceramic samples of $YBa_2Cu_3O_{7-\delta}$ with $\delta = 0.4$–0.6 cooled rapidly from temperatures 500– 650 °C show that the resistance and crystal lattice parameters decrease in the course of annealing at room temperature, while the superconducting transition temperature increases. These variations are associated with oxygen ordering in the Cu–O plane at room temperature. This raises the question about the basic reason underlying the decrease in the transition temperature. According to Widder *et al.*,[13,14] the increase in the transition temperature and the decrease in resistance are due to an increase in the carrier concentration which is attributed to a change in the oxygen environment of copper atoms in the Cu–O plane, i.e., to a change in the occupancy of the oxygen positions O(1) and O(5) which in turn causes a redistribution of charge between Cu–O planes and chains. On the other hand, neutron diffraction studies reveal[9] that annealing of samples at room temperature practically does not change the occupancy of the positions O(1) and O(5). This raises doubts about the validity of the assumption that the transition temperature and carrier concentration increase due to a redistribution of charge between the Cu–O planes and chains.

Another reason behind the increase in the value of T_c may be a decrease in the lattice parameters. It can be seen from Fig. 2 that the application or removal of a pressure of 4.2 kbar leads to a variation of about 10 % in the transition temperature and resistance if we do not take into consideration the thermally activated relaxation of resistance to its equilibrium value. After relaxation of the resistance to its equilibrium value following the application or removal of a pressure of 4.2 kbar, its value changes further by 20 %. The transition temperature does not change in this case, although the onset and termination of the superconducting transition are displaced by about 1 K. Thus the change in the transition temperature is determined mainly by a change in the applied pressure, and not by a redistribution of oxygen. This means that the value of T_c depends primarily on the crystal lattice parameters rather than the degree of oxygen ordering.

The correlation between the magnitudes of variation in the transition temperature and resistance associated with a change in the unit cell volume following the application or removal of pressure may suggest that the variation of these characteristics has the same origin. The resistance variation under pressure may be due to a change in the electron–phonon interaction constant and carrier concentration. In the latter case, it is presumed that the variation of T_c and resistance changes the density of states $N(E_F)$ at the Fermi level: an increase(decrease) in pressure causes an increase(decrease) in the value of $N(E_F)$.

It was mentioned above that relaxation of the resistance to the equilibrium value is followed by a variation in the width and shape of superconducting transitions. For example, it can be seen from Fig. 2 that, following the relaxation of resistance due to an increase in pressure, the step shape of the superconducting transition becomes more pronounced. The step on the resistive transition to the superconducting state in crystals with an oxygen deficit $\delta \sim 0.5$ indicates the existence in such crystals of at least two phases characterized by different concentrations of oxygen and different types of ordering in it, and hence having different transition temperatures.[8] Hence the most plausible reason behind the change in the width and shape of superconducting transitions is the redistribution of oxygen between these phases. For example, a part of oxygen from the phase with a lower transition temperature migrates to the phase with a higher T_c upon an increase in pressure, while the opposite redistribution occurs upon a decrease in pressure. The diffusion length $L_0 = (Dt)^{1/2}$ of oxygen at room temperature over one day is estimated at 30–300 Å.[9] This is comparable with the distance 50–400 Å[14,15] over which oxygen ordering occurs at room temperature in single crystals with $\delta \sim 0.5$.

It should also be observed that the absence of steps on resistive transitions of crystals $K1$ and $K2$ does not rule out the possibility of the existence of two or more phases having different transition temperatures. For example, the existence of percolation channels for current flow in the phase with the highest transition temperature means that a transition to the superconducting state of just this phase will be observed on the resistive transition. Hence it cannot be stated unequivocally from the available experimental data that the crystals $K1$ and $K2$ are single-phase structures.

It was mentioned above that the derivatives dT_c/dP and dR/dP are much smaller for the $K1$ single crystal than for crystals $K2$ and $K3$. For example, it can be seen from Fig. 4 that $dT_c/dP \sim 0.15$ K/kbar for the crystal $K1$ and $dT_c/dP \sim 0.85$ K/kbar for the crystals $K2$ and $K3$. The relatively weak effect of pressure on the transition temperature and conductivity of crystals with $\delta \leqslant 0.1$ may be explained by using the model based on the existence of a van Hove singularity in the electronic spectrum which is characteristic for a two-dimensional lattice with a strong coupling. For crystals with $T_c \sim 90$ K, the Fermi level lies in the valley between two density of states peaks, and the density of states $N(E_F)$ at the Fermi level depends significantly on the ratio $(a-b)/a$.[16,17] An increase in the value of this ratio increases the separation between the density of states peaks, and hence decreases the values of $N(E_F)$ and T_c. On the other hand, a decrease in this ratio brings the peaks closer, which leads to an increase in the values of $N(E_F)$ and T_c. Such a variation of T_c was indeed observed in the studies of the effect of uniaxial compression along **a** and **b** axes on the superconducting transition temperature of single crystals with $T_c \sim 90$ K[18]: the application of a load along the **a** axis increases the transition temperature, while the application of a load along the **b** axis decreases the transition temperature. The ratio $(a-b)/a$ changes weakly under hydrostatic pressure since it is determined only by the difference in the moduli of compression along the **a** and **b** axes. Hence the variation of the transition temperature under hydrostatic pressure is relatively small.

For crystals with $T_c \sim 60$ K, the Fermi level is displaced from the middle of the band, and lies on the side of the van Hove singularity. Hence, if the transition temperature is determined primarily by the number density of charge carriers,

the application of hydrostatic pressure must move the Fermi level towards the density of states peak.

The authors thank V. A. Shklovskii for a discussion of the results and for a number of helpful comments during the preparation of the manuscript.

This research was financed partially by the Ukrainian State Committee on Science and Technology under the project ''Term.''

*E-mail: mikhail.a.obolenski@univer.kharkov.ua

[1] I. V. Medvedeva, Yu. S. Versen'ev, and S. V. Mamaev, Fiz. Met. Metalloved. **64**, 820 (1987).
[2] Yu. F. Revenko and V. M. Svistunov, Fiz. Tverd. Tela (Leningrad) **31**, 310 (1989) [Sov. Phys. Solid State **31**, 2017 (1989)].
[3] I. V. Medvedeva and Yu. S. Versen'ev, Fiz. Met. Metalloved. **66**, 621 (1989).
[4] S. W. Tozer, J. L. Koston, and E. M. McCarron III, Phys. Rev. B **47**, 8089 (1993).
[5] V. N. Kachinsky, V. N. Kochetkov, I. N. Makarenko *et al.*, Physica C **247**, 347 (1995).
[6] M. A. Obolenskii, A. V. Bondarenko, and M. O. Zubareva, Fiz. Nizk. Temp. **15**, 1152 (1989) [Sov. J. Low Temp. Phys. **15**, 635 (1989)].
[7] E. S. Itskevich, Prib. Tekh. Eksp. No. 4, 148 (1963).
[8] M. A. Obolenskii, A. V. Bondarenko, R. V. Vovk, and A. A. Prodan, Fiz. Nizk. Temp. **23**, (1997) [to be published].
[9] D. Jorgensen, S. Pei, P. Lightfoot *et al.*, Physica C **167**, 571 (1990).
[10] M. Lei, J. L. Sarrao, W. M. Visscher *et al.*, Phys. Rev. B **47**, 6154 (1993).
[11] B. W. Veal, H. You, A. P. Paulikas *et al.*, Phys. Rev. B **42**, 4770 (1990).
[12] H. Claus, S. Yang, A. P. Paulikas *et al.*, Physica C **171**, 205 (1990).
[13] J. Kircher, M. Cardona, A. Zibold *et al.*, Phys. Rev. B **48**, 9684 (1993).
[14] K. Widder, A. Zibold, M. Merz *et al.*, Physica C **232**, 82 (1994).
[15] F. Heinmaa, H. Lutgemeier, S. Pecker *et al.*, Appl. Magn. Reson. **3**, 689 (1992).
[16] V. M. Gvozdikov, Fiz. Nizk. Temp. **19**, 1285 (1993) [Low Temp. Phys. **19**, 914 (1993)].
[17] V. M. Gvozdikov, Physica C **235–240**, 2127 (1994).
[18] U. Welp, M. Grimsditch, S. Flesher *et al.*, Phys. Rev. Lett. **69**, 2130 (1992).

Translated by R. S. Wadhwa

Nonlinear microwave properties of epitaxial HTS films

G. A. Melkov, V. Yu. Malyshev, and S. K. Korsak

Taras Shevchenko University, 252601 Kiev-33, Ukraine[*]
(Submitted February 27, 1997; revised April 18, 1997)
Fiz. Nizk. Temp. **23**, 1041–1045 (October 1997)

The surface resistance R_s of epitaxial HTS films of $YBa_2Cu_3O_{7-\delta}$ on sapphire is studied experimentally at a frequency of 8.95 GHz in the presence of an additional powerful microwave signal of frequency 9.4 GHz ensuring the ac magnetic field amplitude up to 20 Oe on the film. It is found that the surface resistance R_s of the HTS film increases with the amplitude of the additional signal. The value of R_s of the HTS film virtually coincides with the value of the nonlinear surface resistance of the film at the same amplitude of the ac magnetic field. In other words, the surface resistances of the film for a weak signal in the presence of an additional powerful signal and for the powerful signal alone are close. The observed phenomena are explained under the assumption that the HTS film is a Josephson medium containing various types of Josephson junctions. Under the influence of a powerful microwave signal, the properties of this medium can vary due to switching of a part of the junctions, causing a transition of the medium to a new state which is manifested identically both for a weak and for a powerful signal. [S1063-777X(97)00210-7]

INTRODUCTION

The most promising application of HTS films at present is the creation of a passive linear resonant structure in the microwave range.[1] The application of HTS films instead of copper analogs makes it possible to improve considerably both electric parameters (losses in the transmission band and steepness of fronts at the band edges), and mass and size parameters of instruments. However, an HTS-based device must satisfy a number of requirements, among which is the absence of noticeable nonlinear changes in parameters up to powers of a few watts, which corresponds to high microwave magnetic fields in resonant systems, which are of the order of tens and even hundreds of oersteds.[2] The situation is complicated even more by the fact that in actual practice an HTS film is subjected to the action of several signals with different frequencies and amplitudes. The nonlinearity problem can be solved successfully only if we know the physical reasons behind its emergence for the development of technological conditions for obtaining epitaxial HTS films with an extended linearity range and for creating devices whose construction would ensure the lowest values of maximum amplitudes of microwave magnetic fields and currents for a given power.[3]

In Ref. 4, a model of an epitaxial HTS film taking into account both linear and nonlinear properties was proposed. According to this model, an HTS film is an aggregate of series-connected regions with different physical parameters (Fig. 1). Some of these regions are perfect defect-free superconductors (regions I, III, and V in Fig. 1), while others (II and IV) contain various defects shunted by regions with ideal conductivity, like regions of a superconductor deoriented in the basal plane and surrounded by large-angle boundaries. Such boundaries form weak links of various types and make a decisive contribution to the surface resistance of epitaxial HTS films.[5] For this reason, an equivalent circuit diagram of a real superconducting film[4] must include elements corresponding to regions with ideal conductivity as well as elements responsible for various types of weak links shunted by a perfect superconductor which, as a rule, is a small inductive reactance. We assume that weak links formed in a natural way during deposition of an HTS film can be classified into two different types. The first-type links are formed at low-resistance *SNS* or bridge junctions, while second-type links are formed at high-resistance (e.g., tunnel) junctions. In the linear mode for small amplitudes of a microwave signal, the main contribution to the surface resistance of epitaxial HTS films comes from low-resistance junctions,[4] whose resistance is smaller than the inductive reactance of the regions of the perfect superconductor shunting them. According to the nonlinear resistive model of tunnel junctions,[6] an increase in the signal amplitude causes a transition of these junctions to a low-resistance state, which increases their contribution to the surface resistance; such a switching is responsible for nonlinear properties of real HTS films. The switching of junctions starts when the signal amplitude exceeds a certain threshold value for which the voltage across the junction shunted by the inductive reactance of a perfect superconductor attains the value of the gap voltage V_g.[6] Obviously, the voltage across the junction increases with the frequency for the same exciting currents in the film in view of the presence of the shunting inductance. This clarifies the regularity observed but not explained by Nguyen *et al.*[2]: nonlinearities are exhibited by epitaxial HTS films for signals with a higher frequency for smaller amplitudes of ac currents or smaller values of ac magnetic fields in the film corresponding to these currents.

Thus, the linear surface resistance in the model proposed in Ref. 4 is mainly due to the presence of low-resistance weak links, while nonlinear surface resistance is associated with switching of high-resistance links to the low-resistance state. However, the former statement should apparently be corrected in the case when two or more microwave signals are acting on the film if the amplitude of at least one signal is

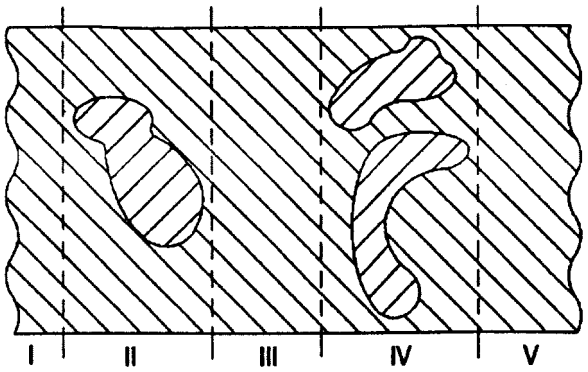

FIG. 1. A model of epitaxial HTS film.

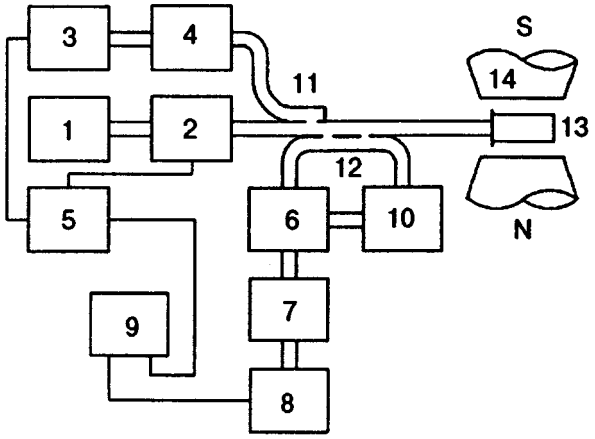

FIG. 2. Block diagram of experimental setup: low-power microwave generator (*1*), microwave modulator (*2*), magnetron generator (*3*), precision attenuator (*4*), low-frequency pulse modulator (*5*), waveguide switch (*6*), band transmission filter (*7*), running wave valve microwave amplifier and pulse detector (*8*), oscillograph (*9*), precision attenuator (*10*), directional divisor (*11*), two-directional divisor (*12*), measuring section in a magnetic field (*13*), and magnet (*14*).

sufficient for switching the junctions. In this case, some links are transformed to low- resistance state even for another (also weak) signal irrespective of its amplitude as a result of the action of a strong signal, and the effective surface resistance for the weak signal in the presence of the strong signal must increase.

This research aims at experimental investigation of the linear surface resistance of an epitaxial HTS film for a weak signal in the presence of a powerful additional microwave signal whose frequency and amplitude differ from those of the first signal. The obtained experimental dependences proved that the linear surface resistance increases indeed upon an increase in the amplitude of the additional signal; in this case, the linear surface resistance for the weak signal virtually coincides with the nonlinear surface resistance of the additional powerful signal.

EXPERIMENT

We studied the surface resistance of *C*-oriented HTS films of $YBa_2Cu_3O_{7-\delta}$ on sapphire, obtained by laser sputtering.[7] The film thickness varied from 0.1 and 0.15 μm, the critical current in the helium temperature range exceeded 10^7A/cm^2, the critical temperature T_c was of the order of 89 K, and the residual surface resistance varied from 100 to 500 $\mu\Omega$ for different films in the 3-cm wavelength range. According to Landerman *et al.*,[5] the volume fraction of large-angle boundaries in the films under investigation did not exceed 0.3–4%.

We determined the relative change in the surface resistance R_S of an HTS film in the presence of an additional signal of a finite amplitude h by using the method of open dielectric resonator (ODR)[4,8] consisting of measuring the Q-factor of an ODR with an HTS film pressed against one of its faces. The size of the rectangular resonator was chosen so as to ensure resonance simultaneously at the frequency ω_s at which the surface resistance is measured for a weak signal and at the frequency ω_l corresponding to an additional signal of large amplitude. W used the lowest magnetic type oscillations $H_{\delta 11}$ and $H_{1\delta 1}$ whose magnetic fields on the film were orthogonal to each other. The film with the ODR was placed at the middle of a standard 3-cm rectangular waveguide at the antinode of the ac magnetic field of the waveguide, which was tangential to the film surface. In our measurements, we used an ODR prepared from a thermostable ceramic with permittivity $\varepsilon \sim 80$, whose size was $3\times 2.6\times 3.5$ mm, which ensured resonance at frequencies $\omega_s/(2\pi)\sim 8.95$ GHz and $\omega_l/(2\pi)\sim 9.4$ GHz.

The block diagram of the experimental setup is shown in Fig. 2. The maximum amplitude of magnetic field of frequency ω_l at the HTS film attains a value of 20 Oe. All the measurements were made in a pulsed mode to avoid film overheating by the electromagnetic power. The pulse duration was 2 μs and the pulse repetition frequency was 50 Hz.

Figure 3 shows the relative change in the linear surface resistance $R_S(h)/R_S(0)-1$ of the HTS film at a frequency $\omega_s/(2\pi)=8.95$ GHz in the presence of an additional microwave signal of frequency $\omega_l/(2\pi)=9.4$ GHz as a function of the amplitude h of the microwave magnetic field of the additional signal. Here $R_S(h)$ and $R_S(0)$ are the linear sur-

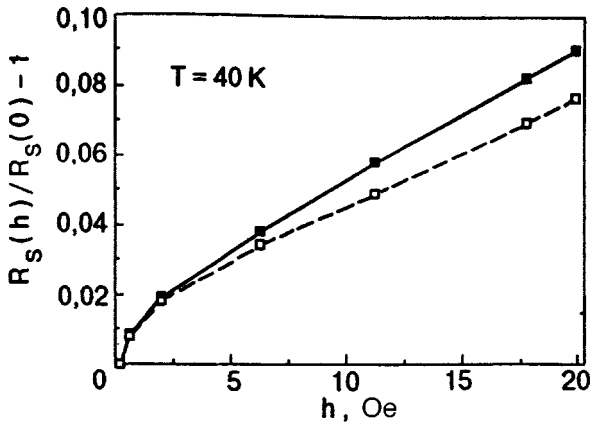

FIG. 3. Relative linear surface resistance of an epitaxial HTS film at a frequency 8.95 GHz as a function of the amplitude h of an additional powerful signal of frequency 9.4 GHz (■, solid curve); the dashed curve (□) shows for comparison the experimental dependence of the nonlinear surface resistance of the same HTS film for a signal of frequency 9.4 GHz on the amplitude of the signal.

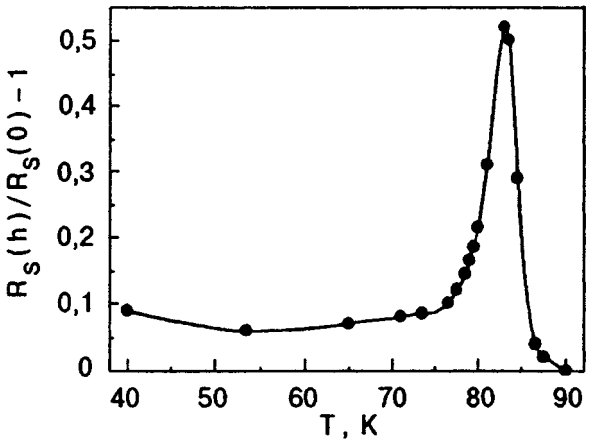

FIG. 4. Temperature dependence of the relative surface resistance of the same HTS film as in Fig. 3 for frequency 8.95 GHz in the presence of an additional signal of frequency 9.4 GHz with the microwave magnetic field amplitude $h=20$ Oe.

face resistances of the HTS film in the presence of an additional power signal of amplitude h and without it. The dashed curve in the same figure shows for comparison the experimental dependence of the relative change in the nonlinear surface resistance of the same HTS film for a signal of frequency 9.4 GHz as a function of the amplitude of this signal. It should be recalled that such dependences were studied in detail in Ref. 4. In our case, $R_S(h)$ is the surface resistance of the HTS film for the magnetic field amplitude equal to h, which is measured with the same signal (which played the role of the additional signal in basic measurements). It can be clearly seen from Fig. 3 that the linear surface resistance of the HTS film in the presence of an additional power microwave signal of amplitude h and the nonlinear surface resistance of the film for the same amplitude virtually coincide quantitatively; the qualitative type of the dependences on the ac magnetic field amplitude h is also the same. These results are in complete agreement with the model of epitaxial HTS film proposed in Ref. 4 and with the arguments presented at the beginning of this paper, according to which any real HTS film is in fact a Josephson medium. The properties of this medium depend on the state of weak links forming it, which are switched from one state to another by the measuring signal itself as well as with the help of an additional powerful signal. In the former case, we have a nonlinear surface resistance, while in the latter case we are dealing with an equivalent linear surface resistance independent of the amplitude of the measuring signal and determined by the amplitude of the additional signal.

Another proof of the correctness of the assumption made here and in Ref. 4 is the temperature dependence of the relative surface resistance of an epitaxial HTS film in the presence of an additional powerful signal, which is presented in Fig. 4. This dependence resembles in many respects the temperature dependences of the nonlinear surface resistance of epitaxial HTS films measured in Ref. 8. Our analysis of the effect of a constant magnetic field up to 4 kOe applied parallel as well as at right angles to the surface of an HTS film on the dependences shown in Figs. 3 and 4 also leads to similar conclusions. The effect of constant magnetic fields on the surface resistance of epitaxial HTS films in the presence of an additional signal turned out to be similar to the effect of these fields on the nonlinear impedance of HTS films, which was studied in Refs. 4 and 8.

In addition to the switching of Josephson weak junctions to a new state by an additional microwave signal described above, an attempt was made to carry out a similar switching with the help of a power videopulse. For this purpose, ohmic contacts required for the transmission of low-frequency current pulses were deposited on an HTS film. As in the case of microwave signals, the duration of pulses was 2 μs and the current amplitude was ~ 5 A, which ensured the magnetic field in the film of the order of 10 Oe. This value is close in order of magnitude to the parameters ensured by an additional powerful microwave signal. However, we did not observe any noticeable effect of the additional signal on linear microwave properties of films even when the low-frequency current parameters were close to the parameters of the maximum current produced by the additional microwave signal. This fact can also be explained by using the proposed model of the epitaxial HTS film. It was mentioned in the Introduction that the voltage across Josephson junctions is determined by shunting inductances and increases in proportion to the signal frequency. The frequency of spectral components of a videopulse of duration 2 μs is obviously much lower than the frequency of an additional microwave signal, which amounts to 9.4 GHz. This confirms the strong dependence of nonlinear properties of epitaxial HTS films on the signal frequency: the nonlinearity increases with the frequency of the signal.

CONCLUSION

It has been proven experimentally that the linear surface resistance of an epitaxial HTS film can be changed with the help of an additional powerful external microwave signal, which differs from the weak measuring signal in frequency and amplitude. It was found that the linear surface resistance for a weak signal in the presence of a strong signal as well as the nonlinear surface resistance for the latter signal are similar both quantitatively and qualitatively. This matching is preserved in the presence of constant magnetic fields also. The effect of an additional signal on the linear surface resistance depends on the frequency of the additional signal and was not observed for videopulses of duration 2 μs.

The reason behind the observed phenomena lies in the fact that an epitaxial film is a Josephson medium consisting of various Josephson junctions: *SNS*, bridge, tunnel junctions, etc. For small amplitudes of the microwave field, the surface resistance of the film is mainly determined by low-resistance (*SNS* and bridge) junctions. For large amplitudes, high-resistance junctions are switched to the low-resistance state and start to make a contribution to the surface resistance, which begins to increase as a result. This increase is virtually the same for a strong signal and for a weak signal in the presence of a powerful signal which is responsible for a transition of the Josephson medium to a new state in both cases. Such a transition is determined by the frequency of the powerful signal due to the shunting of Josephson junctions

by regions of an ideal superconductor. The potential drop across these regions depends on frequency: the higher the frequency, the easier the attainment of potentials required for the switching of tunnel junctions.

*E-mail: melkov@boy.rpd.univ.kiev.ua

[1] N. Newman and W. G. Lyons, J. Supercond. **6**, 119 (1993).
[2] P. P. Nguyen, D. E. Oates, G. Dresselhaus, and M. S. Dresselhaus, Phys. Rev. B **B43**, 6400 (1993).
[3] G. Liang, D. Zhang, C. Shih *et al.*, IEEE Trans. Appl. Supercond. **5**, 2656 (1995).
[4] G. A. Melkov, V. Yu. Malyshev, and A. V. Bagada, Fiz. Nizk. Temp. **21**, 1192 (1995) [Low Temp. Phys. **21**, 911 (1995)].
[5] S. S. Laderman, R. C. Taber, R. D. Jacowitz *et al.*, Phys. Rev. **43**, 2922 (1991).
[6] K. K. Likharev, *Introduction to Dynamics of Josephson Junctions* [in Russian], Nauka, Moscow (1985).
[7] O. D. Pustylnik, A. A. Dymnikov, I. V. Voinovsky *et al.*, Proc. SPIE–International Society for Optical Engineering, Vol. 2104, *Eighteenth Int. Conf. on Infrared and Millimeter Waves*, Colchester, UK (1993).
[8] G. A. Melkov, A. L. Kasatkin, and V. Yu. Malyshev, Fiz. Nizk. Temp. **20**, 868 (1994) [Low Temp. Phys. **20**, 680 (1994)].
[9] M. E. Il'chenko and E. V. Kudinov, *Ferrite Dielectric Microwave Resonators* [in Russian], Izd. KGU, Kiev (1973).
[10] E. L. Glinston, *Microwave Measurements*, McGraw Hill, New York (1957).

Translated by R. S. Wadhwa

Activation spin waves in the Landau theory of Fermi liquid

A. I. Akhiezer, N. V. Laskin, and S. V. Peletminskii

National Science Center ''Kharkov Physicotechnical Institute,'' 310108 Kharkov, Ukraine[*]

(Submitted April 10, 1997)
Fiz. Nizk. Temp. **23**, 1046–1053 (October 1997)

The activation spectra of collective oscillations with a quadratic energy–momentum relation are studied for magnetically ordered Fermi liquid. It is shown that the spectrum of activation spin waves depends considerably on the structure of the Landau interaction amplitude as a function of the angle between quasimomenta of fermions. The existence of activation spin waves is manifested in neutron and light scattering processes as well as in the transformation of waves in magnetically ordered media. © *1997 American Institute of Physics.* [S1063-777X(97)00310-1]

1. INTRODUCTION

The Landau theory of Fermi liquid is one of the widely used methods of self-consistent field.[1] The Landau Fermi liquid theory is successfully employed in analysis of thermodynamic and kinetic processes for systems of strongly interacting fermions such as a normal or superfluid Fermi liquid, electrons in metals, and nuclear matter.

Landau and Silin[1,2] were the first to study collective processes in a normal Fermi liquid, such as zero sound and spin zero sound, which are characterized by a linear energy– momentum relation. Later, Abrikosov and Dzyaloshinskii[3] applied the theory of Fermi liquid for studying spectra of oscillatory modes in a magnetically ordered Fermi liquid. These authors established the possibility of existence of oscillations with a quadratic energy–momentum relation, viz., spin waves in a magnetized Fermi liquid. It should be noted that, according to Silin,[2] a normal (disordered) Fermi liquid in a magnetic field is also characterized by a quadratic energy-momentum relation.

However, Abrikosov and Dzyaloshinskii[3] studied only one case of collective oscillations with a quadratic energy-momentum relation. In actual practice, the spectrum of spin waves in a magnetically ordered Fermi liquid is richer. This work is devoted to an analysis of this problem. It will be shown that along with the activationless spectrum of spin waves established in Ref. 3 on the basis of Fermi liquid theory, collective oscillations with an activation energy and a quadratic energy-momentum relation also exist, their activation energy being determined to a great extent by the structure of the Landau interaction amplitude as a function of the angle between quasimomenta of fermions. In the simplest case when the Landau amplitude is constant and independent of the angle between quasimomenta of fermions, an infinitely degenerate activation mode also exists along with the activationless mode.

The activation spectra should be taken into account in an analysis of neutron and light scattering processes as well as in the transformation of waves in magnetically ordered media.

2. SMALL OSCILLATIONS IN A MAGNETICALLY ORDERED FERMI LIQUID

Let us first recall the basic concept of the Landau theory of a Fermi liquid. The state of the Fermi liquid can be described by the one-particle density matrix $f_{\kappa,\kappa'}$, where $\kappa=\mathbf{p}$, i, $\mathbf{p}$ being the momentum of a quasiparticle (fermion) and i the quantum numbers associated with internal degrees of freedom of the fermion. The Landau theory describes a quantum liquid at low temperatures, whose energy spectrum is similar to the spectrum of an ideal Fermi gas (consisting of particles with a spin 1/2). The starting point of the theory is that the energy spectrum of the ideal gas is in one-to-one correspondence with the spectrum of interacting fermions. In other words, the role of particles forming the gas is played by elementary excitations (quasiparticles) whose number is equal to the number of particles and which obey the Fermi-Dirac statistics. It should be emphasized, however, that the total energy of the liquid in this case is not equal to the sum of the energies of quasiparticles, but is a certain functional $E(f)$ of the one-particle density matrix $f_{\kappa,\kappa'}$.

In view of the coincidence of the energy spectrum of the liquid and the ideal Fermi gas, we can describe the equilibrium properties of the Fermi liquid proceeding from the combinatorial definition of entropy

$$S=\operatorname*{Tr}_{(\kappa)}(f\ln f+(1-f)\ln f)), \tag{1}$$

where the trace is taken in the space of quantum numbers κ.

The equilibrium density matrix $f_{\kappa,\kappa'}$ corresponds to the maximum of the entropy S for a fixed energy $E(f)$ and a fixed spin $S_i/2$,

$$S_i=\operatorname*{Tr}_{(\kappa)}\sigma_i f, \tag{2}$$

where σ_i are the Pauli matrices. (We assume that the energy $E(f)$ is invariant to spin rotations.)

Instead of determining of the conditional maximum of entropy, we can find the unconditional minimum of the potential $\Omega(f,Y)$,

$$\Omega(f,Y)=-S(f)+Y_0E(f)+\sum_i Y_iS_i, \tag{3}$$

where Y_0 and Y_i are thermodynamic forces (Lagrangian multipliers) conjugate to the integrals of motion. Solving this problem, we arrive at the following nonlinear equation for determining the equilibrium density matrix:

$$f=\left\{\exp\left(Y_0\varepsilon(f)+\sum_i Y_iS_i\right)+1\right\}^{-1}, \tag{4}$$

where the self-consistent Hamiltonian $\varepsilon(f)$ of a quasiparticle is connected with the energy functional through the following relation:

$$\varepsilon(f)=\frac{\partial E(f)}{\partial f}. \tag{5}$$

Thus, assuming that the energy functional $E(f)$ is given, we can consider expressions (4) and (5) as a system of equations for determining the equilibrium properties of the Fermi liquid.

An analysis of nonequilibrium properties of a Fermi liquid is based on the time-dependent one-particle density matrix $f(t)$ whose evolution obeys a kinetic equation of the type

$$i\frac{\partial f(t)}{\partial t}=[\varepsilon(f),f] \tag{6}$$

if we disregard the collisions between quasiparticles.

Since the energy functional $E(f)$ is invariant to spin transformations, we have

$$E(UfU^+)=E(f), \quad U=\mathrm{e}^{ig_i\sigma_i} \tag{7}$$

(g_i are arbitrary real-valued parameters). By varying the latter relation in g_i, we obtain

$$\underset{\kappa}{\mathrm{Tr}}\ \sigma_i[\varepsilon(f),f]=0. \tag{8}$$

This equation together with the kinetic equation (6) lead to the law of conservation of the quantity S_i. It should also be noted that relations (7) together with definition (5) lead to the relation

$$U^+\varepsilon(UfU^+)U=\varepsilon(f).$$

For a specific choice of the functional $E(f)$, Eqs. (4) and (6) form a system of equations for an analysis of the oscillator modes in a Fermi liquid.

Going over from the description in terms of the one-particle density matrix f to the description in terms of the Wigner distribution function

$$f(\mathbf{x},\mathbf{p},t)=\frac{1}{V}\sum_{\mathbf{q}}\mathrm{e}^{i\mathbf{q}\cdot\mathbf{x}}f_{\mathbf{p}+\mathbf{q}/2,\mathbf{p}-\mathbf{q}/2}$$

(which is a function in the space of $\mathbf{x}$ and $\mathbf{p}$ and a matrix in indices σ), we obtain from (6) the following equation in the approximation of small gradients:

$$i\frac{\partial f(t)}{\partial t}=[\varepsilon(f),f]-\frac{i}{2}\left\{\frac{\partial\varepsilon(f)}{\partial\mathbf{p}},\frac{\partial f}{\partial\mathbf{x}}\right\}+\frac{i}{2}\left\{\frac{\partial\varepsilon(f)}{\partial\mathbf{x}},\frac{\partial f}{\partial\mathbf{p}}\right\}, \tag{9}$$

where [...,...] and {...,...} denote the commutator and anticommutator, respectively, in the ''spin space.'' [4]

Formula (5) and Eq. (9) form a closed self-consistent system of equations, which will form the basis for a analysis of small oscillations in a magnetically ordered Fermi liquid.

For solving equation (9), we choose for the equilibrium state the spin-ordered state, assuming that $Y_i=0$. This means that we are dealing with a second-order phase transition, while for $Y_i\neq 0$ the phase transition to the magnetically ordered state is a first-order phase transition.

According to (4), this state can be described by the density matrix

$$f(\hat{\varepsilon})=(\mathrm{e}^{Y_0\hat{\varepsilon}+Y}+1)^{-1}=\frac{1+\boldsymbol{\sigma}\cdot\mathbf{n}}{2}f_+ +\frac{1-\boldsymbol{\sigma}\cdot\mathbf{n}}{2}f_-, \tag{10}$$

where

$$f_\pm=(\mathrm{e}^{Y_0\varepsilon_\pm+Y}+1)^{-1}=f(\varepsilon_\pm), \tag{11}$$

$$\hat{\varepsilon}=\frac{1+\boldsymbol{\sigma}\cdot\mathbf{n}}{2}\varepsilon_+ +\frac{1-\boldsymbol{\sigma}\cdot\mathbf{n}}{2}\varepsilon_-. \tag{12}$$

In this case, Eq. (9) has a solution corresponding to oscillations of density and spin over the spin-ordered state. The one-particle density matrix $f(t)=\hat{f}$ describing such oscillations can be written in the form

$$\hat{f}=\frac{1+\boldsymbol{\sigma}\cdot\mathbf{n}}{2}\hat{f}_+ +\frac{1-\boldsymbol{\sigma}\cdot\mathbf{n}}{2}\hat{f}_-+\frac{1}{2}\boldsymbol{\sigma}\cdot\mathbf{f}, \quad \mathbf{n}\cdot\mathbf{f}=0. \tag{13}$$

It can be easily seen that the quantities $\hat{f}_\pm$ and $\mathbf{f}$ are connected with $\hat{f}$ through the relations

$$\hat{f}_\pm=\frac{1}{2}\mathrm{Tr}\ \hat{f}\pm\frac{1}{2}\mathrm{Tr}\ \hat{f}\sigma\mathbf{n}, \tag{14}$$

$$\mathbf{f}=\mathrm{Tr}\ \hat{f}\sigma-\mathbf{n}n_i\ \mathrm{Tr}\ \sigma_i\hat{f}. \tag{15}$$

In this case, the energy functional $E(\hat{f})$ has the form

$$E(\hat{f})=E_0(\hat{f})+E'(\hat{f}),$$

where $E_0(\hat{f})$ is the functional of the fermion kinetic energy:

$$E_0(\hat{f})=\sum_{\mathbf{p}}\varepsilon_{\mathbf{p}}\ \mathrm{Tr}\ \hat{f}=\sum_{\mathbf{p}}\varepsilon_{\mathbf{p}}(\hat{f}_+ +\hat{f}_-)$$

and $E'(\hat{f})$ is the functional of fermion interaction energy:

$$\begin{aligned}E'(\hat{f})=\frac{1}{2V}\sum_{\mathbf{p},\mathbf{p}'}\{&\mathrm{Tr}\ \hat{f}F(\mathbf{p},\mathbf{p}')\mathrm{Tr}\ \hat{f}'\\&+\mathrm{Tr}\ \sigma\hat{f}F_s(\mathbf{p},\mathbf{p}')\mathrm{Tr}\ \sigma\hat{f}'\}=\frac{1}{2V}\sum_{\mathbf{p},\mathbf{p}'}\{(\hat{f}_+\\&+\hat{f}_-)F(\mathbf{p},\mathbf{p}')(\hat{f}'_+ +\hat{f}'_-)+(\hat{f}_+-\hat{f}_-)F_s(\mathbf{p},\mathbf{p}')\\&\times(\hat{f}'_+-\hat{f}'_-)+\mathbf{f}F_s(\mathbf{p},\mathbf{p}')\mathbf{f}'\}.\end{aligned} \tag{16}$$

This allows us to write the Hamiltonian of a quasiparticle in the form

$$\hat{\varepsilon}=\frac{1+\boldsymbol{\sigma}\cdot\mathbf{n}}{2}\varepsilon_+ +\frac{1-\boldsymbol{\sigma}\cdot\mathbf{n}}{2}\varepsilon_-+\frac{1}{2}\sigma\varepsilon, \quad \mathbf{n}\varepsilon=0, \tag{17}$$

where

$$\varepsilon_+ = \frac{\partial E(\hat{f})}{\partial \hat{f}_+} = \varepsilon_{\mathbf{p}} + \frac{1}{V}\sum_{\mathbf{p}'} \{F(\mathbf{p},\mathbf{p}')(\hat{f}'_+ + \hat{f}'_-) + F_S(\mathbf{p},\mathbf{p}') \times (\hat{f}'_+ - f'_-)\},$$

$$\varepsilon_- = \frac{\partial E(\hat{f})}{\partial \hat{f}_-} = \varepsilon_{\mathbf{p}} + \frac{1}{V}\sum_{\mathbf{p}'} \{F(\mathbf{p},\mathbf{p}')(\hat{f}'_+ + \hat{f}'_-) - F_s(\mathbf{p},\mathbf{p}') \times (\hat{f}'_+ - \hat{f}'_-)\}, \quad (18)$$

$$\frac{1}{2}\,\varepsilon = \frac{1}{V}\sum_{\mathbf{p}'} F_s(\mathbf{p},\mathbf{p}')\mathbf{f}'. \quad (19)$$

Since $\hat{f}_\pm = f_\pm$, $\mathbf{f}=0$ in statistical equilibrium, formulas (18) and (10) form a closed system of equations for determining the equilibrium density matrix $f(\hat{\varepsilon})$.

Putting $f(t)=f+\hat{g}$ in Eq. (9) and linearizing in $\hat{g}$ (f is the equilibrium density matrix (10) and $\hat{g}\sim e^{-i\omega t+i\mathbf{k}\cdot\mathbf{r}}$ is the small deviation from equilibrium), we obtain

$$-i\omega g + i[\hat{\varepsilon},\hat{g}] + i[\delta\hat{\varepsilon},f] + \frac{i}{2}\left\{\mathbf{k}\,\frac{\partial\varepsilon(f)}{\partial\mathbf{p}},\hat{g}\right\} - \frac{i}{2}\left\{\delta\hat{\varepsilon},\mathbf{k}\,\frac{\partial f}{\partial\mathbf{p}}\right\} = 0, \quad (20)$$

where

$$\delta\hat{\varepsilon} = \frac{1+\boldsymbol{\sigma}\cdot\mathbf{n}}{2}\,\delta\varepsilon_+ + \frac{1-\boldsymbol{\sigma}\cdot\mathbf{n}}{2}\,\delta\varepsilon_- + \frac{1}{2}\,\boldsymbol{\sigma}\cdot\delta\boldsymbol{\varepsilon}, \quad (21)$$

and the quantities $\delta\varepsilon_+$, $\delta\varepsilon_-$, and $\delta\boldsymbol{\varepsilon}$ are defined by the formulas

$$\delta\varepsilon_+ = \frac{1}{V}\sum_{\mathbf{p}'} \{F(\mathbf{p},\mathbf{p}')(g'_+ + g'_-) + F_s(\mathbf{p},\mathbf{p}')(g'_+ - g'_-)\}, \quad (22)$$

$$\delta\varepsilon_- = \frac{1}{V}\sum_{\mathbf{p}'} \{F(\mathbf{p},\mathbf{p}')(g'_+ + g'_-) - F_s(\mathbf{p},\mathbf{p}')(g'_+ - g'_-)\}, \quad (23)$$

$$\frac{1}{2}\,\delta\varepsilon = \frac{1}{V}\sum_{\mathbf{p}'} F_s(\mathbf{p},\mathbf{p}')\mathbf{g}', \quad (24)$$

where

$$\hat{g} = \frac{1+\boldsymbol{\sigma}\cdot\mathbf{n}}{2}\,g_+ + \frac{1-\boldsymbol{\sigma}\cdot\mathbf{n}}{2}\,g_- + \frac{1}{2}\,\boldsymbol{\sigma}\cdot\mathbf{g}, \quad \mathbf{n}\cdot\mathbf{g}=0. \quad (25)$$

The system of equations (20)–(25) will serve as the basis for finding the oscillatory spectra of density and spin density over the spin-ordered state of the Fermi liquid. It should be noted that (see below) Eqs. (20)–(25) in the absence of magnetic ordering [$f_+=f_-$, see (11)] describe acoustic oscillations of a normal Fermi liquid. In a magnetically ordered Fermi liquid, additional transverse oscillations branches (spin waves) appear along with longitudinal branches. Note that one of transverse branches is activationless (Goldstone's theorem).

The system of equations (20)–(25) has two classes of solutions, viz., longitudinal oscillations) (spin oscillates along the direction $\mathbf{n}$) for which $\mathbf{g}=0$, $g_+\neq 0$, $g_-\neq 0$ and transverse oscillations (spin oscillates in a plane orthogonal to the direction $\mathbf{n}$) for which $\mathbf{g}\neq 0$, $\mathbf{n}\cdot\mathbf{g}=0$, $g_+=g_-=0$.

Before analyzing transverse modes, let us find out how longitudinal modes are modified in the case of magnetic ordering. For this purpose, we note that Eq. (9) has a solution for which $\mathbf{g}=0$ (longitudinal oscillations) and $\delta\boldsymbol{\varepsilon}=0$, while $g_\pm$ satisfies the equations

$$(\omega - \mathbf{k}\cdot\mathbf{v})g_\pm - \mathbf{k}\,\frac{\partial f}{\partial\mathbf{p}}\,\delta\varepsilon_\pm = 0, \quad (26)$$

$\delta\varepsilon_\pm$ being connected with $g_\pm$ through formulas (22) and (23), which will be presented in the form

$$\delta\varepsilon_\pm = \frac{1}{V}\sum_{\mathbf{p}'} \{F_\pm(\mathbf{p},\mathbf{p}')g'_+ + F_\mp(\mathbf{p},\mathbf{p}')g'_-\}, \quad F_\pm(\mathbf{p},\mathbf{p}') = F(\mathbf{p},\mathbf{p}') \pm F_s(\mathbf{p},\mathbf{p}'). \quad (27)$$

Oscillations described by Eq. (26) will be referred to as longitudinal relative to the direction of magnetization $\mathbf{n}$.

Noting that $\partial f_\pm/\partial\mathbf{p} = \mathbf{v}_\pm(\partial f_\pm/\partial\varepsilon_\pm)$ ($\mathbf{v}_\pm = \mathbf{n}v_\pm$), and introducing the notation

$$K_\pm(s_\pm) = \int d^3p\,\frac{\cos\vartheta}{s_\pm - \cos\vartheta}\,\frac{\partial f_\pm}{\partial\varepsilon_\pm}, \quad s_\pm = \frac{\omega}{kv_\pm},$$

we arrive at the dispersion equation in the case when the amplitudes $F_\pm$ are constant quantities independent of momenta:

$$1 + (K_+ + K_-)F_+ + K_+K_-(F_+^2 - F_-^2) = 0 \quad (28)$$

or

$$1 + (K_+ + K_-)(F + F_s) + 4K_+K_-FF_s = 0. \quad (29)$$

In the absence of magnetic ordering, when $s_+=s_-=s$, $K_+(s)=K_-(s)=K(s)$, these equations split into the two equations

$$K(s) = -\frac{1}{2F}, \quad K(s) = -\frac{1}{2F_s} \quad (30)$$

in accordance with the results of the Landau theory.[1] The first dispersion equation corresponds to acoustic oscillations of density, while the second corresponds to oscillations of spin density.

3. ACTIVATION SPIN WAVES

Let us now go over to the description of oscillations transverse relative to the direction of magnetization $\mathbf{n}$, for which $g_+=g_-=0$, and hence $\delta\varepsilon_+=\delta\varepsilon_-=0$. In this case, we have $g=\frac{1}{2}\sigma\cdot\mathbf{g}$, $\mathbf{n}\cdot\mathbf{g}=0$, $\delta\varepsilon=\sigma\delta\varepsilon$, $\mathbf{n}\delta\varepsilon=0$. Since

$$[\hat{g},\hat{b}] = i(b_+ - b_-)[\mathbf{g},\mathbf{n}]\sigma, \quad \{\hat{g},\hat{b}\} = (b_+ + b_-)\mathbf{g}\cdot\boldsymbol{\sigma},$$

where the matrix $\hat{b}$ has the form

$$\hat{b} = \frac{1+\mathbf{n}\cdot\boldsymbol{\sigma}}{2}\,b_+ + \frac{1-\mathbf{n}\cdot\boldsymbol{\sigma}}{2}\,b_-,$$

we can write the kinetic equation (20) in the form

$$\left(\omega-\frac{1}{2}\,\mathbf{k}\cdot(\mathbf{v}_+ +\mathbf{v}_-)\right)\mathbf{g}+i(\varepsilon_+-\varepsilon_-)[\mathbf{g}\cdot\mathbf{n}]-i(f_+-f_-)$$
$$\times[\delta\varepsilon,\mathbf{n}]+\frac{1}{2}\,\mathbf{k}\left(\frac{\partial f_+}{\partial\mathbf{p}}+\frac{\partial f_-}{\partial\mathbf{p}}\right)\delta\varepsilon=0. \tag{31}$$

Equations (26) and (31) form a complete system of equations for finding the spectra of oscillatory modes for a magnetized Fermi liquid. Let us show how this system is transformed in the absence of magnetic ordering. Equations (26) are transformed into the following two equations:

$$(\omega-\mathbf{k}\cdot\mathbf{v})g-\mathbf{k}\,\frac{\partial f}{\partial\mathbf{p}}\,\delta\varepsilon=0,$$
$$(\omega-\mathbf{k}\cdot\mathbf{v})g-\mathbf{k}\,\frac{\partial f}{\partial\mathbf{p}}\,\delta\varepsilon_s=0, \tag{32}$$

where

$$\delta\varepsilon=\frac{2}{V}\sum_{\mathbf{p}'}F(\mathbf{p},\mathbf{p}')g(\mathbf{p}'),$$
$$\delta\varepsilon_s=\frac{2}{V}\sum_{\mathbf{p}'}F_s(\mathbf{p},\mathbf{p}')g(\mathbf{p}').$$

The first equation from (32) describes oscillations of density of a Fermi liquid (zeroth sound), while the second equation is one of the three equations describing triply degenerate acoustic oscillations of spin density. Two other equations for spin oscillations (and having the same form as the second equation from (32)) can be obtained in the limit of zero magnetization from Eqs. (31).

Thus, we have proved that Eqs. (26) and (31) describe acoustic and spin-acoustic oscillations for a normal Fermi liquid in the absence of magnetic ordering [$f_+=f_-$, see (11)].

Let us return to Eq. (31). Going over in this equation to the circular components of the vectors **g** and $\delta\boldsymbol{\varepsilon}$ relative to the vector **n** (z-axis),

$$g_{(\pm)}=g_1\pm ig_2,\quad \delta\varepsilon_{(\pm)}=\delta\varepsilon_1\pm i\delta\varepsilon_2$$

and noting that $[\mathbf{g},\mathbf{n}]_{(\pm)}=\mp ig_{(\pm)}$, we transform Eq. (31) to

$$\left(\omega-\frac{1}{2}\,\mathbf{k}\cdot(\mathbf{v}_+ +\mathbf{v}_-)\right)g_{(\pm)}\pm(\varepsilon_+-\varepsilon_-)g_{(\pm)}\mp(f_+$$
$$-f_-)\,\delta\varepsilon_{(\pm)}+\frac{1}{2}\,\mathbf{k}\left(\frac{\partial f_+}{\partial\mathbf{p}}+\frac{\partial f_-}{\partial\mathbf{p}}\right)\delta\varepsilon_{(\pm)}=0, \tag{33}$$

where

$$\delta\varepsilon_{(\pm)}=\frac{2}{V}\sum_{\mathbf{p}'}F_s(\mathbf{p},\mathbf{p}')g'_{(\pm)}\equiv 2\int d\tau' F_s(\mathbf{p},\mathbf{p}')g'_{(\pm)}, \tag{34}$$

and in statistic equilibrium state we have, according to (18),

$$\varepsilon_+-\varepsilon_-=2\int d\tau' F_s(\mathbf{p},\mathbf{p}')(f'_+-f'_-). \tag{35}$$

Obviously, the solution $g_{(\pm)}$ can be obtained from the solution $g_{(-)}\equiv g$ by changing the signs of the frequency ω and the wave vector **k**.

Let us first analyze the solution of Eq. (33) in the case when the spin amplitude F_s does not depend on $\mathbf{p},\mathbf{p}'$. In this case, for $T\ll\mu$ ($\mu=-Y/Y_0$ is the chemical potential of the Fermi system), Eq. (33) assumes the form

$$(\omega-\mathbf{ku})g+2\beta g+2(f_+-f_-)F_s q-F_s q(\mathbf{kv}_+\,\delta(\varepsilon_+$$
$$-\mu)+\mathbf{kv}_-\,\delta(\varepsilon_--\mu))=0, \tag{36}$$

where

$$\beta=-F_s\int d\tau(f_+-f_-),$$
$$q=\int d\tau' g(\mathbf{p}'),\quad \mathbf{u}=\frac{1}{2}\,(\mathbf{v}_+-\mathbf{v}_-). \tag{37}$$

This equation shows that for $q\neq 0$ the following dispersion equation holds:

$$1/F_s=\int\frac{d\tau}{\omega-\mathbf{ku}+2\beta}\,(\mathbf{kv}_+\,\delta(\varepsilon_+-\mu)+\mathbf{kv}_-\,\delta(\varepsilon_--\mu)$$
$$-2(f_+-f_-)), \tag{38}$$

whose solution for small values of k has the form[1]

$$\omega=\frac{\int d\tau u^2\{(f_+-f_-)-\beta(\,\delta(\varepsilon_+-\mu)+\delta(\varepsilon_--\mu)\}}{6\beta\int d\tau(f_+-f_-)}\,k^2. \tag{39}$$

(We have used relation (37) in this case.) In addition to this solution, for $\mathbf{k}=0$ we have an infinitely degenerate activation solution $\omega=-2\beta$, $q=0$.

Solution (38) corresponds to Goldstone spin waves emerging due to spontaneous symmetry breaking.

In the range of large values of k (and large ω), Eq. (38) assumes the form

$$\frac{1}{F_s}=\int\frac{d\tau}{\omega-\mathbf{k}\cdot\mathbf{u}}\,[\mathbf{v}_+\,\delta(\varepsilon_+-\mu)+\mathbf{v}_-\,\delta(\varepsilon_--\mu)]\mathbf{k} \tag{40}$$

and its solution corresponds to the spin sound $\omega=sk$ transverse relative to **k** in a magnetically ordered state.

In the weak magnetism approximation (or near the transition temperature), solution (39) assumes the form

$$\omega=k^2\,\frac{2v_F^2}{3\alpha_F}, \tag{41}$$

where the quantity α_F is connected with magnetization through the relation

$$\alpha_F\nu_F=-2\int d\tau\ \mathrm{Tr}\ f\sigma\mathbf{n},$$
$$\nu_F=2\int d\tau\,\delta[\varepsilon(\mathbf{p})-\mu]. \tag{42}$$

Equation (40) is transformed in the case of weak magnetism to the ordinary equation for spin sound [see (30)].

Let us now analyze Eq. (33) in the case when the Landau amplitude $F_s(\mathbf{p},\mathbf{p}')$ is a function of the angle between **p** and $\mathbf{p}'$. We will use the weak magnetism approximation, i.e., assume that $f_+-f_-=(\partial f_0/\partial\varepsilon)(\varepsilon_+-\varepsilon_-)$. In addition, as-

suming that the wave vector $\mathbf{k}$ is small, we neglect the difference between ε_+ and ε_- is the corresponding terms in Eq. (33), which assumes as a result the form

$$(\omega-\mathbf{k}\cdot\mathbf{v})g-(\varepsilon_+-\varepsilon_-)g+\frac{\partial f_0}{\partial\varepsilon}(\varepsilon_+-\varepsilon_-)\delta\varepsilon_-$$

$$+\mathbf{k}\cdot\mathbf{v}\frac{\partial f_0}{\partial\varepsilon}\delta\varepsilon_-=0.$$

Noting that

$$\delta\varepsilon_-=2\int d\tau' F_s(\mathbf{p},\mathbf{p}')d(\mathbf{p}')$$

in accordance with (34) and using (35) for $T\ll\mu$, i.e.,

$$1=2\int d\tau' F_s(\mathbf{p},\mathbf{p}')\delta(\varepsilon-\mu)$$

(this equation defines the chemical potential μ for $T=0$), we obtain

$$(\omega-\mathbf{kv})g-(\varepsilon_+-\varepsilon_-)2\int d\tau' F_s(\mathbf{p},\mathbf{p}')\delta(\varepsilon'-\mu)g(\mathbf{p}')$$

$$-(\varepsilon_+-\varepsilon_-)\delta(\varepsilon-\mu)2\int d\tau' F_s(\mathbf{p},\mathbf{p}')g(\mathbf{p}')$$

$$-\mathbf{kv}\delta(\varepsilon-\mu)2\int d\tau' F_s(\mathbf{p},\mathbf{p}')g(\mathbf{p}')=0.$$

It follows hence that the solution of this equation should be sought in the form

$$g(\mathbf{p})=\frac{\partial f_0}{\partial\varepsilon}g(\cos\vartheta),$$

(ϑ is the angle between the momentum vector $\mathbf{p}$ of a particle and the wave vector $\mathbf{k}$). The quantity $g(\cos\vartheta)$ in this case satisfies the equation

$$(\omega-\mathbf{kv})g(\cos\vartheta)-\alpha_F g(\cos\vartheta)\frac{\nu_F}{4\pi}\int do' F_s(\cos\theta)$$

$$+\alpha_F\frac{\nu_F}{4\pi}\int do' F_s(\cos\theta)g(\cos\vartheta')$$

$$+\mathbf{kv}\frac{\nu_F}{4\pi}\int do' F_s(\cos\theta)g(\cos\vartheta')=0, \qquad (43)$$

where θ is the angle between the vectors $\mathbf{p}$ and $\mathbf{p}'$, and notation (42) is used.

We expand $g(\cos\vartheta)$ and $\nu_F F_s(\cos\theta)\equiv B(\cos\theta)$ into power series in the Legendre polynomials:

$$g(\cos\vartheta)=\sum_{l=0}^{\infty} g_l P_l(\cos\vartheta),$$

$$B(\cos\theta)=\sum_{l=0}^{\infty} B_l P_l(\cos\theta), \qquad (44)$$

where g_l and B_l are expansion coefficients.

Taking into account the summation rule

$$P_l(\cos\theta)=P_l(\cos\vartheta)P_l(\cos\vartheta')$$

$$+\sum_{m=1}^{l}\frac{2(l-m)!}{(l+m)!}P_l^m(\cos\vartheta)$$

$$\times P_l^m(\cos\vartheta')\cos m(\varphi-\varphi'),$$

as well as the orthogonality condition for Legendre polynomials

$$\int do P_l(\cos\vartheta)P_{l'}(\cos\vartheta)=\frac{4\pi}{2l+1}\delta_{ll'},$$

we obtain

$$\int do' B(\cos\theta)=4\pi B_0,$$

$$\int do' B(\cos\theta)g(\cos\vartheta')=4\pi\sum_{l=0}^{\infty}\frac{B_l g_l}{2l+1}P_l(\cos\vartheta). \qquad (45)$$

Substituting (44) and (45) into Eq. (41) and taking into account the fact that Legendre polynomials satisfy the relation

$$xP_l(x)=\frac{l+1}{2l+1}P_{l+1}(x)+\frac{l}{2l+1}P_{l-1}(x),$$

we can write Eq. (43) in the form

$$(\omega-\omega_l)g_l=a_l g_{l-1}+b_l g_{l+1}, \qquad (46)$$

where the following notation has been introduced:

$$\omega_l=\alpha_F\left(B_0-\frac{B_l}{2l+1}\right), \qquad (47)$$

$$a_l=\mathbf{k}\cdot\mathbf{v}\frac{l}{2l-1}\left(1-\frac{B_{l-1}}{2l-1}\right), \qquad (48)$$

$$b_l=\mathbf{k}\cdot\mathbf{v}\frac{l+1}{2l+3}\left(1-\frac{B_{l+1}}{2l+3}\right). \qquad (49)$$

Expression (47) defines the frequencies of transverse oscillations for $\mathbf{k}=0$. It can be seen that the mode with $l=0$ is activationless ($\omega_0=0$), while the frequencies ω_l for $l=1,2,\ldots$ differ from zero. It should be noted that, if the spin Fermi amplitude is independent of $\mathbf{p}$ and $\mathbf{p}'$, expression (47) assumes the form

$$\omega_l=\alpha_F B_0(1-\delta_{l,0}). \qquad (50)$$

Obviously, in this case we have for $k=0$ and infinitely degenerate activation mode

$$\omega_l=\alpha_F B_0, \quad l=1,2,\ldots. \qquad (51)$$

Degeneracy is removed by taking into account the dependence of the Landau spin Fermi amplitude on the angle θ between $\mathbf{p}$ and $\mathbf{p}'$.

We can seek the solution of Eq. (46) in the form of a power series in $|\mathbf{k}|$ (it should be recalled that according to (48) and (49), $a_l\sim|\mathbf{k}|$ and $b_l\sim|\mathbf{k}|$):

$$\omega=\omega^{(0)}+\omega^{(1)}+\omega^{(2)}+\ldots.$$

$$g_l=g_l^{(0)}+g_l^{(2)}+g_l^{(3)}+\ldots.$$

Let us fix a certain nonnegative integer r. For the solution of Eq. (46) in the zeroth approximation, we have in this case

$$\omega^{(0)}=\omega_r, \quad g_l^{(0)}=g_r^{(0)}\delta_{r,l}.$$

Taking this into account, we can write the equation for determining the first approximation in the form

$$\omega_r^{(1)}g_l^{(0)}+\omega_r g_l^{(1)}-\omega_l g_l^{(1)}=a_l g_{l-1}^{(0)}+b_l g_{l+1}^{(0)}.$$

Putting $l=r$, we obtain $\omega_r^{(1)}=0$, while for $l\neq r$ we have

$$g_l^{(1)}=g_r^{(0)}\,\frac{a_l\delta_{l-1,r}+b_l\delta_{l+1,r}}{\omega_r-\omega_l}. \tag{52}$$

It follows hence that the spectrum of transverse oscillations in a magnetically ordered Fermi liquid does not contain terms that are linear in $|\mathbf{k}|$.

In the second approximation in the perturbation theory in the wave vector $\mathbf{k}$, Eq. (46) assumes the form

$$\omega_r^{(2)}g_l^{(0)}+\omega_r g_l^{(2)}-\omega_l g_l^{(2)}=a_l g_{l-1}^{(1)}+b_l g_{l+1}^{(1)}$$

for $l=r$, this equation can be written in the form

$$\omega_r^{(2)}g_r^{(0)}=a_r g_{r-1}^{(1)}+b_r g_{r+1}^{(1)}.$$

Noting that, according to (52),

$$g_{r-1}^{(1)}=g_r^{(0)}\,\frac{b_{r-1}}{\omega_r-\omega_{r-1}}, \quad g_{r+1}^{(1)}=g_r^{(0)}\,\frac{a_{r+1}}{\omega_r-\omega_{r+1}},$$

we obtain

$$\omega=\omega_r+\frac{a_r b_{r-1}}{\omega_r-\omega_{r-1}}+\frac{a_{r+1}b_r}{\omega_r-\omega_{r+1}}+\ldots, \tag{53}$$

where a_r and b_r are defined by formulas (48) and (49) respectively.

Expression (53) is valid for $r=1, 2, 3,\ldots$. However, it follows from the derivation of this equation that for $r=0$ we have the formula

$$\omega=-\frac{a_1 b_0}{\omega_1}, \tag{54}$$

according to which $\omega\sim k^2$. Consequently, for $r=0$ we arrive at an activationless spectrum of spin waves, which was established in Ref. 3 on the basis of the Fermi liquid model. The oscillatory branch (54) is a Goldstone branch emerging in the case of spontaneous symmetry breaking in statistical equilibrium, which is associated with the emergence of magnetization. If $F_s=\text{const}$, the spectrum (54) is defined by the formula

$$\omega=\frac{2(kv_F)^2}{3\alpha_F}, \quad B_0=-1,$$

which coincides with formula (41) as expected.

The activation frequency (53) in the spectrum is determined by the value of ω_r. For $F_s=\text{const}$, the activation frequency $\omega_r=\alpha_F B_0$ [see (51)] is the same for all values of r (see above). For this reason, formulas (53) for $r=1, 2, 3,\ldots$ become invalid if $F_s=\text{const}$. In order to find the range of applicability of these formulas, we assume that $B_r\sim B_{r-1}$. In this case, $\omega_r-\omega_{r-1}\sim\alpha_F B_r$, $\omega_r\sim\alpha_F$, $a_l\sim b_l\sim kv_F(1+B_r)$. Consequently, the condition for the applicability of formulas (53) has the form

$$(1+B_r)^2(kv_F)^2\ll\alpha_F^2|B_r|.$$

If the amplitude F_s is close to a constant, $|B_r|\ll 1$, and this condition can be written in the form

$$(kv_F)^2\ll\alpha_F^2|B_r|.$$

It can be seen that formulas (53) become applicable only for anomalously small k.

The authors are grateful to INTAS for supporting this research (grant No. 94-3941). Thanks are also due to the International Soros Program Supporting Education in Science (ISSEP).

*E-mail: nlaskin@kipt.kharkov.ua

[1)]Note that the second term in the numerator of a similar formula (17) in Ref. 3 contains incorrect coefficient.

[1] L. D. Landau, Zh. Éksp. Teor. Fiz. **30**, 1058 (1956) [Sov. Phys. JETP **3**, 920 (1956)].
[2] V. P. Silin, Zh. Éksp. Teor. Fiz. **35**, 1243 (1958) [Sov. Phys. JETP **8**, 870 (1958)].
[3] A. A. Abrikosov and I. E. Dzyaloshinskii, Zh. Éksp. Teor. Fiz. **35**, 771 (1958) [Sov. Phys. JETP **8**, 535 (1958)].
[4] A. I. Akhiezer, V. G. Bar'yakhtar, and S. V. Peletminskii, *Spin Waves*, North-Holland Publ. Co., Amsterdam (1968).

Translated by R. S. Wadhwa

Electron density of states and spin fluctuations in weak itinerant magnets

A. A. Povzner, A. G. Volkov, and P. V. Bayankin

*Ural State Technical University, 620002 Ekaterinburg, Russia**
(Submitted September 30, 1996; revised May 5, 1997)
Fiz. Nizk. Temp. **23**, 1054–1059 (October 1997)

The influence of zero-point and thermal spin fluctuations on the electronic structure and magnetic properties of weak itinerant magnets is considered. The possibility of considerable complex reconstruction of electron state density in fluctuating exchange and charge fields is demonstrated for $Fe_{1-x}Co_xSi$. The temperature dependence of paramagnetic susceptibility is in agreement with experimental data obtained for $Fe_{1-x}Co_xSi$. © *1997 American Institute of Physics.* [S1063-777X(97)00410-6]

1. Weak itinerant magnets include a group of compounds of transition metals characterized by anomalously small values of the Curie and Néel temperatures ($T_c \sim 10$ K) and magnetization in the ground state ($m_0(0)=0.1\mu_B$, where μ_B is Bohr's magneton). This group of substances contains weak itinerant ferromagnets ($ZrZn_2$, Ni_3Al, etc.)[1] as well as helimagnets (e.g., MnSi and $Fe_{1-x}Co_xSi$)[1,2] with small magnitudes of wave vectors ($q_0 \sim 10^{-2}$–10^{-3} Å^{-1}),[2,3] which become weakly ferromagnetic in comparatively weak applied magnetic fields ($h_0 > h_{0,c}, h_{0,c} \sim 10$ kOe). In addition to thermal spin fluctuations (with an amplitude $\langle m\rangle_T = \langle m^2\rangle_T^{1/2} \propto T^{2/3}$),[1] weak itinerant magnets are characterized by another important and insufficiently studied peculiarity, viz., zero-point spin fluctuations whose amplitude $\langle m\rangle_0 = \langle m^2\rangle_0^{1/2}$ depends weakly on temperature and can become comparable to or even larger than the amplitude of magnetization in the ground state $m_0(0)$.[4–6] The results of experiments on inelastic scattering of neutrons in MnSi can serve as an experimental evidence of realization of such a possibility.[7]

In this publication, an approach to the theory of a weak itinerant magnetism is developed, which describes the influence of thermal and zero-point spin fluctuations on the electron density of states for weak itinerant magnets. An analysis of this effect as well as estimates of the spin fluctuation amplitudes were made for $Fe_{1-x}Co_xSi$ alloys in which the renormalization of the electron density of states is significant according to experimental results on magnetic, magnetoelastic, and bulk characteristics.[8–12]

2. We shall analyze the influence of thermal and zero-point spin fluctuations on the electron density of states of weak itinerant magnets by using the Hubbard model in which intraatomic repulsion of electrons at a lattice site is taken into account in addition to their motion in the band (see, for example, Ref. 1). The Hamiltonian of the electron system can be written in the form

$$H = H_0 + \sum_{\mathbf{q}} I N_{\mathbf{q},\sigma} N_{\mathbf{q},-\sigma} - h_0 S_0^{(z)}, \tag{1}$$

where

$$H_0 = \sum_{\mathbf{k},\sigma=\pm 1/2} \varepsilon_{\mathbf{k}} a^+_{\mathbf{k},\sigma} a_{\mathbf{k},\sigma}, \tag{2}$$

$\varepsilon_{\mathbf{k}}$ is the energy of band motion of electrons, $a^+_{\mathbf{k},\sigma}(a_{\mathbf{k},\sigma})$ is the creation (annihilation) operator for electrons in a state with the quasimomentum $\mathbf{k}$ and spin $\sigma = \pm 1/2$, I the electron–electron spin and charge interaction parameter,

$$N_{\mathbf{q},\sigma} = \sum_{\mathbf{k}} a^+_{\mathbf{k},\sigma} a_{\mathbf{k}+\mathbf{q},\sigma} \tag{3}$$

the operator of the Fourier transform of the electron density with the wave vector $\mathbf{q}$ and spin σ, $\mathbf{S_q}$ the vector of the spin density operator,

$$S^z_{\mathbf{q}} = \sum_{\sigma} \sigma N_{\mathbf{q},\sigma}, \quad S^{\pm}_{\mathbf{q}} = \sum_{\mathbf{k}} a^+_{\mathbf{k},\sigma} a_{\mathbf{k}+\mathbf{q},-\sigma} \delta_{\sigma,\pm 1/2}$$

are its longitudinal (parallel to the Z-axis) and circular components, and h_0 the strength of a magnetic field directed along the Z-axis.

In Ref. 5, this model was used for a self-consistent calculation of the electron thermodynamic potential. The formalism of the Stratonovich–Hubbard functional transformations, which reduce the model under investigation to an analysis of motion of electrons in fluctuating exchange (ξ) and charge (η) fields, was developed. Here we shall apply the formalism developed in Ref. 5 for calculating the Matsubara one-electron Green's function,[13] which is directly connected with the electron density of states:

$$G_{\mathbf{k},\sigma} = \frac{1}{T} \langle T_\tau a^+_{\mathbf{k},\sigma} a_{\mathbf{k},\sigma} \sigma(1/T)\rangle_0, \tag{4}$$

where T_τ is the operator of ordering over the imaginary time τ, $k=(\mathbf{k},\omega_{2n+1})$, $\omega_{2n+1}=(2n+1)T$ is the Fermi-Matsubara frequency (n is an integer), $\sigma(1/T)$ the scattering matrix, T the temperature in energy units, and $\langle \ldots\rangle_0$ the quantum-statistical mean with the Hamiltonian H_0.

In order to calculate (5), we introduce the generating functional

$$\Omega(\lambda_{\mathbf{k},\sigma}) = \Omega_0 - T \ln\left\langle \exp\left(-\left[H - H_0 + \sum_{\mathbf{k},\sigma} \lambda_{\mathbf{k},\sigma} a^+_{\mathbf{k},\sigma} a_{\mathbf{k},\sigma} \right] \Big/ T \right) \right\rangle_0 \tag{5}$$

(Ω_0 is the thermodynamic potential of noninteracting electrons) and write the required Green's function in the form

$$G_{\mathbf{k},\sigma}=\lim_{\lambda_{\mathbf{k},\sigma}\to 0}\partial\Omega(\lambda_{\mathbf{k},\sigma})/\partial\lambda_{\mathbf{k},\sigma}. \tag{6}$$

Expressing now (5) in terms of functional integrals with respect to ξ and η variables, we obtain for $\Omega(\lambda_{\mathbf{k},\sigma})$ an expression which differs from that obtained in Ref. 5 for thermodynamic potential in the substitution $\varepsilon_{\mathbf{k}}\to\varepsilon_{\mathbf{k}}+\lambda_{\mathbf{k},\sigma}$. Applying the saddle point method in the variables $m_q^{\gamma}=|\xi_q^{\gamma}|$ and η_q $(q=(\mathbf{q},\omega_{2n})$, where $\omega_{2n}=2nT$ in the Bose-Matsubara frequency,[13]) for estimating $\Omega(\lambda_{\mathbf{k},\sigma})$ and using (6), we obtain the electron Green's function

$$G_{\mathbf{k},\sigma}=\frac{1}{2N_0}\sum_{\nu,\sigma'=\pm 1}\int\prod_{q,\gamma}\frac{d\Theta_{q,\gamma}}{2\pi}(i\omega_{2n+1}-\varepsilon_{\mathbf{k}}-\sigma'\xi_{\nu})^{-1}\left(1+2\sigma\sigma'\frac{\xi_{\nu}^{z}}{\xi_{\nu}}\right). \tag{7}$$

Here

$$\sum_{\nu}(\ldots)=\frac{T}{N_0}\sum_{\nu}\int_0^{1/T}(\ldots)d\tau;\quad \nu=(\nu,\tau);$$

ξ_{ν} is the magnitude of fluctuating exchange field at the site ν in the representation of the imaginary time τ, ξ_{ν}^{γ} the component of the exchange field vector along the axis $\gamma(\gamma=x,y,x)$, $\Theta_{q,\gamma}=\arg\xi_q^{\gamma}$, ξ_q^{γ} is the Fourier transform of ξ_{ν}^{γ} in the variables ν and τ (see Ref. 5), and N_0 the number of crystal lattice sites occupied by d-atoms.

Continuing expression (7) analytically to the real axis $(i\omega_{2n+1}\to\omega+i\theta)$ and going over to two-time temperature Green's functions,[14] we obtain the following expressions for the electron density of states and the amplitude of spin fluctuations:

$$g_{\sigma}(\varepsilon,\xi,m_0)=\frac{1}{2}\sum_{\sigma'=\pm 1}g(\varepsilon+\sigma'\xi)[1+(2\sigma\sigma' m_0/m_L)\times(1+\langle m^2\rangle)/3m_L^2], \tag{8}$$

$$\langle m^2\rangle=\frac{T}{I}\sum_{q,\gamma}m_q^{\gamma}=\frac{1}{I\pi N_0}\sum_{\mathbf{q},\gamma}\int_0^{\infty}\left[f_B(\omega/T)+\frac{1}{2}\right]\times\mathrm{Im}\{D^{-1}(\xi)+X(\mathbf{q},\omega)\}^{-1}d\omega, \tag{9}$$

where $g(\varepsilon)$ is the density of states for noninteracting electrons (i.e., for $I=0$), $\xi=Im_L$; $m_L^2=m_0^2+\langle m^2\rangle$, $m_0(T)$ is the uniform magnetization, $\langle m^2\rangle=\langle m^2\rangle_0+\langle m^2\rangle_T$ the square of spin fluctuation amplitude, $\langle m^2\rangle_0$ corresponding to the term with the coefficient 1/2 in (9), while $\langle m^2\rangle_T$ corresponds to the term with the Bose–Einstein function $(f_B(\omega/T))$,

$$D(\xi)^{-1}=1-\frac{I}{3}\chi^{\parallel}(\chi)-\frac{2I}{3}\chi^{\perp}(\xi), \tag{10}$$

$$\chi^{\parallel}(\xi)=2g(\mu+\xi)g(\mu-\xi)\Big/\sum_{\sigma=\pm 1}g(\mu+\sigma\xi),$$

$$\chi^{\perp}=\sum_{\sigma=\pm 1}(\sigma/2\xi)\int g(\varepsilon+\sigma\xi)f(\varepsilon-\mu)d\varepsilon,$$

$$X_{q,\omega}=I\chi_0^0-I\chi_{q,\omega}^0=[a\mathbf{q}^2-(iIb\omega/v_F|\mathbf{q}|)\theta(\omega-v_F|\mathbf{q}|)]\theta(\mathbf{q}-\mathbf{q}_c), \tag{11}$$

$f(\varepsilon-\mu)$ is the Fermi–Dirac function, $\chi_{q,\omega}^0$ the Pauli nonuniform susceptibility, v_F the velocity of the Fermi surface, a and b are the parameters that can be determined from neutron diffraction experiments or from direct band calculations, and $\mathbf{q}_c$ is the cutoff vector.

The obtained relations (8)–(10) not only describe the effect of spin fluctuations on the electron density of states, but also contain the renormalized density of states $g_{\sigma}(\varepsilon,\xi,m_0)$ in the expressions for their amplitudes, or its component $g(\varepsilon+\sigma'\xi)$. In the paramagnetic case and for $h_0=0$, we have

$$g(\varepsilon,\xi,m_0=0)=\frac{1}{2}\sum_{\sigma'=\pm 1}g(\varepsilon+\sigma'\xi).$$

Using formula (8), we can find equations of the magnetic state and electroneutrality equations renormalized by spin fluctuations:

$$m_0=\sum_{\sigma=\pm 1/2}\sigma\int g_{\sigma}(\varepsilon,\xi,m_0)f(\varepsilon-\mu)d\varepsilon, \tag{12}$$

$$N=\sum_{\sigma=\pm 1/2}\int g_{\sigma}(\varepsilon,\xi,m_0)f(\varepsilon-\mu)d\varepsilon, \tag{13}$$

where N is the number of d-electrons.

Differentiating magnetization with respect to external magnetic field, we obtain the expression for uniform paramagnetic susceptibility,

$$\chi=\partial m_0/\partial h_0|_{h_0=0}=2(1-D^{-1}(\xi))I^{-1}D(\xi), \tag{14}$$

according to which $D(\xi)$ is a factor of exchange enhancement of magnetic susceptibility, and $\chi^{\parallel}$ and $\chi^{\perp}$ correspond to the longitudinal and transverse Pauli susceptibility renormalized by spin fluctuations.

It should be noted that the derived expressions (10) and (14) differ from those obtained earlier[1,15] in that it takes into account not only transverse, but also longitudinal spin and charge fluctuations (associated with a change in the magnitude of exchange field at a lattice site). This combined influence of three types of fluctuation of electron density ensures, along with change in the number of states in subbands corresponding to different spin directions, leads to the emergence of the term $\chi^{\parallel}$ and the weight factor 2.3 in the transverse component of nonenhanced susceptibility in formula (10). In the case when either $(\mu+\xi)$ or $(\mu-\xi)$ is beyond the d-band or a narrow peak on the $g(\varepsilon)$ curve, the system of d-electrons acquires temperature-induced local magnetic moments. As in Refs. 1, 15, local moments are induced at $T>T^*$ such that

$$T^*=(Ib)^{-1}\left[\mu^*-\frac{2}{3}IN^*\right]\Big/[1+(a/2)],$$

where μ^* is the chemical potential counted from the lower (for $N>5N_0$) or upper (for $N<5N_0$) edge of the d-band and is determined from the electroneutrality condition (13) at $T=T^*$, $\xi=\xi(T^*)$, $m_0=0$, and $2N^*$ is the number of vacant $(N>5N_0)$ or occupied $(N<5N_0)$ states in the initial $(I=0)$ five-fold degenerate d-band. The expression for the characteristic temperature T^* in this case virtually coincides with

that given in Ref. 15 (to within the substitution $I \to 2I/3$). Calculating the amplitude of zero-point and thermal spin fluctuations in accordance with (9), we find that the amplitude of zero-point fluctuations decreases with increasing temperature, while the amplitude of thermal fluctuation increases with it. The decrease in the amplitude of zero-point fluctuations of spin density in approximation (11) is described by the relation

$$\langle m^2 \rangle_0 = (3/\pi Ib)[1-(aD(\xi))^{-2}] \times \{1+\ln(1+b\varepsilon_F(D(\xi)^{-1}+a)^{-1}\}, \quad (15)$$

the amplitude vanishing for $D(\xi)^{-1} \geqslant a$. The amplitude of thermal spin fluctuations for $T<T^*$ and $D(\xi)^{-1} \leqslant a$ is calculated by the formula

$$\langle m^2 \rangle_T = (T/T_0)^{4/3}, \quad (16)$$

while in the temperature range $T>T^*$ and for $D(\xi)^{-1} \geqslant a$ it satisfies the relation

$$\langle m^2 \rangle_T = (bT)^2 D^{-1}(\xi)[D^{-1}(\xi)+a]^{-1}, \quad (17)$$

where

$$T_0 = a 3^{5/8} 2^{2/3} [b\Gamma\{4/3\}\zeta(4/3)\}]^{-3/4} I^{1/4},$$

$\Gamma(x)$ and $\zeta(x)$ being the gamma and zeta functions. It can be seen that the temperature T^* of formation of temperature-induced local magnetic moments can coincide approximately with the temperature of vanishing of zero-point spin fluctuations. This is confirmed by an analysis of the properties of weak itinerant magnets and strong paramagnets at $T>T^*$, which was carried out in Refs. 8, 10, 12, 15, 16.

3. A quantitative analysis of the effect of spin fluctuations on the electron density of states and paramagnetic susceptibility of weak itinerant magnets will be carried out for alloys in which temperature-induced local magnetic moments were studied earlier.[10,12,16] We shall estimate the amplitudes of zero-point spin fluctuations on the basis of Eqs. (11) and (12) by using the experimental data on the magnetization of the weakly ferromagnetic states of these alloys,[1)] induced by an applied magnetic field. We use the $g(\varepsilon)$ curve shown in Fig. 1a and the parameter $I=0.76$ eV (see Ref. 12). The values of $\langle m \rangle_0$ obtained in this way are given in Table I. The same table contains the results of experiments[3,16] and of earlier calculations[12,16] of other magnetic and spin-fluctuation parameters of the alloys under investigation. It was found that the calculation of the value of $\langle m \rangle_0$ by formula (15) involves the replacements of the frequency spectrum parameters b corresponding to thermal spin fluctuations by the quantities b' whose values are also given in Table I.

In the quantitative analysis, we must also take into account the effect of concentration fluctuations associated by the substitution of Si atoms for d-atoms and vice versa on the magnetic properties. For this purpose, it is sufficient to carry out the following substitution in the formulas containing the enhancement factor:[18]

$$D^{-1}(\xi) \to D^{-1}(\xi)[1+\Delta p^2 D(\xi)],$$

where the parameter $\Delta p^2 = 1/N_0 \Sigma (p_\nu - p)^2$; p_ν is the probability of occupation of a given lattice site by d-metal atoms, and p is the mean value of p_ν.

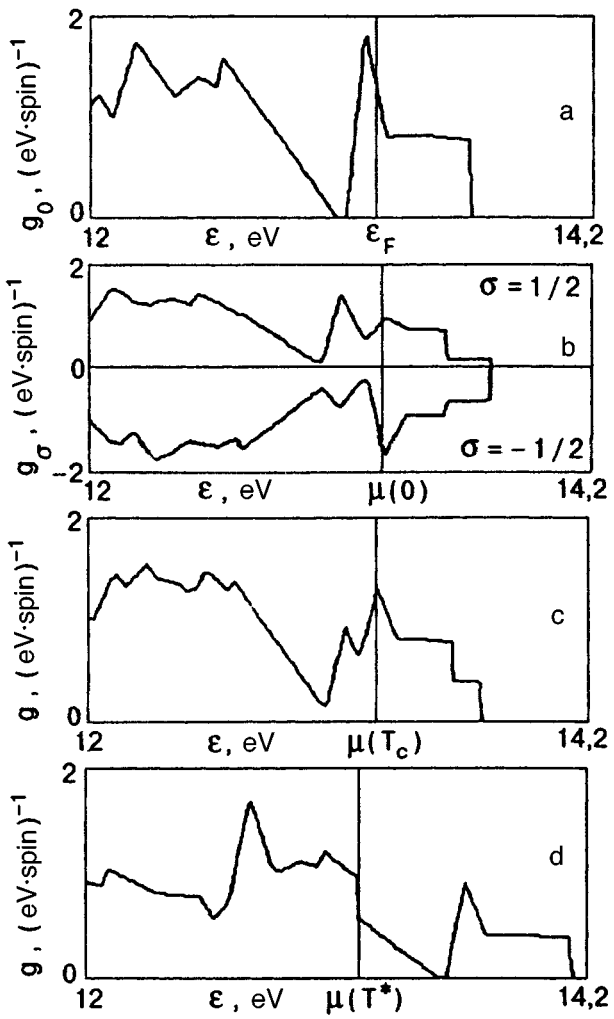

FIG. 1. Electron density of states as a function of energy and temperature: the model curve plotted according to the results obtained in Ref. 12 for electron density of states for $Fe_{1-x}Co_xSi$, which is not renormalized by exchange fields (the value of the Fermi energy is indicated for $x=0.3$) (a), for $Fe_{0.7}Co_{0.3}Si$ in subbands with different directions of spin at $T=0$ K and ferromagnetic ordering (b), for $Fe_{0.7}Co_{0.3}Si$ in subbands at $T=T_C$ (c) and T^* (d) (without degeneracy in spin).

Following Ref. 18, we estimate the value of Δp^2 for $Fe_{1-x}Co_xSi$ alloys from the experimentally obtained dependences of magnetization on the applied magnetic field.[3] It was found that the effect of concentration fluctuations on the magnetic and electronic properties of the samples under investigation can be neglected since $\Delta p^2 \sim 10^{-2}$.

TABLE I. Experimental[3,12,16,17] and theoretical magnetic and spin-fluctuation parameters for $Fe_{1-x}Co_xSi$ alloys.

x	$\frac{m_0}{2\mu_B}$	ε_F, eV	T_c, K	$\frac{\langle m \rangle_0}{2\mu_B}$	T^*, K	$a \times 10^2$	Ib	Ib'
0.10	0.050	13.220	15.0	0.000	650	3.0	5.55	0.00
0.30	0.075	13.294	44.0	0.106	350	3.6	4.80	9.80
0.40	0.100	13.324	39.0	0.439	275	4.0	4.60	2.38
0.50	0.085	13.356	34.0	0.536	200	4.4	4.40	1.95
0.60	0.050	13.391	4.8	0.049	150	4.0	1.14	21.36

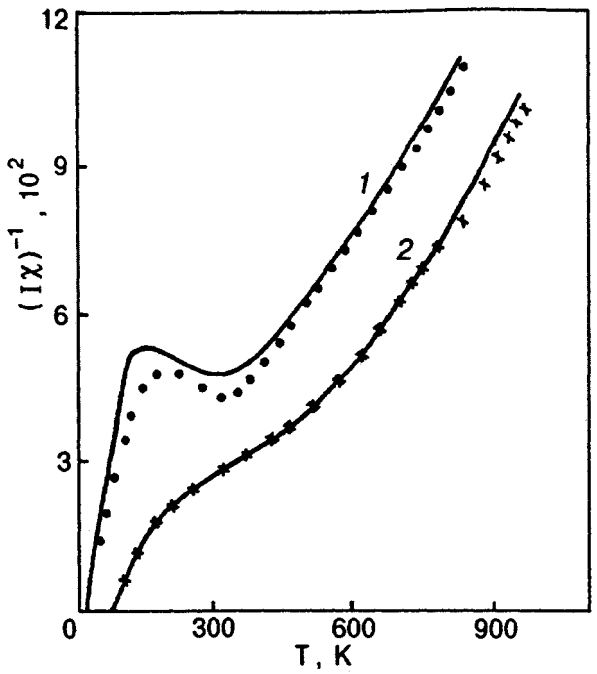

FIG. 2. Temperature dependences of the paramagnetic susceptibility of $Fe_{0.9}Co_{0.1}Si$ (curve *1*) and $Fe_{0.7}Co_{0.3}Si$ (curve *2*) alloys. Solid curves correspond to the results of theoretical calculations, ● and × are experimental data.[16,17]

Figures 1b–d show the energy dependences of the electron density of states calculated by formula (8) taking into account the data on the function $g(\varepsilon)$,[14] as well as the values of $\langle m\rangle_0$, m_0 and $\langle m\rangle_T$ for several characteristic temperatures. It can be seen that the renormalization of the electron density of states due to magnetization and zero-point spin fluctuations leads to redistributions of the number of electronic states between the subbands separated by the gap and to the emergence of a peak on the dependence $g(\varepsilon,\xi,m_0)$ near the energy gap even near the absolute zero temperature. As the temperature increases to values close to T_c, the $g(\varepsilon,\xi,m_0)$ curve changes insignificantly, while in the paramagnetic temperature range it changes more strongly, which is especially noticeable at $T>T^*(\langle m\rangle_0=0)$. Also, it should be borne in mind that spin-fluctuation renormalization of electron band results in an additional displacement of the chemical potential of the alloys $Fe_{1-x}Co_xSi$ to the left of $\mu(0)$ [$\mu(0)=\varepsilon_F+0.033$ eV for $x=0.3$, ε_F being the Fermi energy].

The pattern of electron band transformation for weak itinerant magnets $Fe_{1-x}Co_xSi$ associated with thermal and zero-point spin fluctuations is also confirmed by the agreement between the calculated temperature dependence of paramagnetic susceptibility and the experimental data (Fig. 2). The effect of fluctuation-induced renormalization of the chemical potential, as well as of zero-point spin fluctuations on the formation of the dependence $\chi(T)$ for $T<T^*$ is especially significant. At relatively high temperatures $T>T^*$, the fine-structure singularities of the electron density of states become insignificant, while $\langle m\rangle_0$ and $\chi^{\|}$ vanish. In this case, the results of calculations of $\chi(T)$ in the model curve for electron states[12] (see Fig. 1a) for $T>T^*$ are in accord with the data obtained in Ref. 16 on the basis of a rougher approach[15] based on a slightly different model of $g(\varepsilon)$ (obtained as a result of the substitution $I\to 2/3$).[2)]

Thus, spin fluctuations lead to a considerable renormalization of the electron density of states and chemical potential of weak itinerant magnets, which should be taken into account not only in the description of their magnetic properties, but also while estimating the amplitude of spin fluctuations themselves. The spin-fluctuation reconstruction of the electron band determines the amplitudes of zero-point spin fluctuations, which are the smaller, the closer the Fermi level to the left or right edge of the upper subband $g(\varepsilon,0,0)$ (see Table I). For $T>T^*$, the amplitudes become equal to zero, which is accompanied by the formation of temperature-induced local magnetic moments.

We believe that the effects of spin-fluctuation renormalization of $g(\varepsilon)$ may be especially significant for studying the low-temperature singularities of bulk magnetic, thermal, and thermoelectric phenomena in weak itinerant magnets.

This research was partly financed by a grant from the Competition Center for Fundamental Natural Sciences, Russian Ministry of Public and Professional Education (project No. 95-0-7.2-165).

*E-mail: pav@alfa.e-burg.ru

1) Note that the critical field of formation of a weakly ferromagnetic state in weak itinerant helimagnets tends to zero as $T\to T_c$.

2) The model curve $g(\varepsilon)$ used in Ref. 16 was not confirmed by direct band calculations.

[1] T. Moriya, *Spin Fluctuations in Itinerant Electron Magnetism*, Springer Verlag, Heidelberg (1985).
[2] J. Beille, J. Voiron, and M. Roth, Solid State Commun. **47**, 399 (1983).
[3] S. V. Kortov, A. A. Povzner, L. F. Romasheva, and P. V. Geld, Izv. Vuzov. Fizika **2**, 93 (1990).
[4] A. Z. Solontsov, Fiz. Met. Metalloved. **75**, 5 (1993).
[5] A. A. Povzner, Fiz. Nik. Temp. **19**, 1282 (1993) [Low Temp. Phys. **19**, 911 (1993)].
[6] A. Z. Solontsov and D. Wagner, J. Magn. Magn. Mater. **140**, 199 (1995)].
[7] K. R. A. Ziebek, H. Capellman, and P. J. Brown, Z. Phys. B **48**, 241 (1982).
[8] P. V. Geld, A. A. Povzner, and D. V. Likhachev, Dokl. Akad. Nauk SSSR **315**, 86 (1990) [Sov. Phys. Dokl. **35**, 942 (1990)].
[9] P. V. Geld, A. A. Povzner, and A. A. Timofeeva, Dokl. Akad. Nauk SSSR **299**, 1120 (1988) [Sov. Phys. Dokl. **33**, 275 (1988)].
[10] A. A. Povzner, S. K. Kortov, and P. V. Gel'd, Phys. Status Solidi A **114**, 315 (1993).
[11] A. S. Panfilov, I. V. Svechkarev, and L. F. Romasheva, Fiz. Nizk. Temp. **19**, 284 (1993) [Low Temp. Phys. **19**, 200 (1993)].
[12] L. I. Vinokuriva, A. V. Vlasov, and E. T. Kilatov, Trudy IOFAN **32**, 26 (1992)].
[13] A. A. Abrikosov, L. P. Gor'kov, and I. E. Dzyaloshinskii, *Methods of Quantum Field Theory in Statistical Physics*, Prentice Hall, Englewood Cliffs, NJ (1963).
[14] A. G. Tyablikov, *Methods of Quantum Theory of Magnetism* [in Russian], Nauka, Moscow (1975).
[15] A. A. Povzner and A. G. Volkov, Fiz. Met. Metalloved. **66**, 1073 (1988).
[16] P. V. Geld, A. A. Povzner, S. V. Kortov, and L. F. Romasheva, Izv. Vuzov. Fizika **4**, 18 (1988).
[17] S. V. Kortov, Ph.D. thesis, Sverdlovsk (1987).
[18] A. A. Povzner and A. G. Volkov, Metallofizika **13**, 32 (1991).

Translated by R. S. Wadhwa

Hydrodynamic asymptote of Green's functions of a weakly anisotropic multisublattice magnet

A. A. Isayev

National Science Center ''Kharkov Physicotechnical Institute,'' 310108 Kharkov Ukraine[*]
(Submitted February 21, 1997)
Fiz. Nizk. Temp. **23**, 1060–1066 (October 1997)

The hydrodynamic asymptote of Green's functions is determined for weakly anisotropic multisublattice magnets whose reduced description parameters are the total spin density and the matrix of rotation in the spin space. Spectra of spin waves are obtained and the number of Goldstone and activation modes is determined. © *1997 American Institute of Physics.* [S1063-777X(97)00510-0]

1. INTRODUCTION. DYNAMIC EQUATIONS IN AN EXTERNAL FIELD

The method of two-time Green's temperature functions has been widely used for determining the spectra of collective oscillations and kinetic coefficients, and also for obtaining the system response to an external field.[1,2] In the present work, we shall obtain the hydrodynamic asymptotes of Green's functions of a weakly anisotropic multisublattice magnet and use them for determining the spectra of spin waves that may propagate in the system. It is well known that high-frequency processes in a multisublattice magnet can be described by the Landau–Lifshitz equation[3] for sublattice spins. However, such a description is no longer applicable at the hydrodynamic stage of evolution[4] since sublattice spins ceases to be approximate integrals of motion in view of a strong exchange interaction between sublattices. Earlier, it was shown by us[5] that, owing to exchange interaction, rigid spin complexes whose orientation is defined by the rotation matrix $a_{\alpha\beta}(x)$ are formed in times $t \gg \tau_r$ (τ_r is the relaxation time). Thus, the low-frequency dynamics of a multisublattice magnet is described by the total spin density $s_\alpha(x)$ and the rotation matrix $a_{\alpha\beta}(x)$. We shall derive hydrodynamic equations for just these quantities.

The rotation matrix $a_{\alpha\beta}$ is introduced formally by considering the local spin rotation U_φ through an angle $\varphi_\alpha(x)$:

$$U_\varphi^+ \hat{s}_\alpha(x) U_\varphi = a_{\alpha\beta}(\varphi)\hat{s}_\beta(x),$$

$$U_\varphi = \exp\left(-i\int d^3x \varphi_\alpha(x)\hat{s}_\alpha(x)\right).$$

Using the commutation relations for the operators $\hat{s}_\alpha(x)$ of spin density components, viz.,

$$[\hat{s}_\alpha(x),\hat{s}_\beta(x')] = i\varepsilon_{\alpha\beta\gamma}\hat{s}_\gamma(x)\,\delta(x-x')$$

we can obtain a relation between the matrix $a_{\alpha\beta}$ and the rotation angles φ_α (exponential parametrization):

$$a(\varphi) = \exp(-\varepsilon\varphi), \quad (\varepsilon\varphi)_{\alpha\beta} \equiv \varepsilon_{\alpha\beta\gamma}\varphi_\gamma. \tag{1}$$

With the rotation matrix there are related the right ($\underline{\omega}_{\alpha k}$) and left ($\omega_{\alpha k}$) Cartan's differential forms:

$$\omega_{\alpha k}(a) = \frac{1}{2}\,\varepsilon_{\alpha\beta\gamma}a_{\beta\lambda}\nabla_k a_{\gamma\lambda},$$

$$\omega_{\alpha k}(a) = \frac{1}{2}\,\varepsilon_{\alpha\beta\gamma}a_{\lambda\gamma}\nabla_k a_{\lambda\beta}. \tag{2}$$

It can be easily verified that $\underline{\omega}_k(a) = a\,\omega_k(a)$. The definition of Cartan's forms leads to the Maurer–Cartan identities

$$\begin{aligned}&\nabla_k\underline{\omega}_{\alpha i} - \nabla_i\underline{\omega}_{\alpha k} = \varepsilon_{\alpha\beta\gamma}\underline{\omega}_{\beta k}\underline{\omega}_{\gamma i},\\ &\nabla_k\omega_{\alpha i} - \nabla_i\omega_{\alpha k} = -\varepsilon_{\alpha\beta\gamma}\omega_{\beta k}\omega_{\gamma i}.\end{aligned} \tag{3}$$

In the general case, the energy density of the system is an arbitrary functional of variables $s_\alpha(x)$, $a_{\alpha\beta}(x)$: $\varepsilon(x) = \varepsilon[x; s_\alpha(x'), a_{\alpha\beta}(x')]$, which is invariant to uniform spin rotations $s \to s' = cs$, $a \to a' = s\tilde{c}$ (c is the rotation matrix) if we neglect by weak relativistic interactions. In the local limit, when spatial inhomogeneities are small, this property means that $\varepsilon(x)$ is a function of variables $\underline{s} \equiv as$, $\underline{\omega}_k = a\,\omega_k$ only:

$$\varepsilon(s,a,\omega_k) = \varepsilon(as, a\,\omega_k, 1) \equiv \varepsilon(\underline{s},\underline{\omega}_k).$$

However, if anisotropy is taken into consideration, the dependence on the rotation matrix is preserved:

$$\varepsilon = \varepsilon(\underline{s},\underline{\omega}_k,a). \tag{4}$$

In order to obtain the equations of dynamics of the magnetic systems under consideration, we use the Hamilton approach in which the equation of motion for an arbitrary physical quantity A has the form

$$\dot{A} = \{A,\mathscr{H}\}, \tag{5}$$

where $\mathscr{H}$ is the Hamiltonian of the system. The Poisson brackets for the dynamic variables $s_\alpha(x), a_{\alpha\beta}(x)$ were obtained in Ref. 6 and are defined by the formulas

$$\begin{aligned}&\{s_\alpha(x), s_\beta(x')\} = \varepsilon_{\alpha\beta\gamma}s_\gamma(x)\,\delta(x-x'),\\ &\{s_\alpha(x), a_{\beta\gamma}(x')\} = \varepsilon_{\alpha\gamma\rho}a_{\beta\rho}(x)\,\delta(x-x'),\\ &\{a_{\alpha\beta}(x), a_{\gamma\rho}(x')\} = 0.\end{aligned} \tag{6}$$

In the following, we shall obtain Green's functions for a multisublattice magnet as the response of the system to external a perturbation. Taking this into consideration, we can write the Hamiltonian $\mathscr{H}$ in the form

$$\mathscr{H} = \int d^3x(\varepsilon(x) + v(x)) \equiv \mathscr{H}_0 + V, \tag{7}$$

$$V=\int d^3x\,\xi(x,t)b(s(x),\omega_k(x),a(x))\equiv V(t),$$

where V is the interaction Hamiltonian with the external field, $\xi(x,t)$ the field potential, and b is an arbitrary local physical quantity. We assume that the external field varies quite slowly, and the characteristic frequency of its variation is small in comparison with τ_r^{-1}. Hence, for $t\gg\tau_r$ the system can still be described in terms of the quantities s_α, $a_{\alpha\beta}$.

Using the general functional expression (7) and the system (6) of Poisson brackets, we can obtain the equation of motion for dynamic variables of a multisublattice magnet. Since the energy density ε depends only on the quantities $\underline{s}$, $\underline{\omega}$ if we neglect by the anisotropy, we can formulate the equations of dynamics in terms of the variables $\underline{s}$, $\underline{\omega}$, a (such a choice of variables is convenient for a transition to the isotropic case). In this case, taking Eqs. (5)–(7) into consideration, we obtain the following system of dynamic equations in an external field:

$$\begin{aligned}
&\dot{\underline{s}}_\alpha=-\nabla_k\frac{\partial\varepsilon}{\varepsilon\underline{\omega}_{\alpha k}}+\varepsilon_{\alpha\beta\gamma}\left(\underline{s}_\beta\frac{\partial\varepsilon}{\partial\underline{s}_\gamma}+\underline{\omega}_{\beta k}\frac{\partial\varepsilon}{\partial\underline{\omega}_{\gamma k}}\right.\\
&\qquad\left.+a_{\beta\mu}\frac{\partial\varepsilon}{\partial a_{\gamma\mu}}\right)+\eta_\alpha,\\
&\dot{a}_{\alpha\beta}=\varepsilon_{\alpha\rho\gamma}a_{\rho\beta}\frac{\partial\varepsilon}{\partial\underline{s}_\gamma}+\eta_{\alpha\beta},
\end{aligned}\tag{8}$$

where the sources $\eta_\alpha,\eta_{\alpha\beta}$ are defined by the relations

$$\begin{aligned}
&\eta_\alpha=\xi\varepsilon_{\alpha\beta\gamma}\left(\underline{s}_\beta\frac{\partial b}{\partial\underline{s}_\gamma}+\underline{\omega}_{\beta k}\frac{\partial b}{\partial\underline{\omega}_{\gamma k}}+a_{\beta\mu}\frac{\partial b}{\partial a_{\gamma\mu}}\right)\\
&\qquad-\nabla_k\left(\xi\frac{\partial b}{\partial\underline{\omega}_{\alpha k}}\right),\quad \eta_{\alpha\beta}=\xi\varepsilon_{\alpha\rho\gamma}a_{\rho\beta}\frac{\partial b}{\partial\underline{s}_\gamma}.
\end{aligned}\tag{9}$$

The equation of motion for the rotation matrix leads to the following equation of motion for Cartan's right form $\underline{\omega}_{\alpha k}$:

$$\begin{aligned}
&\dot{\underline{\omega}}_{\alpha k}=-\nabla_k\frac{\partial\varepsilon}{\partial\underline{s}_\alpha}+\varepsilon_{\alpha\beta\gamma}\underline{\omega}_{\beta k}\frac{\partial\varepsilon}{\partial\underline{s}_\gamma}+\eta_{\alpha k},\\
&\eta_{\alpha k}=\xi\varepsilon_{\alpha\beta\gamma}\underline{\omega}_{\beta k}\frac{\partial b}{\partial\underline{s}_\gamma}-\nabla_k\left(\xi\frac{\partial b}{\partial\underline{s}_\alpha}\right).
\end{aligned}\tag{10}$$

Let us now derive the time-independent solution of Eqs. (8), (10) in the absence of an external field. It follows from Eqs. (3), (8), and (10) that the following expressions can be written for the steady-state values of the rotation matrix a^0 and Cartan's form $\underline{\omega}_k^0$:

$$\begin{aligned}
&a^0(\mathbf{x},t)=a(\varphi^0)a[\varphi(\mathbf{x},t)],\quad \varphi_\alpha(\mathbf{x},t)=n_\alpha(-\mathbf{p}\cdot\mathbf{x}+\underline{h}t);\\
&\underline{\omega}^0_{\alpha k}=n_\alpha p_k,
\end{aligned}\tag{11}$$

where φ^0_α are the uniform rotation angles,

$$\underline{h}_\alpha\equiv\left.\frac{\partial\varepsilon}{\partial\underline{s}_\alpha}\right|_0=\underline{h}n_\alpha;$$

and p_k is the spiral vector. Taking into consideration formulas (1), (8), and (11), we obtain the following relation between the steady-state values of the quantities $\underline{s}^0_\alpha$, p_k, and $\underline{h}_\alpha$:

$$\varepsilon_{\alpha\beta\gamma}n_\gamma\left\{\underline{h}s^0_\beta-p_k\frac{\partial\varepsilon}{\partial\underline{\omega}_{\beta k}}\right\}+\frac{\partial\varepsilon}{\partial\varphi_\alpha}=0.\tag{12}$$

2. HYDRODYNAMIC ASYMPTOTIC FORM OF GREEN'S FUNCTIONS

We introduce Green's two-time retarding function for arbitrary quasilocal operators $\hat{a}$ and $\hat{b}$:

$$G_{ab}(x,t;x',t')=-i\,\theta(t-t')\mathrm{Tr}\;w[\hat{a}(x,t),\hat{b}(x',t')].\tag{13}$$

Here, w is the equilibrium statistical operator which can be represented in the following form according to the method of quasiaverages:

$$\begin{aligned}
&w=\lim_{\nu\to0}\lim_{V\to\infty}w_\nu,\\
&w_\nu=\exp(\Omega_\nu-Y_0\hat{\mathscr{H}}_0-\underline{Y}_\alpha\hat{S}_\alpha-\nu\hat{G}).
\end{aligned}\tag{14}$$

In this equation, the thermodynamic forces Y_0 and $\underline{Y}_\alpha$ are connected with the temperature T and the magnetizing field $\underline{h}_\alpha$ through the relations $Y_0=1/T$, $-\underline{Y}_\alpha/Y_0=\underline{h}_\alpha$, while the potential Ω_ν is determined from the normalization condition $\mathrm{Tr}\;w_\nu=1$. In accordance with the conditions (11), the equilibrium statistical operator (14) satisfies the following relations:

$$\begin{aligned}
&[w,\hat{P}_k]=[w,\hat{H}]=0,\quad \hat{P}_k=\hat{\mathscr{P}}_k-p_kn_\alpha\hat{S}_\alpha,\\
&\hat{H}=\hat{\mathscr{H}}_0-\underline{h}_\alpha\hat{S}_\alpha,
\end{aligned}\tag{15}$$

where $\hat{\mathscr{P}}_k$ is the momentum operator. The dependence of quasilocal operators $\hat{a}$ and $\hat{b}$ on coordinates and time in Eq. (13) is defined by the expressions

$$\begin{aligned}
&\hat{a}(\mathbf{x},t)=\exp\,i(Ht-\mathbf{P}\cdot\mathbf{x})\hat{a}(0)\exp[-i(Ht-\mathbf{P}\cdot\mathbf{x})],\\
&\hat{b}(\mathbf{x}',t')=\exp\,i(Ht'-\mathbf{P}\cdot\mathbf{x}')\hat{b}(0)\exp[-i(Ht'-\mathbf{P}\cdot\mathbf{x}')].
\end{aligned}\tag{16}$$

In this case, the Green's function G_{ab} possesses properties of translational invariance in space and time:

$$G_{ab}(x,t;x',t')=G_{ab}(x-x',t-t').$$

If the interaction of the system with the external field $\xi(x,t)$ is defined by formula (7), the linear response of the quantity a to external perturbation reads

$$\delta a_\xi(x,t)=\int_{-\infty}^{\infty}dt'\int d^3x'\,\xi(x',t')G_{ab}(x-x',t-t'),$$

or, if we use the Fourier representation,

$$\delta a_\xi(\mathbf{k},\omega)=G_{ab}(\mathbf{k},\omega)\xi(\mathbf{k},\omega).\tag{17}$$

Let us linearize the system of equations (8), (10) with respect to deviations from equilibrium values $\underline{s}^0_\alpha$, $a^0_{\alpha,\beta}$:

$$\begin{aligned}
&\delta\underline{s}_\alpha(x,t)=\underline{s}_\alpha(x,t)-\underline{s}^0_\alpha,\\
&\delta a_{\alpha\beta}(x,t)=-\varepsilon_{\alpha\rho\gamma}\delta\varphi_\gamma(x,t)a^0_{\rho\beta}(x,t).
\end{aligned}\tag{18}$$

The variation of Cartan's $\underline{\omega}_{\alpha k}$ form associated with the transformations (18) has the form

$$\delta\underline{\omega}_{\alpha k}=\nabla_k\delta\varphi_\alpha-\varepsilon_{\alpha\beta\gamma}\underline{\omega}^0_{\beta k}\delta\varphi_\gamma.$$

Going over to the Fourier representation, we arrive at the following system of equations for determining the deviations $\delta\underline{s}(\mathbf{k},\omega), \delta\varphi(\mathbf{k},\omega)$:

$$L_{\alpha\beta}\delta\underline{s}_\beta - Z_{\alpha\beta}\delta\varphi_\beta = \eta_\alpha, \quad K_{\alpha\beta}\delta\varphi_\beta - \varepsilon_{\alpha\beta}\delta\underline{s}_\beta = \overline{\eta_\alpha}. \tag{19}$$

Here, the sources η_α and $\overline{\eta_\alpha}$ can be presented in the following form in accordance with the relation (9):

$$\eta_\alpha = \xi\left(\frac{\partial b}{\partial\varphi_\alpha} - ik_l\frac{\partial b}{\partial\underline{\omega}_{\alpha l}} + \varepsilon_{\alpha\beta\gamma}\left[\underline{s}^0_\beta\frac{\partial b}{\partial\underline{s}_\gamma} + \underline{\omega}^0_{\beta l}\frac{\partial b}{\partial\underline{\omega}_{\gamma l}}\right]\right),$$

$$\overline{\eta_\alpha} = \xi\frac{\partial b}{\partial\underline{s}_\alpha}. \tag{20}$$

The matrices K, L, Z are defined by formulas

$$K = i\omega - \underline{h}N - if + f'N - T,$$

$$L = -i\omega + i\widetilde{f} + \underline{h}N - M\varepsilon - N\widetilde{f}' - \widetilde{T},$$

$$Z = D + iD'N + iMf - Mf'N + iN\widetilde{D}' - ND''N - iG + G'N - i(Q - \widetilde{Q}) - \widetilde{Q}'N + NQ' + H + MT, \tag{21}$$

where

$$\varepsilon_{\alpha\beta} = \frac{\partial^2\varepsilon}{\partial\underline{s}_\alpha\partial\underline{s}_\beta}, \quad f_{\alpha\beta} = k_i\frac{\partial^2\varepsilon}{\partial\underline{s}_\alpha\partial\underline{\omega}_{\beta i}}, \quad f'_{\alpha\beta} = p_i\frac{\partial^2\varepsilon}{\partial\underline{s}_\alpha\alpha\underline{\omega}_{\beta i}},$$

$$D_{\alpha\beta} = k_ik_l\frac{\partial^2\varepsilon}{\partial\underline{\omega}_{\alpha i}\partial\underline{\omega}_{\beta l}}, \quad D'_{\alpha\beta} = k_ip_l\frac{\partial^2\varepsilon}{\partial\underline{\omega}_{\alpha i}\partial\underline{\omega}_{\beta l}},$$

$$D''_{\alpha\beta} = p_ip_l\frac{\partial^2\varepsilon}{\partial\underline{\omega}_{\alpha i}\partial\underline{\omega}_{\beta l}}, \quad N_{\alpha\beta} = \varepsilon_{\alpha\gamma\beta}n_\gamma,$$

$$M_{\alpha\beta} = \varepsilon_{\alpha\gamma\beta}\underline{s}_\gamma, \quad G_{\alpha\beta} = \varepsilon_{\alpha\gamma\beta}k_i\frac{\partial\dot{\varepsilon}}{\partial\underline{\omega}_{\gamma i}},$$

$$G'_{\alpha\beta} = \varepsilon_{\alpha\gamma\beta}p_i\frac{\partial\varepsilon}{\partial\underline{\omega}_{\gamma i}}$$

and the effect of anisotropy is taken into account through the terms

$$H_{\alpha\beta} = \frac{\partial^2\varepsilon}{\partial\varphi_\alpha\partial\varphi_\beta}, \quad T_{\alpha\beta} = \frac{\partial^2\varepsilon}{\partial\underline{s}_\alpha\partial\varphi_\beta},$$

$$Q_{\alpha\beta} = k_i\frac{\partial^2\varepsilon}{\partial\underline{\omega}_{\alpha i}\partial\varphi_\beta}, \quad Q'_{\alpha\beta} = p_i\frac{\partial^2\varepsilon}{\partial\underline{\omega}_{\alpha i}\partial\varphi_\beta}.$$

Using Eqs. (19), we obtain

$$\delta\underline{s} = \frac{1}{\Delta}\varepsilon^{-1}\{KS(\eta + L\varepsilon^{-1}\overline{\eta}) - \Delta\overline{\eta}\},$$

$$\delta\varphi = \frac{S}{\Delta}(\eta + L\varepsilon^{-1}\overline{\eta}), \tag{22}$$

where

$$S_{\nu\gamma} = \frac{1}{2}\varepsilon_{\alpha\beta\gamma}\varepsilon_{\chi\mu\nu}P_{\alpha\chi}P_{\beta\mu}$$

$$P \equiv L\varepsilon^{-1}K - Z, \tag{23}$$

$$\Delta = \det P.$$

We now consider the fact that in the main approximation in k and ω ($\omega\tau_r \ll 1$, $kl \ll 1$, l being a quantity of the type of mean free path), the response of the quantity a (which is a function of dynamic variables) to the external perturbation $\xi(x,t)$ can be presented in the form

$$\delta a(\mathbf{k},\omega) = \frac{\partial a}{\partial\underline{s}_\alpha}\delta\underline{s}_\alpha(\mathbf{k},\omega) + \frac{\partial a}{\partial\underline{\omega}_{\alpha l}}\delta\underline{\omega}_{\alpha l}(\mathbf{k},\omega) + \frac{\partial a}{\partial\varphi_\alpha}\delta\varphi_\alpha(\mathbf{k},\omega).$$

Comparing this formula with (17) and taking (22) into consideration, as well as the fact that

$$\delta\underline{\omega}_{\alpha l}(\mathbf{k},\omega) = (ik_l\delta_{\alpha\beta} - p_lN_{\alpha\beta})\delta\varphi_\beta(\mathbf{k},\omega),$$

we obtain the following expression for the low-frequency asymptote of Green's function of arbitrary dynamic quantities a and b:

$$G_{ab}(\mathbf{k},\omega) = \frac{1}{\Delta}\left\{\frac{\partial a}{\partial\varphi_\alpha} + (ik_l + Np_l)_{\alpha\mu}\frac{\partial a}{\partial\underline{\omega}_{\mu l}} + (M + L(-\mathbf{k},-\omega)\varepsilon^{-1})_{\alpha\mu}\frac{\partial a}{\partial\underline{s}_\mu}\right\}S_{\mu\beta}\left\{\frac{\partial b}{\partial\varphi_\beta} + (-ik_i + Np_i)_{\beta\nu}\frac{\partial b}{\partial\underline{\omega}_{\nu i}} + [M + L(\mathbf{k},\omega)\varepsilon^{-1}]_{\beta\nu}\frac{\partial b}{\partial\underline{s}_\nu}\right\} - \frac{\partial a}{\partial\underline{s}_\alpha}\varepsilon^{-1}_{\alpha\beta}\frac{\partial b}{\partial\underline{s}_\beta}. \tag{24}$$

This formula is invariant to the substitution $a \leftrightarrow b$, $\mathbf{k} \to -\mathbf{k}$, $\omega \to -\omega$. If the anisotropy is neglected, the asymptotic form (24) of Green's function coincides with the corresponding expression presented in Ref. 7. Among other things, formula (24) leads to the asymptotes for the basis of Green's functions:

$$G_{s_a,s_\beta}(\mathbf{k},\omega) = \frac{1}{\Delta(\mathbf{k},\omega)}[\varepsilon^{-1}K(\mathbf{k},\omega)S(\mathbf{k},\omega)\widetilde{K}(-\mathbf{k},-\omega)\varepsilon^{-1}]_{\alpha\beta} - \varepsilon^{-1}_{\alpha\beta},$$

$$G_{s_\alpha,\varphi_\beta}(\mathbf{k},\omega) = \frac{1}{\Delta(\mathbf{k},\omega)}[\varepsilon^{-1}K(\mathbf{k},\omega)S(\mathbf{k},\omega)]_{\alpha\beta}, \tag{25}$$

$$G_{\varphi_\alpha,\varphi_\beta}(k,\omega) = \frac{1}{\Delta(\mathbf{k},\omega)}S_{\alpha\beta}(\mathbf{k},\omega).$$

These formulas contain a dependence on matrices K, L and Z [the dependence on matrix Z is effectively contained in asymptotic forms through the matrix S and the quantity Δ, see Eq. (23)], which is simplified considerably for the case when the energy density has the special form $\varepsilon[\underline{s},\underline{\omega},a(\varphi)] = \varepsilon(\underline{s},\underline{\omega}) + \varepsilon(a(\varphi))$, where $\varepsilon(\underline{s},\underline{\omega}) = \varepsilon(\underline{s}^2,\underline{\omega}^2,\underline{s}\underline{\omega})$. In this case, we arrive at the following expression for the matrices K, L, and Z:

$$K = i\omega - \underline{h}N - if + f'N, L = -i\omega + i\widetilde{f},$$

$$Z = D + iD'N + H.$$

The effect of anisotropy is now considered through the matrix H.

In order to illustrate the obtained results, we choose the energy density in the form[8]

$$\varepsilon=\frac{\underline{s}_\alpha^2}{2\chi}+\frac{\rho_s\underline{\omega}_{\alpha k}^2}{2}+\frac{\beta\varphi^2}{2},$$

where χ is the magnetic susceptibility, ρ_s is the magnetic rigidity constant, β is the anisotropy constant, and the angle φ is measured from a certain direction defined by the anisotropy axis. In this case, formulas (25) assume the form

$$G_{s_\alpha,s_\beta}(\mathbf{k},\omega)=\frac{\beta+\rho_s\mathbf{k}^2}{\chi\omega^2-(\beta+\rho_s\mathbf{k}^2)}\,\chi\delta_{\alpha\beta},$$

$$G_{s_\alpha,\varphi_\beta}(\mathbf{k},\omega)=\frac{i\omega}{\chi\omega^2-(\beta+\rho_s\mathbf{k}^2)}\,\chi\delta_{\alpha\beta},$$

$$G_{\varphi_\alpha,\varphi_\beta}(\mathbf{k},\omega)=\frac{\delta_{\alpha\beta}}{\chi\omega^2-(\beta+\rho_s\mathbf{k}^2)}.$$

It can be seen that, in the absence of anisotropy ($\beta=0$), the Green's function $G_{\varphi_\alpha,\varphi_\beta}$ has the singularity $1/k^2$ for $\omega=0$ in accordance with Bogoliubov's theorem.[9] For $k=0$, the singularities $1/\omega^2, 1/\omega$ belong to Green's functions $G_{\varphi_\alpha,\varphi_\beta}$ and $G_{s_\alpha,\varphi_\beta}$ respectively. For $k=0$, $\omega=0$ and in the presence of anisotropy, the anisotropy singularity of the type $1/\beta$ belongs to the Green's functions $G_{\varphi_\alpha,\varphi_\beta}$.

3. SPIN WAVE SPECTRA

In order to obtain the spin wave spectra, we must define the poles of Green's functions G_{ab}. This leads to the dispersion equation $\Delta(\mathbf{k},\omega)=0$. Taking into account the definition (23) of the matrix P, we can represent this equation in the form

$$\begin{aligned}
&\det[\omega^2 a+\omega(ib_1+b_2)+ic_1+c_2]\equiv\det P=0,\\
&a=-\varepsilon^{-1},\quad b_1=M-aRN-N\widetilde{R}a+aT-\widetilde{T}a,\\
&R=f'-I\underline{h},\quad b_2=-af-\widetilde{f}a,\\
&c_1=-G+(D'+\widetilde{f}aR)N+N(\widetilde{D}'+\widetilde{R}af)+\widetilde{T}af-\widetilde{f}aT\\
&\qquad -Q+\widetilde{Q},\\
&c_2=D-ND''N+\widetilde{f}af-N\widetilde{R}aRN+\widetilde{T}aT+NQ'-\widetilde{Q}'N\\
&\qquad +H+(G'-\underline{h}M)N.
\end{aligned}\tag{26,27}$$

It can easily be seen that the matrices a and b_2 are symmetric, while the matrices b_1 and c_1 are antisymmetric. In matrix c_2, all terms are obviously symmetric with the exception of $(G'-\underline{h}M)N$. The symmetry of this matrix can be studied by using formula (12). In the absence of anisotropy, $\partial\varepsilon/\partial\varphi=0$, and hence we can easily verify by using formula (12) that $[(G'-\underline{h}M)N]_{\alpha\beta}=[(G'-\underline{h}M)N]_{\beta\alpha}$. Hence, in the absence of anisotropy, P is a hermite matrix and this leads to real values for spin wave frequencies.[6] In the presence of anisotropy, we obtain

$$\begin{aligned}
&[(G'-\underline{h}M)N]_{\alpha\beta}-[(G'-\underline{h}M)N]_{\beta\alpha}\\
&\quad=(n_\alpha N_{\beta\gamma}-n_\beta N_{\alpha\gamma})\,\frac{\partial\varepsilon}{\partial\varphi_\gamma},
\end{aligned}$$

which leads to the following condition for the hermite matrix P:

$$N_{\alpha\gamma}\frac{\partial\varepsilon}{\partial\varphi_\gamma}\equiv\varepsilon_{\alpha\beta\gamma}n_\beta\frac{\partial\varepsilon}{\partial\varphi_\gamma}=0,\tag{28}$$

i.e., the anisotropy should be such that rotations about the direction $n_\alpha=\underline{h}_\alpha/\underline{h}$ do not change the energy functional ε. If the energy functional does not satisfy the condition (28), matrix P is no longer hermite and the spectrum acquires frequencies with imaginary components in the general case. This indicates the instability of the corresponding state. Hence if the matrix P is not hermite, the exchange and anisotropy constants must satisfy certain inequalities for the spin wave spectrum to be real. In the following, we shall assume that the condition (28) is satisfied,

For the model energy density

$$\varepsilon[\underline{s},\underline{\omega},a(\varphi)]=\varepsilon(\underline{s},\underline{\omega})+\varepsilon[a(\varphi)],$$

$$\varepsilon(\underline{s},\underline{\omega})=\varepsilon(\underline{s}^2,\underline{\omega}^2,\underline{s}\,\underline{\omega})$$

the expressions for matrices b_i and c_i in (27) are simplified considerably.In this case, we obtain

$$b_1=-aRN,\quad b_2=-af-\widetilde{f}a,\quad c_1=(D'+\widetilde{f}aR)N,$$

$$c_2=\widetilde{f}af+H$$

and the corresponding symmetry properties of the matrices b_i and c_i are ensured by a special form of the energy density.

We can write the dispersion equation (26) in the form

$$\sum_{n=0}^{6}A_n(\mathbf{k})\omega^n=0,\tag{29}$$

where the coefficients A_n ($n=0,...,6$) in terms of the convolution

$$|abc|=\frac{1}{6}\,\varepsilon_{\alpha\beta\gamma}\varepsilon_{uvt}a_{\alpha u}b_{\beta v}c_{\gamma t}$$

are defined by formulas

$$\begin{aligned}
&A_0=|c_2c_2c_2|-3|c_1c_2c_1|,\\
&A_1=-6|b_1c_1c_2|-3|b_2c_1c_1|-3|b_2c_2c_2|,\\
&A_2=-3|ac_1c_1|+3|ac_2c_2|+3|b_2b_2c_2|-6|b_1b_2c_1|\\
&\qquad -3|b_1b_1c_2|,\\
&A_3=|b_2b_2b_2|+6|ab_2c_2|-6|ab_1c_1|-3|b_1b_1,b_2|,\\
&A_4=3|aac_2|-3|ab_1b_1|+3|ab_2b_2|,\\
&A_5=3|aab_2|,\\
&A_6=|aaa|.
\end{aligned}$$

Let us confine our analysis to the small wave vectors k to analyze the possible spin wave spectra. In the absence of anisotropy and $\omega=0$, $k=0$, we have $\det P(0,0)=\det c_2$, and in view of the explicit form of the matrix c_2 in (27), $\det P(0,0)=0$. This means that, in the isotropic case, the

system has at least two Goldstone modes [since $A_{2l+1}(k=0)=0$]. The situation changes in the presence of anisotropy: $\det P(0,0)=\det c_2\neq 0$, which means that all modes of the anisotropic magnet are activation modes in the general case. However, the degree of anisotropy of activation frequencies may vary from first to third. Since we are considering the case of small anisotropy, we confine the analysis to a consideration of anisotropy in the linear approximation only. In this approximation, the modes whose activation frequencies are quadratic or cubic in anisotropy become activationless. We shall consider some particular cases for the equilibrium values of $\underline{s}$, $\underline{h}$, p_k.

1. $\underline{s}=0$, $\underline{h}=0$, $p_k=0$.

The dispersion equation (29) assumes the form

$$A_6\omega^6+(A_4'+A_4''k^2)\omega^4+A_2''k^2\omega^2+A_0'''k^4=0. \tag{30}$$

Here, we have explicitly isolated the dependence on the modulus $|\mathbf{k}|$ for the coefficients A_n in Eq. (29). The solution of Eq. (30) leads to two pairs of Goldstone modes and one pair of activation modes:

$$\omega_{1,2}^2=F_{1,2}k^2,\quad \omega_3^2=\omega_0^2+F_3k^2,$$

where

$$\omega_0^2=-\frac{A_4'}{A_6},\quad F_{1,2}=\frac{1}{2A_4'}\{-A_2''\pm\sqrt{(A_2'')^2-4A_0'''A_4'}\},$$

$$F_3=\frac{A_6A_2''-A_4'A_4''}{A_6A_4'}.$$

For comparison, let us consider the form of the spin wave spectra for an isotropic magnet[10,11] for the case

$$\omega_i^2=\lambda_i^2k^2,\quad i=1,2,3$$

under consideration.

2. $\underline{s}\neq 0$, $\underline{h}=0$, $p_k=0$.

The dispersion equation assumes the form

$$A_6\omega^6+(A_4'+A_4''k^2)\omega^4+(A_2'+A_2''k^2)\omega^2+A_0'''k^4=0. \tag{31}$$

For small k, we obtain two pairs of activation modes and one pair of Goldstone modes:

$$\omega_{1,2}^2=\omega_\pm^2+R_\pm k^2,\quad \omega_3^2=R_3k^4.$$

where

$$\omega_\pm=\frac{1}{2A_6}\{-A_4'\pm\sqrt{(A_4')^2-4A_2'A_6}\},$$

$$R_\pm=\mp\frac{A_2''+A_4''\omega_\pm^2}{A_6(\omega_+^2-\omega_-^2)},\quad R_3=-\frac{A_0'''}{A_2'}.$$

In the analogous case for an isotropic magnet,[10,11] we obtain

$$\omega_1^2=\nu_1k^4,\quad \omega_2^2=\nu_2k^2,\quad \omega_3^2=\omega_0^2+\nu_3k^2.$$

In view of the emergence of activation frequencies in the isotropic case, we note that such a situation is characteristic for multisublattice exchange magnets whose state is characterized by the total spin density as well as an additional dynamic variable, viz, the rotation matrix. This is due to the fact that in the equations of motion for the densities of additive integrals of motion, expansion in spatial gradients begins with terms linear in gradients, while the expansion in the equation of motion for the rotation matrix begins from the zeroth order gradient terms. This corresponds to precession with the corresponding activation frequencies. A simple model example describing such a situation is presented in Ref. 6.

3. $\underline{s}\neq 0$, $\underline{h}\neq 0$, $p_k=0$.

Equation (29) assumes the form

$$A_6\omega^6+(A_4'+A_4''k^2)\omega^4+(A_2'+A_2''k^2)\omega^2+A_0'+A_0''k^2=0. \tag{32}$$

In this case, all branches correspond to activation modes:

$$\omega_i^2=\omega_{0i}^2+c_i^2k^2,\quad i=1,2,3,$$

where the activation frequencies ω_{0i}^2 are determined from the cubic equation obtained from (32) for $k=0$. In this case, we obtain[12] two pairs of activation modes and one pair of Goldstone modes for an isotropic magnet:

$$\omega_{1,2}^2=\omega_\pm^2+\mu_\pm k^2,\quad \omega_3^2=\mu_3k^2.$$

4. $\underline{s}\neq 0$, $\underline{h}\neq 0$, $p_k\neq 0$.

This is the most general case. An analysis of the dispersion equation shows that there exist six activation branches with spatial anisotropy associated with the existence of a spiral structure

$$\omega_i=\omega_{0i}+c_i(\mathbf{p}\cdot\mathbf{k})+d_i'(\mathbf{p}\cdot\mathbf{k})^2+d_i''\mathbf{k}^2.$$

In this case, we obtain[6] the following expression for an isotropic magnet:

$$\omega_{1,2}=\alpha(\mathbf{p}\cdot\mathbf{k})\pm\sqrt{\beta\mathbf{k}^2+\gamma(\mathbf{p}\cdot\mathbf{k})^2},$$

$$\omega_i=\omega_{0i}+\lambda_i'(\mathbf{p}\cdot\mathbf{k})+\mu_i'(\mathbf{p}\cdot\mathbf{k})^2+\mu_i''\mathbf{k}^2\quad(i=3,...,6).$$

In conclusion, it should be remarked that dynamics of a multisublattice magnet with a complete violation of symmetry relative to spin rotations is in many ways similar to the spin dynamics of the superfluid B-phase of ^{3}He.[13,14] Both are described by the same set of hydrodynamic variables, viz., spin density and real rotation matrix (or the corresponding rotation angles). Hence the formulas obtained for the asymptotes of Green's functions can also be used for the B-phase of ^{3}He. In particular, if we neglect the anisotropy and put $\underline{s}^0=0$, $\underline{h}=0$, and $\mathbf{p}=0$, the obtained expressions for asymptotic forms coincide with the results obtained in Ref. 15 if the quantities a and b are replaced by the variables $\underline{s}$ and φ.

The author is grateful to S. V. Peletminskii and M. Yu. Kovalevskii for a discussion of results and for fruitful remarks.

*E-mail: isayev@kipt.kharkov.ua

[1] V. L. Bonch-Bruevich and S. V. Tyablikov, *The Green's Function Method in Statistical Mechanics*. No. Holland, Amsterdam (1962).
[2] V. G. Bar'yakhtar, V. I. Krivoruchko, and D. Ya. Yablonskii, *Green's Function in The Theory of Magnetism* [in Russian], Naukova Dumka, Kiev (1984).
[3] A. I. Akhiezer, V. G. Bar'yakhtar, and S. V. Peletminskii, *Spin Waves*, North-Holland, Amsterdam (1960).

[4] I. E. Dzyaloshinskii and G. E. Volovick, Ann. Phys. (N.Y.) **125**, 67 (1980).
[5] A. A. Isayev and S. V. Peletminskii, Teor. Mat. Fiz. **102**, 470 (1995).
[6] M. Yu. Kovalevskii, S. V. Peletminskii, and A. L. Shishkin, Ukr. Fiz. Zh. **36**, 245 (1991).
[7] M. Yu. Kovalevsky and A. A. Rozhkov, Physica A **A216**, 169 (1995).
[8] W. M. Saslow, Phys. Rev. B **22**, 1174 (1980).
[9] N. N. Bogoliubov and N. N. Bogoliubov, Jr., *Introduction to Quantum Statistical Mechanics* [in Russian], Nauka, Moscow (1984).
[10] D. V. Volkov and A. A. Zheltukhin, Izv. Akad. Nauk SSSR, Ser. Fiz. **44**, 1487 (1980).
[11] B. I. Halperin and W. M. Saslow, Phys. Rev. B **16**, 2154 (1977).
[12] A. F. Andreev and V. I. Marchenko, Usp. Fiz. Nauk **130**, 39 (1980) [Sov. Phys. Usp. **23**, 21 (1980)].
[13] K. Maki, Phys. Rev. B **11**, 4246 (1975).
[14] M. Yu. Kovalevsky and A. A. Rozhkov, Fiz. Nizk. Temp. **21**, 1138 (1995) [Low Temp. Phys. **21**, 873 (1995)].
[15] Z. M. Galasievicz, J. Low Temp. Phys. **57**, 123 (1984).

Translated by R. S. Wadhwa

Formation of long-range ferrimagnetic order in dilute spinels $Li_{0.5}Fe_{2.5-x}Ga_xO_4$ near the multicritical point

N. N. Efimova

Kharkov State University, 310077 Kharkov, Ukraine
(Submitted May 12, 1997; revised May 22, 1997)
Fiz. Nizk. Temp. **23**, 1067–1073 (October 1997)

The influence of spatial inhomogeneity of short-range exchange on the formation of long- range ferrimagnetic order in dilute spinels is investigated. The objects of investigation are two types of polycrystalline samples of $Li_{0.5}Fe_{1.1}Ga_{1.4}O_4$ differing in the extent of heterogeneity in the distribution of magnetic (Fe^{3+}) and nonmagnetic (Ga^{3+}) ions in the lattice. The heterogeneity was created by using two regimes of thermal treatment, i.e., slow cooling (S) and quenching (Q) of samples from 1550 to 300 K. The results of analysis of magnetization isotherms $\sigma_T(H)$ at $T=4.2$ K, (77–300) K, $H\leqslant 16$ kOe and temperature dependences of initial susceptibility $\chi_0(T)$ show that the long-range ferrimagnetic order near the multicritical point ($x_0=1.5$) of the $x-T$ phase diagram is stable to variations of the degree of spatial heterogeneity of the exchange. © *1997 American Institute of Physics.* [S1063-777X(97)00610-5]

INTRODUCTION

Spatial heterogeneity in the exchange interaction is always observed to a certain extent in dilute magnets with short-range exchange in view of a nonequilibrium distribution of atoms of different species in the lattice (composition disorder).[1–5] As a result, cluster magnetic states are formed for a sufficiently high extent of dilution (including those with a long-range magnetic order) if the concentration of magnetic atoms is higher than the percolation threshold c_0.[4] The exchange interaction in a cluster whose size is approximately equal to the size of a region with a higher concentration of the magnetic component is stronger than the exchange in the surrounding space. For this reason, structures of the cluster type can be regarded as two exchange-coupled subsystems, viz., clusters and the matrix.[4,6] Destruction of the long-range magnetic order in such systems (e.g., under the effect of temperature) facilitates the breaking of exchange coupling between clusters while the ordering is still preserved in them (short-range static order). For this reason, states of the superparamagnetic type are realized in the paramagnetic (PM) region close to the transformation temperature.[4,5,7–9]

Theoretical and experimental studies of the concentration phase diagrams of dilute ferro-, ferri-, and antiferromagnets (FM and AFM) proved that the type of the long-range order changes above the percolation threshold c_0 in the presence of competing exchange interaction and frustrated bonds: the FM or AFM order is replaced by the spin glass (SG) order at a certain concentration $c_0'>c_0$ of magnetic atoms.[8,9] However, the available experimental data pertaining to the concentration range close to c_0' are contradictory, which is primarily due to the spatial heterogeneity of states.[8] Not only the type of these states, but also the possibility of the formation of the long-range magnetic order of any of the known types are disputable. For example, according to the results of neutron diffraction experiments, a phase with an infinitely large correlation length, but with zero spontaneous magnetization can exist.[8] Thus, the problem of spatially heterogeneous magnetic states existing in the vicinity of c_0' is important and required further analysis.

PROBLEM AND OBJECTS OF INVESTIGATION

This research aims at an analysis of magnetic states formed near $c_0'(c>c_0')$ in dilute Heisenberg ferrimagnets with short-range interaction. The influence of spatial exchange heterogeneity on the formation of long-range ferrimagnetic (FM) order is of special importance.

We analyzed the magnetization isotherms $\sigma_T(H)$ at $T=4.2$ K, (77– 300) K, and for $H\leqslant 16$ kOe as well as the temperature dependences of the initial susceptibility $\chi_0(T)$. These characteristics make it possible to determine the presence of the FM ordering and its main parameters [the values of the Curie temperature T_C and spontaneous magnetization $\sigma_s(T)$] and provide information on magnetization mechanisms.[10]

The objects of investigations were two types of polycrystalline samples of dilute spinel $Li_{0.5}Fe_{2.5-x}Ga_xO_4$ with $x=1.4$, which were subjected to different thermal treatments: slow cooling or quenching from 1550 to 300 K. Two regimes of thermal treatment were used in order to obtain samples with different degrees of composition disorder.

The chosen concentration of nonmagnetic ions $Ga^{3+}(x=1.4)$ is close to the multicritical point $x_0=1.5$ of the $x-T$ phase diagram.[11] For $x>x_0$, no long-range FM order is observed at any temperature $T\geqslant 4.2$ K, but the spin-glass order with the Edwards–Anderson parameter is present in the interval $1.5<x<2.0$.[12] The concentration $x=1.4$ corresponds to the reentrant region of the $x-T$ diagram, in which a transition to the FM state occurs initially at the Curie point upon cooling, followed by a transition to the ferrimagnetic spin glass (FSG) state at the freezing temperature $T_f<T_C$. For a slowly cooled sample with $x=1.4$, the temperature $T_f=25$ K. The concentration transition to disordered states of the SG-like (FSG or SG) states is induced by a change in the relations between competing short-range inter- and intrasublattice antiferromagnetic interactions. In

this case, the probability of formation of frustrated states for Fe^{3+} ions with a weakened exchange increases with x.

According to the results of neutron diffraction experiments (in the temperature range from $T>T_C$ to $T=4.2$ K) and the results of magnetic measurements in the PM region, i.e., at $T>T_C$ for FM or $T>T_f$ for SG, magnetic states with a cluster-type structure are formed in the vicinity of x_0.[11–13] The average size of a cluster, e.g., for $x=1.35$, amounts to 600 Å and does not depend on temperature in the interval $T_f<T<T_C$.[13] For any type of low-temperature states (FM, FSG, or SG), ferrimagnetic ordering is preserved in clusters.[12,13] Thus, the results of previous investigations of the dilute system $Li_{0.5}Fe_{2.5-x}Ga_xO_4$ speak in favor of the model of heterogeneous states ''clusters–matrix,'' in which the type of the long-range magnetic order of the crystal (FM or SG) as a whole is determined by the state of the matrix.

SYNTHESIS AND THERMAL TREATMENT OF SAMPLES. MEASURING TECHNIQUE

Polycrystalline samples of the spinel $Li_{0.5}Fe_{1.1}Ga_{1.4}O_4$ were obtained by a method similar to that described in Ref. 11, i.e., from carbonates and oxides of corresponding metals of the AR grade through the solid-phase reaction at $T=1550$ K in air. After holding at this temperature for 7 hours, some samples were quenched in air ($T=300$ K), while other samples were cooled slowly (for 10 h) to the same temperature (300 K).

X-ray diffraction analysis was carried out in order to test the one-phase composition of the sample and to clarify the influence of thermal treatment conditions (slow cooling or quenching) on the degree of composition disorder. Both types of samples corresponded to one-phase spinels to within the experimental error of the x-ray diffraction method. In both cases, x-ray diffraction patterns contained lines corresponding to superstructural ordering in the octahedral sublattice of the type $1Li^+:3Me^{3+}$ ($Me^{3+}-Fe^{3+},Ga^{3+}$).

The specific magnetization isotherms $\sigma_T(H)$ were recorded on a ballistic magnetometer (with a sensitivity of $10^{-3}G\cdot cm^3\cdot g^{-1}$) at $T=4.2$ K and on a pendulum magnetometer (with a sensitivity of $3\times10^{-1}G\cdot cm^3\cdot g^{-1}$) in fields $H\leqslant16$ kOe at $T\geqslant77$ K. Temperature dependences of initial susceptibility $\chi_0(T)$ in the field $H=10$ Oe were measured by the ballistic method (with a sensitivity $10^{-4}cm^3\cdot g^{-1}$).

DISCUSSION OF EXPERIMENTAL RESULTS

According to the results of x-ray diffraction studies on slowly cooled (S) and quenched (Q) samples, the two regimes of thermal treatment give samples with different types of composition disorder. An increase in the lattice constant for M and Q samples from $a=(8.2700\pm0.0005)$Å to $a=(8.2740\pm0.0005)$Å, respectively indicates an enhancement of the nonuniformity in the distribution of metal ion (Fe^{3+} and Ga^{3+}) in the lattice as a result of quenching. This leads to a change in the magnetic properties; the results of analysis of these properties are presented in Figs. 1 and 2.

The temperature dependences of the initial susceptibility $\chi_0(T)$ (Fig. 1) for S and Q samples differ significantly both in shape and in the values of the Curie temperature (T_{CS} and T_{CQ}) determined by extrapolating of the high- temperature segments of the $\chi_0(T)$ curves with the maximum derivative $(\partial\chi/\partial T)$ to the T-axis. The obtained temperature values are $T_{CS}=160$ K and $T_{CQ}=242$ K. A distinguishing feature of the temperature dependence $\chi_0(T)$ of the quenched sample is the sharp decrease in the value of χ_0 near $T_1\sim T_{CS}$ as well as in the emergence of a broad peak at $T\rightarrow T_{CQ}$.

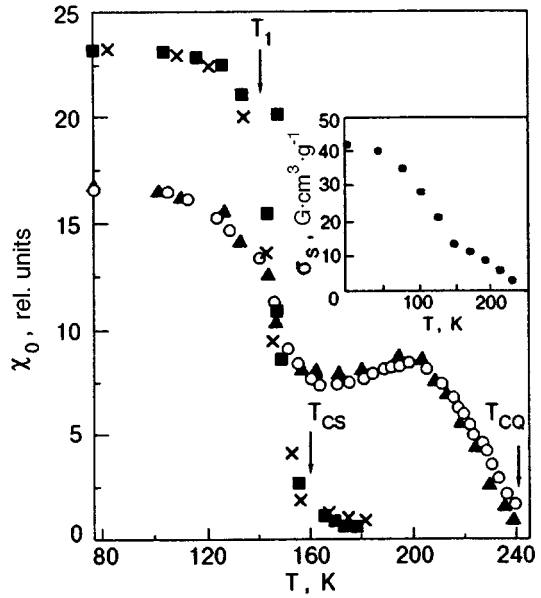

FIG. 1. Temperature dependences of the initial susceptibility $\chi_0(T)$ of samples of $Li_{0.5}Fe_{1.1}Ga_{1.4}O_4$ spinel recorded after different thermal treatment conditions: quenching in air (○) and slow cooling (×) in the temperature interval $T=(1550-300)$K. The results marked by dark squares and triangles correspond to the same sample subjected to cyclic thermal treatment S→Q→S→Q.... The inset shows the temperature dependence of spontaneous magnetization $\sigma_S(T)$ for a quenched sample, determined by the B–A method.

It should be noted that the results presented in Fig. 1 were obtained for different S and Q samples as well as on the same S sample upon multiple cycling of thermal treatment conditions S→Q→S.... This means that the observed effects are not accidental, but are a direct consequence of the change in the thermal treatment conditions. At the same time, aging effects were observed for Q samples: the magnetic properties of these samples changed after 6 months and became the same as for S samples. Therefore, the spatial distribution of metal ions in quenched samples corresponded to nonequilibrium states of the spinel lattice.

The values of T_C and spontaneous magnetization $\sigma_S(T)$ were also determined from the results of analysis of magnetization isotherms $\sigma_T(H)$, some of which are presented in Figs. 2a (S) and b (Q). In accordance with the Belov–Arrott (B–A) method of thermodynamic coefficients, the magnetization isotherms were reconstructed in the $H/\sigma-\sigma^2$ coordinates as shown in Fig. 3 (sample Q). Using the standard procedure, we determined the temperature dependences $\sigma_S(T)$ and the thermodynamic coefficient $\alpha(T)$, which vanish at $T=T_C$.[10] The values of the Curie temperature determined for both types of samples (S and Q) in high fields by using the B–A method and in low fields from the $\chi_0(T)$ dependences coincide to within the experimental error ±2 K.

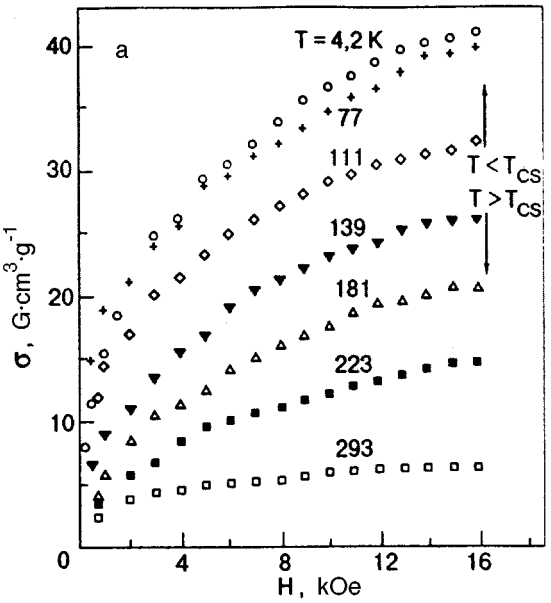

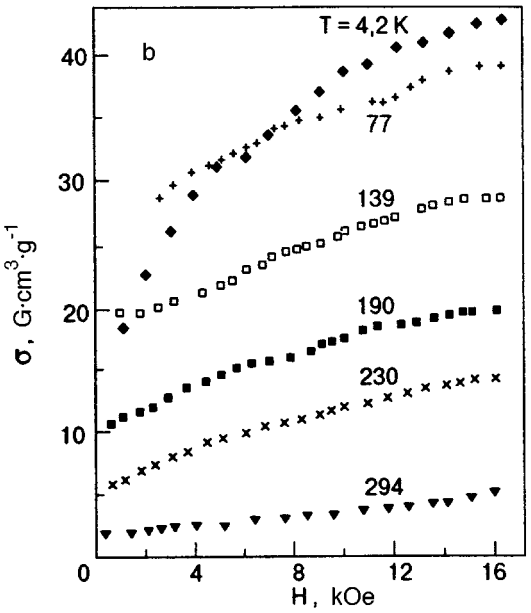

FIG. 2. Magnetization isotherms $\sigma_T(H)$ for a slowly cooled (S) sample.

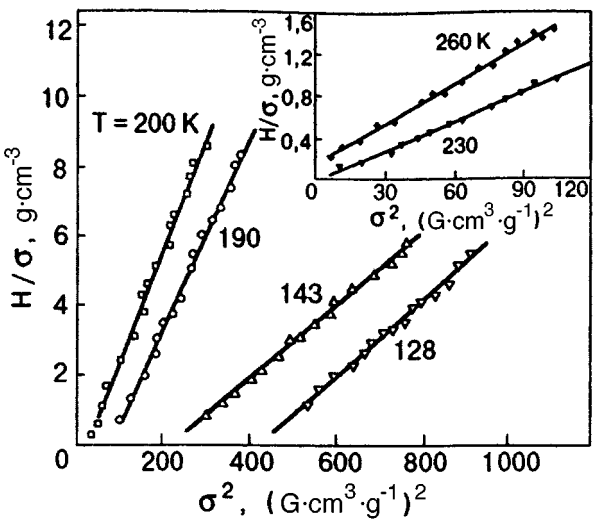

FIG. 3. Magnetization isotherms $\sigma_T(H)$ for a quenched (Q) sample.

This coincidence shows that long-range FM order initially exists in the samples under investigation and is not induced by a magnetic field. Such kind of arguments were used by some authors (see, for example, Ref. 7) who doubt the existence of a long-range FM order near x_0 in systems with a heterogeneous magnetic structure of the cluster type.

Thus, the variation of thermal treatment conditions did not lead to a change in the long- range order which remained ferrimagnetic. However, it resulted in a noticeable change in magnetic properties. In addition to an increase in T_C and a change in the temperature dependence of the initial susceptibility, quenching resulted in another effect. The results presented in the inset to Fig. 1 show that the temperature dependence of spontaneous magnetization $\sigma_S(T)$ determined by the B–A method for Q samples changes in the region of $T_1 \sim T_{CS}$. Before considering possible reasons behind such changes, let us analyze the field dependences of magnetization $\sigma_T(H)$ in greater detail (see Fig. 2).

First of all, it can be seen that the shape of the $\sigma_T(H)$ isotherms in Fig. 2 obviously differs from that for soft magnetic materials including nonsubstituted Li-spinel. The field interval corresponding to technical magnetization region for these samples extends to (12–16)kOe, while the technical saturation field for Li-spinel is $H_S \sim (2-3)$kOe at $T = 4.2$ K. Such a behavior cannot be associated with a change in crystallographic anisotropy determined by one-ion contributions of Fe^{3+} and becomes lower upon the substitution $Ga^{3+} \rightarrow Fe^{3+}$ at all temperatures $T \geqslant 0$.[14] Nevertheless, the shape of the $\sigma_T(H)$ curves shown in Fig. 2 is similar to the shape of magnetization curves due to rotations typical of hard magnetic materials as well as of an ensemble of one-domain or superparamagnetic particles.[10,15] In this connection, the following circumstance is important: it can be seen clearly from Fig. 2a that the shape of $\sigma_T(H)$ isotherms does not change on the whole upon a transition through the Curie point $T_{CS} = 160$ K. However, only the ordering in clusters is preserved at $T > T_{CS}$, and the sample is magnetized due to independent rotation of their magnetic moments **M**. It follows hence that the same type of magnetization also exists in the magnetically ordered region at $T < T_{CS}$. At the same time, the absence of saturation in strong fields (up to 40 kOe at $T = 4.2$ K in our case)[11] indicates the presence of disordered spins in the magnetic structure. Their orientation in the field is associated with the work done against exchange forces, and hence complete saturation can be attained only in fields of the order of hundreds kilooersteds. For $H \leqslant 16$ kOe, the contribution of such spins to the total magnetization of the sample is apparently small. Thus, the difference in the shape of isotherms for S and Q samples should primarily reflect changes in the cluster subsystem caused by quenching. Consequently, we can conclude that the similarity of magnetization curves $\sigma_T(H)$ at $T = 4.2$ K (both in shape and in the values of σ at $H = \text{const}$) is due to the fact that the total number of spins (Fe^{3+} ions) combined is virtually the same in clusters in S and Q samples.

On the other hand, a comparison of the results presented in Figs. 2a and 2b shows that the cluster subsystem experiences changes as a result of quenching. At $T \geqslant 77$ K, the $\sigma_T(H)$ curves in fields $H < 4$ kOe differ significantly. The magnetization of the sample S increases gradually (almost from zero) with the field, while for the Q sample it has a large value even for $H = 0.5$ kOe. At $T \geqslant 77$ K, the methods of measurements were virtually identical in both cases (i.e., without preliminary demagnetization of the samples). Consequently, the peculiarities of the magnetization curves for sample Q under investigation should be naturally attributed to the presence of a residual magnetic moment which is virtually equal to zero in the sample S according to the results presented in Fig. 2a. This means that clusters in S and Q samples (but not the samples as a whole) are in different states.

The behavior of each individual cluster in a magnetic field is determined by whether its spontaneous magnetic moment **M** is fixed in space by anisotropy forces or fluctuates under the action of temperature.[15] Accordingly, it (cluster) plays the role of a one- domain or a superparamagnetic (SPM) particle.[1)] A transition from the one-domain to the SPM state during periods of time typical of static measurements (100 s) occurs under the condition $KV = 25k_BT$, where K is the anisotropy constant, V the volume of a cluster, and k_B the Boltzmann's constant.[15] In the presence of the field H, the energy barrier becomes lower, and the transition from the one-domain to the SPM state occurs at a lower temperature.[15,16] Since remanence preserves only for one-domain clusters, peculiarities of the $\sigma_T(H)$ dependence indicate that a large number of clusters in the sample Q remain in the one-domain state up to high temperatures. The fact that irregularities in the $\sigma_T(H)$ dependence observed for the Q sample is more pronounced that for the S sample at $T \geqslant 77$ K is also in accord with this conclusion. This is manifested most clearly at $T = 77$ K. The magnetization of the S sample increases smoothly with the field up to $H = 16$ kOe. At the same time, the $\sigma_T(H)$ dependence changes noticeably in the sample Q for $H = 12$ kOe: the magnetization increases more strongly in the field interval $H = (12–14)$kOe. The irregularity in the shape of isotherms can be due to the fact that some of one-domain clusters go over to the SPM state under the action of the field at $T = \text{const}$. The same mechanism can also explain the emergence of a low peak on the $\chi_0(T)$ curve for the Q sample near T_{CQ}. Such an effect was predicted theoretically and studied experimentally by Pfeifer and Schuppel.[16]

Thus, the cluster subsystems of samples S and Q are different although the total number of spins combined in clusters in S and Q samples virtually remains unchanged (see above). The difference is obviously manifested in a change in the size distribution function for clusters. If we estimate the linear size of a cubic one-domain particle at $T = 100$ K and $H = 0$, it must be not smaller than (150–320) Å for values of $K = (10^5–10^4)\text{erg/cm}^3$ (Li–Ga spinels).[14] The order of magnitude of this quantity is in accord with the results of neutron diffraction experiments.[13] Taking into account the changes occurring in the cluster subsystems, we have a basis for proposing that the degree of spatial heterogeneity in the arrangement of Ga^{3+} and Fe^{3+} ions also increases in the subsystem of disordered spins (matrix), leading to a change in magnetic properties which directly determine the long-range FM order.

The nature of changes caused by quenching, i.e., an increase in T_C as well as specific features of temperature dependences of the initial susceptibility $\chi_0(T)$ and spontaneous magnetization $\sigma_S(T)$ is in accord with the conclusions of the phenomenological theory.[17] According to Ref. 17, some peculiarities in thermodynamic behavior must be observed for heterogeneous substances with coexisting ferri- and antiferromagnetic phases (FM–AFM) coupled through the exchange interaction. The existence of clearly manifested spatial boundaries between FM and AFM phases is not necessary in this case: the role of the AFM subsystem can be played by two sublattices weakly interacting with other sublattices, which can be singled out in the structure of FM with complex compositions.[10] If we denote by T_N and T_C the Néel and Curie temperatures of hypothetic (i.e., isolated AFM and FM) subsystems, the following situation is observed for $T_N > T_C$. The system as a whole experiences only one (ferrimagnetic) phase transition at a temperature $T_C^* > T_C$. In the region of temperatures close to T_C of the ''pure'' FM phase, a strong (but not jumpwise as in the case of a phase transition) change in the relevant thermodynamic parameters must be observed. For example, the value of $\sigma_s(T)$ near T_C must decrease, but not to zero. In the region $T_C < T < T_C^*$, weak FM order with a spontaneous magnetization $\sigma_s \neq 0$ must be preserved due to the exchange interaction with the AFM subsystem.

If we identify T_{CS} with T_C and T_{CQ} with T_C^* for the samples under investigation, it follows from Fig. 1 that the value of $\chi_0(T)$ decreases sharply, and the dependence $\sigma_S(T)$ changes significantly for the sample Q in the temperature range $T_1 \sim T_{CS}$. The existence of correlation between these characteristics obviously follows from the fact that $\chi_0(T) \sim \sigma_S^2/K$ (one-domain state) and $\chi_0(T) \sim \sigma_S^2/(3k_BT)$ (SPM) for rotations.[10] Taking into account the fact that the exchange between magnetically active ions (Fe^{3+}) in Li–Ga spinels is antiferromagnetic, and the matrix contains Fe^{3+} ions with a large number of broken exchange bonds, we cannot rule out that quenching can lead to changes in the matrix which are favorable for the realization of the mechanism considered in Ref. 17.

CONCLUSION

The influence of spatial heterogeneity of the short-range exchange on the formation of the long-range FM order in frustrated ferrimagnets was analyzed by studying magnetic properties of dilute spinels $Li_{0.5}Fe_{1.1}Ga_{1.4}O_4$ with the concentration of nonmagnetic ions Ga^{3+} ($x = 1.4$) close to the multicritical point $x_0 = 1.5$ of the $x–T$ diagram. The degree of composition disorder, and hence the spatial heterogeneity of exchange and magnetic structure were changed by using two regimes of thermal treatment of the samples, viz., quenching and slow cooling in the temperature range 1550–300 K.

The results of x-ray and magnetic studies as well as the presence of aging effects in quenched samples show that the distribution of magnetic and nonmagnetic ions (Fe^{3+} and Ga^{3+}) in the lattice is more nonuniform in the case of quenching than in the case of slow cooling. On account of the short-range nature of exchange, this corresponds to a higher extent of its spatial heterogeneity.

The data obtained from an analysis of magnetization isotherms $\sigma_T(H)$ at $T=4.2$ K, (77–300) K, and $H\leqslant 16$ kOe as well as temperature dependences of the initial susceptibility $\chi_0(T)$ show that the enhancement of spatial heterogeneity of exchange does not destroy the long-range ferrimagnetic order, but, on the contrary, leads to extension of its temperature range: the values of the Curie temperature increases from 160 to 242 K as a result of quenching. This effect was explained on the basis of the thermodynamic theory for heterogeneous substances with coexisting FM and AFM phases distributed continuously in space.

Thus, the results presented here confirm the possibility of existence of a long-range FM order in heterogeneous frustrated systems of the cluster type and indicate its stability relative to variations of the degree of heterogeneity of the short-range exchange.

[1] K. H. Fischer, Phys. Status Solidi B **116**, 357 (1983); *ibid.* **130**, 13 (1985).
[2] R. J. Birgeneau, R. A. Cowley, G. Shirane *et al.*, Phys. Rev. B **21**, 317 (1980).
[3] J. Hubsch, G. Gavoille, and J. Bolfa, J. Appl. Phys. **49**, 1363 (1978).
[4] I. Ya. Korneblit and E. F. Shender, Usp. Fiz. Nauk **126**, 233 (1978) [Sov. Phys. Usp. **21**, 832 (1978)].
[5] J. A. Midosh, in *Magnetism of Amorphous Systems* [Russian transl.], Metallurgiya, Moscow (1981).
[6] K. Levin, C. M. Soukoulis, and G. S. Grest, J. Appl. Phys. **50**, 1695 (1979).
[7] P. A. Beck, Phys. Rev. B **32**, 7235 (1985).
[8] K. Binder and A. P. Young, Rev. Mod. Phys. **58**, 801 (1986).
[9] C. Y. Huang, J. Magn. Magn. Mater. **51**, 1 (1985).
[10] S. V. Vonsobskii, *Magnetism* [in Russian], Nauka, Moscow (1971).
[11] N. N. Efimova, Yu. A. Popkov, and N. V. Tkachenko, Zh. Éksp. Teor. Fiz. **90**, 1413 (1986) [Sov. Phys. JETP **63**, 827 (1986)]; Fiz. Nizk. Temp. **16**, 1565 (1990) [Sov. J. Low Temp. Phys. **16**, 881 (1990)].
[12] N. N. Efimova, Yu. A. Popkov, and N. V. Tkachenko, Zh. Éksp. Teor. Fiz. **97**, 1208 (1990) [Sov. Phys. JETP **70**, 678 (1990)].
[13] N. N. Efimova, Yu. A. Popkov, G. A. Takzei *et al.*, Fiz. Tverd. Tela (St. Petersburg) **36**, 490 (1994) [Phys. Solid State **36**, 271 (1994)].
[14] M. I. Darby and E. D. Isaac, IEEE Trans. Magn. Mater. **10**, 259 (1974).
[15] Yu. I. Petrov, *Physics of Small Particles* [in Russian], Nauka, Moscow (1982).
[16] H. Pfeifer and W. Schuppel, J. Magn. Magn. Mater. **130**, 92 (1994).
[17] K. B. Vlasov and A. I. Mitsek, Fiz. Met. Metalloved. **14**, 498 (1962).

Translated by R. S. Wadhwa

Magnetic field induced phase transition in $A_{1-x}Ca_xMnO_3$ (A=Nd, Bi, Sm, Eu, Tb)

I. O. Troyanchuk, N. V. Samsonenko, and T. K. Solovykh

Institute of Solid State and Semiconductor Physics, Byelorussian Academy of Sciences, 220072 Minsk, Byelorus

V. A. Sirenko

B. Verkin Institute for Low Temperature Physics and Engineering, National Academy of Sciences of the Ukraine, 310164 Kharkov, Ukraine

H. Szymczak and A. Nabialek

Institute of Physics, Polish Academy of Sciences, 02-668 Warsaw, Poland
(Submitted March 11, 1997; revised May 5, 1997)
Fiz. Nizk. Temp. **23**, 1074–1077 (October 1997)

A study of $Nd_{0.6}Ca_{0.4}MnO_3$ shows that the application of a magnetic field at 4.2 K induces a transition from the insulating antiferromagnetic state to the conducting ferromagnetic state, which is accompanied by a decrease in the sample volume by 0.1%. The replacement of Nd ions by Bi ions leads to stabilization of the antiferromagnetic state, while the substitution of Sm and Eu ions results in manifestation of properties typical of spin glasses.
 [S1063-777X(97)00710-X]

INTRODUCTION

In Refs. 1–3, it is shown that the compounds $Pr^{3+}_{1-x}Ca^{2+}_xMnO_3 (0.3 \leqslant x \leqslant 0.5)$ and $Pr^{3+}_{0.5}Sr^{2+}_{0.5}MnO_3$ in an external magnetic field experience a metamagnetic transition from the antiferromagnetic to the ferromagnetic state. As a result, the electrical conductivity decreases by 6–8 orders of magnitude, and the compounds become a metal. Below 30 K, the transition is irreversible. It was proposed[1–3] that the transition is due to ''melting'' of the charge-ordered phase under the action of the magnetic field. The Mn^{3+} and Mn^{4+} ions in the antiferromagnetic state are structurally ordered in the ratio 1 : 1, while in the ferromagnetic states these ions are disordered. The loss in energy during a metamagnetic transition as a result of disordering of ions and orbitals is compensated by an energy gain during stabilization of the metallic and ferromagnetic states in an external magnetic field. In addition, the antiferromagnetic phase is characterized by smaller structural distortions. Another mechanism of this phenomenon, which is based on field-induced magnetic states of the ''ferron'' type, was proposed by Nagaev.[4]

In this publication, we report on the results of a study of samples of $A_{0.6}Ca_{0.4}MnO_3$ (A=Nd, Bi, Eu, Sm) in magnetic fields up to 120 kOe.

EXPERIMENT

The samples were obtained from simple oxides of AR grade according to the conventional ceramic technology. The final synthesis was carried out at 1720 K. In order to obtain stoichiometric samples, the samples were cooled slowly at a rate of 100 K/h.

Magnetization was measured on a vibrating sample magnetometer, magnetostriction was measured by the strain-gauge technique, electrical conductivity was determined by the conventional four-probe method, and Young's modulus by the resonance method.

DISCUSSION OF RESULTS

It was found that doping of $NdMnO_3$ with Ca ions leads to a transition from a weakly ferromagnetic state of the Dzyaloshinskii–Moriya type to the ferromagnetic state for the Ca concentration $x=0.2$, accompanied by an increase in the critical temperature from 89 to 128 K (Fig. 1). A further increase in the concentration of Ca lowers the magnetization, and compounds with $x=0.4$ become antiferromagnetic. A qualitatively similar behavior was also observed for $Eu_{1-x}Ca_xMnO_3$ (see Fig. 1). However, the magnetization of samples with $x=0.2$ from the europium series is lower than that expected in the case of ferromagnetic ordering of Mn^{3+} and Mn^{4+} ions (the total orbital momentum of Eu^{3+} is equal to zero, and the contribution of the rare- earth sublattice to the magnetization can be neglected). On the other hand, the magnetization of Eu-based compounds with $x=0.3$ and 0.4 is higher than the magnetization of similar Nd-based compounds.

Figure 2 shows temperature dependences of magnetization of samples of $A_{0.6}Ca_{0.4}MnO_3$ (A = Nd, Sm) and $(Nd_{0.45}Bi_{0.15})Ca_{0.4}MnO_3$ in a magnetic field of 200 Oe. At low temperatures, the magnetization of the Sm-based sample is considerably higher, and of the Bi-based sample is much lower than that for Nd-based sample. Above 200 K, the magnetization of Nd- and Bi-based samples increases with temperature. A similar behavior was also observed for $Pr_{0.6}Ca_{0.4}MnO_3$ and was explained in Refs. 1 and 2 by charge ordering leading to antiferromagnetism. At 4.2 K, an external magnetic field induces in $Nd_{0.6}Ca_{0.4}MnO_3$ a transition from the antiferromagnetic to the ferromagnetic state (Fig. 3), which starts in fields above 30 kOe. The transition is irreversible, and a reverse transition to the antiferromagnetic state requires a heating of the sample to a temperature ex-

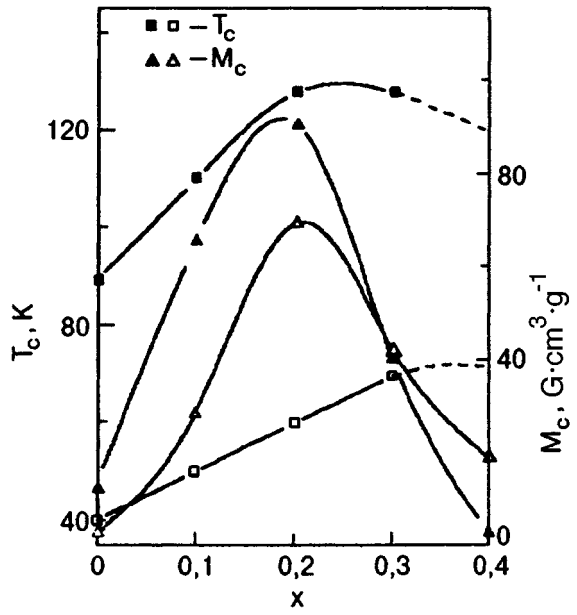

FIG. 1. Concentration dependence of spontaneous magnetization M_s and critical temperature T_c in $Nd_{1-x}Ca_xMnO_3$ (▲,■) and $Eu_{1-x}Ca_xMnO_3$ (△,□) compounds. At temperatures below the dashed curve, the magnetization depends on past history.

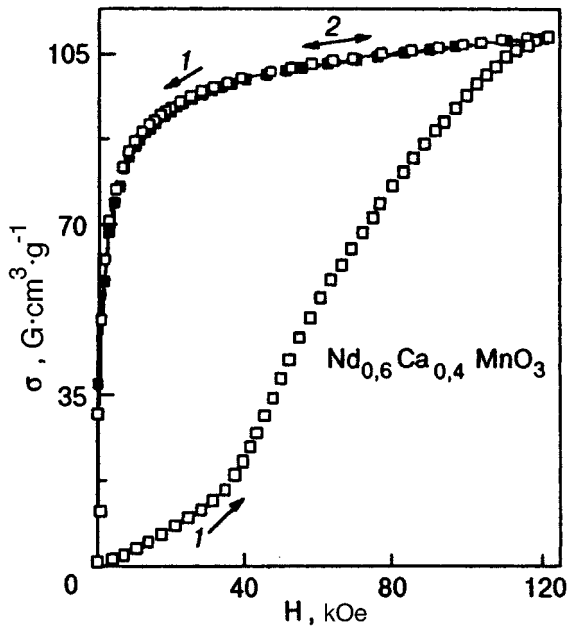

FIG. 3. Field dependence of magnetization for $Nd_{0.6}Ca_{0.4}MnO_3$ at 4.2 K: first cycle of measurements (curve *1*) and second cycle (curve *2*).

ceeding 50 K. The transition is accompanied by negative striction approximately by 0.1% of the sample volume ($3\Delta L/L \approx \Delta V/V$) (Fig. 4). In the field range 30–120 kOe, the resistivity decreases from 10^6 to $10^{-2}\Omega\cdot$cm. The conducting state remains stable after the removal of the field. In a sample of $(Nd_{0.45}Bi_{0.15})Ca_{0.4}MnO_3$, the transition is shifted towards stronger fields and is also reversible in field (Fig. 5).

In $(Nd_{0.3}Bi_{0.3})Ca_{0.4}MnO_3$, no metamagnetic phase transformations were observed up to 120 kOe (see Fig. 5).

A different behavior was observed for the systems $Eu_{1-x}Ca_xMnO_3$ and $Sm_{1-x}Ca_xMnO_3$ (Fig. 6). In these compounds, the magnetization increases nonlinearly with the field, which is typical of superparamagnets and spin glasses. As the Ca concentration increases, the magnetization becomes smaller.

The measurements of Young's modulus revealed a crystal structure phase transition at temperatures slightly lower than the room temperature (Fig. 7). The transition temperature changes insignificantly with the composition. In

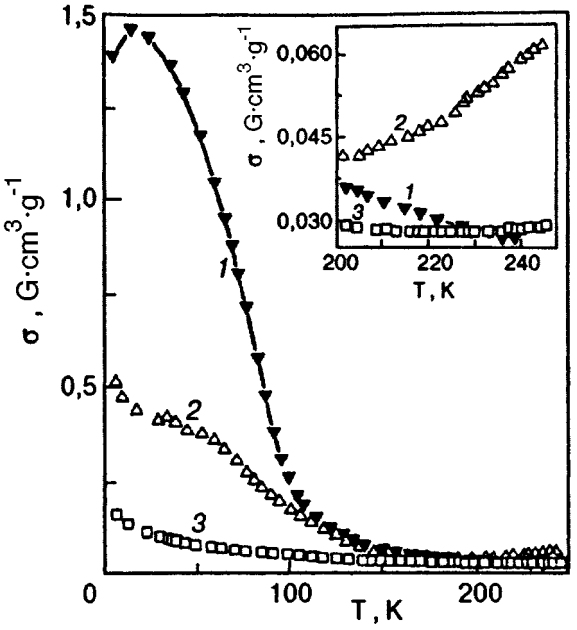

FIG. 2. Temperature dependences of magnetization for $Sm_{0.6}Ca_{0.4}MnO_3$ (curve *1*), $Nd_{0.6}Ca_{0.4}MnO_3$ (curve *2*), and $(Nd_{0.45}Bi_{0.15})Ca_{0.4}MnO_3$ (curve *3*) in a field of 200 Oe (cooling in $H=200$ Oe). The inset shows the behavior of $\sigma(T)$ at temperatures above 200 K.

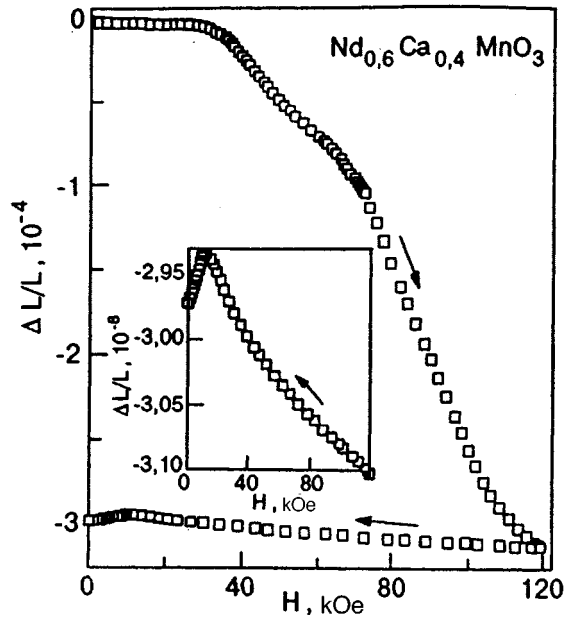

FIG. 4. Magnetostriction isotherms for $Nd_{0.6}Ca_{0.4}MnO_3$ at 4.2 K.

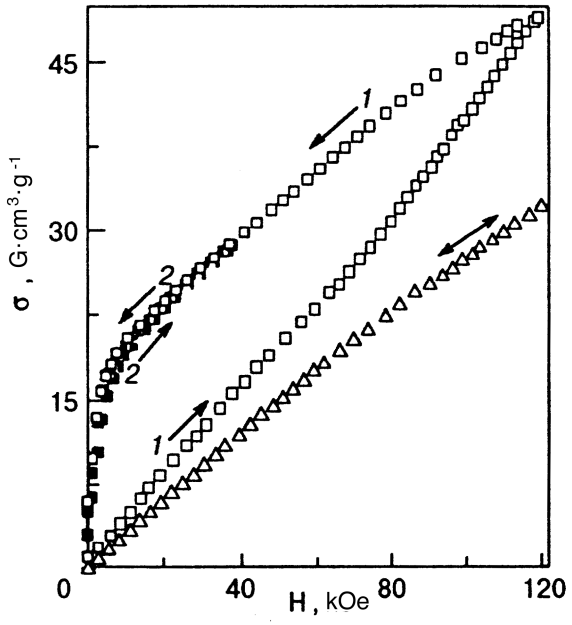

FIG. 5. Magnetization isotherms recorded at 4.2 K for samples of $(Nd_{0.3}Bi_{0.3})Ca_{0.4}MnO_3$ (△) and $(Nd_{0.45}Bi_{0.15})Ca_{0.4}MnO_3$ (□,■): first cycle of measurements (curve *1*) and second cycle (curve *2*).

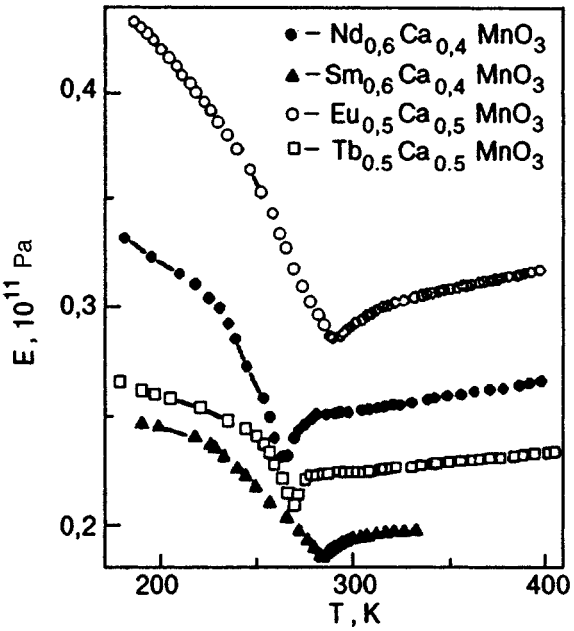

FIG. 7. Temperature dependence of Young's modulus for compounds $A_{0.6}Ca_{0.4}MnO_3$ (A = Nd, Sm) and $A_{0.5}Ca_{0.5}MnO_3$ (A = Eu, Tb).

$Pr_{0.6}Ca_{0.4}MnO_3$, the Mn^{3+} and Mn^{4+} ions are ordered at $T=250$ K.[2] Near 250 K, the magnetization of $Nd_{0.6}Ca_{0.4}MnO_3$ (see Fig. 2) has the maximum value as in $Pr_{0.6}Ca_{0.4}MnO_3$.[2] Consequently, we can assume that the transition in Sm- and Eu-based samples near the room temperature is also due to the ordering of the Mn^{3+} and Mn^{4+} ions. As in the case of $Pr_{1-x}Ca_xMnO_3$, ordering takes place over a wide range of concentrations of Ca ions, which leads to a drop in the spontaneous magnetization in compounds with $x>0.2$.

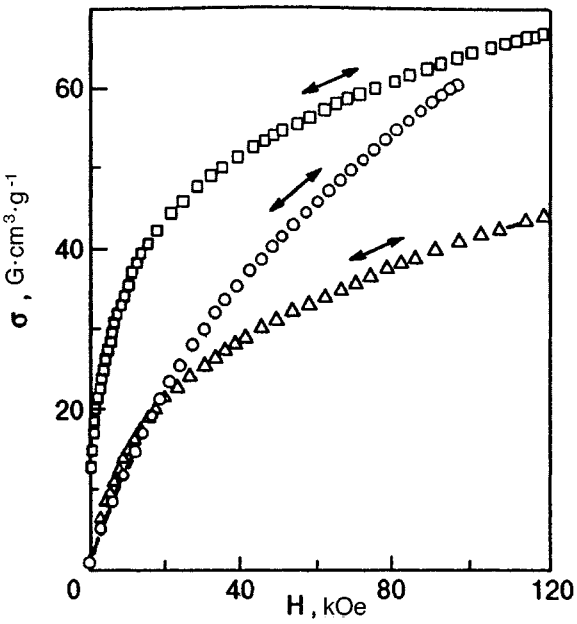

FIG. 6. Magnetization isotherms recorded at 4.2 K for samples of $Sm_{0.6}Ca_{0.4}MnO_3$ (△) and $Eu_{1-x}Ca_xMnO_3$ for $x=0.3$ (□) and 0.4 (○).

However, the magnetic properties of the compounds $A_{0.6}Ca_{0.4}MnO_3$ (A = Bi, Eu, Sm, Nd) differ basically. In Bi-based samples, antiferromagnetic exchange interactions are stabilized, and ferromagnetic clusters are virtually absent (see Fig. 5). In $Nd_{0.6}Ca_{0.4}MnO_3$, the antiferromagnetic structure is stable below 30 kOe (see Fig. 3), while Eu- and Sm-based compounds exhibit properties of spin glasses. For this reason, we believe that $Sm_{0.6}Ca_{0.4}MnO_3$ and $Eu_{0.6}Ca_{0.4}MnO_3$ consist of small antiferromagnetic and ferromagnetic clusters. The magnetic structure of antiferromagnetic clusters is stable in fields up to 120 kOe. Chemical analysis did not reveal any significant deviations from the stoichiometrical composition in Sm- and Eu-based samples. Consequently, the change in the properties in the series $A_{0.6}Ca_{0.4}MnO_3$ (A = Nd, Sm, Eu) is due to increasing mismatching in the ionic radii of Mn and the rare-earth ion. In all probability, the system does not preserve a strictly homogeneous composition, but splits into microscopic domains with different types of crystalline structure.

This research was supported by the Foundation of Fundamental Studies of the Byelorus Republic (Project F96-135) and the Polish Committee on Scientific Research (KBN Grant No. 2 P03B 09512).

[1] A. Asamitsu, Y. Moritomo, Y. Tomioka *et al.*, Nature (London) **373**, 407 (1995).
[2] Y. Tomioka, A. Asamitsu, Y. Moritomo *et al.*, Phys. Rev. Lett. **74**, 5108 (1995).
[3] M. R. Lees, J. Barrat, G. Balakrishnan *et al.*, Phys. Rev. B **52**, R4303 (1995).
[4] E. L. Nagaev, Phys. Usp. **166**, 833 (1996).

Translated by R. S. Wadhwa

Relaxation and effects of potential gradient in a Bi point contact

V. V. Andrievskii, Yu. F. Komnik, and S. V. Rozhok

*B. Verkin Institute for Low Temperature Physics and Engineering, National Academy of Sciences of the Ukraine, 310164 Kharkov, Ukraine**

(Submitted February 28, 1997; revised March 24, 1997)
Fiz. Nizk. Temp. **23**, 1078–1087 (October 1997)

It is shown that electron relaxation in an emitter-type point contact strongly affects the position of the first line of transverse electron focussing (EF) in Bi on the magnetic field scale. As a result, the energy of electrons leaving the point contact region is lower than the energy eV determined by the voltage applied to the point contact. In the case of strong currents, the intrinsic field of the current also affects the position of the EF line. The additional shift of the EF line under the action of this factor depends on V nonlinearly in view of strong nonlinearity of the current–voltage characteristics of Bi point contacts. It is shown that this nonlinearity can be explained by an increase in the concentration of charge carriers in the point contact region under the action of the gradient of potential distribution and interband tunneling. These mechanisms give an accurate description of the nonlinearity of the current–voltage characteristics of Bi point contacts. © *1997 American Institute of Physics.* [S1063-777X(97)00810-4]

Electron focussing by a transverse magnetic field[1] is noticeably affected by relaxation of nonequilibrium charge carriers.[2–4] This makes it possible to use the method of electron focussing (EF) for studying the electron–phonon relaxation on a cyclotron trajectory[5] and in a point contact.[6–9] In these regions, relaxation processes occur differently. The electron–phonon relaxation on a cyclotron trajectory takes place under the conditions of ballistic motion of electrons in a pure metal and leads to a decrease in the amplitude of the EF line. This circumstance was used in Ref. 5 for determining the dependence of electron–phonon relaxation time in Bi on the excess electron energy $\delta\varepsilon$ upon a change in the latter quantity in a wide range (up to $\delta\varepsilon \sim 3\varepsilon_F$).

The electron–phonon relaxation in a point contact occurs under a strong elastic scattering of electrons. If the voltage across the point contact ensures that the electron energy is higher than the limiting Debye energy, the drift velocity of electrons becomes higher than the velocity of sound, leading to the emission of the Cherenkov radiation of nonequilibrium phonons.[9] The EF method makes it possible to determine the phonon modes emitted in such a process. The emission of phonons of preferred frequencies is accompanied by the emergence of additional peaks against the background of the first EF line. These peaks appear due to the fact that discrete relaxation leads to the formation of group of electrons with an energy differing from that of the main group of injected electrons by the phonon relaxation energy. A manifestation of discrete phonon relaxation on the EF curve was called the ''cyclotron'' spectroscopy of the electron– phonon relaxation in a point contact.[3,6] It was found[9] that longitudinal optical phonons with energy ~ 12 meV dominate in the spectrum of emitted nonequilibrium phonons in the case of supersonic drift in a Bi point contact.

If the inelastic energy relaxation length l_ε for electrons is commensurate with the point contact size d, the emission of phonons is observed not only after the attainment of supersonic drift, but also for an infinitely small value of the excess energy for electrons. After the attainment of the Debye energy, phonons are emitted in the entire spectral region. As a result of partial electron energy loss due to electron–phonon relaxation in a point contact, the energy of electrons emitted from the point contact to a ballistic trajectory is lower than the energy eV determined by the voltage applied to the point contact. As a result, an EF line appears for a magnetic field value smaller than that calculated for the energy eV. However, this is not the only reason behind the deviation of the EF line from the calculated position. Among possible reasons, we can also mention the effect of intrinsic magnetic field of the current through the emitter. Here we consider the effect of relaxation and other factors on the position of the EF line. At the same time, we consider another peculiarity in the properties of Bi point contacts, which is interconnected with the above problem (see below), namely, the nonlinearity of their current–voltage characteristics.

POSITION OF EF LINE

In our experiments on bismuth, we used the classical method of electron focussing in a transverse magnetic field.[1] The experimental technique used by us is described in detail in Refs. 8 and 9. A point contact was created on a perfect trigonal face of Bi by the ''needle to anvil'' method. The role of the needle was played by copper wires of diameter 0.1 mm sharpened by electrochemical polishing (in a 10% solution of KOH) to a diameter ~ 1 μm. The point contact was in the form of a hole or a very short channel of length a commensurate with or smaller than the hole diameter d.

In the EF method, the electrons injected through a point contact (emitter) to a perfect metallic single crystal perform

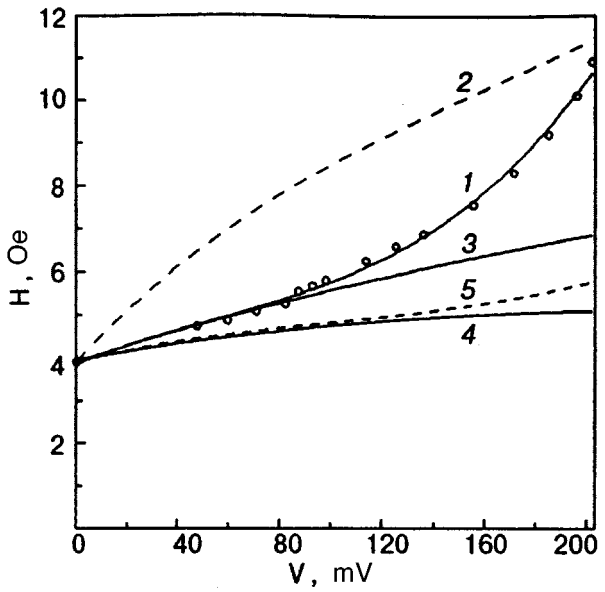

FIG. 1. Magnetic field corresponding to the position of the first EF line as a function of the voltage applied to the emitter: experimental curve (*1*), the dependence predicted by formula (3) (curve *2*), calculated taking into account relaxation in the point contact according to (4) for $l_\varepsilon = \text{const}$ (curve *3*) and $l_\varepsilon \propto \varepsilon^{-1/2}$ (curve *4*), and taking into account the change in the effective concentration of charge carriers in the point contact (curve *5*).

cyclotron motion in a magnetic field parallel to the crystal surface and create a potential across another point contact (collector). The collector potential recorded as a function of the magnetic field $U_0(H)$ has a sharp peak at the field value H_0 for which the largest group of electrons with the maximum radius of trajectory in the real space participates in the formation of the signal. For Fermi electrons, the EF line corresponds to the magnetic field

$$H_{0F} = \frac{2cp_{zF}}{eL}, \tag{1}$$

where p_{zF} is the component of the Fermi quasimomentum, the z-axis is directed along the normal to the surface, and L is the separation between the emitter and the collector. In the EF method, use is made of nonequilibrium electrons which have a correction $\delta\varepsilon$ to the Fermi energy due to the voltage V applied to the emitter. The focussing field H_0 is determined by a relation similar to (1), but p_z corresponds to the constant-energy surface $\varepsilon_F + \delta\varepsilon$ and has the value $p_z = p_{zF}(1 + \delta\varepsilon/\varepsilon_F)^{1/2}$. (Here and below, we will use a quadratic energy–momentum relation as a approximation suitable for analyzing the problems formulated above.) The focussing field H_0 increases with the excess energy of electrons in accordance with the relation

$$H_0 = H_{0F}\left(1 + \frac{\delta\varepsilon}{\varepsilon_F}\right)^{1/2}. \tag{2}$$

It was found[8,9] that the actual increase in the focussing field is slightly smaller than predicted by formula (2) if we assume that $\delta\varepsilon = eV$. Curve *1* in Fig. 1 is the dependence of H_0 on the voltage V across a point contact experimentally observed for one of the samples, while curve *2* is the theoretical curve calculated by using the relation

$$H_{0T} = H_{0F}\left(1 + \frac{eV}{\varepsilon_F}\right)^{1/2}. \tag{3}$$

It was proved in Ref. 10 that for $eV \geqslant \varepsilon_F$, the EF line is blurred to a certain extent, and the position of the peak on the curve may not satisfy relation (2). However, the magnetic field corresponding to maximum electron orbits in the real space from the emitter to the collector and corresponding to the sharp descent of the EF line must correspond to formula (2). The experimental curves in Fig. 1 are plotted on the basis of recording of the derivatives $dU_c/dI_l(H)$, which determine just the field of the sharp descent of the EF line; for this reason, the blurring of the EF line for large values of V cannot be responsible for the discrepancy between the experimental and theoretical curves in Fig. 1. It should be noted that this discrepancy is observed starting from very small values of the applied voltage.

We assume that the reason behind the decrease in the excess energy of electrons emitted from the point contact as compared to eV is partial energy relaxation occurring in the point contact region. In this case,

$$H_{0R} = H_{0F}\left(1 + \frac{eV}{\varepsilon_F}\left(\frac{l_\varepsilon}{a}\right)\right)^{1/2}, \tag{4}$$

where $l_\varepsilon = (D\tau_{\text{in}})^{1/2}$ is the energy relaxation length, a the length of the point contact channel, $D = v_F^2\tau_i/3$ the diffusion coefficient for electrons, τ_i the elastic relaxation time, and τ_{in} the inelastic relaxation time. The ratio l_ε/a takes into account the fact that the applied voltage V creates an electric field over the length a ($V = E/a$), but an electron gains energy in the field E over the length l_ε. In the hole model of a point contact, $a \approx d$. The appearance of the ratio l_ε/a in (4) corresponds to a decrease in the value of H_{0R} relative to H_{0T}.

Let us introduce a certain value $(l_\varepsilon/a)_0$ for the initial segment of experimental dependences $H_0(V)$. It can be easily determined from a comparison of the applied voltage V and the effective voltage $\tilde{V}$,[8] which give the same value of magnetic field corresponding to the position of the EF line on the experimental (*1*) and theoretical (*2*) curves. Curve *3* in Fig. 1 is plotted in accordance with formula (4) for the obtained value $(l_\varepsilon/a)_0$.[1)] It coincides with the experimental dependence $H_0(V)$ only on the initial segment, and then deviates noticeably from the experimental curve upon an increase in V. This increasing difference can be explained by two possible reasons: either the effect of relaxation processes becomes weaker upon an increase in the electron energy, or there exists another factor responsible for the difference between the experimental values of H_0 and theoretical values for a noticeable excess energy of electrons. The intersection of experimental and theoretical dependences for large values of V also points to the existence of an additional reason. Indeed, the theoretical value of H_{0T} in the relaxation model is the maximum possible value for $\delta\varepsilon = eV$.

The suppression of relaxation upon an increase in energy is possible in the case of a special energy dependence of the elastic relaxation time. Indeed, the velocity v_F appearing in the expression for l_ε increases with the energy $\varepsilon = \varepsilon_F + \delta\varepsilon$ in proportion to $\varepsilon^{1/2}$, while the value of τ_{in} obviously changes

with energy in the same way as the value of τ_{ep} changes with temperature (see, for example, Refs. 11–13), i.e., in proportion to ε^{-2}. An increase in the value of l_ε with energy can be observed when τ_i is a function of energy and is described by the dependence $\tau_i \propto \varepsilon^p$, where $p>1$, as, for example, in semiconductors in the case of scattering by charged impurities ($p=3/2$). We will return to the energy dependence of τ_i later.

An additional factor responsible for the difference between the experimental values of H_0 and those calculated according to formula (4) in the relaxation model is the possible influence of thermoelectric effects emerging during heating of the emitter in the case of a strong current. The polarity of the thermoelectric field in a heated Cu–Bi contact coincides with the polarity of the applied electric field ensuring the electron flow to bismuth. The presence of such a field would lead to an increase in the observed focussing field. According to estimates, however, this change in H_0 should not be significant. In Ref. 9, the temperature increase in the point contact region under the action of current is estimated on the basis of the thermal conductivity equation and it is shown that the increase in temperature near the point contact boundary of radius $r\sim 1$ μm amounts to ~ 1.5 K for typical values of the Bi point contact resistance $R\sim 1$ Ω and for the current $I\sim 0.1$ A. The thermoelectric voltage in this case amounts to 10^{-5}–10^{-4} V.

A more realistic factor leading to an increase in experimental values of H_0 relative to the expected dependence $H_{0R}(V)$ for the relaxation model is the intrinsic magnetic field of the current flowing into the crystal through the point contact.[14] In the region of maximum current concentration, i.e., at the boundaries of the point contact aperture, the intrinsic magnetic field of the current can attain a noticeable value (according to our estimates, the field can be as high as ~ 10 Oe for a current ~ 100 mA), but it decreases rapidly with increasing distance in proportion to r^{-1}. The magnitude of the intrinsic magnetic field of current is proportional to the current I, which is a nonlinear function of applied voltage in the case of Bi point contacts.

NONLINEARITY OF THE CURRENT–VOLTAGE CHARACTERISTIC

The current–voltage characteristics (IVC) of Bi point contacts are nonlinear (Fig. 2). We are speaking of a considerable nonlinearity of IVC of a point contact rather than of local nonlinearities which are observed while recording the second derivative d^2I/dV^2, and serve as the basis of point-contact spectroscopy of the electron–phonon interaction in metals[2) 15,16] (it should be noted, by the way, that the application of this method to bismuth proved to be ineffective[17]).

The IVC measured by Bogod *et al.*[18] with the help of the pulse method on Bi single crystal whiskers (of diameter 3 μm and length 0.3–0.6 cm) indicated a nonlinearity of the opposite sign as compared to that observed for point contacts. This nonlinearity of the fracture type, which appears on the current–voltage characteristics for an electric field strength of the order of 10^{-2} V·cm^{-1} is due to generation of phonons by electrons and holes in Bi, which drift in the electric field at a supersonic velocity. The drift of electrons and holes as well as of acoustoelectric flows generated by them occurs in opposite directions; the generation of phonons is accompanied by an increase in the differential resistance of the sample. Such a nonlinearity must also be present in the IVC of Bi point contacts since supersonic electron drift is attained for $eV>h\nu_D$, but this nonlinearity is apparently insignificant in comparison with the dominating smooth nonlinearity presented in Fig. 2 and having a different origin.

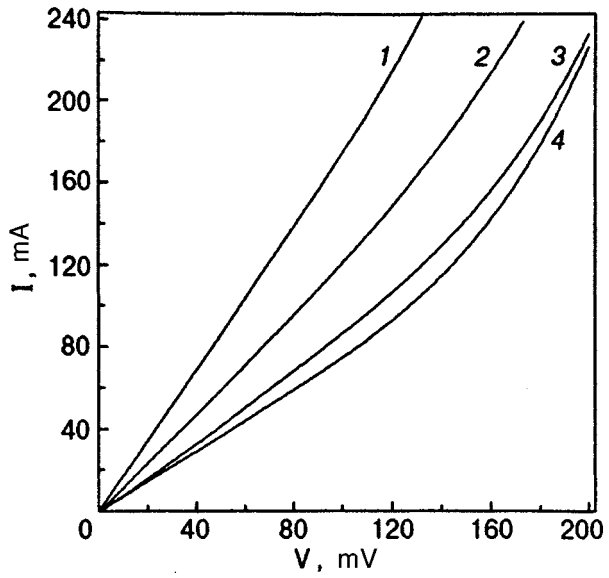

FIG. 2. Current–voltage characteristics for Bi point contacts at $T=4.2$ K and for different point contact resistances R (for $V\to 0$), Ω: 0.55 (curve *1*), 0.86 (curve *2*), 1.21 (curve *3*), and 1.38 (curve *4*).

The nonlinearity of the IVC of Bi point contacts under investigation can be associated, in accordance with the ideas developed in Refs. 19 and 20 with the dependence of the elastic relaxation time τ_i on the electron energy. Shekhter[19] proved that the differential derivative $dI/dV(V)$ in semiconducting point contacts in the diffusive conduction mode and in the case of a small contribution of inelastic relaxation reflects the energy dependence of τ_i. It can be reconstructed from an analysis of the nonlinearity of the IVC for a point contact[19] by using the relation[3)]

$$\frac{\tau_i(\varepsilon)}{\langle \tau_i \rangle} = \frac{3}{2}\,\varepsilon^{-3/2}\int_0^{\varepsilon} du\; u^{1/2}\,\frac{R(0)}{R(u)}, \tag{5}$$

where $R=(dI/dV)^{-1}$ is the differential resistance and $\langle \tau_i \rangle$ is the mean value of τ_i.

Proceeding from the assumption that the nonlinearity of the IVC for Bi point contacts is completely determined by a special dependence $\tau_i(\varepsilon)$, we made an attempt to reconstruct the form of this dependence by using Eq. (5). Calculations led to an odd result: the ratio $\tau_i/\langle \tau_i \rangle$ remains close to unity up to a voltage of 80 mV, and then increases with V in proportion to ε^2, or rather to $\exp \varepsilon$, the increase being not very strong (by 20–40% for the maximum energy value of ~ 200 meV). Functional dependences of τ_i on energy of this type are unknown. Besides, the dependence $\tau_i(\varepsilon)$ obtained for point contacts with different resistances did not coincide

in contrast to what should be observed in the case of a universal physical reason behind the nonlinearity. Thus, the version concerning the reason behind the emergence of nonlinearity on IVC being verified proved to be nonrealistic. Similar assumptions made above in connection with a considerable increase in H_0 at large voltages as compared to the dependence $H_{0R}(V)$ taking relaxation into account should also be rejected since the obtained $\tau_i(\varepsilon)$ dependence fail to describe this discrepancy. If we assume in the limit that τ_i is independent of energy (as in the case of metals) and take into account the most realistic functional energy dependences of the parameters appearing in l_ε (i.e., $v_F \propto \varepsilon^{1/2}$ and $\tau_{\text{in}} \propto \varepsilon^{-2}$, relation (4) assumes the form

$$H_{0R} = H_{0F}\left[1 + \frac{eV}{\varepsilon_F}\left(\frac{l_\varepsilon}{a}\right)_0\left(1 + \frac{eV}{\varepsilon_F}\right)^{-1/2}\right]^{1/2}. \tag{6}$$

The dependences $H_{0R}(V)$ constructed according to (6) for the samples under investigation proved to be still weaker (see curve *4* in Fig. 1) than the dependences plotted for the initial value $(l_\varepsilon/a)_0$ (curve *3*).

Let us now consider other versions of explanation of nonlinearity on the IVC for point contacts.[4)] In view of specific band structure of Bi (small band overlapping), the passage of current through a point contact, i.e., the stabilization of a certain potential distribution in it, can be accompanied by a change in the number of charge carriers. Shik[21] proved that the presence of a potential relief $U(z)$ of any form in a semimetal leads to an increase in the average concentration of charge carriers. Under the condition of nonuniform potential, the concentration of electrons and holes is a position function. If the potential at a certain point of the sample differs from its average value, this leads to a displacement of the Fermi level relative to the band edges and to an increase in the concentration of charge carriers of one polarity and a decreases in the concentration of charge carriers of the opposite polarity at this point. Since the density of states is an increasing function of energy, the total concentration of charge carriers increases, but the condition of compensation of charge carriers of opposite polarities is preserved. It was shown in Ref. 21 that the in the case of a small amplitude of potential variation, we have

$$\overline{n} = n_0\left(1 + \frac{3}{8}\frac{\widetilde{U}^2 - \widetilde{U}^2}{\varepsilon_F^e \varepsilon_F^h}\right). \tag{7}$$

We assume that the potential distribution in the point contact channel is linear, i.e., $U(z) = eEz$, and choose the reference point for the potential so that the mean value of U is equal to zero, i.e., we measure the z-coordinate from the center of the channel. In this case, we have

$$\widetilde{U}^2 = \frac{1}{a}\int_{-a/2}^{a/2}(eEz)^2 dz = \frac{1}{12}(eE)^2 a^2 = \frac{1}{12}(eV)^2. \tag{8}$$

For convenience, we put $\varepsilon_F^h = (1/\gamma)\varepsilon_F^e$ ($\gamma \approx 2$) in (7), which gives

$$\overline{n} = n_0\left[1 + \frac{\gamma}{32}\left(\frac{eV}{\varepsilon_F}\right)^2\right]. \tag{9}$$

The model considered above describes the final pattern of spatial redistribution of charge carriers under a time-independent nonuniform potential. For a time-dependent situation in the current mode, we must apparently introduce a certain coefficient $k_1 < 1$ in the second term in (9), which takes into account the extent to which the actual spatial distribution of charge carriers is close to the expected distribution. It should also be noted that the proposed idealized model cannot correspond completely to the heterojunction used by us.

In the approximation of energy-independence of the probability of elastic scattering of charge carriers, a change in the point contact resistance as a result of an increase in the carrier concentration due to the effect of potential nonuniformity can be described by the following relation:

$$R(V) = R_0\left[1 + k_1\frac{\gamma}{32}\left(\frac{eV}{\varepsilon_F}\right)^2\right]^{-1}. \tag{10}$$

The theoretical dependences $R(V)$ plotted according to (10) (dashed curves in Fig. 3) successfully describe the initial region of experimental dependences (presented in Fig. 3 by different symbols for three samples). In some cases, a satisfactory description of the entire experimental curve can be obtained (see, for example, curve *1*). In this case, we had to take a very small value for the coefficient $k_1 = 0.05 \pm 0.01$ for all the experimental data under consideration. As the voltage V increases, the experimental dependences deviate from those calculated by formula (10); the reason behind this deviation will be considered below. Apparently, the small value of the coefficient k_1 reflects the real efficiency of the model considered above as applied to a heterojunction as well as the assumptions made by using the results obtained by Shik[21] (the application of formula (7) in the case of a large amplitude of potential variation and the assumption concerning the linear distribution of the potential in the point contact channel).

The evolution of the idea about the effect of potential distribution in a point contact on the charge carrier concentration leads to one more statement: the deformation of potential for large values of V can be so strong that interband tunneling becomes possible. The latter is accompanied by an exponential increase in the charge carrier concentration in the conduction band (in the case of semiconductors, this effect is known as the Zinner breakdown). In the case of bismuth, the model of interband tunneling presumes that tunneling of electrons from the valence band to states with the Fermi energy begins when the quantity eV attains values exceeding the electron energy ε_g measured from the top of the valence band (i.e., the sum of the Fermi energy ε_F^e for electrons and the width Δ_L of the energy gap between the valence band and the conduction band at the point L). This leads to generation of holes in the valence band.

The idea of interband tunneling was used for the first time for explaining the nonlinearity of IVC in three-dimensional Bi bridges by Vdovin and Kasumov.[22] According to these authors, the nonlinear correction ΔI to current is correctly described by the law $\Delta I \propto \exp(-V_0/V)$, where V_0 is the effective field determined by the geometrical size of the nanoconstriction. Similar observations were made by van der

Hilst *et al.*[23] for two-dimensional nanoconstrictions in films of $Bi_{0.95}Sb_{0.05}/Bi/Bi_{0.95}Sb_{0.05}$. The measuring technique used by these authors provided information concerning the change in the charge carrier concentration in the constriction region. The authors of Refs. 22 and 23 proceeded from the assumption that the interband tunneling is the only reason behind the nonlinearity of the IVC of the objects under investigation, and hence disregarded the possibility of an increase in the charge carrier concentration under the effect of nonuniform potential. In Ref. 23, the relative rate of generation of additional charge carriers was introduced in the form $\exp(-E_0/E)$, where E_0 is the characteristic field which has the following form in the theory of interband tunneling:

$$E_0=\frac{\pi m^{*1/2}\varepsilon_g^{3/2}}{2^{3/2}e\hbar}. \tag{11}$$

An analysis of experimental data on the basis of this conception made it possible to determine E_0 and the recombination length L_0. According to van der Hilst *et al.*,[23] the obtained value of E_0 increases (from 1.2×10^4 to 5×10^4 V·cm^{-1}) with the magnetic field strength under the effect of the formation of the Landau levels, but is close on the whole to the value of E_0 calculated according to (11). Van der Hilst *et al.*[23] assumed that $m^*=(4\pm2)\times10^{-3}m_0$ and $\varepsilon_g=\varepsilon_F+\Delta_L=27.6+15.3=42.9$ meV for bismuth[24] and obtained $E_0=2.2\times10^4$ V·cm^{-1}.

The mechanism of interband tunneling is supplementary relative to the mechanism of increase in the charge carrier concentration under a nonuniform potential. Let us estimate its relative effect on the process in general. The interband tunneling probability is determined by a function of the form $\exp(-E_0/E)$. Consequently, the charge carrier concentration must increase under the effect of interband tunneling according to the relation

$$n=n_0(1+k_2\ \exp(-E_0/E))=n_0(1+k_2\ \exp(-V_0/V)). \tag{12}$$

The total change in the charge carrier concentration in a point contact with increasing V has the form

$$n=n_0\left(1+k_1\frac{\gamma}{32}\left(\frac{eV}{\varepsilon_F}\right)^2+k_2\ \exp(-V_0/V)\right)=n_0f_c(V), \tag{13}$$

while the change in the point contact resistance must be described by the dependence

$$R=R_0f_c^{-1}(V). \tag{14}$$

In formula (12), we introduced $V_0=E_0a$, assuming that the applied voltage V generates an electric field over the length a. This length is unknown, and in our calculations we used tentative values of a corresponding to the configuration of the curve specified by the function $\exp(-V_0/V)$ for $V\ll V_0$. It was found that the most realistic value is $V_0\approx1$ V,[7] which corresponds to a quite reasonable point contact length $a\approx0.4$ μm. Besides, the coefficients k_1 and k_2 are fitting parameters. It should be noted that in the case when these coefficients are close to unity, the contribution of interband tunneling to the resistance becomes negligibly small as compared to the contribution of the effect of change in the charge carrier concentration under the influence of the field gradient. It was mentioned above, however, that the coefficient k_1 assumes a small value $\approx0.05\pm0.01$ as compared to the experimental value. On the contrary, the coefficient k_2 should be approximately equal to 40–50. In this case, the experimental dependences $R(V)$ can be described to a high degree of accuracy by relations (13) and (14) (solid curves in Fig. 3). In this case, the coefficients k_1 and k_2 for point contacts with different resistances are very close.

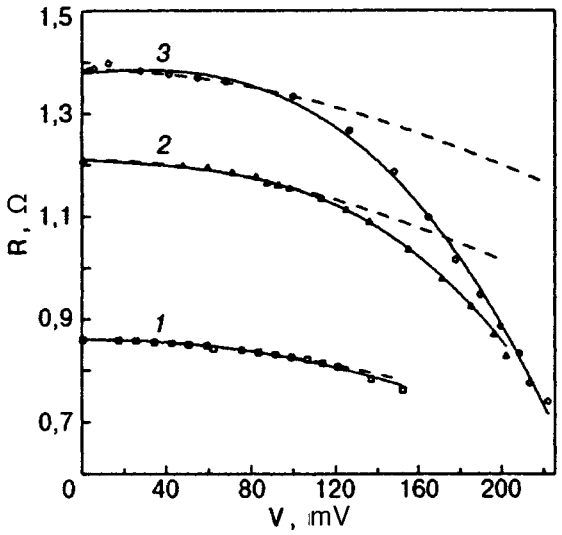

FIG. 3. Resistances of point contacts as functions of applied voltage; symbols correspond to experimental data, dashed curves describe dependences calculated according to (12) taking into account the nonuniform potential, and solid curves are calculated according to (16) taking into account interband tunneling. The point contact resistance (for $V\to0$), Ω: 0.86 (curve *1*), 1.21 (curve *2*), and 1.38 (curve *3*) at 4.2 K.

ONCE AGAIN ON THE POSITION OF THE EF LINE

It would be interesting to estimate whether the positive result obtained while describing the nonlinearity of IVC for a Bi point contact on the basis of the model taking into account potential gradient in the point contact can be used for explaining the dependence of the focussing field H_0 on the voltage applied to the point contact and creating a spatially nonuniform distribution of charge carriers with different polarities. Such a dynamic concentration gradient results in the emergence of a certain intrinsic electric field directed against the applied field. The intrinsic field is probably a reason behind the decrease in the efficiency of the voltage applied to the point contact. This idea requires a special theoretical analysis.

At the same time, we made an attempt to estimate the maximum possible contribution of the increase in the charge carrier concentration in a point contact to the process of focussing. Excess charge carriers can directly affect the position of the EF peak in the case when they reach the collector. In order to estimate the new position of the EF line, we use the familiar relation between the concentration and the boundary value of quasimomentum:

$$p_z=\hbar(3\pi^2)^{1/3}n^{1/3}=\hbar(3\pi^2)^{1/3}n_0^{1/3}f_c^{1/3}(V)=p_{F0}f_c^{1/3}(V).$$

Curve *5* in Fig. 1 illustrates the theoretical dependence (calculated by using formula (6)) with the cofactor $f_c^{1/3}(V)$ in which we have used the values of k_1 and k_2 obtained above. It can be seen that curve *5* is far from the experimental curve *1* and fails to explain the rapid increase in the latter curve relative to the theoretical curve *4* for the relaxation model.

The assumption concerning the possible contribution of excess change carriers generated in a point contact to the focussing curve is problematic. On one hand, electrons and holes emitted from the point contact move in opposite directions and are spatially separated. Consequently, ''recombination'' of charge carriers of opposite polarities on a ballistic trajectory from the emitter to the collector is hardly possible. However, recombination can take place in the region adjoining the point contact (for example, according to estimates,[23] the recombination length for excess charge carriers in Bi does not exceed 2–6 μm), and hence excess charge carriers probably do not reach a ballistic orbit. We also verified the hypothesis on the effect of excess charge carriers in a point contact on the relaxation process in it. If we assume that the cofactor appearing in l_ε in formula (4) change with the concentration n according to the familiar relations ($v_F \propto n^{1/3}$ and $\tau_{ep} \propto n^{-1}$ or $\tau_{ep} \propto n^{-1/3}$ in the ''pure'' and ''dirty'' limit respectively),[25] the theoretical curve deviates from curve *4* only slightly.

At the same time, the models considered above and leading to an increase in the charge carrier concentration in a Bi point contact (to be more precise, the nonlinearity of the IVC for the point contact associated with this effect) have an indirect influence on the displacement of the EF line upon an increase in the applied voltage. It should be noted that the increasing discrepancy between the experimentally observed values of H_0 (curve *1*) and the values of H_{0R} calculated in the relaxation model (curve *4*) resembles the change in the current through the point contact with the applied voltage (cf. curve *3* in Fig. 2). Such a similarity was observed by us for all the samples under investigation with different values of the initial resistance R_0 and with different degrees of nonlinearity. Moreover, it was found that the same values of current flowing through point contacts with different resistances correspond to approximately the same displacement $\Delta H_0 = H_0 - H_{0R}$. This leads to the assumption that the displacement ΔH_0 is due to the intrinsic magnetic field of current.

The intrinsic magnetic field of the current through a point contact bends the electron trajectories in the initial segment and must produce a ''defocussing'' effect on the electron flow since the polarity of this field relative to the applied magnetic field is different for electrons emitted from the point contact at angles φ with opposite signs (the angle φ is measured from the axis of the point contact channel). The electrons emitted along the channel axis and forming a peak on the EF curve experience the influence of the intrinsic magnetic field only in the periphery region relative to the contact axis, i.e., on the initial segment of a ballistic orbit. This leads to a displacement of the peak on the EF curve towards larger values of the applied magnetic field. Van Son *et al.*[14] analyzed theoretically the effect of intrinsic magnetic field on the position of the EF peak for a point contact on a silver single crystal. According to calculations, the relative displacement of the EF peak amounts to $\sim 1\%$ for a current 1.5 A. In the case of Bi, this value must be considerably larger. If we take into account the ratio of microscopic parameters for electrons in silver and bismuth, the relative displacement of the EF curve in Bi for a current 150 mA must be $\sim 10\%$. In actual practice, the shift of the EF line was larger than according to the estimates. The decisive role of the intrinsic magnetic field of current in the displacement of the EF line in question is confirmed by the fact that the relation between the current I and the displacement ΔH_0 is close to linear. An analysis of the entire body of experimental data leads to the empirical relation $\Delta H_0 = AI + BI^2$, where the coefficients A and B assume the average values 9×10^3 and 6×10^{-5} respectively (here I is measured in milliamperes and ΔH_0 in oersteds). Thus, the additional nonuniform magnetic field generated by current in a point contact effectively affects the ballistic trajectories of electrons and leads to a noticeable displacement of the leading edge of the EF line.

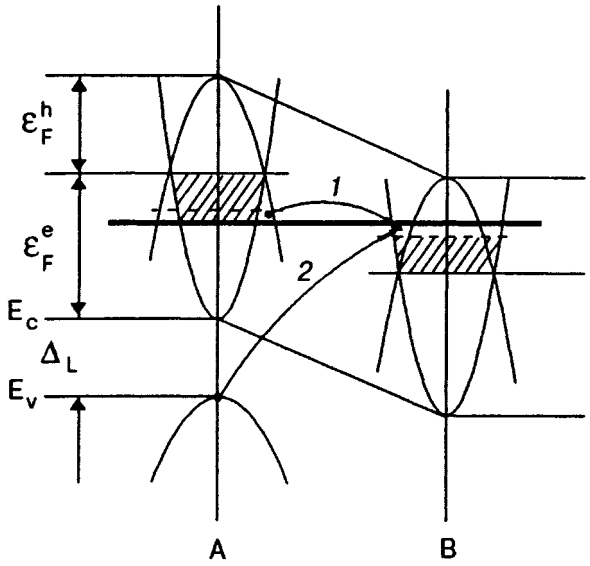

FIG. 4. The change in the mutual arrangement of energy bands in Bi in the region of potential gradient. The formation of electron–hole pairs occurs under the action of potential gradient (curve *1*) and as a result of interband tunneling (curve *2*).

The authors are grateful to Yu. A. Kolesnichenko for fruitful discussions of the results.

APPENDIX

We give a visual description of the physical models used for explaining the nonlinearity of the current–voltage characteristic for Bi point contacts.

1. Potential gradient model

A Bi sample contains electron and hole valleys located at points L and T of the Brillouin zone. We assume that the potential varies linearly between point A and B in the real space (Fig. 4). In the presence of a potential gradient, the concentrations of electrons and holes is a position function.

The potential gradient leads to spatial redistribution of charge carriers of opposite polarities and to the stabilization of a certain level of chemical potential (CP) in this region. In the case under investigation, this level must be exactly at the middle between the positions of CP at the initial states A and B (bold curve in Fig. 4). For the sake of clarity of presentation, we consider the change in the number of electrons and holes only at the extreme points A and B. Electrons occupying states at A above the new level of CP move to states B lying above the initial level of CP. However, the density of states is an increasing function of energy, and the electrons arriving from A fill the states to a certain level lying below the new level of CP. Additional electrons appear as a result of creation of an additional number of holes. Indeed, holes move in the opposite direction, and the number of holes arriving at A from B is insufficient for filling the hole states at A up to the new CP level. This inevitably leads to the creation of additional holes which ensure the emergence of additional electrons at A. This process is associated with intervalley transitions between points L and T of the Brillouin zone. Thus, the presence of a potential relief in a semimetal leads to an increase in the average concentration of electrons and holes while preserving the equality of charge carriers of opposite polarities.

2. Interband tunneling model

In the presence of a potential gradient between points A and B separated by a distance a, electrons can tunnel from a state near the top of the valence band to the Fermi level, the tunneling being accompanied by activation of electrons. Holes are created in the valence band, and additional electrons appear in the conduction band. Transitions occur between states at the point L of the Brillouin zone, but between points A and B separated by the distance a in the real space. The conditions for direct tunneling are created when the level $eE_0a=\Delta_L+\varepsilon_F^e$ is attained.

*E-mail: komnik@ilt.kharkov.ua

[1)]In the given example, $(l_\varepsilon/a)_0=0.3$. In the experiments described above, this quantity assumes the values from 0.7 to 0.2.

[2)]It should be noted that in the above analysis we also neglected fine nonlinearities for the dependences $H_0(V)$, which could emerge in the region of characteristic Debye frequencies.

[3)]In Ref. 19, formula (5) has a misprint.

[4)]The description of the physical models will be given in Appendix.

[1] V. S. Tsoi, Pis'ma Zh. Éksp. Teor. Fiz. **19**, 114 (1974) [JETP Lett. **19**, 70 (1974)].
[2] P. C. van Son, H. van Kempen, and P. Wyder, Phys. Rev. Lett. **58**, 1567 (1987).
[3] V. V. Andrievskii, E. I. Ass, and Yu. F. Komnik, Pis'ma Zh. Éksp. Teor. Fiz. **47**, 103 (1988) [JETP Lett. **47**, 124 (1988)].
[4] Yu. A. Kolesnichenko, I. O. Kulik, and R. I. Shekhter, Zh. Éksp. Teor. Fiz. **94**, 328 (1988) [Sov. Phys. JETP **67**, 834 (1988)].
[5] V. V. Andrievskii, E. I. Ass, and Yu. F. Komnik, Fiz. Nizk. Temp. **16**, 326 (1990) [Sov. J. Low Temp. Phys. **16**, 179 (1990)].
[6] V. V. Andrievskii, E. I. Ass, and Yu. F. Komnik, Fiz. Nizk. Temp. **18**, 513 (1992) [Sov. J. Low Temp. Phys. **18**, 351 (1992)].
[7] V. V. Andrievskii, Yu. F. Komnik, and S. V. Rozhok, Physica B **218**, 7 (1996).
[8] Yu. F. Komnik, V. V. Andrievskii, and S. V. Rozhok, Fiz. Nizk. Temp. **22**, 1406 (1996) [Low Temp. Phys. **22**, 1066 (1996)].
[9] V. V. Andrievskii, Yu. F. Komnik, and S. V. Rozhok, Fiz. Nizk. Temp. **22**, 1418 (1996) [Low Temp. Phys. **22**, 1076 (1996)].
[10] Yu. A. Kolesnichenko, R. I. Shekhter, and V. A. Buldovskii, Fiz. Nizk. Temp. **14**, 263 (1988) [Sov. J. Low Temp. Phys. **14**, 144 (1988)].
[11] A. N. Friedman, Phys. Rev. **159**, 553 (1967).
[12] V. F. Gantmakher and Yu. S. Leonov, Pis'ma Zh. Éksp. Teor. Fiz. **8**, 264 (1968) [JETP Lett. **8**, 162 (1968)].
[13] V. V. Andrievskii, E. I. Ass, and S. V. Rozhok, Fiz. Nizk. Temp. **20**, 1057 (1994) [Low Temp. Phys. **20**, 832 (1994)].
[14] P. C. van Son, H. van Kempen, and P. Wyder, J. Phys.: Met. Phys. **17**, 1471 (1987).
[15] I. K. Yanson, Fiz. Nizk. Temp. **11**, 854 (1985) [Sov. J. Low Temp. Phys. **11**, 465 (1985)].
[16] I. K. Yanson and A. V. Khotkevich, *Atlas of Point Contact Spectra of Electron–Phonon Interaction in Metals* [in Russian], Naukova Dumka, Kiev (1986).
[17] I. K. Yanson, O. I. Shklyarevskii, and N. N. Gribov, J. Low Temp. Phys. **88**, 135 (1992).
[18] Yu. A. Bogod, D. V. Gitsu, and A. D. Grozav, Zh. Éksp. Teor. Phys. **84**, 2194 (1983) [Sov. Phys. JETP **57**, 1275 (1983)].
[19] P. I. Shekhter, Fiz. Tekh. Poluprovodn. **17**, 1463 (1983).
[20] R. I. Shekhter, Fiz. Nizk. Temp. **11**, 854 (1985) [Sov. J. Low Temp. Phys. **11**, 469 (1985)].
[21] A. Ya. Shik, Fiz. Tverd. Tela (Leningrad) **16**, 2801 (1974) [Sov. Phys. Solid State **16**, 1822 (1974)].
[22] E. E. Vdovin and A. Ya. Kasumov, Pis'ma Zh. Éksp. Teor. Fiz. **46**, 440 (1987) [JETP Lett. **46**, 556 (1987)].
[23] J. B. C. van der Hilst, J. A. van Hulst, N. N. Gribov *et al.*, Physica B **218**, 109 (1996).
[24] G. E. Smith, G. A. Baraff, and J. M. Rowell, Phys. Rev. **135**, A1118 (1964).
[25] Yu. F. Komnik, V. Yu. Kashirin, B. I. Belevtsev, and E. Yu. Belyaev, Fiz. Nizk. Temp. **20**, 158 (1994) [Low Temp. Phys. **20**, 127 (1994)].

Translated by R. S. Wadhwa

Drag effects between two-dimensional superfluid charged Bose gases separated by a rigid partition

S. I. Shevchenko and S. V. Terent'ev

B. Verkin Institute for Low Temperature Physics and Engineering, National Academy of Sciences of the Ukraine, 310164 Kharkov, Ukraine[*]

(Submitted April 17, 1997)
Fiz. Nizk. Temp. **23**, 1088–1091 (October 1997)

The drag effect in a system of two-dimensional superfluid charged Bose gases separated by a thin insulating partition is analyzed microscopically. It is shown that in contrast to normal systems, the drag effect is observed at $T=0$. The temperature dependence of the entrainment current is determined. An experiment for observing the effect is proposed. © *1997 American Institute of Physics.* [S1063-777X(97)00910-9]

The possibility of transfer of motion through a solid partition was indicated for the first time by Andreev and Meierovich who predicted the drag of one liquid by another separated from the first liquid by a fixed partition.[1] The drag through a wall separating electron gases due to the Coulomb interaction between electrons was predicted by Pogrebinskii[2] and later by Price,[3] while the drag through the electron-phonon interaction was predicted by Gurzhi and Kopeliovich.[4] Recently, perfect low-dimensional systems were created, and the drag in two-dimensional electron gases separated by an insulating partition has become an object of numerous experimental[5–8] and theoretical[9–13] investigations.

In most of the publications, the problem of drag between electrons in normal systems is considered. To our knowledge, the drag between electrons in superconductors separated spatially was analyzed in a single theoretical paper.[14] The analysis carried out by Duan and Yip[14] is of qualitative nature and provides no answers to a number of questions. For example, the expression for drag current given in Ref. 14 does not contain superconducting parameters of the system, i.e., the current is independent of the pairing potential. This result is astonishing; the existence of the dependence on the pairing potential will be demonstrated in the present paper. For this purpose, we shall consider the problem of the drag between charged Bose gases, i.e., the case of a strong pairing potential. Our results differ from those presented in Ref. 14.

Let us consider a system consisting of two identical two-dimensional Bose gases separated by an insulating partition of thickness d.

The Hamiltonian of the system has the form

$$H=\sum_{\alpha}=\int \frac{\hbar^2}{2M}\nabla\hat{\psi}_{\alpha}^{+}(\mathbf{r})\nabla\hat{\psi}_{\alpha}(\mathbf{r})d^2r + \frac{1}{2}\sum_{\alpha,\beta}\int \hat{\psi}_{\alpha}^{+}(\mathbf{r})\hat{\psi}_{\beta}^{+}(\mathbf{r}')V_{\alpha\beta}(\mathbf{r}-\mathbf{r}') \times\hat{\psi}_{\beta}(\mathbf{r}')\hat{\psi}_{\alpha}(\mathbf{r})d^2rd^2r'. \quad (1)$$

Here $\hat{\psi}_{\alpha}^{+}$ and $\hat{\psi}_{\alpha}$ are the creation and annihilation operators for a boson in the layer $\alpha=1,2$, and the potentials are given by

$$V_{\alpha\alpha}=Q^2/\varepsilon_0 r, \quad V_{\alpha\bar{\alpha}}=Q^2/(\varepsilon_0\sqrt{r^2+d^2}), \quad (2)$$

where $Q=2e$ is the boson charge and ε_0 the permittivity of the interlayer.

Let us first find the energy spectrum of the system. At $T=0$, it could be determined by using the well-known Bogoliubov procedure of replacement of condensate operators by C numbers. However, the Bose condensate is absent in two-dimensional systems at $T\neq 0$, and we will find the spectrum by going over to the $\rho-\varphi$ representation, i.e., we write the operators $\hat{\psi}_{\alpha}$ in the form

$$\hat{\psi}_{\alpha}(\mathbf{r})=\exp[i\hat{\varphi}(\mathbf{r})]\sqrt{\hat{\rho}_{\alpha}(\mathbf{r})}\cong\exp(i\hat{\varphi}_{\alpha}(\mathbf{r}))\sqrt{\rho_0} \times\left(1+\frac{1}{2}\frac{\delta\hat{\rho}_{\alpha}}{\rho_0}\right). \quad (3)$$

Here $\hat{\rho}_{\alpha}(\mathbf{r})$ and $\hat{\varphi}_{\alpha}(\mathbf{r})$ are the density and phase operators for bosons in the α, which satisfy the commutation relations

$$[\hat{\rho}_{\alpha}(\mathbf{r}),\hat{\varphi}_{\beta}(\mathbf{r}')]=i\delta_{\alpha\beta}\delta(\mathbf{r}-\mathbf{r}'), \quad (4)$$

$\rho_0=\langle\hat{\rho}_{\alpha}\rangle$ is the average density of bosons, which is the same for both conducting layers, and $\delta\hat{\rho}_{\alpha}\equiv\hat{\rho}_{\alpha}-\rho_0$. The second equality in (3) is valid for $\rho_0^2\geqslant\langle\delta\hat{\rho}_{\alpha}^2\rangle$. It can be proved that this inequality is satisfied for a two-layer system in the case of a high density, i.e., for $\rho_0\geqslant(me^2/\hbar^2\varepsilon_0)^2$. Substituting (3) into (1) and taking into account only the terms quadratic in φ and $\delta\hat{\rho}_{\alpha}$, we obtain

$$H=S\sum_{\mathbf{k}}\left\{\sum_{\alpha}\frac{\hbar^2k^2n}{2M}\hat{\varphi}_{\alpha}^{+}(\mathbf{k})\hat{\varphi}_{\alpha}(\mathbf{k}) + \frac{1}{2}\sum_{\alpha,\beta}\hat{\rho}_{\alpha}^{+}(\mathbf{k})V_{\alpha\beta}(k)\hat{\rho}_{\beta}(\mathbf{k})\right\}. \quad (5)$$

Here S is the area of the system and $V_{\alpha\beta}(k)$ are the Fourier components of the potentials, which are given by

$$V_{\alpha\alpha}(k)=\frac{2\pi Q^2}{\varepsilon_0 k} \quad \text{and} \quad V_{\alpha\bar{\alpha}}(k)=\frac{2\pi Q^2}{\varepsilon_0 k}\,\mathrm{e}^{-kd}, \tag{6}$$

(for brevity the notation $n=\rho_0$ has been introduced).

After a transition to the new variables

$$\hat{\rho}_{\pm}(\mathbf{k})=\frac{1}{\sqrt{2}}\,[\hat{\rho}_1(\mathbf{k})\pm\hat{\rho}_2(\mathbf{k})],$$

$$\hat{\varphi}_{\pm}(\mathbf{k})=\frac{1}{\sqrt{2}}\,[\hat{\varphi}_1(\mathbf{k})\pm\hat{\varphi}_2(\mathbf{k})] \tag{7}$$

The Hamiltonian (5) is reduced to the sum of the Hamiltonians for two independent modes. Introducing the operators of annihilation of an elementary excitation of species $\sigma=\pm$, i.e.,

$$\hat{b}_{\sigma}(\mathbf{k})=\frac{1}{2}\left\{\left(\frac{E_{\sigma}(k)S}{\varepsilon(k)n}\right)^{1/2}\hat{\rho}_{\sigma}(\mathbf{k})+2i\left(\frac{\varepsilon(k)nS}{E_{\sigma}(k)}\right)^{1/2}\hat{\varphi}_{\sigma}(\mathbf{k})\right\} \tag{8}$$

and the creation operators $\hat{b}^{+}_{\sigma}(\mathbf{k})$ conjugate to them, we diagonalize these Hamiltonians and obtain the energy of an elementary excitation:

$$E^2_{\sigma}(k)=\varepsilon^2(k)+2n[V_{11}(k)+\sigma V_{12}(k)]\varepsilon(k), \tag{9}$$

where $\varepsilon(k)=\hbar^2k^2/2M$. It can be easily seen that the mode $E_{+}(k)$ corresponds to vibrations of the Bose gas in two conducting films as a whole, while the mode $E_{-}(k)$ corresponds to density oscillations in one film relative to the other for a constant total density. For $kd\ll 1$, equation (9) leads to

$$E^2_{+}(k)=\frac{4\pi Q^2 n\hbar^2}{\varepsilon_0 M}\,k, \quad E^2_{-}(k)=\frac{2\pi Q^2 n\hbar^2 d}{\varepsilon_0 M}\,k^2. \tag{10}$$

It is expedient to note that these expressions coincide with the expressions for the spectrum of collective excitations in a two-layer normal Fermi system, which are derived by taking into account screening effects.[13] (We should only replace the fermion charge e and mass m by the boson charge $Q=2e$ and mass $M=2m$.) There is no need to take into account additionally the screening effects for the system under investigation since Hamiltonian (5) has been diagonalized exactly.

Let us now consider the problem of entrainment of bosons from one layer by moving bosons of the other layer. If layer 1 carries a uniform supercurrent, the field operator $\hat{\psi}_1$ in this layer should be written in the form

$$\hat{\psi}_1(\mathbf{r})=\exp[i\mathbf{r}\cdot\mathbf{k}_{s1}+i\hat{\varphi}_1(\mathbf{r})]\sqrt{\hat{\rho}_1(\mathbf{r})}. \tag{11}$$

In this case, the average momentum per boson in layer 1 is equal to $\hbar\mathbf{k}_{s1}$, and the average superfluid velocity in this layer is given by $\mathbf{v}_{s1}=\hbar\mathbf{k}_{s1}/M$. As a result, the Hamiltonian (5) is supplemented with the term

$$iS\sum_{\mathbf{k}}\ \frac{\hbar\mathbf{k}\cdot\mathbf{v}_{s1}}{2}\,[\hat{\varphi}_1(\mathbf{k})\hat{\rho}_1(-\mathbf{k})+\hat{\rho}_1(-\mathbf{k})\hat{\varphi}_1(\mathbf{k})]$$
$$\equiv MS\hat{\mathbf{j}}_{s1}\cdot\mathbf{v}_{s1}. \tag{12}$$

Here $\hat{\mathbf{j}}_{s1}$ is the operator of two-dimensional current density in layer 1. Assuming that the velocity $\mathbf{v}_{s1}$ is small and taking into account (12) in the perturbation theory, we obtain the average current in layer 2 induced by the current in layer 1:

$$\hat{\mathbf{j}}_{21}=\frac{1}{2MS}\sum_{\mathbf{k}}\hbar\mathbf{k}\Bigg\{n_{+}(\mathbf{k})+n_{-}(\mathbf{k})$$
$$+\frac{\hbar\mathbf{k}\cdot\mathbf{v}_{s1}}{4E_{+}E_{-}}\left[\frac{(E_{+}-E_{-})^2}{E_{+}+E_{-}}\,(n_{+}(\mathbf{k})+n_{-}(-\mathbf{k})+1)\right.$$
$$\left.-\frac{(E_{+}+E_{-})^2}{E_{+}-E_{-}}\,[n_{+}(\mathbf{k})-n_{-}(\mathbf{k})]\right]\Bigg\}. \tag{13}$$

Here n_{+} and n_{-} are the Bose distribution functions:

$$n_{\sigma}(\mathbf{k})=\left[\exp\left(\frac{E_{\sigma}(k)+\hbar\mathbf{k}\cdot\mathbf{v}_{s1}/2}{T}\right)-1\right]^{-1}. \tag{14}$$

Further calculations will be made by assuming that the following inequalities hold:

$$d\gg\left[\frac{\hbar^2\varepsilon_0}{8\pi Q^2 nM}\right]^{1/3}, \quad T\ll\left[\frac{2\pi Q^2 n\hbar^2}{M\varepsilon_0 d}\right]^{1/2}\equiv T_0. \tag{15}$$

The first inequality allows us to assume that the energy-momentum relation $E_{\sigma}(k)$ is linear for all the boson momenta significant for the problem. By virtue of the second inequality, we can neglect the excitation of E_{+} modes at nonzero temperatures. This statement follows from the fact that, for a given temperature T, the modes satisfying the inequality $E_{-}(k)\leqslant T$ are excited. The maximum wave number satisfying this condition is $k_c\simeq(M\varepsilon_0T^2/2\pi Q^2n\hbar^2d)^{1/2}$, and for $k<k_c$ we have $E^2_{+}/E^2_{-}>T_0/2T\gg 1$.

Taking into account (15) and retaining only the terms linear in $\mathbf{v}_{s1}$, we obtain from (13)

$$\mathbf{j}_{21}=\frac{1}{8\pi n_s}\,\frac{\hbar^2}{Md^4}\,\frac{1}{T_0}\left\{0.0406-2\zeta(3)\left(\frac{T}{T_0}\right)^3\right\}\mathbf{j}_1. \tag{16}$$

Here $\zeta(y)$ is the Riemann zeta function, T_0 is the temperature defined by (15), and $\mathbf{j}_1=n_s\mathbf{v}_{s1}$. For characteristic values of $n=10^{15}$ cm^{-2}, $M=2m_0$, where m_0 is the mass of a free electron, $Q=2e$, $\varepsilon_0=10$, $d=10^{-6}$ cm, we have $T_0\approx 4\times 10^3$ K.

It follows from (16) that the current in one superconducting film induces a current in the other superconducting film owing to the Coulomb interaction between spatially separated electrons even at $T=0$, the entrainment supercurrent decreasing with increasing temperature. It should be emphasized that this result was obtained by us as a result of consistent microscopic analysis and not by using qualitative arguments as in Ref. 14. According to Ref. 14, the entrainment current at $T=0$ must be equal to $\sqrt{2}\hbar\mathbf{j}_1/48\pi n_s m v_F d^3$. Considering that the velocity of sound for the E_{-} mode is $c_{-}=(2\pi nQ^2d/M\varepsilon_0)^{1/2}$ [see (10)], we can write our result at $T=0$ in the form $\mathbf{j}_{21}=\hbar\mathbf{j}_1/200\pi n_s M c_{-} d^3$. In our opinion, the result obtained in Ref. 14 is valid only in the weak coupling approximation. As the electron–electron attraction increases, the result obtained in Ref. 14 should be modified, and in the limit of two Bose gases, the Fermi velocity of pairing electrons should be replaced by the velocity of sound c_{-} for the slow mode. Since this velocity is a function of the separation d between the conducting layers, this changes the dependence of entrainment current on d.

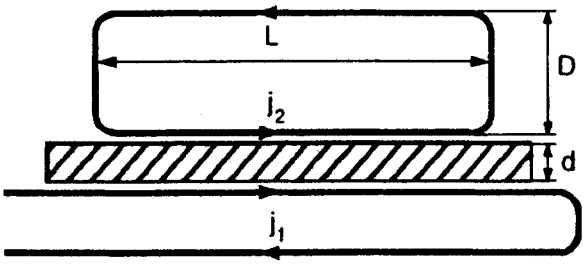

FIG. 1. Schematic diagram of an experiment for detecting the drag effect between superconducting layers. The lower superconducting layer is bent in order to avoid the excitation of current in the upper layer by the magnetic field of the lower layer.

In order to observe entrainment between electrons in the case of spatially separated normal systems, current is passed through one conducting layer, and the potential difference is measured in another (disconnected) layer. However, this method is inapplicable in the case of superconducting layers since no electric field can exist in a superconductor. One of possible ways for observing the entrainment current is to close the secondary circuit and to measure the magnetic flux created in it. The circuit diagram for such an experiment is shown in Fig. 1.

In order to find the electric current $\mathbf{j}_2$ in the secondary circuit, we must take into account the fact that in the general case this current is given by

$$\mathbf{j}_2=\frac{Qn_s}{M}\left(\hbar\nabla\varphi-\frac{Q}{c}\mathbf{A}\right)+\mathbf{j}_{21}. \tag{17}$$

Here $\mathbf{A}$ is the vector potential of the magnetic field generated by the current $\mathbf{j}_2$, and $\mathbf{j}_{21}$ stands for electric current rather than for the flux of particles. Since the phase φ must satisfy the condition

$$\oint \nabla\varphi\cdot d\mathbf{l}=2\pi n,$$

in a closed circuit, where n is an integer, the energy minimum corresponds to zero phase for small currents $\mathbf{j}_{21}$. Consequently, the total entrainment current $\mathbf{j}_2$ in the circuit under investigation must be equal to $-(Q^2n_s/Mc)A_L+\mathbf{j}_{21}$ in the lower film and to $-(Q^2n_s/Mc)\mathbf{A}_H$ in the upper film, where $\mathbf{A}_L$ and $\mathbf{A}_H$ are the values of the vector potential in the lower and upper films. Solving the Maxwell equation curl $\mathbf{H}=4\pi\mathbf{j}/c$, we can easily find that

$$j_2=\frac{j_{21}}{2+\gamma}, \quad \text{where} \quad \gamma=\frac{4\pi n_sQ^2D}{Mc^2}. \tag{18}$$

Here D is the separation between the upper and lower films in the secondary circuit (see Fig. 1). The magnetic flux between the films associated with the current j_2 is given by

$$\Phi\equiv HDL=\frac{4\pi}{c}\frac{j_{21}}{2+\gamma}DL. \tag{19}$$

For $\gamma\ll 1$, the magnetic flux increases linearly with D. For $\gamma\simeq 1$, it attains saturation, and the flux Φ does not depend on D for $\gamma\gg 1$. In this case, we have

$$\Phi=\Phi_{\max}=\frac{0.02e\hbar Lj_1}{Q^2T_0(2\pi n_sd^2)^2}\Phi_0, \tag{20}$$

where $\Phi_0=hc/2e$ is the magnetic flux quantum.

Let us consider the numerical estimates. For $n_s=n=10^{15}$ cm^{-2}, $Q=2e$, $M=2m_0$, the dimensionless constant γ is of the order of unity for $D\simeq 10^{-4}$ cm. If $D\gg 10^{-4}$ cm, then $\gamma\gg 1$, and the flux $\Phi=\Phi_{\max}$. While estimating the flux $\Phi_{\max}$, we must take into account the fact that it strongly depends on d ($\Phi_{\max}\sim d^{-7/2}$), and the value of d must be as small as possible. On the other hand, the value of d must be large enough in order to neglect tunneling through the insulating layer separating the primary and secondary circuits. For $d\approx 50$ Å, $L=1$ cm, $v_{s1}=10^5$ cm/s, and the flux $\Phi_{\max}\approx 3\times 10^{-6}\Phi_0$.

Thus, we have proved that the drag current between two superconductors differs from zero even at $T=0$ and depends on the pairing potential for electrons. It is remarkable that we have obtained a simple test for distinguishing between the ''boson'' and ''fermion'' superconductivity. In the former case, the entrainment current and the flux $\Phi_{\max}$ are proportional to $d^{-7/2}$, while in the latter case they are proportional to d^{-3}, where d is the thickness of the partition separating the two superconducting layers.

*E-mail: shevchenko@ilt.kharkov.ua

[1] A. F. Andreev and A. È. Meierovich, JETP Lett. **15**, 39 (1972).
[2] M. B. Pogrebinskii, Fiz. Tekh. Poluprovodn. **11**, 637 (1977).
[3] P. J. Price, Physica B **117**, 750 (1983).
[4] R. N. Gurzhi and A. I. Kopeliovich, JETP Lett. **26**, 140 (1977).
[5] P. M. Solomon, P. J. Price, D. J. Frank, and D. C. L. Tulipe, Phys. Rev. Lett. **63**, 2508 (1989).
[6] T. J. Gramila, J. P. Eisenstein, A. H. MacDonald *et al.*, Phys. Rev. Lett. **66**, 1216 (1991).
[7] U. Sivan, P. M. Solomon, and H. Shtrikman, Phys. Rev. Lett. **68**, 1196 (1992).
[8] H. Rubel, E. H. Linfield, D. A. Ritchie *et al.*, Semicond. Sci. Technol. **10**, 1229 (1995).
[9] B. Laikhtman and P. M. Solomon, Phys. Rev. B **41**, 9921 (1990).
[10] A. G. Rojo and G. D. Mahan, Phys. Rev. Lett. **68**, 2074 (1992).
[11] H. C. Tso, P. Vasilopulos, and F. M. Peeters, Phys. Rev. Lett. **68**, 2516 (1992).
[12] L. Zheng and A. H. MacDonald, Phys. Rev. B **48**, 8203 (1993).
[13] K. Flensberg and B. Y.-K. Hu, Phys. Rev. B **52**, 14796 (1995).
[14] J.-M. Duan and S. Yip, Phys. Rev. Lett. **70**, 3647 (1993).

Translated by R. S. Wadhwa

High-frequency spin susceptibility of a two-dimensional electron gas with electron impurity states

N. V. Gleizer, A. M. Ermolaev, and A. D. Rudnev

Kharkov State University, 310077 Kharkov, Ukraine
(Submitted February 28, 1997)
Fiz. Nizk. Temp. **23**, 1092–1097 (October 1997)

The high-frequency asymptotic form of dynamic spin susceptibility of a two-dimensional electron gas is obtained. Local states of electrons in impurity atoms and the quantizing magnetic field are taken into consideration. The susceptibility has resonant singularities at frequencies of electron transitions between Landau levels and local levels. In the absence of a magnetic field, the real part of susceptibility has a logarithmic singularity while the imaginary part has a peak at the threshold frequency of bound electron activation by a variable magnetic field. © *1997 American Institute of Physics.* [S1063-777X(97)01010-4]

1. INTRODUCTION

The reaction of a two-dimensional electron gas to a weak varying magnetic field is characterized by the dynamic spin susceptibility tensor $\chi(\mathbf{q},\omega)$ which depends on the wave vector $\mathbf{q}$ and the field frequency ω. The peculiarities of susceptibility on the complex plane of frequency ω determine the spectrum and attenuation of magnetic excitations in a system. The knowledge of susceptibility allows us to obtain the spectrum of spin magnetization fluctuations of a two-dimensional electron gas, cross-section of magnetic scattering of neutrons by spin magnetization current of conduction electrons, and other quantities.

A large number of works have been devoted to the computation of spin susceptibility of two-dimensional electron systems.[1] Shoenberg[2] calculated the static susceptibility of a free electron gas in a magnetic field perpendicular to the plane of motion of electrons, while Isihara *et al.*,[3] took into account the Coulomb interaction of electrons. Exact expressions for the dynamic spin susceptibility as well as the density-density reaction function for a free degenerate two-dimensional electron gas were obtained in Refs. 1 and 4. The quantizing magnetic field was taken into consideration by Glasser,[5] while Yarlagadda and Giuliani[6] obtained the high-frequency asymptotic form for the spin susceptibility of a two-dimensional Fermi liquid. The effect of impurity atoms potentially scattering conduction electrons on susceptibility was considered by Nkoma.[7] Fukuyama[8] compiled a review of the properties of two-dimensional disordered systems in a magnetic field.

Spin susceptibility, which is sensitive to the dynamics of conduction electrons, experiences the effect of impurity atoms in the system. In particular, the impurity states of electrons must affect the susceptibility and other quantities associated with it. It is important to take such states into consideration since an impurity atom in the two-dimensional case forms a bound state with electrons even if it attracts them quite weakly. The corresponding local level lies near the lower edger of the two-dimensional conduction band. The local levels are ''multiplied'' in a magnetic field, and exist in a field of both attracting and repelling scatterers. Local levels are arranged between the Landau levels.

In this work, we consider the effect of local states on the high-frequency spin susceptibility of a two-dimensional electron gas at low temperatures. We shall use the method of local perturbations[9] which was employed earlier[10] for calculating the conductivity tensor. It is assumed that the frequency ω of the field is high in comparison with the electron collision frequency.

In Sec. 2, we shall consider the effect of local electron states in the field of isolated impurity atoms on high-frequency spin susceptibility of a two-dimensional electron gas. In Sec. 3 we take into account the quantizing magnetic field perpendicular to the electron layer. The results obtained in this work are briefly summarized and their possible applications are discussed in Sec. 4.

2. EFFECT OF LOCAL ELECTRON STATES ON DYNAMIC SPIN SUSCEPTIBILITY

In order to calculate the spin susceptibility tensor, we use Kubo's formula

$$\chi_{\alpha\beta}(\mathbf{q},\omega)=i\int_0^\infty dt e^{i\omega t}\langle[M_\alpha(\mathbf{q},t),M_\beta(-\mathbf{q},0)]\rangle, \qquad (1)$$

where $\mathbf{M}(\mathbf{q},t)$ is the spatial Fourier component of the Heisenberg operator for the spin magnetization of two-dimensional electrons; brackets denote the commutator of operators, while angle brackets describe Gibbs averaging and averaging over impurity atom configurations, $\alpha,\beta=x,y$. The sample area and the quantum constant are assumed to be equal to unity. In secondary quantization representation, the spin magnetization operator has the form

$$M_\alpha(\mathbf{q})=-\mu\sum_{\mathbf{p}ss'}\sigma^\alpha_{s's}a^+_{(\mathbf{p}-\mathbf{q})s'}a_{\mathbf{p}s}, \qquad (2)$$

where μ is the electron magnetic moment, $\mathbf{p}$ and s stand for momentum and the spin quantum number, while $a_{\mathbf{p}s}$ and $a^+_{\mathbf{p}s}$ are the operators of annihilation and creation of electrons in the state $|\mathbf{p}s\rangle$, and σ^α are Pauli matrices. Substituting formula (2) into (1), we obtain the following relation between the susceptibility tensor and Fourier component of a retarded two-electron Green's function. The latter quantity is calculated by using Green's temperature function method.[11]

In the one-electron approximation, the two-particle Green's function is reduced to the product of two one-particle Green's functions averaged over impurity atom configurations. Disregarding vortex corrections,[11] this average is reduced to the product of average one-particle Green's functions. Using their spectral representations,[11] we obtain the following expression for the tensor (1):

$$\chi_{\alpha\beta}(\mathbf{q},\omega)=-\mu^2\sum_{\mathbf{p}ss'}\sigma^{\alpha}_{s's}\sigma^{\beta}_{ss'}\int_{-\infty}^{\infty}d\varepsilon\int_{-\infty}^{\infty}d\varepsilon' \times\frac{f(\varepsilon)-f(\varepsilon')}{\varepsilon-\varepsilon'-\omega-i0}\,\rho_s(\mathbf{p},\varepsilon)\rho_{s'}(\mathbf{p}-\mathbf{q},\,\varepsilon'), \tag{3}$$

in which $f(\varepsilon)$ is the Fermi function, and $\rho_s(\mathbf{p},\varepsilon)$ is the spectral density of one-electron Green's function averaged over impurity configurations. In a pure sample, this quantity is defined as

$$\rho_0(\mathbf{p},\varepsilon)=\delta(\varepsilon-\varepsilon_{\mathbf{p}}),$$

where $\varepsilon_{\mathbf{p}}=p^2/2m$, m being the effective electron mass.

The one-particle Green's function G is connected with the operator T of electron scattering by impurity centers through the relation[9]

$$G=G_0+G_0T\,G_0, \tag{4}$$

where G_0 is the Green's function of free electrons. The exact expression for the mean value of the operator of short-range electron scattering by impurity atoms in the one-center approximation was derived in Ref. 9. Hence the spectral density of the averaged Green's function (4) can be represented in the form $\rho=\rho_0+\delta\rho_i$, where $\delta\rho_i$ is the impurity correction. In the linear approximation in density n_i of impurity atoms, this correction is proportional to n_i. Consequently, $\chi=\chi_0+\delta\chi_i$, where χ_0 is the spin susceptibility tensor for the pure sample, and $\delta\chi_i$ is the impurity contribution which is defined as $\delta\chi^{(i)}_{\alpha\beta}=\delta\chi_i\delta_{\alpha\beta}$, where

$$\delta\chi_i(\mathbf{q},\omega)=-2\mu^2\sum_{\mathbf{p}}\int_{-\infty}^{\infty}d\varepsilon\;\delta\rho_i(\mathbf{p},\varepsilon) \times[f(\varepsilon)-f(\varepsilon_{\mathbf{p}+\mathbf{q}})]\left(\frac{1}{\varepsilon-\varepsilon_{\mathbf{p}+\mathbf{q}}-\omega-i0}+\frac{1}{\varepsilon-\varepsilon_{\mathbf{p}+\mathbf{q}}+\omega+i0}\right). \tag{5}$$

It can be seen from formula (4) that the function G has additional singularities associated with the singularities of the scattering operator. These singularities correspond to local electron energy levels in isolated impurity atoms. The contribution of local levels to the spectral density of the average Green's function is given by

$$\delta\rho(\mathbf{p},\varepsilon)=|v_0|n_i(\varepsilon-\varepsilon_{\mathbf{p}})^{-2}\delta[1-v_0F(\varepsilon)], \tag{6}$$

where v_0 is a constant characterizing the intensity of short-range impurity potential, and $F(\varepsilon)$ is a function appearing in the Lifshits equation[9] $1-v_0F(\varepsilon)=0$ for local levels. It can be seen from formula (6) that the spectral density has a delta-shaped peak at the local levels:

$$\delta\rho(\mathbf{p},\varepsilon)=n_i\sum_l r_l(\varepsilon_p-\varepsilon_l)^{-2}\delta(\varepsilon-\varepsilon_l), \tag{7}$$

where ε_l is the position of the l-th local level, and

$$r_l=\left|\frac{dF(\varepsilon)}{d\varepsilon}\right|^{-1}_{\varepsilon=\varepsilon_l}$$

is the residue of the amplitude of electron scattering by an isolated impurity center at the pole ε_l. For a shallow ($m|v_0|\ll 1$) local level, this residue is defined as

$$r=2\pi|\varepsilon_l|/m.$$

Formulas (5) and (7) lead to the contribution of local levels to the high-frequency spin susceptibility:

$$\delta\chi(\mathbf{q},\omega)=2\mu^2n_i\sum_{\mathbf{p}l}r_l(\varepsilon_{\mathbf{p}-\mathbf{q}}-\varepsilon_l)^{-2}[f(\varepsilon_{\mathbf{p}})-f(\varepsilon_l)] \times\left(\frac{1}{\varepsilon_l-\varepsilon_{\mathbf{p}}-\omega-i0}+\frac{1}{\varepsilon_l-\varepsilon_{\mathbf{p}}+\omega+i0}\right). \tag{8}$$

As expected, the real part of this equation is an even function of frequency, while the imaginary part is an odd function.

If the energy spectrum of the system contains just one local level situated near the lower edge of a two-dimensional conduction band, integration over the directions of the vector $\mathbf{p}$ in (8) leads to the following expression:

$$\delta\chi(q,\omega)=4\pi m\mu^2rn_i\int_0^{\infty}d\varepsilon[f(\varepsilon)-f(\varepsilon_l)] \times\left(\frac{1}{\varepsilon_l-\varepsilon+\omega+i0}+\frac{1}{\varepsilon_l-\varepsilon-\omega-i0}\right) \times|\varepsilon-\varepsilon_l+\varepsilon_q|[(\varepsilon-\varepsilon_l+\varepsilon_q)^2-4\varepsilon\varepsilon_q]^{-3/2}. \tag{9}$$

In the case of a weak spatial dispersion ($\varepsilon_q\ll|\varepsilon_l|$), we can confine ourselves to an expansion of the real part of the function (9) into a series in powers of $\varepsilon_q/\varepsilon_l$. In this case, we arrive at the following expression for degenerate electrons, taking into account terms of the order of q^2:

$$\mathrm{Re}\;\delta\chi(q,\omega)=4\pi m\mu^2rn_i\omega^{-2}\left\{\left[1-\frac{4\varepsilon_q}{\omega} \times\left(1-\frac{3}{2}\frac{\varepsilon_l}{\omega}\right)\right]\ln\left|\frac{\varepsilon_F-\varepsilon_l}{\omega+\varepsilon_F-\varepsilon_l}\right|+\frac{4\varepsilon_q}{\varepsilon_l} \times\left(1-\frac{\varepsilon_F}{\varepsilon_l}\right)^{-1}\left[1-\frac{3}{4}\left(1-\frac{\varepsilon_F}{\varepsilon_l}\right)^{-1}\right]\right\} +(\omega\to-\omega), \tag{10}$$

where ε_F is the Fermi energy, and $(\omega\to-\omega)$ indicates the term obtained from the preceding one by reversing the sign of frequency. The function (10) has a logarithmic singularity at the threshold frequency $\varepsilon_F+|\varepsilon_l|$ of activation of electrons localized at impurities by a varying magnetic field. The impurity absorption of the varying field energy has a threshold at this frequency.

The imaginary component of (9) for any degree of electron degeneracy and for any q is given by

$$\text{Im}\ \delta\chi(q,\omega)=4\pi^2 m\mu^2 r n_i|\omega_+|\Theta(\omega+\varepsilon_l)\times[f(\varepsilon_l)-f(\varepsilon_l+\omega)][\omega_+^2-4\varepsilon_q(\omega+\varepsilon_l)]^{-3/2}-(\omega\to-\omega), \tag{11}$$

where $\omega_\pm=\omega\pm\varepsilon_q$, and Θ is the Heaviside function. At a finite temperature, Eq. (11) has a threshold at the frequency $\omega_g=|\varepsilon_l|$ of activation of the local level. As the temperature decreases, the threshold is displaced towards the point $\varepsilon_F+|\varepsilon_l|$ in accordance with Pauli's principle. As the imaginary part (11) of the susceptibility passes through the threshold frequency, it experiences a jump defined (for $q=0$) by $4\pi^2 m\mu^2 r n_i\omega_g^{-2}$. With increasing frequency, the quantity (11) decreases in proportion to ω^{-2}. The jump is naturally blurred if we take into account the finite width of the local level.

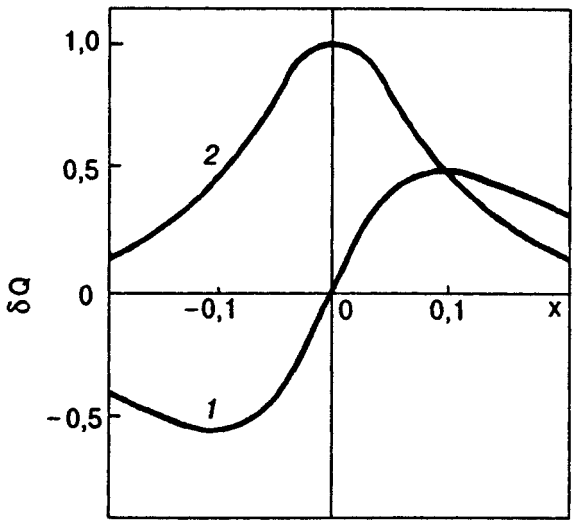

FIG. 1. Dependence of the real (curve *1*) and imaginary (curve *2*) parts of the susceptibility (14) on frequency in the vicinity of resonance.

3. EFFECT OF MAGNETIC FIELD ON SPIN SUSCEPTIBILITY

The method of local perturbations used above is also applicable in the case when a two-dimensional electron gas is in a quantizing magnetic field perpendicular to the plane $z=0$ in which the electrons move. In this case, the electrons are situated at Landau levels and the local levels detached from them. In order to calculate the spin susceptibility tensor of such a system, it is convenient to use the Landau representation. In particular, the spatial Fourier component of spin magnetization operator in this representation has the form

$$M_\alpha(\mathbf{q})=-\mu\sum_{vv'ss'}\sigma^\alpha_{s's}I_{v'v}(-\mathbf{q})a^+_{v's'}a_{vs},$$

where v is a set of orbital quantum numbers for an electron in a magnetic field, and $I_{vv'}(\mathbf{q})=\langle v|e^{i\mathbf{qr}}|v'\rangle$ are the matrix elements of a plane wave in the Landau basis.

The above transformations lead to the following contributions of local levels to the high-frequency spin susceptibility tensor of two-dimensional electrons:

$$\delta\chi_{\alpha\beta}(q,\omega)=\frac{m\mu^2\omega_c n_i}{2\pi}\sum_{knn'ss'}r_{ks}\frac{\varphi^2_{nn'}(q)}{(\varepsilon_{ns}-\varepsilon^l_{ks})}[f(\varepsilon_{n's'})-f(\varepsilon^l_{ks})]\left(\frac{\sigma^\alpha_{ss'}\sigma^\beta_{s's}}{\varepsilon^l_{ks}-\varepsilon_{n's'}+\omega+i0}+\frac{\sigma^\alpha_{s's}\sigma^\beta_{ss'}}{\varepsilon^l_{ks}-\varepsilon_{n's'}-\omega-i0}\right). \tag{12}$$

Here ω_c is the cyclotron frequency, while ε_{ns} and ε^l_{ks} are the positions of the nth Landau level and kth local level respectively,

$$\varphi_{n'n}=\left(\frac{n!}{n'!}\right)^{1/2}\xi^{1/2(n'-n)}\exp\left(-\frac{\xi}{2}\right)L_n^{n'-n}(\xi),$$

$L_n^{n'-n}$ are generalized Laguerre polynomials, $\xi=q^2/(2m\omega_c)$, and the wave vector $\mathbf{q}$ is parallel to the y-axis. If the separation ω_0 between the Landau level and the local level detached from it is small in comparison with ω_c, the residue of the amplitude of scattering of electrons by an impurity atom at the pole ε^l_{ks} is equal to

$$r=2\pi\omega_0^2/(m\omega_c).$$

For $\xi\ll 1$, the spatial dispersion of the tensor (12) can be disregarded. In this case, the circular components of susceptibility are defined as

$$\delta\chi_\pm(\omega)=\delta\chi_{xx}(\omega)\pm i\delta\chi_{yx}(\omega)=\frac{m\mu^2\omega_c n_i}{\pi}\sum_{kn}\frac{r_{k+}}{(\varepsilon_{n+}-\varepsilon^l_{k+})^2}[f(\varepsilon_{n-})-f(\varepsilon^l_{k+})]\frac{1}{\varepsilon^l_{k+}-\varepsilon_{n-}\pm\omega\pm i0}+(+\leftrightarrow-), \tag{13}$$

where the indices $\pm$ in $r_{k\pm}$, $\varepsilon_{n\pm}$ and $\varepsilon^l_{k\pm}$ correspond to the electron spin orientations along and against the magnetic field, and $(+\leftrightarrow-)$ indicates the term obtained from the preceding one by reversing the sign of the electron spin projection, as well as the sign of $\omega+i0$. It can be seen from formulas (12) and (13) that the spin susceptibility of a two-dimensional electron gas has resonant singularities at the frequencies of electron transitions between the Landau levels and local levels that are accompanied by a spin flip. The resonance frequencies are equal to $|\varepsilon_{n\pm}-\varepsilon^l_{k\mp}|$.

The dependence of the real (1) and imaginary (2) parts of the quantity

$$\delta Q=\frac{\omega_1\gamma}{2\mu^2 n_i}\delta\chi_- \tag{14}$$

on $x=1-\omega/\omega_1$ is shown in Fig. 1 near the frequency $\omega_1=\omega_c-\omega_0$ of resonant electron transitions between a Landau level and a local level involving a spin flip $(-\to+)$ within a single Landau subband. Here, $\gamma=\Gamma/\omega_1$, where Γ is the total width of levels participating in transitions. Calcula-

tions were made for $\gamma = 0.1$. The ratio of the maximum value of Re $\delta\chi_-$ to the Pauli susceptibility of a two-dimensional electron gas[2]

$$\chi_0 = e^2/(4\pi m c^2)$$

is equal to

$$k = \frac{\pi n_i}{m\omega_1 \gamma}.$$

Substituting in the above expression the values $n_i = 10^{12}$ cm^{-2}, the constant magnetic field strength $H = 10^4$ Oe, and $\omega_0/\omega_c = 0.1$ that are typical for experiments with an inversion layer at the Si–SiO_2 boundary, we obtain $k = 218$.

4. CONCLUSION

In the present work, we have considered the effect of localization of electrons on the high-frequency spin susceptibility tensor of a two-dimensional electron gas in the field of impurity atoms. It is assumed that the mean separation between impurity atoms is large as compared to the radius of the bound state of an electron and the radius of the electron orbit in a magnetic field, while the frequency of the varying magnetic field considerably exceeds the electron collision frequency. This allows us to expand the susceptibility into a series in powers of the density n_i of impurity atoms and to single out the contribution of local levels proportional to n_i. The local levels are the poles of the one-electron Green's function averaged over the impurity configurations. These levels are manifested in the form of delta-peaks on the dependence of the spectral density of the average Green's function on the electron energy. A consideration of these peaks leads to the value of the contribution to the susceptibility resulting from electron transitions between bound and band states induced by a varying magnetic field. This contribution is obtained both in a quantizing magnetic field perpendicular to the electron layer, and without the field.

In the absence of a magnetic field, the real part of the dynamic spin susceptibility of degenerate electrons has a logarithmic singularity at the threshold frequency of transitions of localized electrons to the two-dimensional conduction band. The imaginary part of susceptibility has a threshold and experiences a discontinuity at this frequency. A consideration of the finite width of the local level leads to a blurring of the jump and to the emergence of a peak at the frequency dependence of susceptibility in a quantizing magnetic field.

The susceptibility has resonance singularities at frequencies of electron transitions between Landau levels and the local levels alternating with them. As a function of frequency, the real part of susceptibility has simple poles at resonance frequencies, while the imaginary part has delta-shaped peaks. Formulas (10)–(13) were derived just by using the fact of the existence of local levels in the electron energy spectrum. The characteristics of these levels (their positions ε_{ks}^l and the residues r_{ks} of the scattering amplitude) were not specified. Hence formulas (10)–(13) can be used for obtaining these characteristics by comparing theory with experiments.

The results obtained by us can be used for studying the high- frequency magnetic properties of inversion layers at the boundary between a semiconductor and an insulator, in heterojunctions, superlattices, two-dimensional and layered metals, and thin metallic films in the case when the electrons fill only the lower energy level associated with spatial quantization.[1] The above peculiarities of the real part of susceptibility must be taken into consideration in the dispersion equation for the spin wave spectrum in a two-dimensional nonferromagnetic Fermi liquid. Apparently, these singularities lead to a rearrangement of the wave spectrum near resonance frequencies. The peaks of the imaginary part of the susceptibility must be manifested in the absorption of high-frequency field energy, and in the cross section of inelastic magnetic scattering of neutrons by a two-dimensional electron gas.

[1] T. Ando A. Fowler, and F. Stern, *Electronic Properties of Two-dimensional Systems*, Amer. Phys. Soc., New York (1982).
[2] D. Shoenberg, J. Low Temp. Phys. **56**, 417 (1984).
[3] A. Isihara and D. Y. Kojima, Phys. Rev. B **19**, 846 (1979).
[4] F. Stern, Phys. Rev. Lett. **18**, 546 (1967).
[5] M. L. Glasser, Phys. Rev. B **22**, 472 (1980).
[6] S. Yarlagadda and G. F. Giuliani, Phys. Rev. B **39**, 3386 (1989).
[7] J. S. Nkoma, J. Phys. C **14**, 1685 (1981).
[8] H. Fukuyama, Techn. Rep. ISSP, Ser. A, No. 1304, 1 (1983).
[9] I. M. Lifshits, S. A. Gredeskul, and L. A. Pastur, *Introduction to the Theory of Disordered Systems*, Wiley, New York (1988).
[10] N. V. Gleizer and A. M. Ermolaev, Fiz. Nizk. Temp. **23**, 73 (1997) [Low Temp. Phys. **23**, 55 (1997)].
[11] A. A. Abrikosov, L. P. Gor'kov, and I. E. Dzyaloshinskii, *Methods of Quantum Field Theory in Statistical Physics*, Prentice Hall, Englewood Cliffs, NJ (1963).

Translated by R. S. Wadhwa

Interference phenomena and ballistic transport in a one-dimensional ring

M. V. Moskalets

Il'ich Prospect 93a, Flat 48, 310020 Kharkov, Ukraine
(Submitted February 11, 1997; revised March 24, 1997)
Fiz. Nizk. Temp. **23**, 1098–1105 (October 1997)

The dependence of the conductance of a one-dimensional ballistic ring on a potential barrier at one of the branches of the ring is considered at a nonzero temperature. The case of a small potential barrier (Aharonov–Bohm electrostatic effect) as well as a tunnel barrier is considered. The possibility of direct measurement of the electron wave function phase variation upon tunneling is discussed. © *1997 American Institute of Physics.* [S1063-777X(97)01110-9]

INTRODUCTION

The preservation of phase coherence during propagation of electrons in mesoscopic samples[1] at low temperatures makes the transport properties of such objects sensitive to the phase of the electron wave function. This makes it possible to observe the Aharonov–Bohm (AB) effect in solids.[2,3]

It was shown earlier[4,5] that the physical properties of doubly connected systems containing an AB magnetic flux Φ are periodic in Φ with a period $\Phi_0=h/e$. Such a periodicity was indeed observed in Refs. 6–10 during measurement of conductance oscillations in isolated conducting rings in a magnetic field. Calculations of conductance for one-dimensional[11–14] as well as multichannel[15] rings also show that the dependence $G(\Phi)$ must have a period Φ_0. However, experiments on chains formed by many rings[16,17] display a $\Phi_0/2$ periodicity which is associated with the ensemble averaging of macroscopically identical but microscopically different characteristics of the rings (length, impurity distribution, etc.).[1,13,15,18] It can be stated that the $\Phi_0/2$ periodicity may be caused by interference of electrons moving along various trajectories as well as along the same trajectory but in opposite directions. The contribution of the latter processes, which was first considered in the weak localization theory by Al'tshuler, Aronov, and Spivak (AAS),[19] is independent of microscopic characteristics of the sample and is therefore preserved upon averaging. According to the prevailing concepts, averaging over an ensemble of rings is equivalent to averaging over electron energy (see Ref. 1).

In analogy with optical phenomena, attempts were made to control the interference pattern in an AB magnetic interferometer (a mesoscopic ring containing the AB magnetic flux) by changing the electron wave function phase with the help of a variable potential barrier created on one of the branches of the ring. Thus, the phase change in Refs. 20 and 21 was caused by the Aharonov–Bohm electrostatic effect. A potential barrier with resonance levels (quantum dot) was used in Ref. 22. It was assumed in these works that the electron wave function phase variation by a quantity θ caused by a potential barrier with transmission coefficient $t=t_0\exp(i\theta)$ (where i is the imaginary unit) leads to an identical phase shift in the dependence $G(\Phi)$. However, no such phase shift was observed in the dependence $G(\Phi)$. Moreover, the existence of such a phase shift would contradict the requirement of parity of the kinetic coefficients of doubly connected two-terminal mesoscopic samples upon a reversal of the magnetic field,[23] which is confirmed in experiments.[24] Hence Yacoby *et al.*[25] concluded that a two-terminal interferometer cannot be used in principle for a direct measurement of the phase of the transmission coefficient of an electron passing through a potential barrier.

The present paper aims at determining the effect of a potential barrier of height $e\varphi$ on the conductance of an interferometer with an AB magnetic flux, and at illustrating the possibility of using a two-terminal ballistic interferometer to study the coefficient of transmission of an electron through a potential barrier. Such a formulation of the problem is justified by the following arguments. According to Landauer's formula,[1,26] the conductance G of a sample with two terminals connected with the banks is proportional to the square of the amplitude τ of transmission of a Fermi electron through the sample:

$$G=G_0|\tau(k_F)|^2. \tag{1}$$

Here, $G_0=2e^2/h$. In other words, if the contacts are mounted directly on the potential barrier, it is not possible to measure the phase of the transmission coefficient during conductance measurements. The situation becomes quite different if we locate the potential barrier at one of the branches of the ballistic ring. In this case, $\tau\simeq A_{L1R}+A_{L2R}$, where A_{L1R} is the amplitude of transition through the branch containing the potential barrier, and A_{L2R} is the amplitude of transition through the other (ballistic) branch. Writing the dependence on t explicitly ($A_{L1R}=A_{01}t$), we obtain

$$G\simeq G_0(|A_{01}|^2t_0^2+|A_{L2R}|^2+2\,\mathrm{Re}(A_{01}A_{L2R}^*t)).$$

The third term in this expression is proportional to the first power of the coefficient t of electron transmission across the potential barrier and depends on its phase θ.

We shall consider the case of a small potential barrier (potential step) $e\varphi\ll\varepsilon_F$ (where ε_F is the Fermi energy of electrons at the banks), as well as a potential barrier of arbitrary height (including a tunnel barrier with $e\varphi\geqslant\varepsilon_F$).

In the former case, the Aharonov–Bohm electrostatic effect is realized. It will be shown below that, in spite of the additive nature of the contributions from vector and scalar potentials to the electron wave function phase, the magnetic and electrostatic AB effects in a one-dimensional ballistic ring are independent of each other as far as the phase is

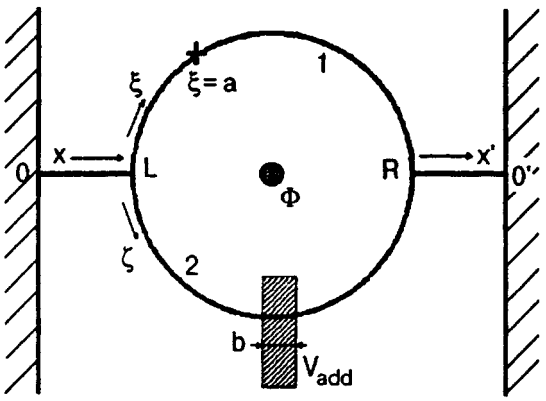

FIG. 1. Model of a one-dimensional ring connected with the banks. The arrows show the positive direction of the coordinate axes. The numbers correspond to the branches of the ring. $0,0'$ are points of contact with the banks, L and R are contact points for terminals, Φ is the magnetic flux, and V_{add} is the potential of the metallic shutter creating a potential step of length b. The cross shows the impurity position, and a is the impurity coordinate.

concerned. In other words, a change in the phase of the electron wave function during the passage across a potential barrier does not change continuously the phase of the dependence $G(\Phi)$. This is due to the different ways in which the vector and scalar potentials affect the spectrum of electron states in the ring.[27] Because of this effect, the interference phenomena in doubly connected systems differ from analogous effects in ballistic flows of particles[28] when the electromagnetic potentials affect only the amplitude of electron transition from the initial to the final point. This is confirmed by the results obtained in Ref. 29 where a phase variation in the dependence $G(\Phi)$ was observed under a scalar potential acting on an electron beam in a two-slit interferometer formed in a two-dimensional electron gas. Such a phase shift corresponds to the additive contribution from scalar and vector potentials to the electron wave function phase. No such phase shift was observed in Refs. 20 and 21 where measurements were made on conducting rings with two terminals.

1. FORMULATION OF THE PROBLEM AND BASIC EQUATIONS

Our aim is to find the conductance G of a one-dimensional ballistic ring with a potential barrier connected to macroscopic banks through one-dimensional conductors (Fig. 1). Following Büttiker *et al.*,[12] we shall solve this problem by using the transfer matrix technique in the approximation of the quantum waveguide theory.[14]

For this purpose, we consider the passage of a plane wave $\exp(ikx)$ through the ring from left to right. According to formula (1), the square of the transmission amplitude $\tau(k_F)$ for an electron with Fermi energy defines the conductance of the system at zero temperature. We single out four one-dimensional segments $0L$, $L1R$, $L2R$, and $R0'$. In each segment, we introduce a coordinate axis with positive direction as indicated by arrows in Fig. 1. We denote the solution of the one-dimensional Schrödinger equation for the wave function of noninteracting electrons at each segment by Ψ_L, Ψ_1, Ψ_2 and Ψ_R and present it in the form

$$\begin{cases} \Psi_L(x)=\exp(ikx)+r(k)\exp(-ikx), \\ \Psi_1(\xi)=(A_1\ \exp(ik\xi)+B_1\ \exp(-ik\xi))\exp\left(i2\pi\dfrac{\xi\Phi}{L\Phi_0}\right), \\ \Psi_2(\zeta)=(A_2\ \exp(ik\zeta)+B_2\ \exp(-ik\zeta))\exp\left(-i2\pi\dfrac{\zeta\Phi}{L\Phi_0}\right), \\ \Psi_R(x')=\tau(k)\exp(ikx'). \end{cases} \tag{2}$$

Here k is the electron wave vector, Φ the magnetic flux in the ring, and L the length of the ring. In order to find the six unknowns r, A_1, B_1, A_2, B_2, and τ, we use the conditions of continuity of the wave function at the points of intersection of one-dimensional conductors L (coordinates $x=0$, $\xi=0$, $\zeta=0$) and R (coordinates $\xi=L/2$, $\zeta=L/2$, $x'=0$):

$$\begin{cases} \Psi_L(0)=\Psi_1(0)=\Psi_2(0), \\ \Psi_R(0)=\Psi_1(L/2)=\Psi_2(L/2), \end{cases} \tag{3}$$

as well as the conditions of conservation of current at these points:[14]

$$\begin{cases} \dfrac{d\Psi_L}{dx}\,(x=0)=\dfrac{d\Psi_1}{d\xi}\,(\xi=0)+\dfrac{d\Psi_2}{d\zeta}\,(\zeta=0), \\ \dfrac{d\Psi_R}{dx}\,(x'=0)=\dfrac{d\Psi_1}{d\xi}\,(\xi=L/2)+\dfrac{d\Psi_2}{d\zeta}\,(\zeta=L/2). \end{cases} \tag{4}$$

It is convenient to use the matrix approach for solving these equations. For this purpose, we put the column vector $\hat{\Psi}(x)$ in correspondence with the wave function $\Psi(x)=A\ \exp(ikx)+B\ \exp(-ikx)$:

$$\hat{\Psi}(x)=\begin{pmatrix} \Psi_+(x) \\ \Psi_-(x) \end{pmatrix}, \tag{5}$$

where $\Psi_+(x)=A\ \exp(ikx)$ and $\Psi_-(x)=B\ \exp(-ikx)$. In this case, the wave function $\Psi(x)$ is equal to $\hat{I}\hat{\Psi}(x)$, where $\hat{I}=(1,1)$ is the unit row vector. The boundary conditions (3) and (4) can be represented in matrix form as follows:

$$\begin{cases} \hat{\Psi}_2(0)=\begin{pmatrix} 1 \\ -1 \end{pmatrix}+\hat{T}_L\hat{\Psi}_1(0), \\ \hat{\Psi}_2(L/2)=\hat{T}_R\hat{\Psi}_1(L/2), \end{cases} \tag{6}$$

where

$$\hat{T}_L=\begin{pmatrix} -1 & 1 \\ 3 & 1 \end{pmatrix}, \quad \hat{T}_R=\begin{pmatrix} 1 & 3 \\ 1 & -1 \end{pmatrix}. \tag{7}$$

Here

$$r=-1+\hat{I}\hat{\Psi}_1(0), \tag{8}$$

$$\tau=\hat{I}\hat{\Psi}_2(L/2). \tag{9}$$

Equations (6) must be supplemented by relations connecting the wave function values $\hat{\Psi}_l(0)$ at the beginning and $\hat{\Psi}_l(L/2)$ at the end of each branch ($l=1,2$). In each particular case, we can obtain such a relation with the help of the transfer matrix.[12,30]

It is well known[12,14] that at a temperature $T=0$, the value of G depends significantly on the product k_FL. In or-

der to study the effect of potential barriers, we also consider the conductance G_T of the ring at a nonzero temperature:[1]

$$G_T = G_0 \int \frac{d\varepsilon}{4T} |\tau(k)|^2 \cosh^{-2}\left(\frac{\varepsilon - \varepsilon_F}{2T}\right), \tag{10}$$

where $\varepsilon = (\hbar k)^2/(2m)$.

2. ELECTROSTATIC AHARONOV–BOHM EFFECT IN THE CONDUCTIVITY OF A ONE-DIMENSIONAL BALLISTIC RING

Let us place a metallic gate over one of the branches of the ring (Fig. 1) with a potential V_{add} which forms a potential step of length b and height $e\varphi$ in the ring. If the condition $|e\varphi| \ll \varepsilon_F$ is satisfied, the coefficient r_φ of reflection of a Fermi electron by the step can be put equal to zero. In this case, the transmission coefficient will be defined as[27]

$$t_\varphi = \exp[i(\delta_F + k_F b)], \tag{11}$$

$\delta_F = 2\pi\varphi/\varphi_0$; $e\varphi_0 = \Delta_F L/b$. The transfer matrix $\hat{T}_\varphi$ for the potential step can be represented in the following form: $\hat{T}_\varphi = \hat{T}_0(\delta_F + k_F b)$, where the ballistic transfer matrix $\hat{T}_0(x)$ is defined as

$$\hat{T}_0(x) = \begin{pmatrix} \exp(ix) & 0 \\ 0 & \exp(-ix) \end{pmatrix}. \tag{12}$$

In this case, the complete transfer matrices for the corresponding branches of the ring can be represented in the form

$$\hat{T}_{L1R} = \hat{T}_0(k_F L/2); \quad \hat{T}_{L2R} = \hat{T}_0(\delta_F + k_F L/2). \tag{13}$$

Note that in, view of the diagonality of matrices $\hat{T}_\varphi$ and $\hat{T}_0$, the matrix $\hat{T}_{L2R}$ does not depend on the position of the potential step.

The relations between the values of wave functions required for solving Eqs. (6) have the following form

$$\begin{cases} \hat{\Psi}_1(L/2) = \hat{T}_{L1R}\hat{\Psi}_1(0)\exp\left(i\pi\dfrac{\Phi}{\Phi_0}\right), \\ \hat{\Psi}_2(L/2) = \hat{T}_{L2R}\hat{\Psi}_2(0)\exp\left(-i\pi\dfrac{\Phi}{\Phi_0}\right). \end{cases} \tag{14}$$

Substituting the solution of Eq. (6) and taking (13) and (14) into account in (9) and then in (1), we obtain

$$G = G_0 \frac{(1-\cos\Delta)(1+\cos\delta_F) + (\cos\delta_F - \cos\Delta)(\cos(2\pi\Phi/\Phi_0) - 1)}{[\cos(2\pi\Phi/\Phi_0) - \cos\Delta + (\cos\delta_F - \cos\Delta)/4]^2 + \sin^2\Delta}. \tag{15}$$

Here $\Delta = k_F L + \delta_F$. Similar expressions were obtained earlier for $\delta_F = 0$ in Refs. 12 and 14.

It follows from formula (15) that G is periodic in φ with a period φ_0. Thus, a long potential barrier of small height ($e\varphi \ll \varepsilon_F$) has a considerable effect on the conductance of a ballistic ring.

For $T = 0$, the shape of the curve $G(\varphi)$ depends on the product $k_F L$ (see Fig. 2), and is not symmetric relative to the reversal of the sign of the potential step. However, such a dependence vanishes for $T > T_0 = 0.5\Delta_F$, where $\Delta_F = 2\varepsilon_F \lambda_F/L$ is the separation between the electron energy levels in the ring near the Fermi energy (Fig. 2, curve *3*), and the curve becomes symmetric:

$$G_T(\varphi) = G_T(-\varphi) \quad \text{for } T > T_0. \tag{16}$$

From a formal point of view, the presence of a potential step is equivalent to the nonsymmetric connection of terminals to the ring considered by Xia.[14] Here, $L + \delta_F/k_F \to L_1 + L_2$ and $\delta_F \to k_F \Delta L$, where $\Delta L = L_1 - L_2$, L_1 and L_2 being the lengths of the branches constituting the ring. However, such a correspondence is valid only for $T = 0$. For a nonzero temperature, the dependence of G on $k_F \Delta L$ vanishes for $T \geqslant \Delta_F L/\Delta L$, while the dependence on φ is preserved.

The main conclusion that can be drawn from formula (15) is that vector and scalar potentials exert different influence on the conductance of the ring, which is in accord with the results of measurements.[20,21]

Presenting the dependence (15) in the form of a series

$$G(\Phi) = \sum_n C_n(\varphi)\cos\left(2\pi n\frac{\Phi}{\Phi_0}\right), \tag{17}$$

we find that the quantity φ affects only the amplitudes of harmonics of the conductance $G(\Phi)$, and does not affect their phase. Figure 3 shows the dependence of C_1 (curve *1*)

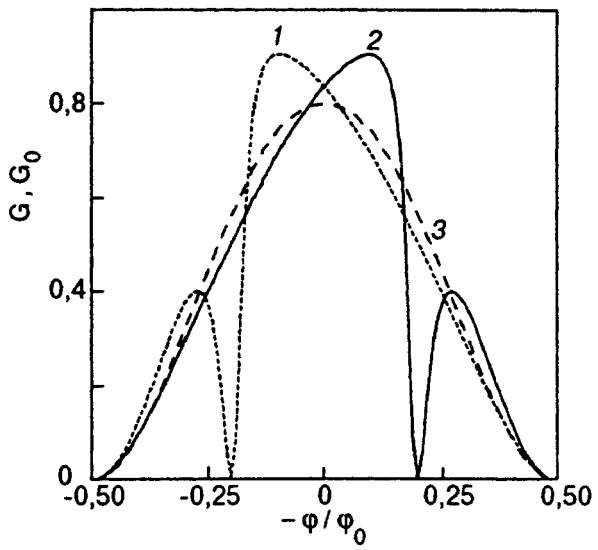

FIG. 2. Dependence of the conductance G of the ring (in units of G_0) on the height φ of the potential step for $T = 0$, $\Phi = 0$ for $L/\lambda_F = 200.2$ (curve *1*), 200.8 (curve *2*), and at $T = \Delta_F/2$ (curve *3*).

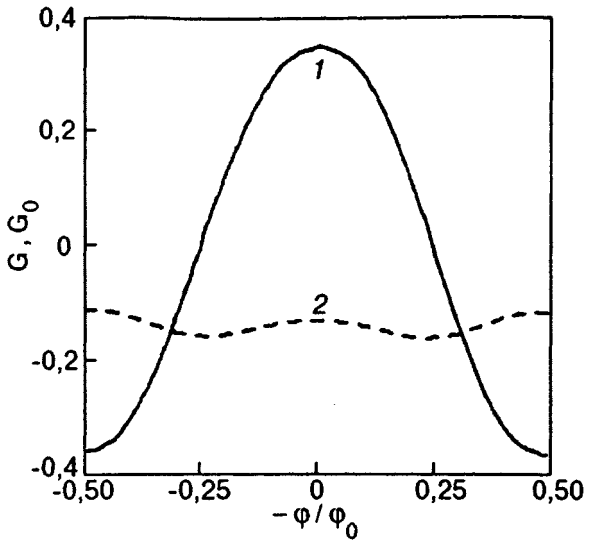

FIG. 3. Dependence of the amplitude of the first (curve *1*) and second (curve *2*) harmonics $G(\Phi)$ (in units of G_0) on the height φ of the potential step for $T=\Delta_F/2$.

and C_2 (curve *2*) on φ/φ_0 at $T=T_0$. For $\varphi=\varphi_1=\pm\varphi_0/4$, C_1 becomes equal to zero, while $C_2(\varphi_1)\neq 0$ and the dependence $G(\Phi)$ near $\varphi=\varphi_1$ is periodic in magnetic flux with a period $\Phi_0/2$. Such a transition was observed experimentally by Yacoby *et al.*[25] Note that the presence of a φ-independent component in the amplitude of the second harmonic C_2 is associated with the contribution from the AAS effect.

For $T>T_0$, the value of G_T remains unchanged upon a sign reversal of Φ or φ.[16] Separating the first harmonic, we can write

$$G_T=0.35\cos\left(2\pi\frac{\Phi}{\Phi_0}\right)\cos\left(2\pi\frac{\varphi}{\varphi_0}\right)+g(\Phi,\varphi). \tag{18}$$

The second term, which contains higher harmonics, is usually smaller than the first term except for the values

$$\Phi=\pm\Phi_0/4, \tag{19a}$$

$$\varphi=\pm\varphi_0/4, \tag{19b}$$

near which G_T is periodic in φ with a period $\varphi_0/2$ (Eq. (19a)) and in Φ with a period $\Phi_0/2$ [Eq. (19b)].

3. BALLISTIC RING WITH A SINGLE IMPURITY

The effect of a single impurity on the conductance of a ballistic ring at $T=0$ was considered earlier in Refs. 12 and 31. We shall consider the case $T\neq 0$. In addition, we shall also consider the effect of the tunneling coefficient phase on the conductance of a ring.

Suppose that an impurity of length d is introduced in one of the branches of the ring at a distance a from the starting point. We denote the transmission and reflection coefficients of a Fermi electron by $t_i=t_0\exp(i\theta)$ and $r_i=r_0\exp(i\rho)$. The other branch of the ring contains a potential step with a transfer matrix $\hat{T}_\varphi$ (see Fig. 1).

Calculations made in a similar manner as above give

$$G=G_0|2X/(Y+Z)|^2,$$

$$X=r_0\exp(i\rho)\cos\left[k_F\left(\frac{L}{2}-d-2a\right)\right]-i\exp(i\theta)\left[\sin\Sigma'+t_0\sin\Delta'\exp\left(2\pi i\frac{\Phi}{\Phi_0}\right)\right],$$

$$Y=r_0\exp(i\rho)\cos\left[k_F\left(\frac{L}{2}-d-2a\right)\right][\cos\Delta'+\exp(-i\Delta')]$$

$$Z=2\exp(-i\Delta)-\exp(i\theta)\left[\sin\Sigma'\sin\Delta'+2t_0\cos\left(2\pi\frac{\Phi}{\Phi_0}\right)\right]. \tag{20}$$

Here $\Delta=k_F(L-d)+\delta_F$; $\Delta'=k_FL/2+\delta_F$; $\Sigma'=k_F(L/2-d)+\theta$.

Formula (20) is symmetric relative to the sign reversal of the magnetic flux: $G(\Phi)=G(-\Phi)$. This can be verified through appropriate transformations. Also, the above expression is also symmetric relative to change in the impurity coordinate a: $G(a)=G(L/2-a-d)$, which indicates that the magnitude of conductance is independent of the direction of the measuring current I: $G(I)=G(-I)$.

For numerical computations, we consider a point impurity $(d=0)$ with a potential U:

$$U(\xi)=\Omega\hbar^2/m\,\delta(\xi-a). \tag{21}$$

The presence of an impurity affects the dependence $G(k_FL)$. This is due to the emergence of new channels of transition from L to R (involving reflection at the barrier) for $r_0>0$. Among other things, this causes a ''large-scale'' modulation (with a period larger than 2π) of the dependence $G(k_FL)$. The amplitude of such a modulation increases with r_0. As the temperature increases, oscillations associated with the interference of waves with the shortest path difference are preserved for the longest period of time. Such oscillations have a period $\Delta(L/\lambda_F)\simeq\max[L/(2a), L/(L-2a)]$ and vanish at $T\geqslant T_{0i}=T_0\Delta(L/\lambda_F)$ (see Fig. 4). The following circumstance is worth noting. If we consider a ring with an overlapping branch $(t_0=0)$, the separation between electron energy levels near ε_F in such a ring will be half the value of Δ_F for a pure ring. Hence it would be natural to expect that a decrease in t_0 causes a decrease in temperature at which oscillations on the dependence $G(k_FL)$ vanish. However, this is not true. This is due to the fact that the conductivity of the ring depends not only on the position of the Fermi level relative to the electron energy levels in the ring, but also on the amplitude of the electron transition through the ring.

A decrease in the barrier transparency causes a decrease in the amplitude of oscillations of the dependence $G(\Phi)$.[31] In this case, the amplitude of the second harmonic increases (Fig. 5) due to an increase in the contribution from the AAS processes to the field dependence of the conductance.

It follows from formula (20) that the dependence $G(\varphi)$ is sensitive to the amplitude and phase of the transmission coefficient t_i. In order to determine the dependence on θ, we write

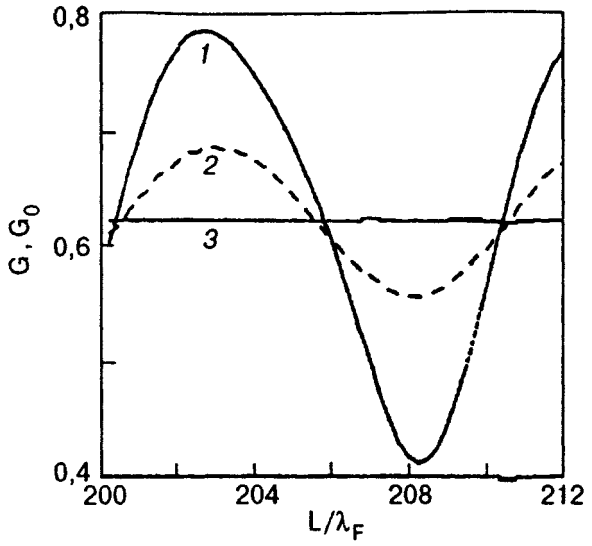

FIG. 4. Dependence of the conductance G of a ring with a single impurity (in units of G_0) on the parameter L/λ_F for $T=\Delta_F/2$ (curve *1*), 1.5 Δ_F (curve *2*) and 5 Δ_F (curve *3*). The values of the parameters are $\Phi=0$, $\varphi=0$, $\Omega/k_F=1$, and $2a/L=0.1$.

$$G(\varphi)=\sum_n D_n \cos\left(2\pi n \frac{\varphi}{\varphi_0}-\gamma_n\right), \tag{22}$$

where D_n and γ_n are the amplitude and phase of the nth harmonic.

Calculations show that the following relation holds for $T\geqslant T_0$:

$$\gamma_1=\theta. \tag{23}$$

In other words, a change in the phase of the transmission coefficient causes a corresponding variation in the phase of the first harmonic in the dependence $G(\varphi)$. Note that the parity condition (16) was obtained for a symmetric ring (for $\varphi=0$), and is not valid in the present case.

The presence of a magnetic flux $\Phi\neq 0$ does not change the relation (23). The only exception are the values $\Phi=\pm\Phi_0/4$ [see Eq. (19a)] near which D_1 vanishes.

One more circumstance deserves attention. A change in the barrier transparency may cause a sign reversal for the first harmonic in the dependence $G(\Phi)$ (Fig. 5, curve *3*). Calculations show that the amplitude of the first harmonic for $T\geqslant T_0$ vanishes if the following condition is satisfied:

$$\delta_F-\theta=\pi/2. \tag{24}$$

Thus, if we keep the amplitude of the first harmonic in the dependence $G(\Phi)$ equal to zero, the change in the height of the potential barrier is proportional to the variation in the phase of the coefficient of transmission of a Fermi electron through the potential barrier.

Yacoby *et al.*[22] found a variation π in the phase of the dependence $G(\Phi)$ in an AB interferometer with a quantum dot (QD) (a potential barrier with a resonance level) upon the passage of a QD level E_n through a resonance: $\varepsilon_F=E_n+V_p$, where V_p is the QD potential relative to the ring. Theoretical studies reveal[25,32,33] that this is due to the vanishing of the first harmonic amplitude near the resonance. It is shown in this section that such an effect may also be observed for a nonresonance potential barrier.

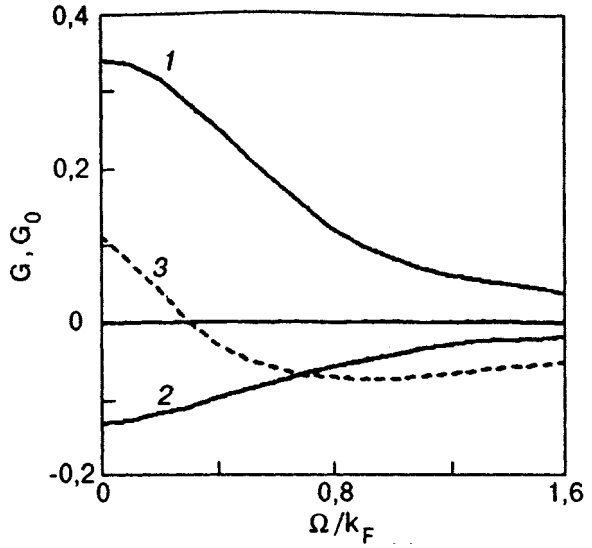

FIG. 5. Dependence of the amplitude of the first (curve *1*) and second (curve *2*) harmonics $G(\Phi)$ (in units of G_0) for $\varphi=0$, and amplitude of the first harmonic for $\varphi=0.2$ (curve *3*) on the ratio Ω/k_F. The values of the parameters are $2a/L=0.5$, $T=\Delta_F$.

CONCLUSION

In this work, we have studied the effect of a potential barrier of arbitrary height on the conductivity of an AB magnetic interferometer. Results obtained for nonzero temperatures are presented. In this case, the effect of uncontrollable geometrical size (parameter k_FL) is ruled out, but controllable parameters like the magnetic flux Φ and the height $e\varphi$ of the potential barrier continue to exert an influence.

For a small potential step ($e\varphi\ll\varepsilon_F$), the interference of electron waves propagating along different branches of the ring (Aharonov–Bohm electrostatic effect) causes an oscillatory dependence of the conductance G of the ring on φ. It is shown that the quantity δ_F (phase change of the electron wave function due to the presence of a step) does not affect the phase of the dependence $G(\Phi)$ in accordance with the experimental results.[20,21] It is also shown that a change in δ_F may cause a reversal of the sign of the amplitude of the first harmonic C_1 in the dependence $G(\Phi)$. Near the value $C_1(\delta_F)=0$, the period of oscillations changes from Φ_0 to $\Phi_0/2$, which was indeed observed by Yacoby *et al.*[25]

The effect of a tunnel barrier on the conductance of the ring is studied. It is shown that for certain values of parameters, the sign of the amplitude of C_1 may be reversed upon a change in the value of the tunneling coefficient. This effect was observed earlier in the case of resonance tunneling.[22] However, it is shown in the present work that such an effect may also occur during ordinary (nonresonance) tunneling.

It is found that an increase in the coefficient of electron reflection at the potential barrier causes a relative increase in

the amplitude of the second harmonic in the dependence $G(\Phi)$ (with a period $\Phi_0/2$) due to an increase in the contribution from the AAS processes.

It is also shown that the use of a ballistic ring with a small potential barrier (electrostatic AB interferometer) allows us to determine directly the change in the phase of the electron wave function upon tunneling through the barrier formed in one of the branches of the ring.

[1] Y. Imry, *Physics of Mesoscopic Systems: Directions in Condensed Matter Physics* [Ed. by G. Grinstein and G. Mazenco], World Scientific, Singapore (1986)
[2] Y. Aharonov and D. Bohm, Phys. Rev. **115**, 484 (1959).
[3] Y. Aharonov and D. Bohm, Phys. Rev. **123**, 1511 (1961).
[4] N. Byers and C. N. Yang, Phys. Rev. Lett. **7**, 46 (1961).
[5] F. Bloch, Phys. Rev. B **2**, 109 (1970).
[6] R. A. Webb, S. Washburn, C. P. Umbach, and R. B. Laibowitz, Phys. Rev. Lett. **54**, 2696 (1985).
[7] V. Chandrasekhar, M. J. Rooks, S. Wind, and D. E. Prober, Phys. Rev. Lett. **55**, 1610 (1985).
[8] S. Datta, M. R. Mellock, S. Bandhopadhyay *et al.*, Phys. Rev. Lett. **55**, 2344 (1985).
[9] G. Timp, A. M. Chang, J. E. Cunwugham *et al.*, Phys. Rev. Lett. **58**, 2814 (1987).
[10] C. J. B. Ford, T. J. Thornton, R. Newbury *et al.*, J. Phys. C **21**, L325 (1988).
[11] Y. Gefen, Y. Imry, and M. Ya. Azbel, Phys. Rev. Lett. **52**, 129 (1984).
[12] M. Büttiker, Y. Imry, and M. Ya. Azbel, Phys. Rev. A **30**, 1982 (1984).
[13] M. Murat, Y. Gefen, and Y. Imry, Phys. Rev. B **34**, 659 (1986).
[14] J. Xia, Phys. Rev. B **45**, 3593 (1992).
[15] A. D. Stone and Y. Imry, Phys. Rev. Lett. **56**, 189 (1986).
[16] B. Pannetier, J. Chaussy, R. Rammal, and P. Gandit, Phys. Rev. Lett. **53**, 718 (1984).
[17] D. J. Bishop, J. C. Licini, and G. J. Dolan, Appl. Phys. Lett. **46**, 1000 (1985).
[18] D. A. Browne, J. P. Carini, K. A. Muttalib, and S. R. Nagel, Phys. Rev. B **30**, 6798 (1984).
[19] B. L. Al'tshuler, A. G. Aronov, and B. Z. Spivak, Pis'ma Zh. Éksp. Teor. Fiz. **33**, 101 (1981) [JETP Lett. **33**, 94 (1981)]
[20] S. Washburn, H. Schmid, D. Kern, and R. A. Webb, Phys. Rev. Lett. **59**, 1791 (1987).
[21] P. G. N. de Verger, G. Timp, P. M. Mankiewich *et al.*, Phys. Rev. B **40**, 3491 (1989).
[22] A. Yacoby, M. Heiblum, D. Mahalu, and H. Shtrikhman, Phys. Rev. Lett. **74**, 4047 (1995).
[23] M. Büttiker, IBM J. Res. Dev. **32**, 317 (1988).
[24] C. J. B. Ford, A. B. Fowler, J. M. Hong *et al.*, Surf. Sci. **229**, 307 (1990).
[25] A. Yacoby, R. Schuster, and M. Heiblum, Phys. Rev. B **53**, 9583 (1996).
[26] R. Landauer, IBM J. Res. Dev. **1**, 223 (1957).
[27] M. V. Moskalets, Fiz. Nizk. Temp. **23**, 425 (1997) [Low Temp. Phys. **23**, 312 (1997).
[28] H. Schmid, in *Proceedings of the 8th European Congress on Electron Microscopy*, Budapest, Hungary (1984).
[29] A. Yacoby, M. Heiblum, V. Umansky *et al.*, Phys. Rev. Lett. **73**, 3149 (1994).
[30] B. S. Andereck and E. Abrahams, J. Phys. C **13**, L383 (1980).
[31] J. M. Mao, Y. Huang, and J. M. Zhou, J. Appl. Phys. **73**, 1853 (1993).
[32] G. Hackenbroich and H. A. Weidenmüller, Phys. Rev. Lett. **76**, 110 (1996).
[33] G. Hackenbroich and H. A. Weidenmüller, Phys. Rev. B **53**, 16379 (1996).

Translated by R. S. Wadhwa

Energy spectrum of a finite chain of cylindrical potential wells

E. Ya. Glushko

State Pedagogical Institute, 324086 Krivoy Rog, Ukraine[*]
(Submitted March 26, 1996; revised April 21, 1997)
Fiz. Nizk. Temp. **23**, 1106–1111 (October 1997)

An approximate analytic solution of the Schrödinger equation is obtained for a finite quasi-one-dimensional system of cylindrical potential wells. The system is considered as a model of an atomic chain or a quantum filament. It is shown that a smooth variation of the transverse size of a cylindrical quasi-one-dimensional system may modify the spectrum due to the creation (annihilation) of transverse quanta. The threshold nature of the states of a wide chain associated with the quantization of longitudinal motion is considered. [S1063-777X(97)01210-3]

1. INTRODUCTION

Low-dimensional solid structures display an enormous number of physical phenomena, such as the quantum Hall effect, high-temperature superconductivity, reversible memory, etc. In particular, quasi-one-dimensional systems like quantum filaments, atomic and molecular chains, and tips of scanning tunnel microscopes (STM) have continued to attract the attention of researchers. Apparently, the chain structure of layers in metaloxide cuprates plays an important role in the mechanism of high-temperature superconductivity.[1] Atomic chains of real structures may be simulated by potential well chains. Such a system of one-level weakly interacting potential wells was considered in Ref. 2 where the connection between the topology of a one-dimensional atomic chain and the energy spectrum was analyzed. It was shown that a variation of the connectivity of the chain (formation of a ring) causes a detachment of local states. Maslova *et al.*[3,4] calculated the contribution to the STM tunnel current from a local state formed due to interaction of the electrode tip with the sample surface. Demicheva *et al.*[5] studied experimentally the sharp increase in the conductivity of microscopic conducting channels formed in oxidized polypropylene under the action of a current. Using the spectra of radiative recombination of electrons in the heterojunction GaAs–AlGaAs with quantum filaments having photo-excited holes, Kukushkin *et al.*[6] obtained the magnetic field dependence of the energy spectrum and discovered a dimensional increase in the electron effective mass. They confirmed experimentally (see also the review in Ref. 7) the absence of a size miniband energy quantization. The theoretical proof of this effect is obtained from an analysis of exactly solvable terminated superlattice models without using the translational invariance approximation,[8,9] as well as in the framework of such an approximation.[10]

In general, the conventionally used theoretical models of quasi-one-dimensional systems[2,5–7] are strictly one-dimensional since they do not take into consideration the transverse degrees of freedom. However, a disregard of quantization in the transverse direction displaces the entire energy diagram downwards by a quantity of the order of the energy of transverse quanta. The resulting uncertainty in energy measured in this case can be avoided by confining a quasi-one-dimensional system in an impermeable potential box as was done in Refs. 8 and 11. Tikhodeev[11] used this approach to solve the problem of tunnel oscillations of the electron density in paired quantum wires. The two-dimensional problem of states in a cylindrically symmetric infinite potential well was studied in detail in Refs. 12 and 13. The three- and multidimensional cases were analyzed by Ul'yanov.[14]

In this work, we use the exact solutions for a finite system of one-dimensional potential wells to obtain an approximate analytic solution for band and local states of a terminated cylindrical quasi-one-dimensional chain of finite-depth potential wells. The obtained spectrum contains local states of two types, viz., intrinsic and extrinsic. The condition of smallness of perturbation theory corrections to the energy of actual states near the bottom of the conduction band of the chain is analyzed. The existence of the threshold effect of expulsion of states from quantum chains with a shallow potential well caused by longitudinal quantization is considered.

2. FINITE CYLINDRICAL CHAIN OF POTENTIAL WELLS

Let us consider a system of N coaxial cylindrical potential wells, each having a length a and radius R. In this model, the wells have a depth U_0 and are separated by infinitely narrow partitions with opacity coefficient Ω (Fig. 1a). The potential energy of such a system can be presented in the form of the sum $U(\rho,z)=U_0(\rho,z)+\Delta U(\rho,z)$, where the additive part in cylindrical variables ρ and z has the form $U_0(\rho,z)=U_\rho+U_z$,

$$U_z\begin{cases}\dfrac{\hbar^2\Omega}{m^*}\displaystyle\sum_{l=1}^{N-1}\delta(z-la), & z\in(0,\,Na),\\ U_0, & z\notin(0,\,Na);\end{cases} \tag{1}$$

$$\Delta U(\rho,z)=\begin{cases}0, & \rho<R,\\ -U_z, & \rho>R, \quad z\in(0,\,Na),\\ -U_0, & \rho>R, \quad z\notin(0,\,Na).\end{cases}$$

The potential energy U_ρ is equal to zero for $\rho<R$ and U_0 for $\rho>R$, ρ being the radius vector in the cylindrical system of

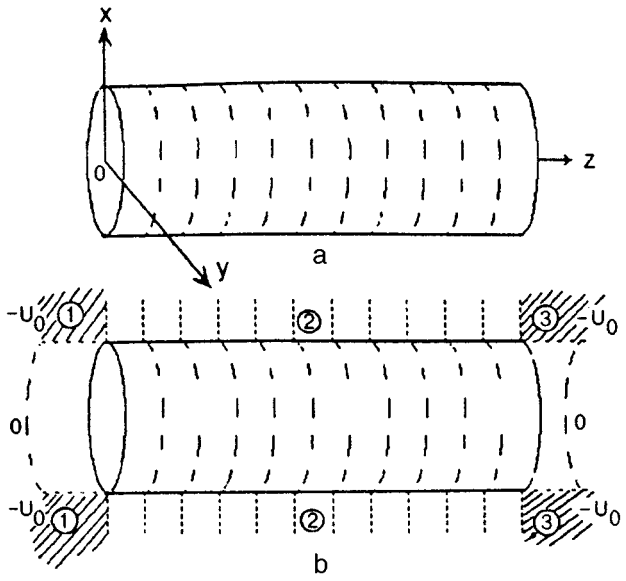

FIG. 1. A cylindrical chain of finite-depth potential wells: U_0, is the depth of the cell. The potential inside the chain is equal to zero (a). Correcting potential energy $\Delta U(\rho,z)$. The dashed curves correspond to δ-notches with opacities Ω (b).

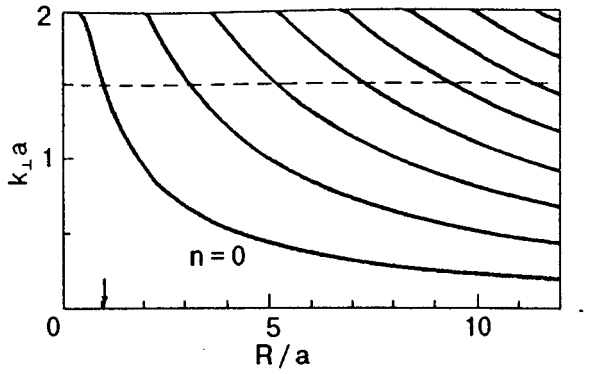

FIG. 2. Transverse quantum motion. The solid curves correspond to transverse branches. The quantum numbers N_r are measured from below. The arrow shows the position of the limiting radius $R_{\min}\approx 1.1a$ of the chain in zeroth approximation. The dashed horizontal line corresponds to the limiting wave number $k_{\max}\approx 1.486/a$.

coordinates. The exact solution of the problem can be obtained with the help of the zeroth approximation potential chosen in the form of a superposition of one-dimensional terminated Kronig–Penney potential lowered into the common potential well of depth U_0, and the potential of an infinite cylindrical well of depth U_0 with a flat bottom. In view of a large number of wells in the system, the correction $\Delta U(\rho,z)$ weakly alters the zeroth approximation spectrum (see below) and can be taken into account in the perturbation theory. Using the notation

$$\Delta_\rho=\frac{d}{\rho d\rho}\left(\rho\,\frac{d}{d\rho}\right)+\frac{1}{\rho^2}\,\frac{d^2}{d\varphi^2},\quad \Delta_z=\frac{d^2}{dz^2},$$

where φ is the azimuthal angle, we obtain the following expression for the additive part of the Hamiltonian:

$$\hat{H}_0=-\frac{\hbar^2}{2m^*}\,(\Delta_\rho+\Delta_z)+U_\rho+U_z. \tag{2}$$

The correction $\Delta U(\rho,z)$ to the zeroth Hamiltonian (see Fig. 1b) annihilates the δ-barriers in the space outside the cylinder and ''trims'' the excessive increase in potential in the hatched regions 1 and 3 by U_0. Since the variables in the Hamiltonian $\hat{H}_0$ are separated, we obtain for the l fragment of the wave function in the zeroth approximation

$$(\psi_{kk_\perp}(z,\rho))_l=(A_l e^{ikz}+B_l e^{-ikz})e^{in\varphi}\begin{cases}A_\perp \mathbf{K}_n(\overline{k_\perp}\rho), & \rho>R,\\ B_\perp \mathbf{J}_n(k_\perp\rho), & \rho<R,\end{cases} \tag{3}$$

where k and $k_\perp$ are the longitudinal and transverse wave vectors, $n=0,\pm1,\pm2,\ldots$ is the angular quantum number, $l\in[0,\,N+1]$ labels the quantum wells, the terminal values of l corresponding to the left and right banks of the one-dimensional potential with appropriate modifications of the first bracket, $\mathbf{J}_n$ is the nth order Bessel function, $\mathbf{K}_n$ the nth order McDonald function, and $A_\perp, B_\perp$ are the normalizing constants of the transverse part of the wave function,

$$k^2+k_\perp^2=\frac{E}{E_0a^2},\quad k_\perp^2+\overline{k_\perp^2}=g_0^2;$$

$$g_0^2=\frac{2m^*U_0}{\hbar^2},\quad E_0=\frac{\hbar^2}{2m^*a^2}. \tag{4}$$

Here E is the energy eigenvalue in the three-dimensional problem. The boundary conditions at any point (z,φ) on the lateral wall of the cylinder lead to the equation of quantization of transverse motion:

$$\overline{k_\perp}\,\mathbf{J}_n(k_\perp R)\mathbf{K}_{n+1}(\overline{k_\perp}R)=k_\perp \mathbf{J}_{n+1}(k_\perp R)\mathbf{K}_n(\overline{k_\perp}R). \tag{5}$$

This equation is an exact dispersion relation describing the energy spectrum of a particle in an infinite cylindrical potential well of finite depth.[13,14] Figure 2 shows the energy spectrum of transverse motion calculated according to formula (5) for $U_0=4E_0$ and the angular quantum number $n=0$ as a function of radius R.[1)] It can be seen that states in an infinite cylindrical well with a flat bottom and finite depth are formed for an indefinitely small radius R, since the lower branch of transverse motion begins directly at the point $R=0$. This result is in accord with the general conclusion about the absence of a threshold for the existence of states in an arbitrary cylindrical well.[12] Higher branches of states do possess such a threshold which is defined for $n=0$ by the zeros of $\mathbf{J}_1(k_\perp R)$. In the limit $U_0\to\infty$, we obtain a quantum filament in a cylindrical potential box.[9,11] The growth of the transverse size of the system is described by the appropriate displacement of the vertical section in Fig. 2 defining the radial quantum numbers $N_r=1,2,\ldots,N_{\max}$. For $R=9a$, for example, we obtain $N_{\max}=6$ for $n=0$ and $N_{\max}=5$ for $n=1$.

The longitudinal quantization is defined by the Hamiltonian

$$\hat{H}_z = -\frac{\hbar^2}{2m^*}\Delta_z + U_z. \tag{6}$$

The solution of the eigenvalue problem for a terminated system of potential wells without using the translational invariance approximation is based on a convolution of the product of transfer matrices $\hat{\Lambda}$ connecting the vectors (A_l, B_l) in adjacent wells:[12]

$$\hat{\Lambda}^m = \frac{1}{2}\begin{bmatrix} (\mu+\sqrt{\lambda\nu})^m + (\mu-\sqrt{\lambda\nu})^m, & \\ [(\mu+\sqrt{\lambda\nu})^m - (\mu-\sqrt{\lambda\nu})^m]\bar{\xi}\sqrt{\lambda/\nu}, & \\ & \xi\sqrt{\nu/\lambda}[(\mu+\sqrt{\lambda\nu})^m - (\mu-\sqrt{\lambda\nu})^m] \\ & (\mu+\sqrt{\lambda\nu})^m + (\mu-\sqrt{\lambda\nu})^m \end{bmatrix}, \tag{7}$$

where $\xi = \operatorname{sgn}\nu$, $\bar{\xi} = \operatorname{sgn}\lambda$, $m = N-2$,

$$\hat{\Lambda} = \begin{bmatrix} \mu & \nu \\ \lambda & \mu \end{bmatrix};$$

$$\lambda = (\Omega^2 - \kappa^2)\sin\kappa a + 2\Omega\kappa\cos\kappa a,$$

$$\nu = \sin\kappa a, \quad \mu = -\Omega\sin\kappa a - \kappa\cos\kappa a. \tag{8}$$

Local states exist inside the energy gaps ($\lambda\nu > 0$). It was shown by us earlier[8] that, for $N \gg 1$, the equation of local states for the one-dimensional system (6) has the form

$$\sqrt{\lambda/\nu} = \xi\begin{cases} \lambda_0/\nu_0 \\ (\Omega^* - \Omega)/2 \end{cases}, \tag{9}$$

where $\zeta = \xi\ \operatorname{sgn}\mu$; $\nu_0 = \kappa_0\sin\kappa a + \kappa\cos\kappa a$, $\lambda_0 = (\Omega\kappa_0 - \kappa^2)\sin\kappa a + \kappa(\Omega+\kappa_0)\cos\kappa a$; $\kappa_0^2 = g_0^2 - \kappa^2$; Ω^* is the opacity coefficient of a single perturbed barrier away from the edges, κ is the wave number of longitudinal motion, λ_0/ν_0 corresponds to local states near the ends, while $(\Omega^* - \Omega)/2$ corresponds to the intrinsic local state. The band states correspond to negative radicands $\lambda\nu$. In this case, transformation of the general dispersion relation leads to the generalized Kronig–Penney equation for the energy spectrum of longitudinal motion:

$$\cos\frac{\pi s + 2\varphi_0}{m} = \cos\kappa a + \frac{\Omega}{\kappa}\sin\kappa a, \tag{10}$$

where $\varphi_0 = \operatorname{arctg}((\nu_0/\lambda_0)\xi\sqrt{-\lambda/\nu}$, $s \in Z$, $(\pi s + 2\varphi_0)/m \in [0,\pi]$. This equation differs from the known result for an infinite one-dimensional system of δ-barriers (see, for example, Ref. 14) in the additional phase $2\varphi_0$ which slightly modifies the states near the band edges. However, exact wave functions of band states of a terminated system differ considerably from the conventionally used Bloch wave functions in that they are in the form of standing waves and do not reveal a tendency towards translational invariance for $N \to \infty$.[8,9]

The simple form of the relations (5), (9) and (10) allows us to obtain the energy diagram of states in a certain range of variation of opacities Ω of barriers separating the wells ($E - \Omega$ diagram). Figure 3 shows such a diagram for a terminated chain of potential wells for the smallest transverse quantum number $N_r = 1$ for $n = 0$. The chosen depth U_0 of the potential well in Figs. 2 and 3 corresponds to a work function of 4.7 eV (carbon, $a = 0.142$ nm).[15] The characteristic band gap 1.88 eV for fullerenes is reached at $\Omega a \approx 0.8$. Figure 2 shows that $N_{\max} = 3$ for $R = 5a$. It follows from Fig. 3 that the system being studied by us does not have any local states for such values of parameters, and its conduction band stretches from $E_{g1} \approx 1.6E_0$ to the vacuum level (continuum). A transition in the chain to the state $N_r = 2$ without a change in the angular quantum number raises the bottom of the conduction band to the level $E_{g2} \approx 2.25E_0$ ($E_0 = U_0/4$). The state with a transverse quantum number $N_r = 3$ is not realized for the given values of R and U_0. This is due to the presence of an energy gap in the longitudinal spectrum. The horizontal dashed line in Fig. 2 separates the transverse states with energy $E_\perp > U_0 - E_{g1}$ which combine with longitudinal states and fall into the continual spectrum region. Here, $E_\perp = \kappa_\perp^2 a^2 E_0$. The energy gap is responsible for the emergence of a threshold for the existence of a bound state in the chain of shallow cylindrical potential wells separated by barriers. The arrow in Fig. 2 shows the minimum chain radius for which electron conductivity still exists in the zeroth approximation for the above values of parameters.

3. SMALL PARAMETERS OF THE PROBLEM

The spectrum for the multiplicative wave function (3) obtained in the zeroth approximation does not take into ac-

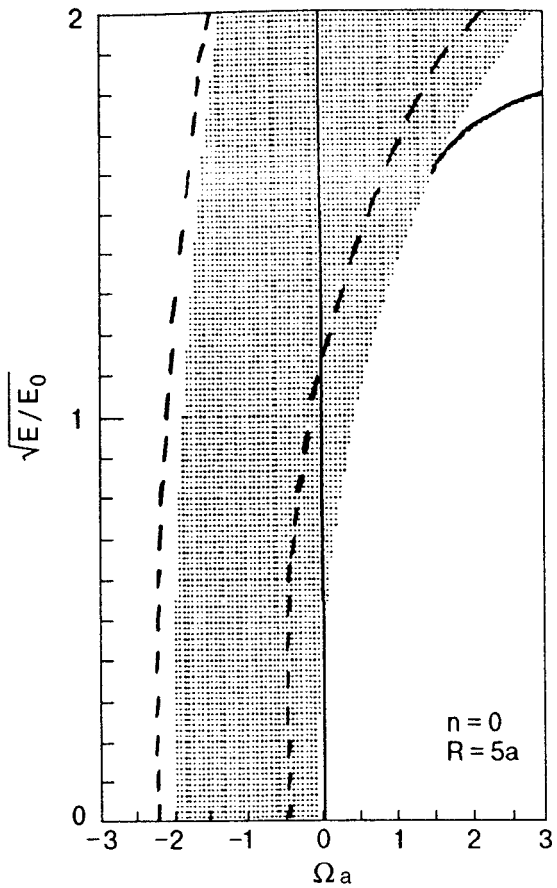

FIG. 3. $E - \Omega$ diagram in the quasi-one-dimensional model. The hatched region corresponds to the band states for $N_r = 1$, $n = 0$. The solid line is the external local state calculated by using formula (9). The dashed curves show the position of the band states for $N_r = 2$, $n = 0$; the local state is expelled to the continuous spectral region.

count the effect of the potential correction $\Delta U(z,\rho)$. Before proceeding further, we remark that only ''tails'' of the wave functions of band states penetrate the regions 1 and 3 (Fig. 1b) where this potential is quite high: $\Delta U(z,\rho)=-U_0$. However, $\Delta U(z,\rho)=0$ in the region of the chain proper, where the main density of band states is concentrated. This indicates that the separable approximation chosen by us is effective, at least for band states and deep local states (which attenuate rapidly in the outer region). Let us estimate the magnitude of corrections to the obtained energy values.

The lth order correction to the energy in perturbation theory is defined by the expression

$$\Delta E=\int d\varphi \int \rho\, d\rho \int dz\ \psi^2_{kk_\perp}(z,\rho)\Delta U(\rho,z). \tag{11}$$

The integration in this equation is carried out over the entire space, but only regions 1 and 3 make a nonzero contribution (ΔE_1) in the halfspace to the left and right of the cylinder, where $\Delta U(\rho,z)=-U_0$. Region 2 of compensating δ-barriers also makes a nonzero contribution ΔE_2 (Fig. 1b). Taking into consideration the properties of the amplitudes $A_l=-B_l^*$, the expression in the first brackets in (3) can be presented in real form:[12]

$$\psi_\parallel(z)=A_\parallel\begin{cases}\exp(\pm\kappa_0 z), & z\notin[0,\ Na],\\ C_l\ \sin(\kappa z+\varphi_l), & z\notin[0,\ Na],\end{cases} \tag{12}$$

where C_l and $\varphi_l=\arctan(\mathrm{Im}\,A_l/\mathrm{Re}\,A_l)$ are defined by the system of boundary conditions, and $A_\parallel$ is determined from the normalization condition for the longitudinal part of the wave function. The components ΔE_1 and ΔE_2 have different values for different types of states. In the case of band states, ΔE_1 contains an asymptotically small factor $A_\parallel^2/\kappa_0=l_{\mathrm{ex}}/L$, where $L=Na$ is the crystal size and l_{ex} is the length of the ''tail'' part of the probability density that falls in the external medium.

The contribution from the second region is more significant. Taking into account the relation between the amplitudes of the transverse part of the wave function

$$A_\perp=B_\perp \mathbf{J}_n(k_\perp R)/\mathbf{K}_n(\overline{k_\perp R}), \tag{13}$$

we obtain for $n=0$

$$\Delta E_2=-2E_0\Omega a\left[\frac{\Sigma_{l=1}^{N-1}C_l^2\ \sin^2(\kappa a+\varphi_l)}{a/A_\parallel^2}\right]\frac{E_\perp}{U_0}$$
$$\times\left(1-\frac{\mathbf{K}_0^2(\overline{k_\perp R})}{\mathbf{K}_1^2(\overline{k_\perp R})}\right). \tag{14}$$

Here $E_\perp$ is the energy of the transverse quantum which can be determined from Fig. 2. It follows from the explicit form of $A_\parallel^{-2}$ that the quantity in the square brackets in Eq. (14) does not exceed unity. For $N_r=1$ and the values of parameters obtained above, the last two factors in (14) are equal to 0.05 and 0.091, respectively. For $N_r=2$, these factors are equal to 0.105 and 0.25. It can be easily calculated that $|\Delta E_2|\leqslant 0.006E_{g1}$ in the first case and $|\Delta E_2|\leqslant 0.02E_{g2}$ in the second case. Hence the main correction ΔE_2 narrows the energy gap by not more than 0.6% for the lower branch of transverse motion and 2% for the upper branch.

The correction ΔE_1 is significant for local states. Putting the expression within square brackets in (14) equal to unity, we arrive at the following expression for the sum of two contributions:

$$\Delta E=-\frac{E_\perp}{U_0}\left(2\Omega a E_0+U_0\frac{l_{\mathrm{ex}}}{l_{\mathrm{ex}}+l_{\mathrm{in}}}\right)\left(1-\frac{\mathbf{K}_0^2(\overline{k_\perp R})}{\mathbf{K}_1^2(\overline{k_\perp R})}\right), \tag{15}$$

where l_{in} is the effective length over which the state penetrates from the endface into the chain. For deep states, when $l_{\mathrm{ex}}\ll l_{\mathrm{in}}$, the correction ΔE becomes small in comparison with the total energy $E=E_\perp+E_s$, where E_s is the energy of the local state detachment from the one-dimensional band.

4. STATES IN A NARROW OR SHALLOW CHAIN

In the general case, the formation of an energy level in a system of shallow potential wells is essentially inseparable and we cannot disregard the correlation between transverse and longitudinal motion. However, for broad and long chains ($R\gg a$, $N\gg 1$), the problem of threshold depth of a common potential well into which a quasidiscrete level falls from the continuum can be solved in the separable approximation. Since $E_\perp\ll E_g$ for $R\gg a$, the threshold depth for a very long chain ($N\geqslant 20$) can be assumed to be equal to $U_0\approx E_g$, where the band gap E_g is defined in accordance with (8) and (10) by the condition $\lambda=0$. This conclusion is also valid in the case of a finite depth of barriers separating the potential wells. In the notation used in Refs. 8 and 9, E_g is defined by the equation $\lambda_\nu=0$.

As regards the threshold radius $R_{\min}$ for which a bound state is formed in a chain of finite depth, we have presented above just a qualitative estimate of this parameter in the first order perturbation theory. Substituting into (14) the limiting value $k_\perp=1.486/a$ ($k_\perp=1.339/a$) obtained from the condition $E_\perp+E_g=0$, we can compute the correction $\Delta E_g\cong 0.1E_\perp$ for $R\approx 1.1a$ whence, in accordance with Fig. 2, we obtain the interval of values $R_{\min}$ between $1.1a$ and $1.2a$. This result can be refined by using integral approach, e.g., the Green's function method (see Ref. 14 in this connection).

5. DISCUSSION OF RESULTS

The method of separation of the additive part of potential used in Sec. 2 can be applied to solve the problem of a quantum wire which can be described by the model of parallelepiped wells forming parallel filaments. The zeroth-approximation wave functions in this case have the form of triple product of the expression in the first brackets in formula (3) written for various degrees of freedom. The conditions of smallness of corrections are analogous to those considered while discussing Eq. (14).

It follows from the dimensional dependence of the energy spectrum that a smooth decrease in the value of R to $R_{\min}$ leads to a continuous upward displacement of the energy pattern (Fig. 3) accompanied by an expulsion of bound states into the continuous spectrum. Such spectral variations can be observed experimentally during extension or com-

pression of the initial quantum chain caused, say, by the interaction of chain atoms with the substrate. An increase in the separation between the centers of the wells is accompanied by a narrowing of the transverse dimensions of the wells and a corresponding increase in the band gap. For the parameters chosen by us, a transition to the insulating state occurs for $R \approx a$. It must be borne in mind, however, that this conclusion is valid for a solitary chain of potential wells with a flat bottom. In real semiconducting quantum wires,[10] transverse waves are considerably distorted due to scattering at the interatomic barriers. For a thick quantum wire, i.e., a bunch of cylindrical chains considered above, the model proposed here indicates that the integral characteristics of the energy spectrum, e.g., band width and position of the bottom of the band, are completely independent of the number of chains in the bunch if the number is of the order of several dozens.

The model gives a slightly distorted initial band spectrum [see Eq. (10)] for the case when the chain of potential wells is intersected by another chain at considerable angles. The results obtained above are not applicable if the number of intersections is large, i.e., close to N.

A consideration of the finite thickness of interatomic barriers does not produce any major changes in the pattern described here.[8]

The author sincerely thanks the reviewers of this paper for a number of helpful comments.

This research was financed by the International Soros Foundation.

*E-mail: eyagl@kpi.dp.ua

[1)]Branches corresponding to $n=1$ in Fig. 2 lie almost exactly in the middle between the branches $n=0$, while the branches corresponding to $n=2$ lie in the middle between branches $n=1$.

[1] È. A. Pashitskii, Fiz. Nizk. Temp. **21**, 1091 (1995) [Low Temp. Phys. **21**, 837 (1995)].
[2] Yu. M. Abrukina and B. L. Oksendgendler, Pis'ma Zh. Éksp. Teor. Fiz. **60**, 258 (1994) [JETP Lett. **60**, 270 (1994)].
[3] P. I. Arseev and N. S. Maslova, Zh. Éksp. Teor. Fiz. **102**, 1056 (1992) [Sov. Phys. JETP **74**, 575 (1992)].
[4] N. S. Maslova, Pis'ma Zh. Éksp. Teor. Fiz. **51**, 627 (1990) [JETP Lett. **51**, 712 (1990)].
[5] O. V. Demicheva, D. N. Rogachev, S. G. Smirnova *et al.*, Pis'ma Zh. Éksp. Teor. Fiz. **51**, 228 (1990) [JETP Lett. **51**, 258 (1990)].
[6] I. V. Kukushkin, A. S. Plaut, K. von Klitzing *et al.*, Pis'ma Zh. Éksp. Teor. Fiz. **51**, 176 (1990) [JETP Lett. **51**, 201 (1990)].
[7] K. Schuller, Solid State Commun. **92**, 141 (1994).
[8] E. Ya. Glushko, Fiz. Tverd. Tela (St. Petersburg) **36**, 2417 (1994); **38**, 2051 (1996) [Phys. Solid State **36**, 1313 (1994); **38**, 1132 (1996)].
[9] E. Ya. Glushko and V. N. Evteev, Preprint of the State Pedagogical Inst., Krivoy Rog (1994); Ukr. Fiz. Zh. **40**, 719 (1995).
[10] V. R. Gushin, Zh. Eksp. Teor. Fiz. **100**, 924 (1991) [Sov. Phys. JETP **73**, 510 (1991)].
[11] S. G. Tikhodeev, Zh. Éksp. Teor. Fiz. **99**, 1871 (1991) [Sov. Phys. JETP **72**, 1047 (1991)].
[12] L. D. Landau and E. M. Lifshitz, *Quantum Mechanics* [in Russian], Nauka, Moscow (1989).
[13] V. M. Galitskii, B. M. Karnakov, and V. I. Kogan, *Problems in Quantum Mechanics* [in Russian], Nauka, Moscow (1981).
[14] V. V. Ul'yanov, *Problems in Quantum Mechanics and Quantum Statistics* [in Russian], Vysha Shkola, Kharkov (1980).
[15] A. V. Eletskii and B. V. Smirnov, Phys. Usp. **165**, 977 (1995).

Translated by R. S. Wadhwa

Noncentrality effects of impurity ions in an icosahedral environment

A. B. Roitsin, L. V. Artamonov, and A. A. Klimov

Institute of Semiconductor Physics, National Academy of Sciences of the Ukraine, Prospekt nawki, 45, 252650 Kiev, 28 Ukraine

(Submitted April 2, 1997)
Fiz. Nizk. Temp. **23**, 1112–1121 (October 1997)

The multivalley potential corresponding to the displacement of impurity ions from the center of symmetry to the centers of faces of icosahedrons, dodecahedron vertices, and centers of hexagonal faces of fullerenes is considered. The generalized effective Hamiltonian describing the behavior of endohedral complexes with noncentral ions in external electric fields of any orientation is derived. Its eigenvalues are obtained and line intensities of all possible transitions between tunnel levels are calculated. The paraelectric resonance spectrum is predicted and analyzed without an electric field as well as in the presence of a field. [S1063-777X(97)01310-8]

INTRODUCTION

The discovery of fullerenes and crystals based on them (fullerites)[1–3] has created many new trends in various branches of science, including low-temperature physics. Interest has also been aroused for symmetries whose elements include rotation by an angle divisible by $2\pi/5=72°$, e.g., C_5, C_{5v}, D_5, D_{5h}, Y, Y_h, etc., especially for the last two of these. The peculiar structure and symmetry of these new formations are as interesting as their unusual and diverse properties. For example, it was shown that the introduction of atoms of other elements into fullerites may lead to the formation of materials with semiconducting, metallic, including superconducting properties. It was also found that atoms (molecules) of elements belonging to various groups of the periodic table (right up to lanthanides and even uranium) can be introduced directly into fullerenes.[4–6] Such formations were called endohedral fullerenes and denoted by $M@C_N$, where M is the atom (ion) or the group of atoms being introduced into the fullerene and N is the number of carbon atoms in the latter. This form of notation is used to distinguish these compounds from ordinary compounds in which elements exist next to each other (in the case of fullerenes, they are attached from outside).

The large diameter of the fullerene cavity ($d\simeq 7.1$ Å in the case of C_{60}) points towards the possibility of the emergence of noncentrality which was observed earlier in crystals with a local symmetry lower than icosahedral.[7–9] The effect consists in the displacement of the minimum of the potential energy of interaction of the implanted atom with the fullerene framework from the center of symmetry of the latter. The noncentrality effect usually arises in the case when the atomic radius of the particle being implanted is smaller than the radius of the implantation cavity. This statement has been verified by calculations. Thus, Wang *et al.*[10] calculated the equilibrium positions $r_{\min}$ for a large group of ions of the periodic table implanted in C_{60}, and showed that $r_{\min}\neq 0$ for many of them, i.e., the atom is not situated at the center of symmetry of C_{60}. In particular, $r_{\min}\approx 1.3$ Å for Li^+. This result was confirmed in the theoretical work of Joslin *et al.*[11] Calculations for Na^+ show[12,13] that $r_{\min}\simeq 0.7$ Å. For comparison, we note that $r_{\min}=0$ for heavier atoms (like K^+)[14] and atoms of noble gases.[15–17]

Fullerene C_{20} and one of the highest fullerenes C_{180} also possess icosahedral symmetry with (IS).[18] Side by side fullerenes, the clusters formed by other atoms and possessing different symmetries, including icosahedral are also investigated.[19–21] Thus, Jinlong *et al.*[22] studied an icosahedral cluster $M@Co_{12}$ consisting of 12 cobalt atoms and containing atoms of various elements of the iron group, from Ti to Ni. It was shown that in all cases except Ti, Mn, and Co atoms which have a closed shell inside the cluster, a displacement from the icosahedron center is possible.

The formation of condensed materials from endohedral fullerenes and other clusters opens new avenues in low- temperature physics research. For example, it was mentioned in Ref. 23 that the introduction of polar molecules with a constant dipole moment into fullerenes may form the basis for creating a new class of ferroelectric crystals, while Wang *et al.*[10] indicated the possibility of formation of a new class of high-temperature superconductors with a specific electron–phonon coupling based on endohedral fullerenes (in contrast to the impurity fullerites tested earlier, in which the impurity is implanted between fullerenes.[3])

The noncentrality effect is accompanied by the presence of several (n) equivalent equilibrium positions. In the case of impurity ions, these positions are displaced from the symmetry center along the symmetry directions, while for dipole molecules displacement or dipole orientation along these directions may take place. Overlapping of potential valleys and wave functions of a particle moving in them leads to an intervalley tunneling of the latter and a splitting of the n-fold degenerate energy level. The resulting characteristic system of tunnel energy levels causes a diversity of effects including paraelectric resonance (PER),[7,8] which provides a technique for direct investigation of the noncentrality effect. In view of the strong ion–lattice coupling and the short relaxation

TABLE I. Characters of IR of group Y_h.

Irreducible representations	$1E$	$12C_5^{1,4}$	$12C_5^{2,3}$	$20C_3^{1,2}$	$15C_2^1$	I	$12C_5^{1,4}I$	$12C_5^{2,3}I$	$20C_3^{1,2}I$	$15C_2^1I$
A_g	1	1	1	1	1	1	1	1	1	1
A_u	1	1	1	1	1	−1	−1	−1	−1	−1
F_{1g}	3	ε_+	ε_-	0	−1	3	ε_+	ε_-	0	−1
F_{1u}	3	ε_+	ε_-	0	−1	−3	$-\varepsilon_+$	$-\varepsilon_-$	0	1
F_{2g}	3	ε_-	ε_+	0	−1	3	ε_-	ε_+	0	−1
F_{2u}	3	ε_-	ε_+	0	−1	−3	$-\varepsilon_-$	$-\varepsilon_+$	0	1
G_g	4	−1	−1	1	0	4	−1	−1	1	0
G_u	4	−1	−1	1	0	−4	1	1	−1	0
H_g	5	0	0	−1	1	5	0	0	−1	1
H_u	5	0	0	−1	1	−5	0	0	1	−1

Remark. C_n^m is the m-fold rotation around the nth order axis. The digit preceding the elements indicates the number of such elements. $\varepsilon_\pm=(1\pm\sqrt{5})/2$.

times associated with it, PER is usually observed at low temperatures only.

Thus, a large number of publications point towards the possibility of emergence of tunnel levels in many endohedral complexes, between which quantum transitions may occur. In the present work, we shall study the energy structure of noncentral ions (NI) in the intracrystalline electric field of IS produced for different atomic configurations (icosahedron, dodecahedron, fullerene). We shall consider transitions between tunnel levels under the action of a varying external electric field.

ENERGY STRUCTURE AND RESONANCE TRANSITIONS. GENERAL ANALYSIS

Earlier investigations[7–9] of the high-symmetry systems (O_h group) show that NI are displaced along symmetry directions of the type [111], [100], and [110], i.e., towards vertices, centers of faces, and edges. In view of this and taking into account the results of calculations of $r_{\min}$,[10–17] we shall consider below the symmetric displacement directions. We shall analyze a 20-valley potential that corresponds simultaneously to the NI displacements towards the centers of icosahedron faces, pentagonal dodecahedron vertices, and centers of hexagonal faces of fullerenes. All these figures have the symmetry group Y_h whose irreducible representation (IR) characters are presented in Table I.[24] The reducible representation Π_{20} which transforms the potential valleys was obtained by direct mutual transformation of 20 dodecahedron vertices defining the displaced equilibrium positions of NI of all the figures considered here. From Table I we obtain for the above representation the decomposition

$$\Pi_{20}=A_g+F_{1u}+F_{2u}+G_g+G_u+H_g, \tag{1}$$

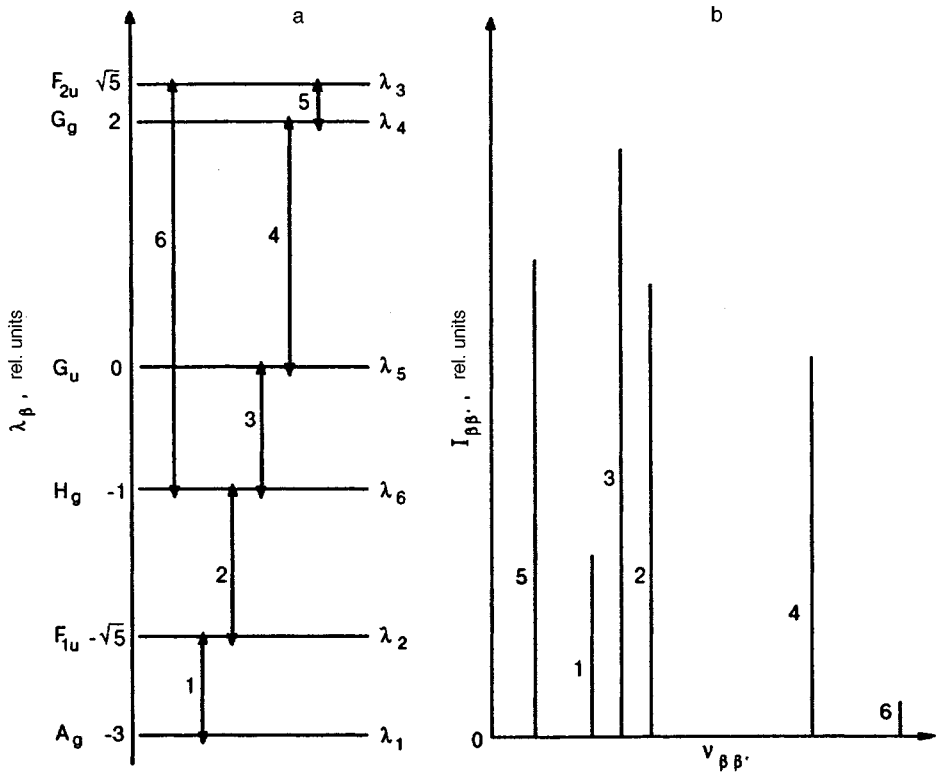

FIG. 1. System of tunnel levels λ_i. Possible resonance transitions in field-free PER (a). Relative line intensities (b): $1\to\nu_{21}$, $2\to\nu_{62}$, $3\to\nu_{56}$, $4\to\nu_{45}$, $5\to\nu_{34}$, $6\to\nu_{36}$.

TABLE II. Point groups of polyhedra in an external electric field.

Polyhedron	Direction from center to face	vertex	edge
Icosahedron	C_{3v}	C_{5v}	C_{2v}
Dodecahedron	C_{5v}	C_{3v}	C_{2v}
Fullerene	C_{5v}/C_{3v}	C_s	C_s/C_{2v}

indicating the origin and number of tunnel levels.

Let us consider the resonance transitions in the system of equations (1) in the absence of the external static electric field $\mathbf{E}_0$, i.e., a field-free PER. Transitions in PER take place under the action of a varying electric field whose vector $\mathbf{e}$ is transformed according to the IR F_{1u}. An analysis of direct products of IR of the group Y_h[25] leads to allowed transitions indicated in Fig. 1a. In this case, transitions are induced by the vector $\mathbf{e}$ oriented arbitrarily in space.

Quite frequently, PER is realized as the external field $\mathbf{E}_0$ by passing through resonance. For convenience of spectral analysis the field is oriented along the symmetry directions and hence some of the point group elements are preserved. For the symmetry directions of the field $\mathbf{E}_0$, we choose the directions from the inversion center towards vertices, centers of faces, and edges of different figures. Table II shows the symmetry groups emerging for such field directions. The presence of two point groups in one square for fullerene is associated with two types of faces and edges. The upper symbols correspond to a pentagon and the edge between a pentagon and a hexagon, while the lower symbols correspond to a hexagon and the edge between two hexagons. Data on the nature of splitting of levels under the action of a field $\mathbf{E}_0$ are presented in Table III. The digits correspond to the number of times the IR indicated at the top of the column together with the subgroup is contained in the IR of the group Y_h indicated at the beginning of the row. It can be seen from the Table that it is sufficient to consider each IR of any point subgroup not more than twice for formulating the selection rules in an arbitrary case. The results of calculations are presented in Fig. 2, the arrows showing the allowed electric dipole transitions. The indices at the arrows show the directions of components of the field $\mathbf{e}$, the symbols $\parallel$ and $\perp$ replacing the letters (x,y) and z, respectively. The absence of a notation indicates that a transition is possible for any direction of the field $\mathbf{e}$.

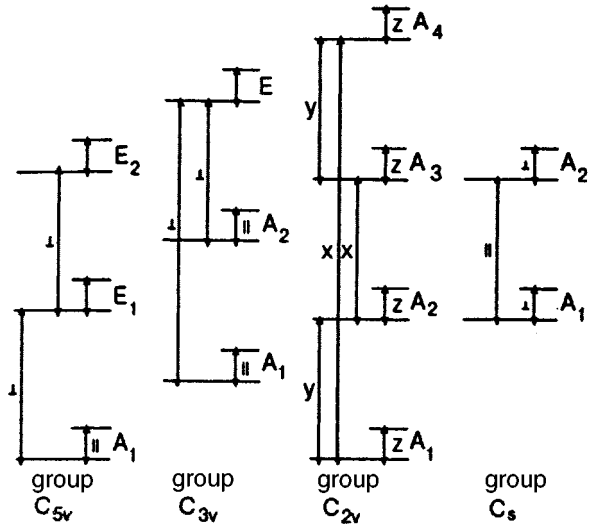

FIG. 2. Allowed transitions between tunnel levels in a constant electric field oriented along the symmetry directions.

GENERALIZED EFFECTIVE HAMILTONIAN

The method of obtaining generalized effective Hamiltonian for centers with a multivalley potential and an arbitrary local symmetry is described in Ref. 26. In the case under consideration, the Hamiltonian is a 20×20 matrix $\mathbf{M}_{20}$ whose matrix elements (ME) are defined in the basis of symmetric functions ψ^{β} corresponding to certain IR β of the group Y_h. The initial perturbation operator can be presented in the form $\hat{\mathbf{W}}=\hat{\mathbf{W}}_K+\hat{\mathbf{W}}_E$, $\hat{\mathbf{W}}_K$ and $\hat{\mathbf{W}}_E$ being the operators of energy of interaction of NI with intracrystalline and external electric fields, respectively. The operator $\hat{\mathbf{W}}_K$ is invariant with respect to all operations of the group Y_h, $\hat{\mathbf{W}}_E$ has the form $\hat{\mathbf{W}}_E=-\mathbf{dE}$, where $\mathbf{d}$ is the operator of the dipole moment of NI which is transformed according to the IR F_{1u}, and $\mathbf{E}$ in the general case is the sum of the external electric fields $\mathbf{E}_0+\mathbf{e}$ acting on NI. Using the method of perturbation matrix[26,27] and matrix of IR of the group Y_h,[28] we first ob-

TABLE III. Splitting of tunneling levels in an electric field applied along the symmetry directions.

Irreducible representations of Y_h group	C_{5v}				C_{3v}			C_{2v}				C_s	
Y_h	A_1 z	A_2	E_1 x,y	E_2	A_1 z	A_2	E x,y	A_1 z	A_2 y	A_3	A_4 x	A_1 x,y	A_2 z
A_g	1	0	0	0	1	0	0	1	0	0	0	1	0
F_{1u}	1	0	1	0	1	0	1	1	1	0	1	2	1
F_{2u}	1	0	0	1	1	0	1	1	1	0	1	2	1
G_g	0	0	1	1	1	1	1	1	1	1	1	2	2
G_u	0	0	1	1	1	1	1	1	1	1	1	2	2
H_g	1	0	1	1	1	0	2	2	1	1	1	3	2
Dimensionality of secular equations	4	0	4	4	6	2	6	7	5	3	5	12	8

Remark: A and E are one- and two-dimensional IR. The letters x, y, z below the IR notation indicate the appurtenance of the corresponding polar vector components to these IR.

tain nonzero perturbation matrices $M(\beta\times\beta')$ of the operator $\hat{\mathbf{W}}$ for all pairs of IR β and β' $(\beta\neq\beta')$. The results of calculations are presented in Appendix 1. The nondiagonal matrices $(\beta\neq\beta')$ do not contain nonzero ME of the operator $\hat{\mathbf{W}}_K$ because of its invariance to all transformations of the group Y_h. Nonzero ME of it will be present only in square matrices of the type $M(\beta\times\beta)$. These elements are arranged along the principal diagonal, and all ME are identical for each IR β. We introduce the following notation for them:

$$\lambda_\beta=\int (\psi^{(\beta)})^*\hat{W}_K\psi^{(\beta)}d\tau. \tag{2}$$

Since the operator $\hat{\mathbf{d}}$ does not possess parity relative to inversion, the matrices $M(\beta\times\beta)$ do not contain nonzero ME of the operator $\hat{\mathbf{W}}_E$.

The required matrix $\mathbf{M}_{20}$ can be represented as a combination of the perturbation matrices presented in Appendix 1:

$$\mathbf{M}_{20}=\begin{bmatrix} M(1\times1) & M(1\times2), & 0, & 0, & 0, & 0 \\ & M(2\times2), & 0, & 0, & 0, & M(2\times6) \\ & & M(3\times3), & M(3\times4), & 0, & M(3\times6) \\ & & & M(4\times4), & M(4\times5), & 0 \\ & \text{c.c.} & & & M(5\times5), & M(5\times6) \\ & & & & & M(6\times6) \end{bmatrix} \tag{3}$$

where c.c. stands for complex conjugate, and zeros indicate that all ME of the block are zeros. The rows and columns in (3) are arranged according to IR in the following order: A_g, F_{1u}, F_{2u}, G_g, G_u, H_g. The equation contains six parameters $\alpha_{\beta\beta'}$ describing the effect of external fields $\mathbf{E}$, as well as six parameters λ_β characterizing the intracrystalline electric field.

For any orientation of the field $\mathbf{E}_0$, the exact analytic expressions for eigenvalues of the operator (3) cannot be presented in a general form. Hence it is expedient to consider the approximate solutions using the perturbation theory in the presence of degeneracy[29] for two possible cases $\hat{\mathbf{W}}_K\gg\hat{\mathbf{W}}_E$ and $\hat{\mathbf{W}}_E\gg\hat{\mathbf{W}}_K$. For symmetric directions of the field $\mathbf{E}_0$, the 20th order secular equation splits into equations of lower order. The numbers in the last row of Table III indicate the dimensionality of such equations, the latter corresponding to a definite IR of the subgroup. For two- dimensional representations, two identical equations of the indicated dimensionality are obtained. Thus, if the field $\mathbf{E}_0$ is directed along the Z-axis, the symmetry of Y_h drops to C_{5v} and the secular equation is split into five fourth-order equations. One of these corresponds to the IR A_1, while the IR E_1 and E_2 have two identical equations each. These equations have the form

IRA_1:

$$\mathscr{E}^4-\mathscr{E}^2(E_{12}^2+E_{26}^2+E_{36}^2)+E_{12}^2E_{36}^2=0,$$

IRE_1:

$$\mathscr{E}^4-\mathscr{E}^2\left(\frac{3}{4}E_{26}^2+E_{56}^2+E_{45}^2\right)+\frac{3}{4}E_{26}^2E_{45}^2=0,$$

IRE_2:

$$\mathscr{E}^4-\mathscr{E}^2\left(\frac{1}{3}E_{36}^2+\frac{1}{4}E_{56}^2+E_{34}^2+E_{45}^2\right)+\frac{1}{4}E_{56}^2E_{34}^2$$

$$+\frac{1}{3}E_{36}^2E_{45}^2+\frac{1}{\sqrt{3}}E_{36}E_{56}E_{34}E_{45}=0, \tag{4}$$

where $E_{\beta\beta'}=\alpha_{\beta\beta'}E_z$. For the sake of simplicity, we put $\lambda_i=0$ when deriving the above expressions, which corresponds to zeroth approximation for the case $\hat{\mathbf{W}}_E\gg\hat{\mathbf{W}}_K$. We can use the biquadratic equations (4) to obtain all energy levels in the analytic form. For the case $\hat{\mathbf{W}}_K\gg\hat{\mathbf{W}}_E$, the zeroth approximation is determined by the levels λ_β. For this case, the data presented in Appendix 1 can be used for exact computations of the squares of ME for transitions in the system of levels presented in Fig. 1a: e_{12}^2, $^{5/2}e_{26}^2$, $^{5/3}e_{36}^2$, $^{5/2}e_{56}^2$, $2e_{34}^2$, $4e_{45}^2$, respectively, for transitions $A_g\leftrightarrow F_{1u}$, $F_{1u}\leftrightarrow H_g$, $F_{2u}\leftrightarrow H_g$, $G_u\leftrightarrow H_g$, $F_{2u}\rightarrow G_g$, $G_g\leftrightarrow G_u$ where $e_{\beta\beta'}=\alpha_{\beta\beta'}e$; $e^2=e_x^2+e_y^2+e_z^2$.

PHYSICAL MEANING OF PARAMETERS λ_β AND $\alpha_{\beta\beta'}$

We shall use the valley approximation, which is the oscillatory analog of the MO LCAO method in quantum chemistry.[30] Let φ_i $(i=1,2,\ldots,20)$ be the valley function of a particle in the ith quasiequilibrium position (Fig. 3). The functions φ_i carry out the reducible representation Π_{20} transforming them into each other under the action of the operations of group Y_h. As a result, we obtain orthonormal symmetrized functions ψ_j^β:

$$\psi_j^\beta=D^\beta\sum_{i=1}^{20}k_{ij}^\beta\varphi_i. \tag{5}$$

For each of the 20 functions, the coefficients k_{ij}^β and D^β are presented in Appendix 2, The nonorthogonality integrals $\sigma_{i\neq0}$ are presented below in descending order:

$$\sigma_1=\int\varphi_1^*\varphi_2d\tau,\quad \sigma_2=\int\varphi_1^*\varphi_3d\tau,$$

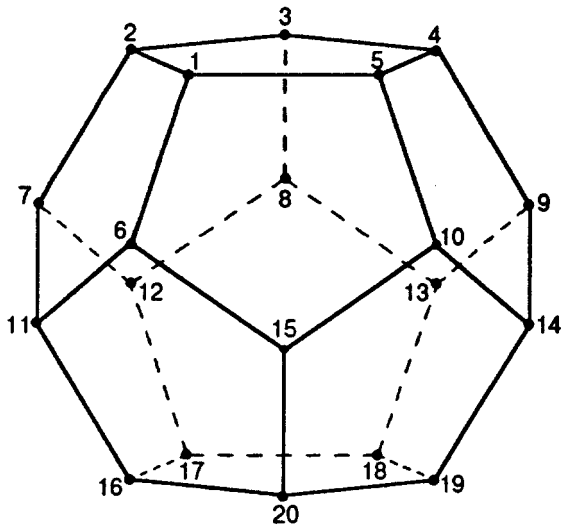

FIG. 3. Equilibrium positions i of noncentral ions (dipole directions) for a 20-valley potential in endohedral complexes of icosahedral symmetry. The points i are located at the vertices of a pentagonal dodecahedron.

$$\sigma_3=\int \varphi_1^*\varphi_{20}d\tau, \quad \sigma_4=\int \varphi_1^*\varphi_{19}d\tau,$$

$$\sigma_5=\int \varphi_1^*\varphi_{18}d\tau; \quad \sigma_0=1.$$

Substituting (5) into (2), we obtain

$$\lambda_\beta=\sum_{i=0}^{5} n_i^\beta V_i/S_\beta,$$

where

$$V_0=\int \varphi_1^*\hat{W}_K\varphi_1 d\tau, \quad V_1=\int \varphi_1^*\hat{W}_K\varphi_2 d\tau,$$

$$V_2=\int \varphi_1^*\hat{W}_K\varphi_3 d\tau, \quad V_3=\int \varphi_1^*\hat{W}_K\varphi_{20} d\tau,$$

$$V_4=\int \varphi_1^*\hat{W}_K\varphi_{19} d\tau, \quad V_5=\int \varphi_1^*\hat{W}_K\varphi_{18} d\tau.$$

Similar relations can be obtained for the parameters $\alpha_{\beta\beta'}$. In this case, ME of the type

$$\int \varphi_i\hat{\mathbf{d}}_z\varphi_j d\tau$$

will appear together with the integrals σ_i as parameters of the theory.

Let us estimate the highest overlapping integral σ_1. For the valley function we choose an oscillator function of the type

$$\varphi_i=(l/\pi)^{3/4}\exp\{-(l/2)[(x-x_i)^2+(y-y_i)^2+(z-z_i)^2]\},$$

normalized to unity, where x_i, y_i, z_i are the coordinates of the center of the ith valley, $l=m\omega/\hbar$ where m is the mass of an NI, and ω is the frequency of oscillations in a potential well. Putting $r_{\min}=1.4$ Å, $m=1.2\times10^{-23}$ g, and $\omega=3\times10^{12}$ rad/s,[32] we find that $\sigma_1=0.4$. Neglecting all nondiagonal ME, we obtain

$$\lambda_\beta=V_0(i=1,...,6);$$

$$\alpha_{12}=\frac{R_1}{2\sqrt{S_{12}}}; \quad \alpha_{26}=\frac{R_2}{2\sqrt{S_{26}}}; \quad \alpha_{36}=\frac{R_3}{2\sqrt{S_{36}}};$$

$$\alpha_{56}=\frac{R_2}{\sqrt{3S_{56}}}; \quad \alpha_{34}=\frac{R_1}{\sqrt{3S_{34}}}; \quad \alpha_{45}=\frac{t_3r_{11}-t_4r_{66}}{\sqrt{6S_{45}}};$$

$$R_{1,2}=t_1r_{11}\pm t_2r_{66}; \quad R_3=-(t_2r_{11}+t_1r_{66});$$

$$S_{\beta\beta'}=S_\beta S_{\beta'}; \quad t_{1,2}=\sqrt{1\pm2/p};$$

$$t_{3,4}=\sqrt{1\pm1/p}; \quad r_{ii}=\int \varphi_i^*\hat{\mathbf{d}}_z\varphi_i d\tau.$$

Putting $r_{ii}=\int\varphi_i^*\mathbf{Z}\varphi_i d\tau$, we obtain $r_{11}/r_{66}=4.3$, which indicates that terms which are proportional to r_{66} can be disregarded (except for the case α_{36}, but this ME will be much smaller than other α_{ij} and its role will be insignificant). In this approximation, the tunnel splitting does not occur, and the system is described by a single parameter $d_0=r_{11}$, viz., by the local electric dipole moment. Such an approximation can be used for strong fields $\mathbf{E}_0(\hat{\mathbf{W}}_E\gg\hat{\mathbf{W}}_K)$.

Let us consider the tunnel approximation[7,8] in which all nondiagonal matrix elements of the operator $\hat{\mathbf{W}}_K$ and nonorthogonality integrals are assumed to be small, and only integrals corresponding to nearest neighbors are preserved. Moreover, all nondiagonal ME of the operator $\hat{\mathbf{W}}_E$ are put equal to zero. In this approximation, $\lambda_\beta=V_0+a_\beta U$, where $U=V_0\sigma_1-V_1$, and a_β are equal to -3, $-\sqrt{5}$, $+\sqrt{5}$, $+2$, 0, and -1, respectively for $\beta=1$, 2, 3, 4, 5, 6, and the separation between levels is determined by a single parameter U. This scale is used for the system of levels presented in Fig. 1a. For the transition frequencies (in units of U), we have $\nu_{21}=3-\sqrt{5}$, $\nu_{62}=\sqrt{5}-1$, $\nu_{56}=1$, $\nu_{45}=2$, $\nu_{34}=\sqrt{5}-2$, $\nu_{36}=\sqrt{5}+1$, where $\nu_{\beta\beta'}=\lambda_\beta-\lambda_{\beta'}$. Using the relations for parameters $\alpha_{\beta\beta'}$ and squares of transition ME in the field-free PER, we can also obtain an expressions for line intensities in the tunnel approximation. These data (in units of $e^2d_0^2$) are presented in Fig. 1b together with the corresponding data for transition frequencies (in units of U). The obtained results describe nonparametrically the relative values of frequencies and transition intensities, and can be used for identifying the PER lines.

CONCLUSION

The number of lines in the PER spectrum and their intensities depend on the presence (or absence) of the external field $\mathbf{E}_0$ and its orientation relative to the coordinate axes attached to a certain cluster of icosahedral symmetry. Thus, for $\mathbf{E}_0=0$, we obtain six lines whose frequencies $\nu_{\beta\beta'}$ and intensities $I_{\beta\beta'}$ are in the ratio 0.24:0.76:1.0:1.2:2.0:3.2 and 1.3:0.47:1.6:1.20:0.96:0.044, respectively. For $\mathbf{E}_0\neq0$ and for field orientation along the fifth-order axis, there will be fifty PER lines in all, of which six will be observed for $\mathbf{e}\|\mathbf{E}_0$, 32 for $\mathbf{e}\perp\mathbf{E}_0$, and 12 for any orientation of the vector $\mathbf{e}$.

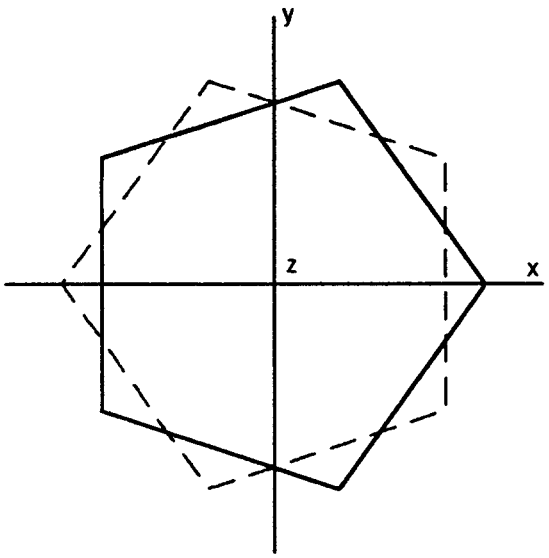

FIG. 4. Projection of an icosahedron on the (x,y) plane passing through its center and perpendicular to the z-axis. The z-axis passes through the vertices of the icosahedron and is directed towards the reader. The solid line indicates the projection of a part of the figure lying above the plane, while the dashed line corresponds to the part below the plane.

Two situations must be distinguished in experiments. The first of these is a random orientation of paraelectric centers for an orientationally disordered condensed cluster. Here, the axes of the centers are distributed randomly in space, and the description of the PER spectrum requires a preliminary averaging of transition frequencies (resonance electric fields) over angles characterizing the orientation of the axes of complexes. Such an averaging causes an additional broadening of PER lines. The second situation corresponds to the same type of orientation of centers in identical or several nonequivalent positions. Such a situation can arise in a number of supercooled liquids or crystals of fullerite type. In this case, the above expressions for transition frequencies will realize directly, and the line broadening will be caused by other factors, the most important of which in PER is the defect structure of the condensed phase. It should be observed, however, that for $\mathbf{E}_0=0$ the field-free PER spectra in two cases will be identical since the spectra are independent of orientation of the field **e** responsible for the transitions. This circumstance extends the range of materials that can be subjected to investigation, including the gaseous phase, solutions, and powders.

Finally, it should be remarked that all possible cases of PER realization can be described on the basis of the Hamiltonian (3). The relations for frequencies, intensities, and other characteristics of spectral lines are simplified considerably in the tunnel approach which can be used expediently for describing the first experimental results. The Hamiltonian (3) may also serve as the basis for studying other properties of materials that are determined by noncentral impurities in endohedral complexes.

This research was carried out under financial support from the Ukrainian State Committee on Science and Technology.

APPENDIX 1

The matrices of the perturbation operator $\hat{\mathbf{W}}$ are defined as follows:

$$M(1\times 2)=\frac{\alpha_{12}}{\sqrt{2}}\,(P,\sqrt{2}E_z,-P^*);$$

$$M(2\times 6)=\frac{\alpha_{26}\sqrt{3}}{2}\begin{pmatrix} P & E_z, & -P^*/\sqrt{6}, & 0, & 0 \\ 0, & P/\sqrt{2}, & 2E_z/\sqrt{3}, & -P^*/\sqrt{2}, & 0 \\ 0, & 0, & P/\sqrt{6}, & E_z & -P^* \end{pmatrix};$$

TABLE A1. Coefficients k_{ij}^{β} for symmetrized functions.

			k_{ij}^{β}																			
			i																			
IR	β	j	1	2	3	4	5	6	7	8	9	10	11	12	13	14	15	16	17	18	19	20
A_g	1	1	$+1$	$+1$	$+1$	$+1$	$+1$	$+1$	$+1$	$+1$	$+1$	$+1$	$+1$	$+1$	$+1$	$+1$	$+1$	$+1$	$+1$	$+1$	$+1$	$+1$
F_{1u}	2	1	$+c_3$	$+a_3$	$+c_3^*$	$-c_2$	$-c_2^*$	$+c_5$	$+1$	$+c_5^*$	$-c_6$	$-c_6^*$	$+c_6$	$+c_6^*$	$-c_5$	-1	$-c_5^*$	$+c_2$	$+c_2^*$	$-c_3$	$-a_3$	$-c_3^*$
		2	$-a_2$	$-a_2$	$-a_2$	$-a_2$	$-a_2$	$-a_5$	$-a_5$	$-a_5$	$-a_5$	$-a_5$	$+a_5$	$+a_5$	$+a_5$	$+a_5$	$+a_5$	$+a_2$	$+a_2$	$+a_2$	$+a_2$	$+a_2$
F_{2u}	3	1	$-c_4^*$	$+a_4$	$-c_4$	$+c_1$	$+c_1^*$	$+c_6^*$	-1	$+c_6$	$-c_5$	$-c_5^*$	$+c_5$	$+c_5^*$	$-c_6^*$	$+1$	$-c_6$	$-c_1$	$-c_1^*$	$+c_4^*$	$-a_4$	$+c_4$
		2	$+a_1$	$+a_1$	$+a_1$	$+a_1$	$+a_1$	$-a_6$	$-a_6$	$-a_6$	$-a_6$	$-a_6$	$+a_6$	$+a_6$	$+a_6$	$+a_6$	$+a_6$	$-a_1$	$-a_1$	$-a_1$	$-a_1$	$-a_1$
G_g	4	1	$-c_{10}$	$+a_8$	$-c_{10}^*$	$+c_8^*$	$+c_8$	$+c_6$	-1	$+c_6^*$	$-c_5^*$	$-c_5$	$-c_5^*$	$-c_5$	$+c_6$	-1	$+c_6^*$	$+c_8^*$	$+c_8$	$-c_{10}$	$+a_8$	$-c_{10}^*$
		2	$+c_5$	$+1$	$+c_5^*$	$-c_6$	$-c_6^*$	$-c_8$	$-a_8$	$-c_8^*$	$+c_{10}$	$+c_{10}^*$	$+c_{10}$	$+c_{10}^*$	$-c_8$	$-a_8$	$-c_8^*$	$-c_6$	$-c_6^*$	$+c_5$	$+1$	$+c_5^*$
G_u	5	1	$-c_2$	$+a_3$	$-c_2^*$	$+c_3^*$	$+c_3$	$-c_6$	$+1$	$-c_6^*$	$+c_5^*$	$+c_5$	$-c_5^*$	$-c_5$	$+c_6$	-1	$+c_6^*$	$-c_3^*$	$-c_3$	$+c_2$	$-a_3$	$+c_2^*$
		2	$+c_5$	$+1$	$+c_5^*$	$-c_6$	$-c_6^*$	$-c_3$	$-a_3$	$-c_3^*$	$+c_2$	$+c_2^*$	$-c_2$	$-c_2^*$	$+c_3$	$+a_3$	$+c_3^*$	$+c_6$	$+c_6^*$	$-c_5$	-1	$-c_5^*$
H_g	6	1	$-c_7^*$	$+a_7$	$-c_7$	$+c_9$	$+c_9^*$	$-c_6^*$	$+1$	$-c_6$	$+c_5$	$+c_5^*$	$+c_5$	$+c_5^*$	$-c_6^*$	$+1$	$-c_6$	$+c_9$	$+c_9^*$	$-c_7^*$	$+a_7$	$-c_7$
		2	$-c_5$	-1	$-c_5^*$	$+c_6$	$+c_6^*$	$-c_9$	$-a_7$	$-c_9^*$	$+c_7$	$+c_7^*$	$+c_7$	$+c_7^*$	$-c_9$	$-a_7$	$-c_9^*$	$+c_6$	$+c_6^*$	$-c_5$	-1	$-c_5^*$
		3	$+a_9$	$+a_9$	$+a_9$	$+a_9$	$+a_9$	$-a_9$	$-a_9$	$-a_9$	$-a_9$	$-a_9$	$-a_9$	$-a_9$	$-a_9$	$-a_9$	$-a_9$	$+a_9$	$+a_9$	$+a_9$	$+a_9$	$+a_9$

Remark: $k_{i3}^{2,3}=-(k_{i1}^{2,3})^*$, $k_{i3,4}^{4}=(k_{i2,1}^{4})^*$, $k_{i3,4}^{5}=-(k_{i2,1}^{5})^*$, $k_{i5}^{6}=(k_{i1}^{6})^*$, $k_{i4}^{6}=-(k_{i2}^{6})^*$.

$$M(3\times 6)$$

$$= \frac{\alpha_{36}}{\sqrt{3}} \begin{pmatrix} E_z, & P^*, & 0, & 0, & P \\ 0, & -P/\sqrt{2}, & \sqrt{3}E_z, & P^*/\sqrt{2}, & 0 \\ -P^* & 0, & 0, & P & -E_z \end{pmatrix};$$

$$M(5\times 6)$$

$$= \frac{\alpha_{56}}{4} \begin{pmatrix} 3P^*, & 0, & 0, & 2P, & -2E_z \\ -P, & 4E_z, & \sqrt{6}P^*, & 0, & 0 \\ 0, & 0, & -\sqrt{6}P, & 4E_z, & P^* \\ 2E_z, & 2P^*, & 0, & 0, & -3P \end{pmatrix};$$

$$M(3\times 4) = \frac{\alpha_{34}}{2} \begin{pmatrix} P, & P^*, & 0, & -2E_z \\ 0, & \sqrt{2}P, & \sqrt{2}P^*, & 0 \\ 2E_z, & 0, & -P, & -P^* \end{pmatrix};$$

$$M(4\times 5) = \alpha_{45} \begin{pmatrix} -E_z, & 0, & -P, & 0 \\ 0, & -E_z, & 0, & P \\ -P^*, & 0, & E_z, & 0 \\ 0, & P^*, & 0, & E_z \end{pmatrix};$$

where $P = E_x + iE_y$, and the common factor in front of the matrix indicates that all ME must be multiplied by this factor;

$$\alpha_{12} = -\int (\psi^{(1)})^* \hat{\mathbf{d}}_z \psi_2^{(2)} d\tau,$$

$$\alpha_{26} = -\int (\psi_2^{(2)})^* \hat{\mathbf{d}}_z \psi_3^{(6)} d\tau,$$

$$\alpha_{36} = -\int (\psi_2^{(3)})^* \hat{\mathbf{d}}_z \psi_3^{(6)} d\tau,$$

$$\alpha_{56} = -\int (\psi_2^{(5)})^* \hat{\mathbf{d}}_z \psi_2^{(6)} d\tau,$$

$$\alpha_{34} = -\int (\psi_3^{(3)})^* \hat{\mathbf{d}}_z \psi_1^{(4)} d\tau,$$

$$\alpha_{45} = -\int (\psi_4^{(4)})^* \hat{\mathbf{d}}_z \psi_4^{(5)} d\tau,$$

where the subscript of the functions denotes their order number in the base of the corresponding IR, the superscript corresponds to the IR (for convenience of notation, letters defining IR in formulas are replaced by digits: $A_g \to 1$, $F_{1u} \to 2$, $F_{2u} \to 3$, $G_g \to 4$, $G_u \to 5$, $H_g \to 6$); $d\tau$ is the volume element; and all $\alpha_{\beta\beta'}$ are real. The choice of the coordinate system is indicated in Fig. 4.

APPENDIX 2

Coefficients k_{ij}^{β} and D^{β} for symmetrized functions are given in Tables A1 and A2.

$$a_{1,2} = \frac{\sqrt{2}}{p\pm 1}; \quad a_{3,4} = \sqrt{2}a_{1,2}; \quad a_{5,6} = \frac{\sqrt{2}}{3\pm p};$$

TABLE A2. Coefficients A^{β} and n_i for symmetrized functions.

		D^{β}		
β	A^{β}	n_0, n_5	n_1, n_4	n_2, n_3
A_g	$1/p$	1	3	6
F_{1u}	$\sqrt{5+p}/10$	± 1	$\pm p$	± 2
F_{2u}	$\sqrt{5-p}/10$	± 1	$\mp p$	± 2
G_g	$\sqrt{3-p/\sqrt{60}}$	1	-2	1
G_u	$\sqrt{5+p}/10$	± 1	0	∓ 3
H_g	$\sqrt{3+p/\sqrt{60}}$	1	1	-2

$$a_{7,8} = \sqrt{2}a_{5,6}; \quad a_9 = \frac{\sqrt{6}}{p+1};$$

$$c_{1,2} = \frac{1}{2} + \frac{iA^{\pm}}{2}; \quad c_{3,4} = \frac{1}{3\pm p} + \frac{iD^{\mp}}{\sqrt{8}};$$

$$c_{5,6} = \frac{1}{p\pm 1} + \frac{iD^{\pm}}{\sqrt{8}}; \quad c_{7,8} = \frac{1}{p\pm 1} + \frac{iJ^{\mp}}{\sqrt{8}};$$

$$c_{9,10} = \frac{1/(p\pm 2) + iA^{\mp}}{2}; \quad D^{\beta} = A^{\beta}/\sqrt{S_{\beta}}$$

$$S_{\beta} = \sum_{i=0}^{5} n_i^{\beta} \sigma_i;$$

$$A^{\pm} = \sqrt{5\pm 2p}; \quad D^{\pm} = \sqrt{5\pm p}; \quad J^{\pm} = \sqrt{25\pm 11p};$$

$$p = \sqrt{5}.$$

[1] R. F. Curl and R. Z. Smolly, Sci. Am. **12**, 14 (1991).
[2] V. Krechmer, Priroda **1**, 30 (1992).
[3] V. M. Loktev, Fiz. Nizk. Temp. **18**, 217 (1992) [Sov. J. Low Temp. Phys. **18**, 149 (1992)].
[4] F. D. Weiss, J. L. Elkind, S. C. O'Brien *et al.*, J. Am. Chem. Soc. **110**, 4464 (1988).
[5] D. S. Bethune, R. D. Johnson, J. R. Salem *et al.*, Monthly Nature **1**, 67 (1993).
[6] A. V. Eletskii and B. M. Smirnov, Usp. Fiz. Nauk **165**, 977 (1995).
[7] M. D. Glinchuk, V. G. Grachev, M. F. Deigen *et al.*, *Electrical Effects in Radiospectroscopy* [in Russian], Nauka, Moscow (1981).
[8] U. Kh. Kopvillem and R. V. Saburova, *Paraelectric Resonance*, [in Russian], Nauka, Moscow (1982).
[9] V. S. Vikhnin, in *Radiospectroscopy of Solids* [in Russian] (Ed. by A. B. Roitsin), Naukova Dumka, Kiev (1992).
[10] Y. Wang, D. Tomanek, and R. S. Ruoff, Chem. Phys. Lett. **208**, 79 (1993).
[11] C. G. Joslin, J. Yang, C. G. Gray *et al.*, Chem. Phys. Lett. **208**, 86 (1993).
[12] J. Cioslowski and E. D. Fleischmann, J. Chem. Phys. **94**, 3730 (1991).
[13] J. L. Ballester and B. I. Dunlap, Phys. Rev. A **45**, 7985 (1992).
[14] C. G. Joslin, J. Yang, C. G. Gray *et al.*, Chem. Phys. Lett. **211**, 587 (1993).
[15] G. Cardini, P. Procacci, P. R. Salvi, and V. Schettino, Chem. Phys. Lett. **200**, 39 (1992).
[16] L. Pang and F. Brisse, J. Chem. Phys. **97**, 8562 (1993).
[17] J. Breton, J. Gonzales-Platas, and C. Giradet, J. Chem. Phys. **99**, 4036 (1993).
[18] B. Shanker and J. Applequist, J. Phys. Chem. **98**, 6486 (1994).
[19] I. D. Morokhov, V. I. Petinov, L. I. Trusov, and V. F. Petrunin, Usp. Fiz. Nauk **133**, 653 (1981) [Sov. Phys. Usp. **24**, 295 (1981)].
[20] W. Heer, Rev. Mod. Phys. **65**, 611 (1993).
[21] H. Brack, Rev. Mod. Phys. **65**, 677 (1993).
[22] Y. Jinlong, X. Chuayun, X. Shangda, and W. Kelin, Phys. Rev. B **48**, 12155 (1993).
[23] J. Cioslowski and A. Nanayakkara, Phys. Rev. Lett. **69**, 2871 (1992).

[24] A. B. Roitsin, Phys. Status Solidi B **178**, 275 (1993).
[25] A. B. Roitsin, Fiz. Tverd. Tela (St. Petersburg) **35**, 2548 (1993) [Phys. Solid State **35**, (1993)].
[26] A. B. Roitsin, Fiz. Tverd. Tela (St. Petersburg) **37**, 1594 (1995) [Phys. Solid State **37**, 865 (1995)].
[27] A. B. Roitsin, *Some Applications of Symmetry Theory in Radiospectroscopy* [in Russian], Naukova Dumka, Kiev (1973).
[28] A. B. Roitsin, A. A. Klimov, and L. V. Artamonov, Fiz. Tverd. Tela (St. Petersburg) **38**, 741 (1996) [Phys. Solid State **38**, 408 (1996)].
[29] A. B. Roitsin, Ukr. Fiz. Zh. **19**, 1216 (1974).
[30] I. B. Bersuker, *Electronic Structure and Properties of Coordinational Compounds* [in Russian], Nauka, Leningrad (1986).
[31] G. Ya. Lyubarskii, *The Application of Group Theory in Physics*, Pergamon Press, Oxford, 1960.
[32] B. I. Dunlap, J. L. Ballester, and P. P. Schmidt, J. Phys. Chem. **96**, 9781 (1992).

Translated by R. S. Wadhwa

Low-temperature plasticity of Zn-doped β–Sn crystals

A. N. Diulin, G. I. Kirichenko, V. D. Natsik, and V. P. Soldatov

B. Verkin Institute for Low Temperature Physics and Engineering, National Academy of Sciences of the Ukraine, 310164 Kharkov, Ukraine
(Submitted December 12, 1996; revised March 6, 1997)
Fiz. Nizk. Temp. **23**, 1122–1127 (October 1997)

Work hardening curves are obtained for Sn–Zn single crystals with Zn concentration 0.01 and 0.53 at.% in the temperature interval 1.6–300 K. It is found that the Zn impurity significantly affects the shape of the curves as well as the work hardening parameters like the strain-hardening factor, duration of slip stage, temperature dependences of critical shear stress, and strain-rate sensitivity. A comparative analysis is carried out for the effect of Zn on low-temperature creep of Sn, and the effect of the same concentration of Cd impurity (which was studied earlier). © *1997 American Institute of Physics.* [S1063-777X(97)01410-2]

It was shown by us earlier[1,2] that the kinetics of low-temperature plastic deformation of high-purity single crystals of β–Sn (99.9995%) oriented for easy slip in the (100) $\times\langle 010\rangle$ system is determined by the mechanisms of thermally activated or quantum motion of dislocations through the lattice potential relief barriers (Peierls barriers). The Peierls mechanism of dislocation drag significantly affects the plasticity of many pure crystals, e.g., a number of semiconductors and most of bcc metals. However, experimental studies of this mechanism at low temperatures are hampered by the effects of low-temperature embrittlement and discontinuous (jumplike) plastic flow. Pure β–Sn has a unique property for a Peierls crystal to preserve a considerable reserve of plasticity and a smooth plastic flow upon cooling down to subkelvin temperatures. Together with the experimental studies of the plasticity of β–Sn in a wide temperature range 0.5–300 K, this circumstance allowed us to carry out a quantitative verification[1,2] of nearly all conclusions and predictions of the theory of thermal and quantum motion of dislocations in a Peierls relief.[3–6]

Another interesting problem emerging during the study of the Peierls mechanism of dislocation drag concerns the effect of impurity atoms on the dislocation motion through Peierls barriers.[7–10] Impurity atoms deform the potential relief of the matrix and are capable of radically affecting the thermally activated and tunnel transitions of dislocations through Peierls barriers. On a macroscopic scale, this may be manifested in the form of various anomalies on the temperature dependences of plasticity parameters. The most interesting and disputable anomalies are the effect of softening of certain bcc metals by impurities,[9] and the displacement of the threshold temperature of transition to the quantum plasticity region observed for β–Sn.[2] A detailed experimental analysis of these anomalies in bcc metals is hampered not only by the above-mentioned effect of low-temperature embrittlement, but also by an additional embrittlement caused by doping. However, β–Sn continues to be a very convenient object for experimental investigations of impurity effects also. Indeed, first experiments on single crystals of Cd-doped β–Sn showed that the smooth plastic flow in the system $(100)\langle 010\rangle$ is preserved right down to lowest temperatures for low impurity concentrations, while a jumplike deformation is observed only below 4 K in strongly doped samples.[2]

In this connection, we are planning a series of experiments to study the regularities of the low-temperature plasticity of β–Sn single crystals doped with various impurities. We intend to study the effect of impurity concentration and the intensity of impurity barriers on the kinetics of dislocation motion across Peierls barriers in the slip system (100) $\times\langle 010\rangle$ in the regions of thermally activated slip ($T>2$ K) and quantum plasticity ($T\leqslant 1$ K). Earlier, we obtained[11] the stress-strain curves for Sn–Cd alloys with the Cd concentrations 0.01, 0.21, and 0.53 at.% in the temperature range 4.2–100 K. We also constructed the temperature dependences of the yield stress for these alloys. In the present work, we extend our investigations to Sn–Zn alloys. The atomic concentration of Zn in the alloys studied by us was 0.01 and 0.53 at.%. Atoms of Zn and Cd have quite different size- and elasticity parameters. Hence, while preserving identical impurity concentrations, we obtained the experimental results, enabling us to estimate the effect of impurity barrier intensity on the dislocation motion in the Peierls relief.

We study the plasticity of single crystals of Sn–Zn alloys in the temperature range 1.6– 300 K. The main purpose of our investigations was to determine the extent and type of the effect of the Zn impurity on the stress–strain curves and work-hardening parameters in Sn–Zn alloys oriented for slip in the system $(100)\langle 010\rangle$. Besides, the data on the strain-rate sensitivity to small variations of deforming stress, i.e., the differential characteristics of plasticity, are also obtained. This information is essential for the subsequent thermal activation analysis of the process.

1. EXPERIMENTAL TECHNIQUE

Single crystals of Sn–Zn alloys were grown in batches of ten crystals per seed from the melt by using the modified Bridgmann technique.[12] The orientation of the axis of elon-

gation of the single crystals was such that the maximum shear stress was attained in the slip system $(100)\langle 010\rangle$. The initial components used for preparing alloys contained impurities whose concentration did not exceed 10^{-5}–$5\cdot 10^{-6}$. According to Hansen and Anderko,[13] the solubility of Zn in solid Sn is not less than 0.7 at.%, its upper limit at or near the eutectic temperature varying from 2 to 3 at.%.

Single crystals of alloys were deformed under creep conditions by using direct loading technique. The load on the sample was varied in small steps corresponding to an increase of 0.2–0.4 MPa in the shear stress. The strain increments corresponding to each stage of loading were recorded automatically on an electronic recorder with an error not exceeding $5\cdot 10^{-5}$. Such a loading regime ensured an average strain rate of about $5\cdot 10^{-5}\mathrm{s}^{-1}$ in the crystal.

The work-hardening curves $\tau(\varepsilon)$ corresponding to the above average strain rate were constructed from the load increment and the corresponding increase in strain. These curves were used for determining the critical shear stress (CSS) τ_0, the strain-hardening factor κ, and the duration of the work-hardening stage $\tau(\varepsilon)$. The values of CSS were measured in the same sample at different temperatures to reduce the spread in the values of τ_0 for alloys with different structures. First measurements were made at the highest temperature by loading the sample until the onset of plastic flow. The sample was then unloaded, cooled to a certain temperature, and again subjected to loading until the emergence of CSS. This procedure was repeated five or six times for the same sample.

We also measured the differential characteristic of plasticity, viz., the sensitivity $(\partial \ln \dot{\varepsilon}/\partial\tau)_T$ of creep rate to small variations of the deforming stress. For this purpose, the sample was loaded additionally by applying small stresses $\Delta\tau = 0.1$–0.2 MPa during the recording of transient creep curves upon the attainment of a creep rate of about $10^{-5}\mathrm{s}^{-1}$, and the resulting increments $\Delta\dot{\varepsilon}$ of the creep rate were recorded. The required quantity $(\partial \ln \dot{\varepsilon}/\partial\tau)_T$ was estimated as the ratio of finite increments

$$\left(\frac{\partial \ln \dot{\varepsilon}}{\partial \tau}\right)_T \approx \frac{\ln(\dot{\varepsilon}+\Delta\dot{\varepsilon}) - \ln \dot{\varepsilon}}{\Delta\tau}.$$

The above experiments were made in the temperature range 1.6–300 K. Intermediate temperatures were obtained by using the technique described in Ref. 14, while temperatures below 4.2 K were obtained by pumping He vapor. At temperatures below the superconducting transition temperature of Sn ($T_c = 3.7$ K), the samples were deformed in a solenoid whose magnetic field was stronger than the critical value ($H_c = 30.5$ mT).

2. DISCUSSION OF EXPERIMENTAL RESULTS

2.1. Work-Hardening Curves

Figure 1 shows typical work-hardening curves for single crystals of Sn[15] and Sn–Zn alloys at different temperatures. An analysis of the all the curves recorded in this way makes it possible to note the following most important features:

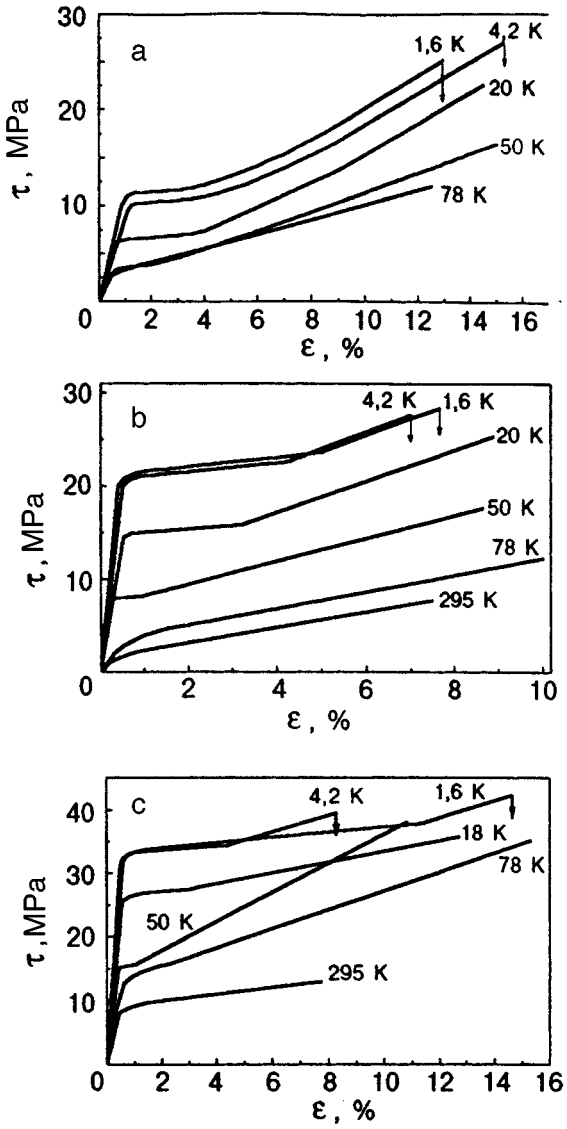

FIG. 1. Work hardening curves for single crystals of pure Sn[15] and Sn–Zn alloys: Sn (99.9995%)(a), Sn + 0.01 at.% Zn (b) and Sn + 0.53 at.% Zn (c).

(1) the stress–strain curves for pure Sn as well as Sn–Zn alloys have a step manifested in the form of two stages on the $\tau(\varepsilon)$ curves, corresponding to easy slip (stage I) and linear work hardening (stage II);
(2) the effect of temperature on the $\tau(\varepsilon)$ curves is manifested in a gradual reduction of stage I with increasing temperature, culminating in its disappearance at a temperature of about 60 K;
(3) as a rule, the stress–strain curves display only the linear work-hardening stage at nitrogen temperatures, while a parabolic shape of $\tau(\varepsilon)$ curves dominates near room temperature;
(4) doping of Sn leads to a stronger manifestation of the step on stress–strain curves at low temperatures.

The lower the temperature, the stronger the effect of impurities on the work-hardening curves. An increase in the impurity concentration leads to an increase in the stress corresponding to the onset of plastic deformation, a sharper step

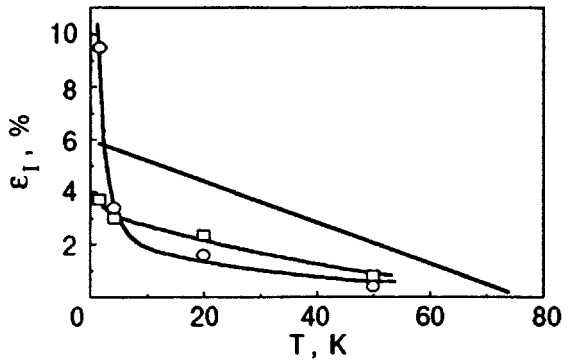

FIG. 2. Temperature dependence of the duration of the easy slip stage for pure Sn[15] (solid curve) and for Sn + 0.01 at.% Zn (□) and Sn + 0.53 at.% Zn (○) alloys.

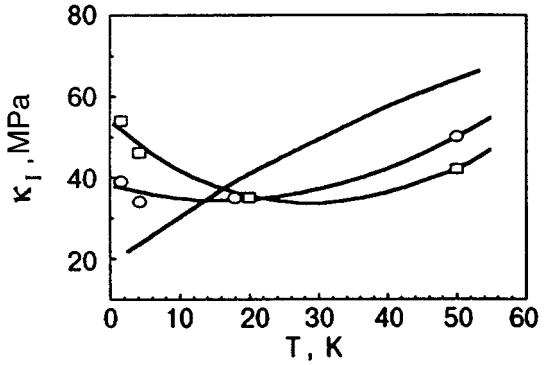

FIG. 3. Temperature dependence of the strain-hardening factor at the easy slip stage for pure Sn[1] (solid curve) and for Sn + 0.01 at.% Zn (□) and Sn + 0.53 at.% Zn (○) alloys.

on the work-hardening curves, and a variation of the kinetics of strain increment at the yield point and immediately behind it, especially at temperatures below 4.2 K. Thus, a transition in the alloy with a Zn concentration 0.53 at.% at 1.6 K through the yield point is accompanied by a catastrophically rapid growth in the sample strain (at a rate of several percent in a fraction of a second) even upon a slight increase in the load. If the level of stress on the sample can be reduced at the initial stage (by removing a part of the load), the increase in deformation continues as a rule, albeit at a lower rate. This behavior points towards the presence of a ''flow tooth'' in the alloy Sn + 0.53 at.%Zn, which is manifested specifically during sample deformation under creep conditions. No such singularity is observed in the alloy Sn + 0.01 at.%Zn at the same temperature.

Another peculiarity distinguishing the Sn–Zn alloys from Sn–Cd alloys can be seen in Fig. 2, showing the temperature dependence of the duration of the easy slip stage ε_I. Irrespective of temperature, the Sn–Cd alloys display a shortening of the easy-slip stage upon an increase in the impurity concentration.[11] Such an effect is also observed in the Sn–Zn alloys, but only at temperatures higher than 4 K. For example, an increase in the Zn concentration to 0.53 at.% at temperatures below 4 K leads to a sharp increase in the value of ε_I. The reason behind such an inversion has not been established thus far.

A similar inversion is also observed on the temperature dependence of the strain-hardening factor κ_I near 20 K upon a transition form a lower to a higher concentration of Zn impurity (Fig. 3). The decrease in κ_I observed below 20 K in alloys with a higher concentration of Zn impurity can be regarded as a manifestation of a peculiar impurity softening effect. Such an effect was also observed in Sn–Cd alloys,[11] and earlier in Fe–C,[9] Fe–N, and Fe–Si alloys,[16] but at higher temperatures.

2.2. Temperature Dependence of the Critical Shear Stress

Figure 4 shows the temperature dependences of the critical shear stress $\tau_0(T)$ for the investigated Sn–Zn alloys and Sn single crystals.[1] For comparison, the inset shows the temperature dependences of CSS for Sn–Cd alloys of the same concentration as Sn–Zn alloys (dashed curves).[11] Two characteristic branches corresponding to a strong (below 100 K) and weak (above 100 K) temperature dependence of the critical shear stress shown in the figure are typical of pure Sn and its alloys with Cd. The $\tau_0(T)$ dependence for pure Sn is characterized by the presence of a sharp kink at about 70 K and a low-temperature plateau in the temperature range 40–60 K. This singularity vanishes upon the doping of Sn, the effect of Zn impurity being stronger than that of Cd: the kink and the plateau on the $\tau_0(T)$ dependence vanish in Sn–Zn alloys with the Zn concentration 0.01 at.%, while this effect in Sn–Cd alloys is observed only for 0.21 at.%Cd.

Above 100 K, the CSS of pure Sn as well as its alloys becomes practically independent of temperature. Apparently, the attainment of a constant value of τ_0 in this temperature range corresponds to the attainment of the intrinsic stress τ_i whose value increases considerably with the impurity concentration in the alloy (Table I).

It can also be seen from Fig. 4 that doping with Zn increases the CSS significantly as compared to its value for pure Sn or Sn–Cd alloy with an equivalent Cd concentration. This can be seen clearly in Table I containing the values of the critical shear stress $\tau_0(0,0)$ for pure Sn and $\tau_0(0,C)$ for Sn–Cd and Sn–Zn alloys extrapolated to zero temperature,

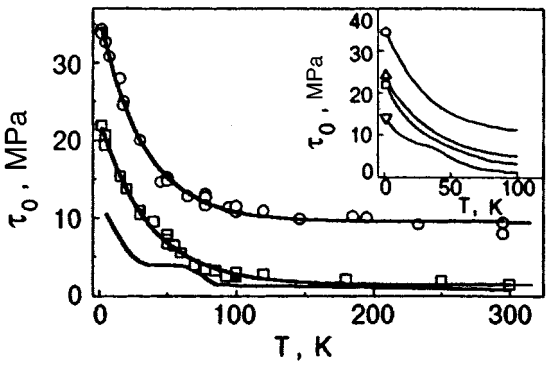

FIG. 4. Temperature dependence of the critical shear stress for single crystals of pure Sn[1] (solid curve) and for Sn + 0.01 at.% Zn (□) and Sn + 0.53 at.% Zn (○) alloys. The inset shows the dependence for Sn + 0.01 at.% Cd (∇), Sn + 0.53 at.% Cd (△),[11] Sn + 0.01 at.% Zn (□), and Sn + 0.53 at.% Zn (○).

TABLE I. Effect of impurities on critical shear stress τ_0.

Alloy	$\tau_0(0,0)$, MPa	$\frac{\tau_0(0,C)}{\tau_0(0,0)}$	τ_i, MPa
Sn (99.9995%)	12.5	1	1
Sn+0.01 at.% Cd	14.7	1.2	1.5
Sn+0.53 at.% Cd	24	1.92	5
Sn+0.01 at.% Zn	23.5	1.9	1.5
Sn+0.53 at.% Zn	35	2.8	9.5

as well as the ratio $\tau_0(0,C)/\tau_0(0,0)$ characterizing the relative increase in the CSS for alloys with different types of impurities.

One of the important results obtained earlier by us[11] is the impurity softening effect observed in the $\tau_0(T)$ dependence: the yield stress of Sn decreased significantly in the temperature interval 60–80 K as a result of doping (0.01 and 0.21 at.%) by Cd impurity. Such an effect was not observed for Zn impurity since the values of $\tau_0(T)$ for samples even with 0.01 at.% Zn are higher than the corresponding value for pure Sn in the entire investigated temperature range.

In all probability, the strong dependence of τ_0 on the type of impurity for the same concentration in the alloy is due to the different intensities of barriers formed by these impurities to hinder the movement of dislocations. According to Refs. 17–19, the barrier intensity is determined by a combination of the parameters of size and modular mismatching of the atoms of impurity and the matrix. According to the data presented in Ref. 20, the difference in the atomic radii of Sn and Cd is 2–6%, while the corresponding difference for Sn and Zn is 21%. The elastic properties of these elements, e.g., the characteristic values of the elastic constant C_{44}($C_{44}=G$, where G is the shear modulus) at helium temperatures differ even more sharply (by 13 and 64%, respectively). If we confine the analysis to a qualitative estimate of size and modular mismatching parameters, the disparity in the impurity atoms of Zn and Cd atoms as dislocation drag centers becomes obvious.

2.3. Creep Rate Sensitivity to Deforming Stress

Figure 5 shows the temperature dependences of the differential creep parameter $(\partial \ln \dot{\varepsilon}/\partial\tau)_T$ for pure Sn and Sn–Zn alloys corresponding to a strain $\varepsilon=5\%$. For pure Sn, this dependence has a well-defined minimum at 70 K corresponding to the kink on the $\tau_0(T)$ dependence. It can be seen that this singularity disappears as a result of doping with Zn, which correlates with the vanishing of the kink and plateau on the $\tau_0(T)$ dependence (see Fig. 4).

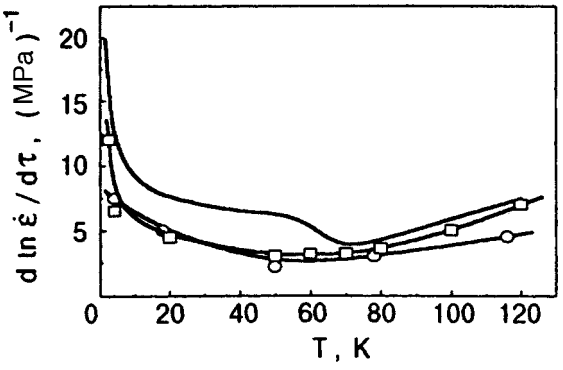

FIG. 5. Temperature dependence of the strain rate sensitivity for $\varepsilon=5\%$ for Sn (99.9995%) (solid curve),[1] Sn + 0.01 at.% Zn (□), and Sn + 0.53 at.% Zn (○).

Two hypotheses have been proposed in the literature to explain the presence of the above singularities on the temperature dependences of τ_0 and $(\partial \ln \dot{\varepsilon}/\partial\tau)_T$ for crystals with the Peierls mechanism of dislocation drag: the two-hump shape of the Peierls barriers,[21–24] and the nonmonotonic temperature dependence of intrinsic stresses at stage I.[1] The relative advantages of these hypotheses can be determined only from a detailed thermal activation analysis of the experimental data, which we are planning to carry out in near future. Here, we can simply state that the temperature dependence of the strain-hardening factor κ_I at stage I varies sharply as a result of doping (see Fig. 3). The possibility of an equally significant variation of the temperature dependence of internal stresses as a result of doping cannot be ruled out and may be attributed to the vanishing of anomalies on the temperature dependences of τ_0 and $(\partial \ln \dot{\varepsilon}/\partial\tau)_T$ observed in the alloys under consideration at temperatures 50–80 K, which were observed in pure Sn.

A comparison of the three curves presented in Fig. 5 indicates that a transition from pure Sn to a weakly doped alloy with 0.01 at.% Zn reduces the characteristic value of $(\partial \ln \dot{\varepsilon}/\partial\tau)_T$ by about 50%. However, a subsequent increase in the Zn concentration by a factor of 50 practically does not change its value or the temperature dependence. This fact seems to be surprising and must be taken into consideration during subsequent studies.

3. CONCLUSIONS

The results presented in this publication mark an important step towards the accumulation of experimental data concerning the effect of impurity atoms of the kinetics of dislocation motion through the Peierls barriers in β–Sn single crystals. We confined ourselves to the description of the effect of the Zn impurity on the low-temperature plastic flow of Sn under the creep conditions in the slip system $(100)\times\langle 010\rangle$ and compared them with our earlier results[11] on the effect of the same concentration of Cd impurities on this process. Both types of impurities are found to exert a strong influence on the parameters of the work-hardening curve for Sn and result in a qualitative variation of the temperature dependence $\tau_0(T)$ of the yield stress and the creep rate sensitivity to the deforming stress variations $(\partial \ln \dot{\varepsilon}/\partial\tau)_T$. However, Cd and Zn impurities affect the plasticity of Sn in quite different ways. For example, the impurity-induced softening observed in the temperature interval 60–80 K as a result of doping with Cd does not occur upon doping with Zn.

Unfortunately, the available experimental data are insufficient for a detailed thermal activation analysis and for drawing unambiguous conclusions about the microscopic mechanisms of the effect of impurities of the dislocation mo-

tion in a Peierls relief. We intend to continue our investigations in this field in the nearest future.

This research was financially supported by the Soros International Foundation (Grants U2P000 and U2P200) and by the State Foundation for Fundamental Research under the Ukrainian State Committee on Science and Technology (Project ''Bion'').

[1] G. I. Kirichenko, V. D. Natsik, and V. P. Soldatov, Fiz. Met. Metalloved. **44**, 410 (1977).
[2] V. D. Natsik, G. I. Kirichenko, V. V. Pustovalov *et al.*, Fiz. Nizk. Temp. **22**, 965 (1996) [Low Temp. Phys. **22**, 740 (1996)].
[3] B. V. Petukhov and V. L. Pokrovskii, Zh. Eksp. Teor. Fiz. **63**, 634 (1972) [Sov. Phys. JETP **36**, 336 (1972)].
[4] A. Seeger, Z. Metallkunde **B72**, 369 (1981).
[5] B. V. Petukhov, Fiz. Nizk. Temp. **11**, 1090 (1985) [Sov. J. Low Temp. Phys. **11**, 601 (1985)].
[6] B. V. Petukhov, Fiz. Nizk. Temp. **12**, 749 (1986) [Sov. J. Low Temp. Phys. **12**, 425 (1986)].
[7] A. Sato and M. Meshii, Acta Metall. **21**, 753 (1973).
[8] B. V. Petukhov and V. Ya. Sukharev, Fiz. Nizk. Temp. **9**, 520 (1983) [Sov. J. Low Temp. Phys. **22**, 264 (1983)].
[9] D. J. Quesnel, A. Sato and M. Meshii, Mater. Sci. Eng. **18**, 199 (1975).
[10] B. V. Petukhov, Pis'ma Zh. Tekh. Fiz. **17**, 29 (1991).
[11] G. I. Kirichenko, V. D. Natsik, and V. P. Soldatov, Fiz. Nizk. Temp. **18**, 1270 (1992) [Sov. J. Low Temp. Phys. **18**, 887 (1992)].
[12] Yu. G. Kazarov, in *Physics of the Condensed State* [in Russian], vol. 11, Kharkov (1973).
[13] M. Hansen and K. Anderko, *Constitution of Binary Alloys*, 2nd ed., McGraw-Hill, NY (1958).
[14] G. I. Kirichenko and V. P. Soldatov, Fiz. Met. Metalloved. **54**, 560 (1982).
[15] V. P. Soldatov and G. I. Shklyarevskaya, Fiz. Met. Metalloved. **44**, 410 (1977).
[16] K. Kitajima, Y. Aono, H. Abe, and E. Kuramoto, in *Proc. 5th Int. Conf. Strength of Metals and Alloys*, Aachen (1979).
[17] P. Haasen, in *Physical Metallurgy* (ed. by R. W. Cahn), North-Holland, Amsterdam (1965).
[18] R. L. Fleischer, Acta Metall. **9**, 996 (1961).
[19] R. Labusch, Phys. Status Solidi **41**, 659 (1970).
[20] G. V. Samsonov (Ed.), *Properties of Elements*, Part 1 [in Russian], Metallurgiya, Moscow (1976).
[21] P. Guyot and J. E. Dorn, Can. J. Psychol. **45**, 983 (1967).
[22] E. Kuramoto, Y. Aono, and K. Kitajima, Scr. Metall. **13**, 1039 (1979).
[23] B. V. Petukhov and Yu. I. Polyakov, Kristallografiya **32**, 324 (1987) [Sov. Phys. Crystallogr. **32**, 778 (1987)].
[24] T. Suzuki, H. Koizumi, and H. O. K. Kirchner, Acta Metall. Mater. **43**, 2177 (1995).

Translated by R. S. Wadhwa

Influence of cyclic change of normal and superconducting states on the deformation of Pb–In alloys

V. P. Lebedev, V. S. Krylovskii, and V. M. Pinto Simoes

Kharkov State University, 310077 Kharkov, Ukraine[*]
(Submitted April 2, 1997; revised May 7, 1997)
Fiz. Nizk. Temp. **23**, 1128–1130 (October 1997)

The effect of cyclic change of the normal and superconducting states of single crystals of Pb–In alloys is manifested in the form of strain hardening. The increase in the deforming stress in this case is attributed to an increase in the density of structural defects. © *1997 American Institute of Physics.* [S1063-777X(97)01510-7]

The rearrangement of the electron energy spectrum during the superconducting transition leads to a decrease in electron drag force acting on moving dislocations[1] and a simultaneous increase in the intensity of structural defects generation.[2] This results in an enhanced strain-hardening of metals in the superconducting state.[3] The effect of the experimental conditions and the state of the object on the change in the electron drag acting on dislocations is usually studied by a cyclic variation of the normal and superconducting states in the course of active loading, creep, or stress relaxation in the same object.[1]

The presence of dynamic processes associated with multiple transitions of the electron subsystem of a metal, the application and removal of an external magnetic field, periodic jumps in mechanical stress, etc., may also affect the strength and plastic characteristics of the metal. This was confirmed by Didenko and Pustovalov[4] who concluded that deformation of metal with multiple variations of the superconducting and normal states followed by load removal and annealing leads to the formation of a defect structure having a lower recovery and higher strain hardening at temperatures exceeding the superconducting transition temperature T_c. The present paper aims at finding the laws governing the deformation of a metal during cyclic variation of the normal and superconducting states at temperatures $T<T_c$.

Measurements were made on single crystals of the alloys Pb–$x$at.%In($x=0-5$) formed by using components with an initial purity 99.9992% for Pb and 99.999% for In. Samples in the form of plane-parallel plates ($1\times5\times30$ mm) were deformed at 4.2 K by stretching at the rate of 1.5×10^{-4} s^{-1}. The error in stress measurements was $\pm2\times10^4$ Pa, while strain was measured to within 0.1%. Cyclic variation of the normal and superconducting states at a rate of two cycles for one percent strain was carried out by using a magnetic field with induction $\mathbf{B}=0.2$ T. The residual resistance of the metal in the normal state was measured by the four-point technique having a sensitivity of $4\times10^{-13}\ \Omega\cdot$m.

The periodically varying mechanical stress was created on the sample at 77 K by magnetostriction variation of the length of a nickel plate (100 mm) in the loading device.

A common feature of the experiments was the existence of a higher shear stress τ_c in single crystals of lead and its alloys with indium (the smoothed shear stress vs. strain curve $\tau(\gamma)$ was obtained by measuring stress in the normal state) upon deformation under cyclic variation of normal and superconducting states as compared to the stress value τ_n obtained upon deformation in the normal state only. Since cycling of the states was started in the elastic region of loading, the yield stress was always higher than in the normal state.

Figure 1 shows the strain-hardening curves $\tau(\gamma)$ for single crystals of the alloy Pb–5 at.%In having the same orientation and deformed under various conditions: curve *1* — normal state, curve *2* — superconducting state, curve *3* — cyclic variation of normal and superconducting states. Earlier, it was shown by us[3] that loading of a metal with a fixed normal electron density leads (almost immediately behind the yield point) to a higher level of deforming stress in the superconducting state than in the normal state ($\tau_s>\tau_n$). In accordance with the chosen pattern of deformation with a periodic variation of normal and superconducting states, when the sample spends nearly the same time in each state, curve *3* should be lying between curves *1* and *2* in Fig. 1. However, a cyclic change of states leads to a plastic flow for higher values deforming stress $\tau_c>\tau_s>\tau_n$. Moreover, at each stage of deformation, we observed $\theta_c>\theta_n$ for the strain hardening modulus, $\tau_{bc}>\tau_{bn}$ for ultimate strength, and an increase of about 20% in plasticity during loading in the normal state. The absolute ($\tau_c-\tau_n$) and relative ($\tau_c-\tau_n$)/τ_n variations of shear stress increase monotonically, attaining the values 0.8 MPa and 85%, respectively, for $\gamma\approx125\%$. The ratio of $\tau_c-\tau_n$ to the isolated stress jump $\delta\tau_{ns}$ is equal to 10.

Like strain defects, impurity atoms also facilitate a more effective role of cycling of states in the metal–superconductor strain hardening process. The inset in Fig. 1 shows a linear increase in $\tau_c-\tau_n$ with concentration of indium atoms in the alloy.

Thus, a cyclic variation of the state of the electronic system of a metal through superconducting transition not only provides information about the magnitude of the electron drag force acting on a moving dislocation,[1] but also allows us to observe the increase in the deforming stress (Fig. 1) due to dynamic processes occurring during a change

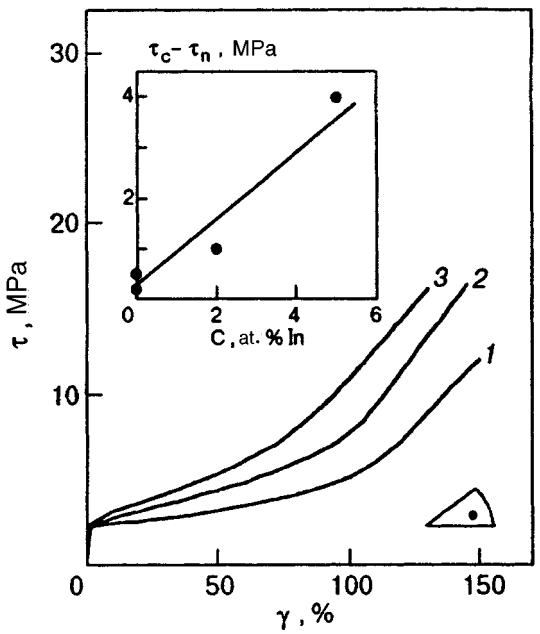

FIG. 1. Strain-hardening curves $\tau(\gamma)$ of single crystals of Pb–5 at.%In alloys corresponding to the normal (curve *1*) and superconducting (curve *2*) states, as well as the cyclic variation of these states (curve *3*). The inset shows the dependence of additional increase in stress $\tau_c-\tau_n$ on the In concentration in the alloy ($\gamma=75\%$).

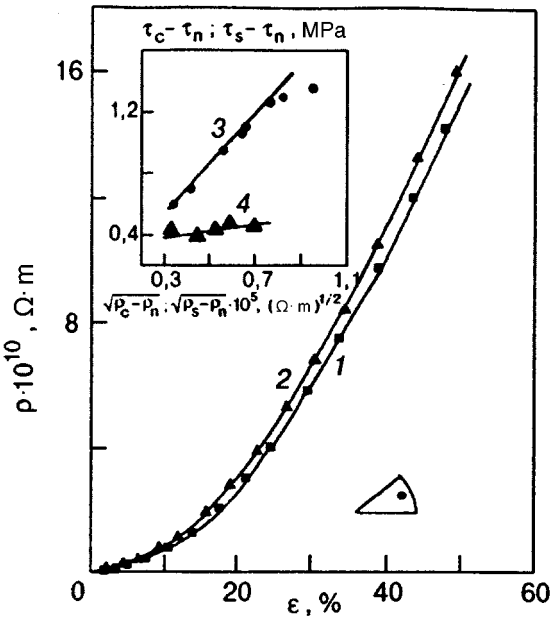

FIG. 2. Variation of the resistivity ρ with the strain ε for single crystals of Pb (99.9992% purity) after loading in the normal (curve *1*) state and upon cyclic variation of states (curve *2*). The inset shows the dependence of $\tau_c-\tau_n$ on $(\rho_c-\rho_n)^{1/2}$ (curve *3*) and of $\tau_s-\tau_n$ on $(\rho_s-\rho_n)^{1/2}$ (curve *4*).

of state, this increase being larger than that in the shear stress even due to deformation in the superconducting state only.[3] A higher intensity of strain-hardening processes may be caused by an increase in the concentration of structural defects and their distribution over the volume of the crystal.

In order to estimate the distortion of a lead crystal (99.9992% purity), we measured the residual resistivity ρ after loading in normal and superconducting states, as well as under cyclic variation of these states. Measurements of ρ were carried out in the absence of external stresses in the sample and in a magnetic field higher than the critical field ($H>H_c, H_{c2}$). The increase in ρ with relative elongation ε is shown in Fig. 2 (the figure does not show the $\rho(\varepsilon)$ dependence for a sample deformed in the superconducting state). It was found that $\rho_c>\rho_n$ for the entire interval of deformations, and the difference $\rho_c-\rho_n$ increases monotonically with ε. For the orientation of the lead single crystal indicated in the lower part of the figure, $\rho_c-\rho_n=0.62\cdot10^{-10}\Omega\cdot\mathrm{m}$ and $(\rho_c-\rho_n)/\rho_n=10\%$ for $\varepsilon=10\%$.

It follows from various models of structural hardening[5] that $\tau(\gamma)=\tau_0+\alpha Gb\sqrt{N_d}$, where τ_0 and $\tau(\gamma)$ define the shear stress of the original and deformed crystal, $\alpha=0.1$–1, G is the shear modulus, and N_d the dislocation density. Assuming that point and line defects make equal contributions to the growth of resistance for lead, we can use the dependences $\rho_c(\varepsilon)$ and $\rho_n(\varepsilon)$ (Fig. 2) to estimate the excess dislocation density $N_d=[\rho(\varepsilon)-\rho_0]/2\rho_d$, where ρ_0 corresponds to the undeformed crystal, and ρ_d is the resistivity of dislocations of unit density. Using the above formula for $\tau(N_d)$, we obtain a linear relation between the additional strain hardening $(\tau_c-\tau_n)$ or $(\tau_s-\tau_n)$ and the quantity $(\rho_c-\rho_n)^{1/2}$ or $(\rho_s-\rho_n)^{1/2}$ (see inset in Fig. 2). Different slopes of straight lines *3* and *4* correspond to an increased intensity of generation of an additional number of deformation defects and the formation of a more effective network of structural obstacles in the path of moving dislocations upon a cyclic change of states than for superconducting and normal states.

A possible reason behind the observed effect of the cyclic change of states can be the influence of the change in mechanical stress in the sample due to the superconducting transition (stress jumps $\delta\sigma_{ns}$). In order to verify this hypothesis, we subjected the alloy Pb–5 at.%In to deformation at 77 K by using normal procedure and under cyclic stress variation (nickel magnetostrictor of length 100 nm in the loading circuit of the sample), whose magnitude corresponds to the jump in stress during the superconducting transition. A comparison of the strain-hardening curves shows that the application of a small pulsating mechanical stress (of amplitude 0.1 – 0.5 MPa and a frequency of two cycles per 1% relative elongation) to the sample during extension does not cause any increase in the deforming stress.

The peculiarities of the superconducting transition itself are the most likely mechanism of the effect leading to an increase in the concentration of deformation defects and the formation of a structure with an enhanced resistance to the plastic flow. The change in the state of the electronic system occurs through an intermediate or mixed state of the superconductor. A change in the external magnetic field in the interval $0\leqslant H\leqslant H_c$, H_{c2} leads to the emergence of a dynamic intermediate state or a mixed state in the metal with moving system of domains or magnetic flux vortices. The interaction of the interface between the normal and superconducting phase with crystal lattice defects[6,7] may facilitate a

more intensive action of the dislocation sources and the creation of dislocation structures with enhanced resistance to the plastic flow of the metal.

This research was carried out under the research project PRAXIS XXI.

*E-mail: vladimir.s.krylovskiy@univer.kharkov.ua

[1] V. I. Startsev, V. Ya. Il'ichev, and V. V. Pustovalov, *Plasticity and Strength of Metals and Alloys at Low Temperatures* [in Russian], Metallurgiya, Moscow (1975).
[2] V. P. Lebedev and V. S. Krylovskii, Fiz. Tverd. Tela (Leningrad) **18**, 3648 (1976) [Sov. Phys. Solid State **18**, 2124 (1976)].
[3] V. P. Lebedev and V. S. Krylovskii, Fiz. Tverd. Tela (Leningrad) **33**, 2994 (1991) [Sov. Phys. Solid State **33**, 1690 (1991)].
[4] D. A. Didenko and V. V. Pustovalov, Fiz. Nizk. Temp. **1**, 1428 (1975) [Sov. J. Low Temp. Phys. **1**, 684 (1975)].
[5] J. Friedel, *Dislocations*, Oxford (1964).
[6] V. P. Lebedev and V. I. Khotkevich, Fiz. Nizk. Temp. **5**, 89 (1979) [Sov. J. Low Temp. Phys. **5**, 42 (1979)].
[7] V. P. Lebedev and Le Khak Hiep, Fiz. Tverd. Tela (Leningrad) **25**, 228 (1983) [Sov. Phys. Solid State **25**, 125 (1983)].

Translated by R. S. Wadhwa

Photon excitation of the third molecular continuum in solid krypton

A. N. Ogurtsov and E. V. Savchenko

B. Verkin Institute for Low Temperature Physics and Engineering, National Academy of Sciences of Ukraine, Lenin Ave., 47, 310164, Kharkov, Ukraine

J. Becker, M. Runne, and G. Zimmerer

II. Institut für Experimental Physik der Universität Hamburg, 22761 Hamburg, Germany
(Submitted May 26, 1997; revised June 6, 1997)
Fiz. Nizk. Temp. **23**, 1131–1133 (October 1997)

Luminescence study of the near-ultraviolet continuum in nominally pure solid krypton under selective excitation by synchrotron radiation is presented. Intrinsic nature of the emission has been established. Clear threshold behavior at the band gap energy reveals the key role of the electron-hole pairs in a population of the continuum forming states. © *1997 American Institute of Physics.* [S1063-777X(97)01610-1]

In addition to the well-known vacuum ultraviolet (VUV) continua stemming from the decay of self-trapped excitons, wide near-UV luminescence bands were observed in rare gas solids.[1] A rebirth of interest in their origin has been stimulated by a prospect of the development of excimer lasers operating in a near-UV range of spectra.[2] Despite the active current theoretical[3] and experimental studies in gas,[4–7] condensed phases,[8–10] and cluster beams,[11] the origin of these bands (the so-called third continua) is still under discussion.

Synchrotron radiation is a very valuable tool for elucidation of primary processes of emitting state population. Luminescence study of the third continuum following selective excitation with synchrotron radiation was performed on solid Xe (Ref. 8) and solid Ar (Ref. 10). In the present paper, the results of the first analysis of the near-UV luminescence of solid krypton following primary selective excitation with synchrotron radiation in the excitonic range and the range of band-to-band excitation are presented.[12]

The experiments were performed at the SUPER-LUMI experimental station of HASYLAB at DESY[13] in an ultrahigh vacuum environment (a basic pressure in the experimental chamber did not exceed the 10^{-10} mbar). The samples were grown from a Kr gas (99.99%) in a special cell attached to a helium cryostat. Preparation of samples under isobaric ($P=80$ Pa) conditions with a constant rate of cooling 0.1 K/s in the temperature range 80–60 K results in high transmittance samples with a small quantity of initial defects of structure. The samples contained inevitable amount of Xe impurity. The Xe concentration is estimated to be in a low ppm range.[14] After condensation the cell was opened and the measurements of photoluminescence and excitation spectra were performed. Selective photon excitation was carried out with $\Delta\lambda=2.5$ Å. In the luminescence and the excitation spectra, the luminescence was spectrally dispersed with a 0.5-m Pouey monochromator equipped with a solar-blind photomultipler ($\Delta\lambda=15$ Å).

The luminescence spectrum in the region of self-trapped exciton emission (the M-band at 8.6 eV) and the third continuum at 5.3 eV is shown in Fig. 1. The M-band consists of four well-known[15,16] M-subbands originating from the radiative decay of $Kr_2^*(M_1,M_2)$ and $XeKr^*(M_1',M_2')$ molecular centers, which are self-trapped in the regular lattice and trapped at the initial and electronically induced defects of the structure. A narrow band A originates from Xe atoms in the Kr matrix.[17]

At low temperatures the third continuum reveals two components: a H-band at 5.3 eV with FWHM=0.3 eV and a H'-subband at 4.9 eV with FWHM=0.4 eV. The H'-subband disappears on heating of the sample, whereas the H-band only reduces its intensity by half, beginning with $T=35$ K. The main component which peaks at 5.3 eV and which remains in the luminescence spectrum, is thought to be of intrinsic nature.

In order to gain insight into the origin of this band, we measured the excitation spectrum. Figure 2 shows the excitation spectra of the H-, the H'-, and the M-bands recorded at the luminescence photon energies indicated in Fig. 1 by arrows. The choice of emission energy (8.3 eV) for measuring the excitation spectrum of the M-band is dictated by its complex internal structure due to the presence of small quantity of Xe impurity. Note that at the chosen energy the contribution of the M_1 subband is dominant. The excitation spectrum of the M_1 subband shows the well-known fine structure in the excitonic range of the spectrum.[18] The most prominent features were observed in the region below the first member of the bulk excitons $\Gamma(3/2)$. This fact clearly demonstrates the association of the subband with the structure defects and with the surface region of the sample. In addition, the excitation spectrum of the M_1 subband yields a step-like behavior at the energy $E=21.78$ eV, which exceeds the band gap energy $E_g=11.61$ eV by the lowest exciton energy $E_1=10.17$ eV. The energy E_1+E_g determines the threshold for creation of excitons during inelastic scattering of secondary photoelectrons by valence electrons.[19]

To check the probable origin of the H-band from impurities, we measured the excitation spectrum in a transparency range of the Kr host. We found that this band cannot be excited below the range of intrinsic absorption. Moreover, the band in question cannot be excited in the excitonic range of energies ($E_1=E<E_g$) and its behavior is in contrast with that of the extrinsic M_1 subband. The tests confirm beyond any doubt the intrinsic nature of the H-band in nominally

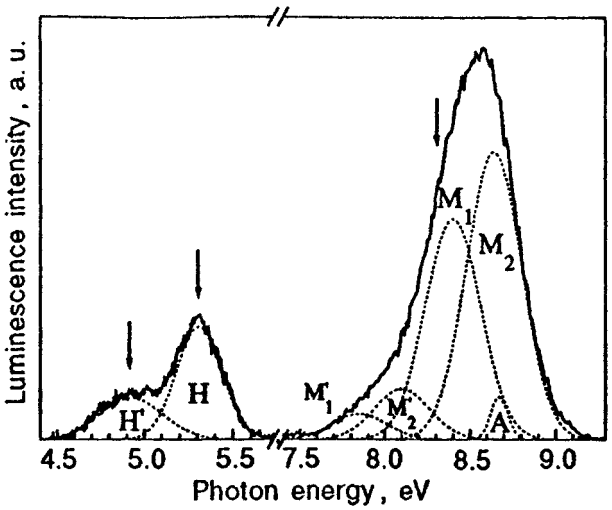

FIG. 1. The luminescence spectrum of solid krypton excited by $h\nu = 14.2$ eV at $T = 5$ K. The arrows indicate the photon energies at which the excitation spectra in Fig. 2 were measured.

pure solid krypton. The excitation spectrum of the H-band yields a pronounced threshold at the band gap energy E_g and a maximum at $2E_g$. The clear threshold behavior testifies that the creation of free electron-hole pairs is the primary process of population of continuum forming states. If the energy position of the H-band is taken into account, the direct recombination of free electrons and holes should be excluded. It is well known that free holes are rapidly self-trapped in atomic cryocrystals,[20] forming molecular-ion-like centers. The radiative recombination of self-trapped holes

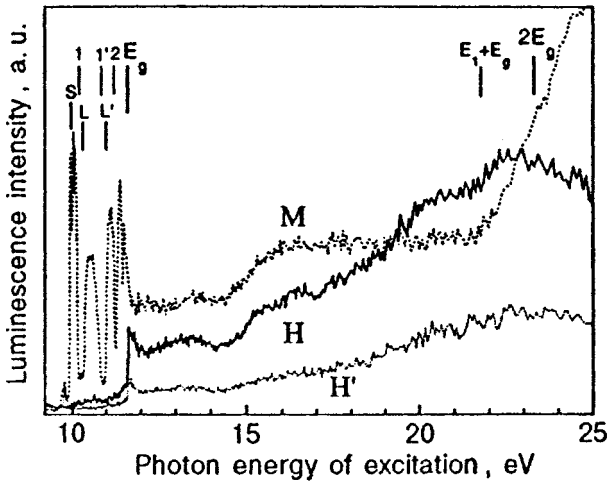

FIG. 2. The excitation spectra of H-, H'-, and M-bands measured at luminescence photon energies indicated in Fig. 1 by arrows. The positions of bulk transverse (1, 1′, 2), bulk longitudinal (L, L'), and surface (S) excitons are marked at the top of the curves according to Ref. 1.

with electrons results in the M-band emission in the VUV range of the spectra and is excluded as a probable channel of population of the third continuum forming states. A more likely assumption about the origin of the H-band seems to be the radiative transition from the excited states of the krypton molecular ion to lower-lying repulsive states. According to this assumption, the population of the continuum forming states is a two-step process: self-trapping of holes followed by their excitation. The key role of the self-trapped holes in the formation of near-UV emission from nominally pure solid krypton is evident from the observed features of the excitation spectrum and from the temperature behavior of the H-band—quenching with increasing temperature starting at 35 K, where electrons are released from their traps.[21] The nature of the H'-band is presently not clear. Perhaps it originates from heteronuclear krypton-xenon ionic centers. Detailed assignment of the emitting states requires further investigation.

Financial support by the BMFT (Grant 05650 GUB) and under the PECO-Project is gratefully acknowledged.

[1] I. Ya. Fugol' Adv. Phys. **1**, 1 (1978).
[2] H. Langhoff Opt. Commun. **68**, 31 (1988).
[3] C. Cachoncinlle, J. M. Pouvesle, G. Durand, and F. Spiegelmann, J. Chem. Phys. **96**, 6085 (1992).
[4] W. Krotz, A. Ulrich, B. Bush, G. Ribitzki, and J. Wieser, Phys. Rev. A **43**, 6089 (1991).
[5] A. Kh. Amirov, O. V. Korshunov, and V. F. Chinnov, J. Phys. B: At. Mol. Opt. Phys. **27**, 1753 (1994).
[6] H. Langhoff, J. Phys. B: At. Mol. Opt. Phys. **2**, L709 (1994).
[7] D. E. Johnson, Chem. Phys. Lett. **238**, 71 (1995).
[8] M. Hävecker, M. Runne, and G. Zimmerer, J. Electron Spectrosc. Relat. Phenom. **79**, 103 (1996).
[9] O. N. Grigorashchenko, S. A. Gubin, A. N. Ogurtsov, and E. V. Savchenko, J. Electron Spectrosc. Relat. Phenom. **79**, 107 (1996).
[10] A. Ogurtsov, M. Runne, A. Karl, J. Becker, and G. Zimmerer, HASYLAB Annual Report 1995, DESY, Hamburg (1996), p. II-75.
[11] E. Rühl, C. Heinzel, and H. W. Jochims, Chem. Phys. Lett. **211**, 403 (1993).
[12] J. Becker, A. N. Ogurtsov, M. Runne, E. V. Savchenko, and G. Zimmerer, HASYLAB Annual Report 1996, DESY, Hamburg (1997), p. 247.
[13] G. Zimmerer, Nucl. Instrum. Methods Phys. Res. A **308**, 178 (1991).
[14] D. Varding, J. Becker, L. Frankenstein, B. Peters, M. Runne, A. Schröder, and G. Zimmerer, Low Temp. Phys. **19**, 427 (1993).
[15] E. V. Savchenko, A. N. Ogurtsov, O. N. Grigorashchenko, and S. A. Gubin, Chem. Phys. **189**, 415 (1994).
[16] A. N. Ogurtsov, E. V. Savchenko, S. A. Gubin, O. N. Grigorashchenko, M. Runne, A. Karl, J. Becker, and G. Zimmerer, in *Excitonic Processes in Condensed Matter*, M. Schreiber (Ed.), Dresden University Press, Dresden (1996).
[17] W. Laasch, PhD Thesis, The University of Hamburg (1992); *Internal Rep. DESY-HASYLAB 92-07*, December 1992.
[18] Ch. Ackermann, R. Brodmann, U. Hahn, A. Suzuki, and G. Zimmerer, Phys. Status Solidi B **74**, 579 (1976).
[19] H. Möller, R. Brodmann, G. Zimmerer, and U. Hahn, Solid State Commun. **20**, 401 (1976).
[20] K. S. Song and R. T. Williams, *Self-Trapped Excitons*, *Springer Series in Solid-State Sciences* **105**, Springer-Verlag Berlin, Heidelberg, New York (1993).
[21] M. Krim and H. Niedrais, J. Lumin. **60-61**, 611 (1994).

This article was published in English in the original Russian journal. It was edited by S. J. Amoretty.

Anisotropic pinning and the mixed-state galvanothermomagnetic properties of superconductors—a phenomenological approach

V. A. Shklovskij

National Science Center-''Kharkov Institute of Physics and Technology,'' Institute of Theoretical Physics. 1 Akademicheskaya St., 310108, Kharkov, Ukraine; Kharkov State University, Physical Department, 4 Svobody Sq., 310077, Kharkov, Ukraine

(Submitted July 4, 1997; revised July 10, 1997)
Fiz. Nizk. Temp. **23**, 1134–1138 (October 1997)

In the presence of isotropic and anisotropic pinning the vortex dynamics is discussed in terms of phenomenologically introduced, nonlinear viscosities. The formulas for linear galvanothermomagnetic effects are derived and analyzed under the condition at which the transport current or temperature gradient is directed at arbitrary angle with respect to the unidirected twins, which cause the anisotropic pinning. It is shown that two new effects which appear due to the anisotropic pinning, namely (with respect to the reversal of the magnetic field direction) even transverse and odd longitudinal voltage, have a distinct origin. The first is due to the guided vortex motion, while the second appears only when anisotropic (in contrast with isotropic) pinning changes the Hall drag coefficient. We also show that the last effect might be masked in the experiment by a large, odd contribution, which has the same angular dependence and which appears due to the Ettingshausen effect. In order to clarify the problem of influence of the twins on the Hall drag coefficient, we discuss the possibility of separating these two contributions in the experiment.
[S1063-777X(97)01710-6]

1. The influence of the pinning on the transport properties of high-T_c superconductors (HTSC) is a very interesting problem. One of the open and rather controversial issues in this field is the influence of the pinning on the Hall drag coefficient. Recently, Vinokur *et al.*[1] have calculated the effect of point (isotropic) pins on the Hall resistivity and showed that the Hall constant is pinning-independent. Is it also true for the anisotropic pinning caused, for example, by a system of unidirected twins in YBCO single crystal? Sonin *et al.*[2] have shown that in the last case, in addition to the usual longitudinal and transverse (Hall) resistivities (even and odd, accordingly, with respect to the reversal of a magnetic field direction) two new contributions to the resistivity appear: the even transverse and the odd longitudinal contributions. These results follow in Ref. 2 from the general form of the linear Ohm's law in anisotropic media which, in turn, was formulated on the basis of symmetry considerations. In fact, it was postulated in Ref. 2 that presence of the twins changes the Hall conductivity. The experimental situation also is still controversial. Recent paper[3] claims that for a twinned (and further irradiated with high-energy Pb ions) YBCO single crystal the mixed-state Hall conductivity does not depend on the pinning strength, in complete agreement with the theory.[1]

The main purpose of this paper is to suggest and develop theoretically a new method for experimental verification of the plausible effect of twins on the Hall drag coefficient within the framework of the phenomenological approach used earlier in Ref. 1 for the case of isotropic pinning. We modify the method of Ref. 1 for considering both the isotropic and anisotropic pinning so that we can derive the Ohm's law, which was postulated in Ref. 2. We can therefore clarify the origin of the earlier introduced[2] four phenomenological resistivities in terms of the drag and pinning vortex viscosities, i.e., on a more detailed level. In the linear case we show that the above-mentioned, new, even, transverse contribution is due completely to the guided vortex motion[4] and does not require the modification of the Hall drag coefficient by twins, whereas the odd longitudinal contribution depends entirely on the different values of this coefficient for motion of vortices along the twins and across them. It follows from this conclusion that in order to justify the influence of the twins on the Hall drag coefficient, we must identify only odd longitudinal contribution in the measurements.

But as we show below, experimental observation of this small (Hall in nature) contribution may be masked by the possible appearance (due to the emergence of a small temperature gradient in the presence of the transport current) of the odd Seebeck contribution with the same angular dependence. In order to give a theoretical basis for the separation of these two contributions, we also calculated the thermomagnetic properties of the sample with anisotropic pinning, using the same approach. We will show that the main contribution to the odd Seebeck resistivity now gives the guided vortex motion, while the possible Hall contribution is small and can be disregarded.

2. Following Ref. 1, we have for the average velocity of vortices $\mathbf{v}$ the equation of motion

$$\eta\mathbf{v}+\alpha\mathbf{v}\times\mathbf{n}=\mathbf{f}+\mathbf{f}_p\,, \tag{1}$$

where η is the isotropic friction coefficient, α is the isotropic Hall drag viscosity, $\mathbf{f}$ is the moving external force (Lorentz or thermal, see below), and $\mathbf{f}_p$ is the average resulting pinning force, which is the sum of the isotropic contribution $\mathbf{f}_p^{\,i}$ and the anisotropic contribution $\varepsilon\mathbf{f}_p^{\,a}$, where $\varepsilon=a_0/d$ is

relative fraction of vortices placed on the twins (a_0 and d are the average distances between vortices and twins, respectively). Considerations which may lead to the equation of motion in the form (1) will be discussed in detail elsewhere. If $\varepsilon=0$, we obtain Eq. (2) in Ref. 1. We assume that the average anisotropic pinning force $\mathbf{f}_p^a$ can be decomposed into two parts $\mathbf{f}_p^a=\mathbf{f}_p^t+\mathbf{f}_p^l$, where, neglecting small Hall viscosities, $\mathbf{f}_p^t=f_p^t\cdot\mathbf{m}$, $\mathbf{f}_p^l\equiv f_p^l\cdot\mathbf{m}_\parallel$. Here $\mathbf{m}$ and $\mathbf{m}_\parallel\equiv\mathbf{z}\times\mathbf{m}$ are the unit vectors directed perpendicularly and parallel to the twins, respectively, $\mathbf{z}$ is the unit vector which is perpendicular to the sample's plane, $f_p^t\equiv\mathbf{f}_p^t\cdot\mathbf{m}$, and $f_p^l\equiv\mathbf{f}_p^l\cdot\mathbf{m}_\parallel$. As in Ref. 1, we assume that $\mathbf{f}_p^i=-\gamma_i(v)\mathbf{v}$, where $\gamma_i(v)>0$ is phenomenological coefficient, which depends only on the value of $v\equiv|\mathbf{v}|$. For $\mathbf{f}_p^t$ and $\mathbf{f}_p^l$ we assume that

$$\mathbf{f}_p^t=-\gamma_t(|v_t|)\mathbf{v}_t-\alpha_t\mathbf{v}_t\times\mathbf{n}, \tag{2a}$$

$$\mathbf{f}_p^l=-\gamma_l(|v|_l)\mathbf{v}_l-\alpha_l\mathbf{v}_l\times\mathbf{n}, \tag{2b}$$

where γ_t and γ_l are the average phenomenological anisotropic viscosities which include also the $\mathbf{v}$-independent terms for the motion of vortices across the twins and along them, respectively; α_t and α_l are the corresponding anisotropic Hall drag coefficients, and $\mathbf{n}$ is the unit vector in the magnetic field direction ($\mathbf{n}=n\mathbf{z}$, where $n=\pm1$). Here $\mathbf{v}_l=v_l\mathbf{m}_\parallel$ and $\mathbf{v}_t=v_t\mathbf{m}$ are longitudinal and transverse vortex velocities, respectively ($\mathbf{v}=\mathbf{v}_l+\mathbf{v}_t$). Below we will show that incorporation of the Hall terms in (2) is equivalent to the assumption that the anisotropic pinning influences the Hall drag coefficient α and leads to a new effect—the odd longitudinal contribution to the resistivity of the sample.

Substitution of the expressions for $\mathbf{f}_p$ into (1) leads to a system of two nonlinear equations for v_t and v_l

$$\begin{cases} \eta_t v_t+n\alpha_{Hl}v_l=f_t, & (3a)\\ -n\alpha_{Ht}v_t+\eta_l v_l=f_l, & (3b)\end{cases}$$

where

$$\eta_t\equiv\eta+\gamma_i(v)+\varepsilon\gamma_t(|v_t|), \tag{4a}$$

$$\eta_l\equiv\eta+\gamma_i(v)+\varepsilon\gamma_l(|v_l|), \tag{4b}$$

$$\alpha_{Hl}\equiv\alpha+\varepsilon\alpha_l,\quad \alpha_{Ht}\equiv\alpha+\varepsilon\alpha_t, \tag{4c}$$

and $f_t\equiv\mathbf{f}\cdot\mathbf{m}$ and $f_l\equiv\mathbf{f}\cdot\mathbf{m}_\parallel$ are the transverse and longitudinal components of the external force, respectively.

In the linear case, where η_t and η_l are constants, i.e., they do not depend on the velocities, the solution of (3) is simple

$$v_t=\Delta^{-1}(\eta_l f_t-n\alpha_{Hl}f_l);\quad v_l=\Delta^{-1}(\eta_t f_l+n\alpha_{Ht}f_t);$$

$$\Delta\equiv\eta_t\eta_l+\alpha_{Hl}\alpha_{Ht}. \tag{5}$$

The electric field induced by the vortex motion is $\mathbf{E}=(1/c)\mathbf{B}\times\mathbf{v}$, and if the external force is equal to the Lorentz force $\mathbf{f}=(\Phi_0/c)\mathbf{j}\times\mathbf{n}$, where Φ_0 is the flux quantum, c is the light velocity, and $\mathbf{j}$ is the transport current density, then from (5) we obtain

$$\mathbf{E}_L=\rho_t\mathbf{m}_\parallel(\mathbf{m}_\parallel\cdot\mathbf{j})+\rho_l\mathbf{m}(\mathbf{m}\cdot\mathbf{j})+n[\rho_{Hl}\mathbf{m}_\parallel(\mathbf{m}\cdot\mathbf{j})-\rho_{Ht}\mathbf{m}(\mathbf{m}_\parallel\cdot\mathbf{j})], \tag{6}$$

$$\rho_t\equiv\beta\eta_l;\rho_l\equiv\beta\eta_t;\quad \rho_{Hl}\equiv\beta\alpha_{Hl};\quad \rho_{Ht}\equiv\beta\alpha_{Ht};$$

$$\beta\equiv B\Phi_0/\Delta c^2. \tag{7}$$

Note that four phenomenological resistivities may be measured in two special, ''basic'' measurements, namely, ρ_l and ρ_{Hl}–in $\mathbf{j}\perp\mathbf{TB}$ (twin boundary) geometry, and ρ_t,ρ_{Ht}–in $\mathbf{j}\parallel\mathbf{TB}$ geometry. Physically, relation (6) shows how to express $\mathbf{E}$ for arbitrary angle between $\mathbf{j}$ and $\mathbf{m}$ in terms of four basic resistivities. It was postulated earlier in Ref. 2 on the basis of the symmetry considerations. In our approach we are able to elucidate the origin of the above-mentioned resistivities [see Eq. (7)] in terms of the drag and pinning viscosities, i.e., at a more detailed level. Equation (6) admits another representation of $\mathbf{E}$ in terms of two mutually perpendicular unit vectors $\mathbf{e}_\parallel\equiv\mathbf{j}/j$ and $\mathbf{e}_\perp\equiv(\mathbf{z}\times\mathbf{j})/j$; then $\mathbf{E}\equiv E_\parallel\mathbf{e}_\parallel+E_\perp\mathbf{e}_\perp$, where

$$E_\parallel=(\rho_\parallel^+ +n\rho_\parallel^-)j;\quad E_\perp=(\rho_\perp^+ +n\rho_\perp^-)j. \tag{8}$$

Here $E_\parallel$ and $E_\perp$ are the longitudinal (dissipative) and transverse (Hall, nondissipative) components of the electric field (in relation to the transport current density), respectively, and

$$\begin{cases}\rho_\parallel^+\equiv x^2\rho_l+y^2\rho_t, & \rho_\perp^-\equiv x^2\rho_{Hl}+y^2\rho_{Ht},\\ \rho_\perp^+\equiv xy(\rho_t-\rho_l), & \rho_\parallel^-\equiv xy(\rho_{Hl}-\rho_{Ht}),\end{cases} \tag{9}$$

where $x\equiv\mathbf{m}\cdot\mathbf{e}_\parallel$ and $y\equiv\mathbf{m}_\parallel\cdot\mathbf{e}_\parallel$. The angle-dependent resistivities $\rho_\parallel^\pm$ and $\rho_\perp^\pm$ (in contrast to the ''intrinsic'' parameters ρ_l, ρ_t, ρ_{Hl}, and ρ_{Ht}) are measurable values for a given sample and they do not depend on the value of n. The sign $(+)$ here means that this value is even with respect to the reversal of the magnetic field direction, where the sign $(-)$ means that the value $n\rho_{\perp,\parallel}^-$ is odd.

In the isotropic limit $\varepsilon=0$; then $\eta_t=\eta_l=\tilde{\eta}\equiv\eta+\gamma_i(v)$ and $\alpha_{Hl}=\alpha_{Ht}=\alpha$. In the limit $\alpha^2\ll\tilde{\eta}^2$ we obtain directly from Eqs. (3) the results of Ref. 1 [including the nonlinear scaling relation $\rho_{xy}=\rho_{xx}^2(\alpha c^2/B\Phi_0)$; Eq. (7) in Ref. 1].

In contrast with the isotropic limit, where only $\rho_\parallel^+$ and $\rho_\perp^-$ are not equal to zero, in general $(\varepsilon\neq0)$, as we can see from (9), two new contributions to the resistivity appear: transverse even $\rho_\perp^+$ and longitudinal odd $n\rho_\parallel^-$. Note that the angular dependence of these two contributions is the same and has the maximum value at $\theta=\pi/4$ (here θ is the acute angle between $\mathbf{m}$ and $\mathbf{j}$). But unlike this similarity, these contributions (as can be seen from their derivation) have a completely different origin.

The even transverse resistivity $\rho_\perp^+$ stems from the evidently different pinning force for the motion of the vortices along and across the twins, and we can see in the experiment[5] the different critical currents for these two directions. Usually, in some temperature interval[5] $\rho_t\ll\rho_l$, and such inequality promotes the so-called guided vortex motion[4], where the vortices prefer to move mostly along the twins than to slip across them. If we define the quantitative measure of guiding as $\cot\varphi\equiv|E_\perp^+/E_\parallel^+|=|\rho_\perp^+/\rho_\parallel^+|$, then $\cot\varphi=(1-u)\tan\theta/(u+\tan^2\theta)$ where $u\equiv\rho_t/\rho_l$ and $0<u<1$. If $u\to0$, then $\varphi\to\theta$ and we have a full guiding. From the above formula follow several conclusions with a simple

physical interpretation:

a) at $0<u<1$ always $\tan\varphi>\tan\theta$ and, in addition, $\tan\varphi$ increases when $\tan\theta$ is increasing with a fixed value of u,

b) if we assume $u=\text{const}$ and change $\tan\theta$, then $\tan\varphi$ as a function of $\tan\theta$ is convex downwards and corresponding minimal value of $(\tan\theta)_{\min}=2\sqrt{u}(1-u)$ is attained at $\tan\theta=\sqrt{u}$,

c) if $\tan\theta>1$, then always $\cot\varphi<1$. But when $\tan\theta\ll1$, then depending on the relation between u and $\tan\theta$ we have several opportunities:

$$\cot\varphi\approx\begin{cases}[(1-u)/u]\tan\theta<1 & u>\tan\theta, \quad (10a)\\ \tan\theta/u\gg1 & \tan^2\theta\ll u\ll\tan\theta, \quad (10b)\\ 1/\tan\theta\gg1 & u\ll\tan^2\theta. \quad (10c)\end{cases}$$

We see that in the cases (10b) and (10c) always $E_\perp^+\gg E_\parallel^+$. The last situation is real, because in the experiment in Ref. 5, u may be well below unity (for example, $u<10^{-6}$ at $T\approx87$ K for YBCO; see Fig. 1, curves *1* and *5* in Ref. 5).

The appearance of the odd longitudinal contribution $\rho_\parallel^-$, as we see from Eqs. (2), (4), (7), and (9), follows from the assumed influence of twins on the ''bare'' Hall drag coefficient α. It must be stressed that such influence should be different for the vortex motion along and across the twins ($\gamma_l\neq\gamma_t$). Physically, it may follow from a different behavior of the Magnus force, whose microscopic origin may be highly complex (see, for example, Ref. 6). It is evident, at least, that the vortices move along the twin at the constant value of the order parameter, whereas the order parameter value is not homogeneous for the vortices that move across the twins.

3. In what follows, however, we consider another mechanism for the $\rho_\parallel^-$ appearance, which implies that the Ettingshausen effect is possible. For this reason, we will initially discuss the case in which, the transport current is zero, but there is a thermal force

$$\mathbf{f}_T=s_\parallel\nabla T+s_\perp\nabla T\times\mathbf{n}. \quad (11)$$

Here ∇T is the temperature gradient vector in the plane of the sample, and $s_\parallel$ and $s_\perp$ are the phenomenological constants ($s_\parallel\equiv S_\varphi$ is the transport entropy per vortex unit length, $s_\perp\equiv\Phi_0Q_n/\rho_n$, where Q_n is the normal state thermoelectric power, and ρ_n is the normal state resistivity; see, for example, Ref. 7). Substitution of the thermal force components f_t^T and f_l^T (instead of f_t and f_l) into Eqs. (3)

$$f_t^T\equiv s_\parallel x_T+ns_\perp y_T, \quad (12a)$$

$$f_l^T\equiv s_\parallel y_T-ns_\perp x_T, \quad (12b)$$

where $f_t^T\equiv\mathbf{m}\cdot\mathbf{f}_T$, $f_l^T\equiv\mathbf{m}_\parallel\cdot\mathbf{f}_T$ and $x_T\equiv\mathbf{m}\cdot\nabla T$, $y_T\equiv\mathbf{m}_\parallel\cdot\nabla T$ leads to the solutions of Eqs. (3) in the form (5)

$$v_t^T=(c/B)(s_\parallel^t x_T+ns_\perp^t y_T),$$

$$v_l^T=(c/B)(s_\parallel^l y_T-ns_\perp^l x_T), \quad (13)$$

where

$$\begin{cases}s_\parallel^t\equiv(B/c\Delta)(\eta_l s_\parallel+\alpha_{Hl}s_\perp),\\ s_\perp^t\equiv(B/c\Delta)(\eta_l s_\perp-\alpha_{Hl}s_\parallel),\end{cases}$$

$$\begin{cases}s_\parallel^l\equiv(B/c\Delta)(\eta_t s_\parallel+\alpha_{Ht}s_\perp),\\ s_\perp^l\equiv(B/c\Delta)(\eta_t s_\perp-\alpha_{Ht}s_\parallel).\end{cases} \quad (14)$$

Finally, we have the following equation for the electric field $\mathbf{E}$ produced by ∇T [compare with Eq. (6)]:

$$\mathbf{E}_T=s_\perp^t\mathbf{m}_\parallel(\mathbf{m}_\parallel\cdot\nabla T)+s_\perp^l\mathbf{m}(\mathbf{m}\cdot\nabla T)+n[s_\parallel^t\mathbf{m}_\parallel(\mathbf{m}\cdot\nabla T)-s_\parallel^l\mathbf{m}(\mathbf{m}_\parallel\cdot\nabla T)]. \quad (15)$$

Comparing (15) and (6), we see that if we change $s_\perp\to(\Phi_0/c)$, $s_\parallel\to0$, and $\nabla T\to\mathbf{j}$, then Eq. (15) transforms into Eq. (6). All physical analysis of Eq. (6) can therefore be repeated for Eq. (15) with only one essential distinction: for thermomagnetic effects all four parameters given by (14) are the values of the same order of magnitude[7], because $s_\parallel$ and $s_\perp$ in Eq. (11) are approximately of the same order of magnitude for HTSC. Note, however, that in Eq. (6) $\rho_{Hl}\ll\rho_l$ and $\rho_{Ht}\ll\rho_t$. From Eqs. (14) and (15) it follows that the Hall contributions ($\sim\alpha_{Ht}$ and α_{Hl}) always are small in comparison with other terms which are proportional to η_t and η_l. Because of this circumstance, all new (i.e., those stemming from anisotropy) thermomagnetic effects, giving $E_\parallel^-(\nabla T)$ and $E_\perp^+(\nabla T)$, might be of the same order of magnitude [unlike galvanomagnetic effects, where usually $E_\parallel^-(j)\ll E_\perp^+(j)$]. Until now, several interesting experimental investigations of the thermomagnetic effects in YBCO single crystals with unidirected twins have been carried out[8]. But below we deal only with ''secondary'' thermomagnetic effects produced by ∇T, which, in turn, is generated by the transport current density $\mathbf{j}$ due to the Ettingshausen effect (the latter in almost adiabatic conditions was measured in YBCO by Battlogg *et al.*[9]). In the case of anisotropic pinning such ''secondary'' thermomagnetic effects produce additional odd longitudinal (''Seebeck'') and even transverse (''Nernst'') contributions to the measured voltages. If the real experiment is carried out in nonisothermal conditions, these additional contributions may mask the ''intrinsic'' odd longitudinal contribution which is attributable to the possible influence of the twins on the Hall drag coefficient. Moreover, it is conceivable that in the case of bad heat removal conditions the intrinsic $E_\parallel^-=0$ (i.e., $\alpha_{Hl}=\alpha_{Ht}=\alpha$), but we measure only $\delta E_\parallel^-$ produced by the Ettingshausen effect. Analysis of the experimental observations of $E_\parallel^-$ (in contrast to $E_\perp^+$) therefore requires more accurate estimates of the heat removal conditions, especially for the case of large transport current densities. Theoretical estimate of the additional odd longitudinal contribution $\delta E_\parallel^-$ in the adiabatically isolated sample can be derived as follows. First, we calculate ∇T_L, which arises due to the heat current flow density $\mathbf{Q}_\varphi$ carried by the vortices which move with the velocity $\mathbf{v}_L$ in the sample with the anisotropic pinning in the presence of the transport current density $\mathbf{j}$

$$\mathbf{Q}_\varphi=U_\varphi\mathbf{v}_L=TS_\varphi\mathbf{v}_L=-\kappa\nabla T_L. \quad (16)$$

Here $U_\varphi=TS_\varphi$ is the thermal energy of the vortices, and κ is the thermal conductivity of the sample. From (16) we have

$$\nabla T_L=-\mu\mathbf{v}_L=-(\mu c/B)(\mathbf{n}\times\mathbf{E}_L). \quad (17)$$

Here $\mu \equiv TS_\varphi/\kappa$ and $\mathbf{E}_L$ is given by Eq. (6). Substitution of (17) into the equation for $\mathbf{E}_T$ (15) after some calculations gives us the desired additional odd longitudinal contribution $\delta E_\parallel^-$:

$$\delta E_\parallel^- = (\mu c/Bj)(xy)[(s_\perp^l \rho_t - s_\perp^t \rho_l) + (s_\parallel^t \rho_{Hl} - s_\parallel^l \rho_{Ht})]. \tag{18}$$

Neglecting a small Hall contribution in the second part of the brackets and comparing (18) with the equation for $E_\parallel^-$ (8), we see that both contributions have the same angular dependence and may have the same order values.

For further estimates we can use (18), in which we replace κ by κ_{eff} in order to take into account the actual heat-transfer conditions (κ_{eff} is always greater than κ). If the heat removal from the sample is effective (in term of κ_{eff} it means that $\kappa_{\text{eff}} \to \infty$), then $\delta E_\parallel^- \to 0$ and we can ignore it. In the opposite case ($\kappa_{\text{eff}} \to \kappa$) we would have $\delta E_\parallel^- \gg E_\parallel^-$.

In conclusion, we stress that Eqs. (3) allow us to consider nonlinear galvanothermomagnetic effects. This will be the subject of the next publication.

It is my pleasure to thank A. A. Prodan for help in preparing this paper for publication.

[1] V. M. Vinokur, V. B. Geshkenbein, M. V. Feigelman, and G. Blatter, Phys. Rev. Lett. **71**, 1242 (1993).
[2] E. B. Sonin and A. L. Kholkin, Fiz. Tverd. Tela **34**, 1147 (1992) [Sov. Phys. Solid State **34**, 610 (1992)]; E. B. Sonin, Phys. Rev. B **48**, 10487 (1993).
[3] A. V. Samoilov, A. Legris, F. Rulier-Albenque, P. Lejay, S. Bouffard, Z. G. Ivanov, and L.-G. Johansson, Phys. Rev. Lett. **74**, 2351 (1995).
[4] A. K. Niessen and C. H. Weijsenfeld, J. Appl. Phys. **40**, 384 (1969).
[5] A. V. Bondarenko, M. A. Obolenskii, R. V. Vovk, A. A. Prodan, V. A. Shklovskij, and A. G. Sivakov, in *Proc. of the 7th Intern. Workshop on Critical Currents in Superconductors*, H. W. Weber (Ed.), World Scientific, Singapore (1994), p. 177.
[6] E. B. Sonin, Phys. Rev. B **55**, 485 (1997).
[7] T. W. Clinton, Wu Liu, X. Jiang, A. W. Smith, M. Rajesuari, R. L. Greene, and C. J. Lobb, Phys. Rev. B **54**, R9670 (1996).
[8] H. Ghamlouch and M. Aubin, Physica C **269**, 163 (1996); H. Ghamlouch, M. Aubin, R. Gagnon, and L. Taillefer, Physica C **275**, 141 (1997).
[9] T. T. M. Palstra, B. Batlogg, L. F. Schneemeyer, and J. V. Waszczak, Phys. Rev. Lett. **64**, 3090 (1990).

This article was published in English in the original Russian journal. It was edited by S. J. Amoretty.

Low-temperature acoustic characteristics of the amorphous alloy $Zr_{41.2}Ti_{13.8}Cu_{12.5}Ni_{10}Be_{22.5}$

A. L. Gaiduk, E. V. Bezuglyi, and V. D. Fil

*B. Verkin Institute for Low Temperature Physics and Engineering, National Academy of Sciences of the Ukraine, 310164 Kharkov, Ukraine**

W. L. Johnson

California Institute of Technology, Pasadena, CA 91125, USA
(Submitted July 22, 1997)
Fiz. Nizk. Temp. **23**, 1139–1143 (October 1997)

The temperature dependences of the sound velocity v and attenuation α of high-frequency (50–160 MHz) sound in the bulk amorphous alloy $Zr_{41.2}Ti_{13.8}Cu_{12.5}Ni_{10}Be_{22.5}$ are studied at helium temperatures in the normal and superconducting states. The alloy is characterized by a relatively small constant C determining the intensity of interaction between an elastic wave and two-level systems. The density of states of the latter systems is estimated. The peculiarities in the variation of v during the superconducting transition point to the possibility of a gapless superconductivity in a narrow temperature interval near T_c. © *1997 American Institute of Physics.* [S1063-777X(97)01810-0]

Low-temperature kinetics of amorphous materials is mainly determined by specific low-energy quasilocal excitations, viz., two-level systems (TLS). The model concept of TLS developed in Refs. 1 and 2 proved to be very fruitful for explaining the thermal, elastic, and electromagnetic properties of insulating glasses and metglasses.[3] A simplest model of a TLS is a heavy tunneling entity in an asymmetric double-well potential. Both the initial model of TLS and its subsequent versions[4] are universal and are not connected with specific features associated with the microscopic origin of double-well potentials.

The properties of a large number of various glasses have been studied extensively. One of the most remarkable results in this field is the conclusion concerning virtual independence of the TLS density of states of the composition and the method of obtaining of glass. As regards metglasses, it should be noted, however, that all the compositions that were investigated before had been obtained at very high cooling rates ($\geqslant 10^3$ K/s), which probably determines the above-mentioned universality.

New classes of glass-forming systems obtained recently are stable over a wide temperature region of supercooled liquid state. Their high resistance to crystallization makes it possible to obtain bulk amorphous samples at very low quenching rates ($\leqslant 10$ K/s). It would be interesting to estimate the density of states of TLS for a typical representative of this family of metglasses. In this connection, we studied the acoustic properties of the amorphous alloy $Zr_{41.2}Ti_{13.8}Cu_{12.5}Ni_{10}Be_{22.5}$[5] at temperatures near 1 K.

Acoustic measurements are known to be one of the most informative methods of studying TLS.[3] The interaction of TLS with sound mainly follows the two principal mechanisms: resonance and relaxation. The former mechanism corresponds to the excitation of direct transitions between tunnel levels with the energy splitting $E=\sqrt{\Delta^2+\Delta_0^2}=\omega$ by sound of frequency ω (Δ is the asymmetry of a double-well potential and Δ_0 the tunnel splitting of energy levels for $\Delta=0$). In the available frequency range ($\omega \ll T$), the resonant contribution to variations of the sound velocity is determined (to within a constant term) by the formula

$$\left(\frac{\delta v_i}{v_i}\right)_{\text{res}} = \frac{\overline{P}\,\overline{\gamma_i^2}}{\rho v_i^2} \ln T = C_i \ln T, \tag{1}$$

where $\overline{P}$ is the TLS density of states, γ the deformation potential, ρ the mass density, and i denotes the longitudinal (l) or transverse (t) polarization.

The resonant contribution to the absorption coefficient α/q (q is the wave number) is small in the parameter ω/T on the C_i scale.

Elastic deformation of the wave also shifts the spectrum of tunnel levels. If there exist the relaxation mechanism which makes it possible for TLS to tune the occupancy of the levels to a new set of E rapidly (on the ω^{-1} scale), the attenuation and the velocity of sound acquire a relaxation component:

$$\begin{pmatrix} \dfrac{\alpha_i}{q_i} \\ \dfrac{\delta v_i}{v_i} \end{pmatrix} = \frac{C_i}{2} \begin{pmatrix} \pi \\ \ln\, \omega\tau_{\min} \end{pmatrix}, \tag{2}$$

where $\tau_{\min}$ is the minimum relaxation time for $\Delta=0$ and $E\sim T$. Expressions (2) are valid for $\omega\tau_{\min}\ll 1$; otherwise, the relaxation interaction can be neglected. In the general case, the TLS relaxation in metglasses is due to interaction with

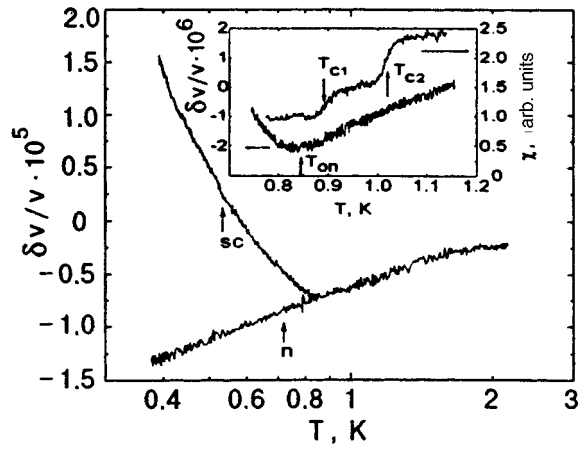

FIG. 1. emperature dependences of relative changes in the velocity of transverse sound in the amorphous alloy $Zr_{41.2}Ti_{13.8}Cu_{12.5}Ni_{10}Be_{22.5}$ at a frequency of 54.3 MHz. The inset shows a fragment of $\delta v/v(T)$ dependence and the diamagnetic response χ in the superconducting transition region.

electrons as well as with phonons, but the contribution of the latter can be neglected at $T<2-3$ K, and the relaxation frequency can be written in the form[3]

$$(\tau_{\min}^{-1})_e=\frac{\pi}{2}\,\eta^2 T, \tag{3}$$

where η is the dimensionless parameter of coupling between electrons and the TLS.

The sample with an acoustic path length of 0.74 cm was cut from an oval ingot.[5] The values of v and α were measured in the pulsed mode by the phase-sensitive bridge method at frequencies close to 54.3 and 162.9 MHz. The diamagnetic response χ was measured at a frequency of 22.5 Hz with the concentric arrangement of the sample, the receiving and exciting coils. Note the high homogeneity of the alloy: 8–10 well-defined reflexes were observed at an acoustic wavelength ~ 15 μm. In order to avoid possible errors of interference origin, main measurements were made by comparing phases and amplitudes of first and second or third pulses. At 77 K, the velocities were $v_l=(5.17\pm 0.03)\times 10^5$, $v_t=(2.49\pm 0.01)\times 10^5$ cm/s.

Figure 1 shows the relative change in the velocity of transverse sound in the alloy under investigation in the normal (n) and superconducting (sc) states. In the former case, the field $H=1.5$ T($\mathbf{H}\|\mathbf{q}$) was applied. It should be noted that above T_c, such fields did not affect the behavior of v and α. In the normal phase, the temperature variation of the velocity is correctly approximated by a logarithmic dependence with the coefficient $C_i/2$ appearing when expressions (1) and (2) are added. To within the error of measurements, the values of the constants C_i ($C_l=(0.58\pm 0.02)\times 10^{-5}$, $C_t=(1.42\pm 0.03)\times 10^{-5}$) were independent of frequency.

In the superconducting phase, freezing out of normal excitations leads to an increase in $\tau_{\min}$[6] and to a sharp decrease in the relaxation contributions to the velocity and absorption of sound, which is reflected in a sharp kink on the $v(T)$ curve in Fig. 1 at the temperature $T_{\rm on}=0.85$ K. The inset to Fig. 1 shows the changes in the velocity near $T_{\rm on}$ measured simultaneously ($H=0$) with the diamagnetic response χ of the sample recorded for the ac field amplitude $\tilde{H}\simeq 4$ mOe. The sample obviously contains two phases with the phase-transition temperatures $T_{c1}\simeq 0.9$ K and $T_{c2}\simeq 1.02$ K. The value of T_{c2} probably corresponds to a surface phase since this transition does not affect the sound velocity in any way. Besides, an increase in $\tilde{H}$ to 40 mOe leads to virtually complete suppression of the jump in χ at T_{c2}, while the peculiarity at T_{c1} is preserved up to $\tilde{H}=1$ Oe. The non-coincidence between the resistive and magnetic superconducting transitions in a glass of the same composition observed by Gerber *et al.*[7] is apparently also connected with the existence of two phases.

It can be seen from Fig. 1 that the temperatures $T_{\rm on}$ and T_{c1} do not coincide. Naturally, we can assume that the sample is not homogeneous as regards T_{c1}, but the small width of the jump in χ at T_{c1} renders this assumption hardly plausible. Probably, the regime of so-called gapless superconductivity is realized in the temperature interval $T_{c1}-T_{\rm on}$.[8]

An analytic expression for $\tau_{\min}$ in a superconductor can be derived only for $E\ll\Delta_{sc}$ (Δ_{sc} is the superconducting gap).[6] Since the main contribution to the measured parameters comes from TLS with $E\leqslant T$, the above limitation boils down to $T\ll\Delta_{sc}$. In this case, we can write

$$(\tau_{\min}^{-1})_{e\,sc}=\frac{\pi}{2}\,\eta^2 T\mathrm{e}^{-\Delta_{sc}/T}. \tag{4}$$

Since the velocity in the superconducting phase continues to grow up to $T\sim 0.4$ K, the condition $\omega\tau_{\min}<1$ obviously remains valid, and expression (2) for the relaxation contribution to $\delta v/v$ still holds. Assuming that the resonant contribution in the normal and superconducting phases is the same, we have the following expression for the difference in the velocities of sound in the sc- and n-phases from (1-4):

$$\frac{\Delta v}{v}=\left(\frac{\delta v}{v}\right)_{sc}-\left(\frac{\delta v}{v}\right)_{n}\sim-\frac{\Delta_{sc}}{T}.$$

In actual practice, the strong inequality between T and Δ_{sc} is not satisfied in our experiments. Nevertheless, we can expect that the experimental dependences $\Delta v/v(T^{-1})$ become linear in a certain temperature interval $T<T_c$, where $\Delta_{sc}(T)\approx\Delta_{sc}(0)$.

A dependence of this type is shown in Fig. 2a. For comparison with theoretical dependences, the temperature scale in Fig. 2 is given in reduced form, and the superconducting transition temperature is assumed to be equal to $T_{\rm on}$. The velocity scale is also normalized to $C_t/2$. It was found that the dependence $\Delta v/v(T^{-1})$ is close to linear in the entire temperature range below $T_{\rm on}$, but its slope is twice the BCS value of $\Delta_{sc}(0)$. In all probability, such a behavior of $\Delta v/v(T^{-1})$ is the result of joint operation of several temperature-dependent mechanisms. For comparison, Fig. 2a presents the results of complete calculation of $\Delta v/v$ for the BCS model ($\eta=0.85$, see below) on the basis of equations from Ref. 6. The agreement between the theoretical and experimental dependences is obviously unsatisfactory over virtually the entire temperature range, although the scale of variation is reproduced correctly on the whole. The agreement can probably be improved in the vicinity of T_c by

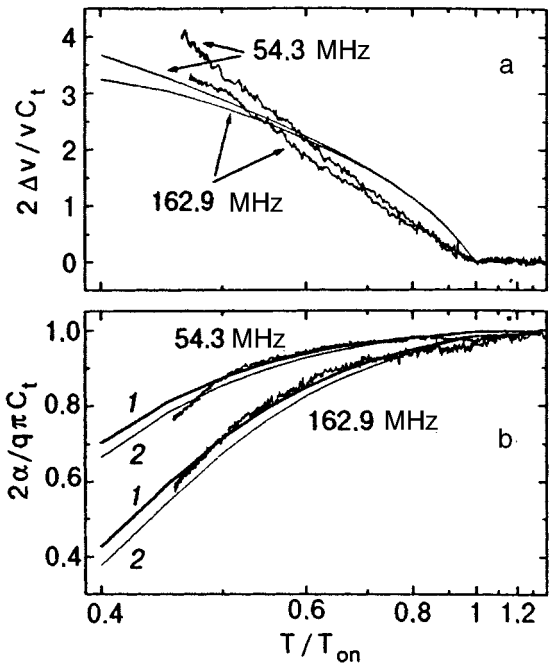

FIG. 2. Difference of the relative changes in the transverse sound velocity in the superconducting and normal states as a function of reduced temperature. Smooth curves correspond to the results of calculation ($\eta=0.85$) (a); absorption in the superconducting phase: $\eta=0.89$ (curve *1*) and 0.81 (curve *2*) (b). The temperature is given on reciprocal scale.

taking into account magnetic scattering effects which eliminate the divergence in the derivatives of the order parameter and energy gap at T_c,[8] but a rigorous theory of interaction between sound and TLS in the presence of magnetic impurities has not yet been constructed. The assumption concerning the equality of the resonant contributions in the *sc*- and *n*-phases might be incorrect due to a considerable narrowing of the tunnel levels upon a decrease in $(\tau_{\min}^{-1})_{e\,sc}$,[9] which can affect the behavior of $\Delta v/v$ at lower temperatures, e.g., can change the normalization of the ordinate axis in Fig. 2a.

Figure 2b shows the temperature dependences of variations in sound absorption, which is also normalized by $\pi C_t/2$ in accordance with (2). Further, the normalized absorption in the normal phase was assumed to be equal to unity in conformity with (2) since the real value of α cannot be determined in the temperature interval under investigation (this can be done only from the difference in absorption in the normal and deep superconducting states). The theoretical dependences in the BCS model correctly reproduce the difference in the behavior of absorption at two frequencies, although the steepness of the variation of α/q for $T/T_{on}\sim 0.45$ is higher than the theoretical value. It should be recalled, however, that the steepness of experimental dependences in Fig. 2b is also determined by the choice of the normalization constant C_t. The estimated value of $\eta\approx 0.85$ naturally depends on the value of Δ_{sc}: the value of η decreases with Δ_{sc}. In this case, theoretical dependences become still more gently sloping, and the estimated value of η can not be reduced by a factor of more than two for the same normalization constant C_t.

Let us now estimate the TLS density of states. This can be done if we know the crossover temperature T_{cr} at which the electron relaxation time becomes equal to the phonon one: $(\tau_e)_{\min}=(\tau_{ph})_{\min}$. Usually it is assumed that the crossover occurs at a temperature at which the velocity of sound passes through its maximum.[3] In our case, $T_{cr}\approx 3.3$ K. The phonon relaxation rate is mainly determined by transverse phonons:[3]

$$(\tau_{\min}^{-1})_{ph}=\frac{8\gamma_t^2}{\pi\rho v_t^5}T^3. \tag{5}$$

Combining (1), (3), and (5), we obtain

$$\overline{P}=8.4(T_{cr}/\eta)^2C_t\cdot 10^{32}\ \ \mathrm{erg}^{-1}\cdot\mathrm{cm}^3 \tag{6}$$

(in this equation, T_{cr} is in degrees). Substituting $T_{cr}=3.3$ K, $\eta=0.85$, $C_t=1.42\cdot 10^{-5}$, we obtain $P=1.8\cdot 10^{29}$ $\mathrm{erg}^{-1}\cdot\mathrm{cm}^{-3}$. This value is two–three orders of magnitude smaller than values known from literature.[4]

In formula (6), we specially singled out the quantities whose values are not known exactly. In actual practice, a noticeable contribution (proportional to T^2) to the velocity of sound is observed in the sample under investigation (we are planning to publish the corresponding results later); the combination of this contribution with the logarithmic dependence can also lead to the formation of a velocity peak. For this reason, the value of T_{cr} can be slightly higher. The fitting value of η (see Fig. 2b) depends on the energy gap for which the BCS value was used. If our assumption concerning the effect of magnetic scattering is confirmed, the energy gap will be smaller,[8] which can reduce the estimated value of η^2 by a factor of several times. The exact value of C_t is not known to us either; it can be obtained from the logarithmic decrease in the velocity of sound in the deep superconducting state. On account all these remarks, the estimated value of P in the alloy under investigation can be an order of magnitude higher than the value given above, but still considerably smaller than the known values from the literature sources.

In summary, the values of the TLS density of states in the amorphous alloy $Zr_{41.2}Ti_{13.8}Cu_{12.5}Ni_{10}Be_{22.5}$ estimated on the basis of acoustic measurements are much smaller than for other metglasses. This is probably due to the very low rate of cooling of the melt (~ 10 K/s). The observed peculiarities of superconducting ordering indicate, on one hand, the two-phase structure of the amorphous alloy under investigation, and on the other hand, the possible realization of a gapless superconductivity in this material in a narrow temperature range.

The authors are grateful to V. Z. Bengus, E. D. Tabachnikova, and A. S. Bakai for fruitful discussions and to E. A. Masalitin for his assistance in preparing the apparatus.

*E-mail: fil@ilt.kharkov.ua

[1] P. W. Anderson, B. I. Halperin, and C. M. Varma, Philos. Mag. **25**, 1 (1972).
[2] W. A. Phillips, J. Low Temp. Phys. **7**, 351 (1972).
[3] S. Hunklinger and A. K. Raychaudhuri, Progr. Low Temp. Phys. **9**, 266 (1986).
[4] D. A. Parshin, Phys. Rev. B **49**, 9400 (1994).

[5] A. Pecker and W. L. Johnson, Appl. Phys. Lett. **63**, 2342 (1993).
[6] J. L. Black and P. Fulde, Phys. Rev. Lett. **43**, 453 (1979).
[7] A. Gerber, A. Milner, A. Voronel *et al.*, Physica C **275**, 333 (1997).
[8] A. A. Abrikosov and L. P. Gor'kov, Zh. Éksp. Teor. Fiz. **39**, 1781 (1960) [Sov. Phys. JETP **12**, 1243 (1960)].
[9] N. Thomas, Philos. Mag. B **48**, 297 (1983).

Translated by R. S. Wadhwa

Erratum: Peculiarities in the electron properties of $\delta\langle$Sb$\rangle$-layers in epitaxial silicon. III. Electron–phonon relaxation [Low Temp. Physics 23, 303–307 (April 1997)]

V. Yu Kashirin, Yu. F. Komnik, A. S. Anopchenko, O. A. Mironov, C. J. Emelius, and T. E. Whall

[S1063-777X(97)01910-5]

The correct spelling of the fifth author's name should read C. J. EMELEUS.

